Journal of Engineering

ISSN 1726-4073

A Scientific Refereed Journal
Published by College of Engineering University of Baghdad

June

2015

Number 6

Volume 21

مجلة الهندسة

ISSN 1726-4073

مجلة علمية محكمة تصدرها
كلية الهندسة ـ جامعة بغداد

حزيران
2015

العدد 6
المجلد 21

ISSN 1726 - 4073

Journal of Engineering

A Scientific Refereed Journal
Published by
College of Engineering
University of Baghdad

June
2015

Number 6
Volume 21


English Section

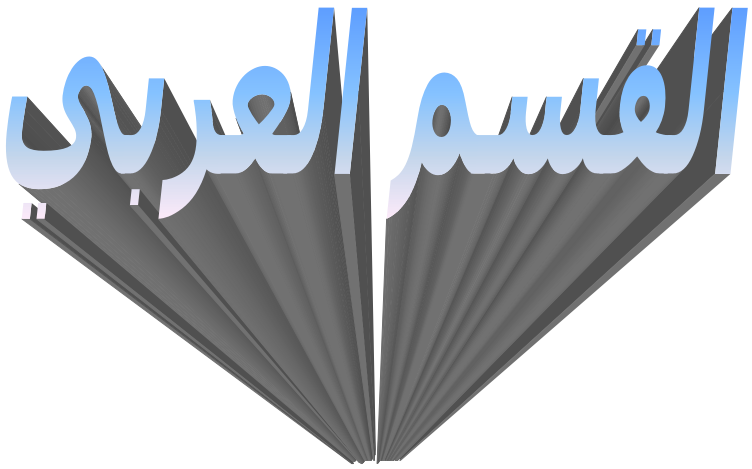
القسم العربي

JOURNAL OF ENGINEERING ISSN 1726-4073

College of Engineering University of Baghdad Baghdad

Editorial Board

The Journal of Engineering is a monthly refereed periodical

Correspondence should be addressed to:

THE EDITOR
JOURNAL OF ENGINEERING
COLLEGE OF ENGINEERING
UNIVERSITY OF BAGHDAD
P. O. BOX 47024 JADERIYAH
BAGHDAD – IRAQ

ISSN 1726-4073

مجلة الهندسة

كلية الهندسة جامعة بغداد

مجلة الهندسة: مجلة شهريه محكمة

تعنون كافة المراسلات وطلبات الاشتراك الى:

رئيس التحرير
مجلة الهندسة
كلية الهندسة
صندوق بريد **47024**
الجادرية
بغداد - العراق

ENGINEERING

College of Engineering Baghdad University Baghdad

List of Contents

English Section: Page

Evaluation of Alum/Lime Coagulant for the Removal of Turbidity from Al-Ahdab Iraqi Oilfields Produced Water

Basma Abbas Abdul-Majeed
Assistance Professor
College of Engineering
University of Baghdad
E-mail:basma1957@yahoo.com

Hussein Basim Oleiwi
Ph.D. Chemical Engineer
College of Engineering
University of Baghdad
E-mail:husseinbasim537@yahoo.com

ABSTRACT

The removal of turbidity from produced water by chemical coagulation/flocculation method using locally available coagulants was investigated. Aluminum sulfate (alum) is selected as a primary coagulant, while calcium hydroxide (lime) is used as a coagulant aid. The performance of these coagulants was studied through jar test by comparing turbidity removal at different coagulant/ coagulants aid ratio, coagulant dose, water pH, and sedimentation time. In addition, an attempt has been made to examine the relationship between turbidity (NTU) and total suspended solids (mg/L) on the same samples of produced water. The best conditions for turbidity removal can be obtained at 75% alum+25% lime coagulant at coagulant dose of 80 mg/l at pH 6 and 120 min for sedimentation time. At these conditions, the turbidity reading was reduced from 92 to 2.1 NTU.

Key words: coagulation, turbidity, alum, produced water.

تقييم مخثر الشب ـ النورة في ازالة العكورة من المياه المصاحبة لأنتاج النفط من حقول الأحدب العراقية

أ.م.د. بسمة عباس عبدالمجيد
كلية الهندسة- جامعة بغداد

حسين باسم عليوي
دكتوراه هندسة كيمياوية

الخلاصة

في هذا البحث تمت دراسة ازالة العكورة من الماء المنتج بطريقة التخثر/ التلبد وباستخدام مخثرات متوفرة محلياً. تم استخدام كبريتات الالمنيوم (الشب) كمخثر رئيسي بينما استخدم هيدروكسيد الكالسيوم (النورة) كمخثر مساعد. تم دراسة اداء هذه المخثرات بطريقة الدفعة وباستخدام فحص الجرة وذلك بمقارنة ازالة العكورة من الماء تحت ظروف مختلفة مثل نسبة المخثر / المخثر المساعد و كمية المخثر و الدالة الحامضية للماء وزمن التركيد. بالاضافة الى ذلك, تم عمل دراسة مختبرية لمعرفة العلاقة بين درجة العكورة (وحدة كدرة) ومجموع المواد الصلبة المعلقة (مليغرام لكل لتر) لنماذج مختلفة من الماء المنتج. بينت النتائج بأن المخثرات المستخدمة اظهرت افضل اداء في ازالة العكورة وان الجرعة الامثل للمخثر هي ٨٠ مليغرام لكل لتر والرقم الهيدروجيني الامثل هو ٦ وافضل زمن التركيد كان١٢٠ دقيقة وان افضل نسبة مخثر/ مخثر مساعد كانت ٧٥% شب مع ٢٥% نورة. تناقصت قراءة العكورة من ٩٢ الى ٢,١ وحدة كدرة عند هذه القيم المثلى.

الكلمات الرئيسية: التخثر, العكورة, الشب, المياه المنتجة.

1. INTRODUCTION

Treating oilfield water can help facilitate additional water management options for operators such as beneficial uses that in the short and long term can potentially provide certain community and economic advantages. Treated produced water has the potential to be a valuable product rather than a waste. A large number of methods were used as treatment technologies such as heat treating, gas flotation, chemical separation, membranes, filtration, and biological degradation. Several methods are available to remove the suspended solids or turbidity (like cuttings, sand, clay particles, and microorganisms) and their methods are filtration, coagulation, gravity separation, and biological treatment, **Arthur, 2005.**

All waters, especially produced water, contain both dissolved and suspended particles. Coagulation and flocculation processes are used to separate the suspended solids portion from the water. The suspended particles vary considerably in source, composition charge, particle size, shape, and density. Correct application of coagulation and flocculation processes and selection of the coagulants depend upon understanding of the interaction between these factors, **Smita, et al., 2012.**

Turbidity is cloudiness or haziness of water (or other fluid) caused by individual particles that are generally invisible to the naked eye. It is a characteristic related to the concentration of suspended solid particles in water and has been adopted as an easy and reasonably accurate measure of overall water quality **,Tseng, 2000.** World Health Organization (WHO) has set the guideline value for the residual turbidity in drinking water at 5 Nephelometric Turbidity units (NTU), **Connachie, et al., 1999.** Although turbidity purports to measure approximately the same water quality property as total suspended solids, the later is more useful because it provides an actual weight of the particulate material present in the sample. While a relationship can be established between turbidity and suspended solids, this relationship can and will change spatially and temporally due to variations in solid composition and stream energy **,Rasmussen, 1995.**

For all water types, there are many parameters that affect coagulation performance for turbidity removal including the character and concentration of the particular material, chemical and physical properties of the water, mixing time, mixing speed, and temperature. The common parameters are coagulant type, dose, pH, and settling time, **Uyak** and **Toroz, 2007.** The coagulation process utilizes what is known as a chemical coagulant to promote particle agglomeration. **Eilbeck** and **Mattock, 1987,** presented a list of common coagulants in treating wastewater. They mentioned that the most frequently used coagulants are iron and aluminum salts and especially, for economic reasons, aluminum sulfate and ferric chloride. Coagulants are sometimes assisted with further chemicals, known as coagulant aids. They essentially are polyelectrolytes and lime alkalinity addition, **Kiely, 1997.**

The aim of this work was to study the feasibility of turbidity removal from real produced water from Al-Ahdab Oilfields by alum and lime coagulants. The process was examined for the

first time in Iraq under different values of coagulant/ coagulants aid ratio, coagulant dose, water pH, and sedimentation time.

2. MATERIALS

2.1 Produced Water

A volume of produced water obtained for sampling from Al-Ahdab Oilfields, 180 km south-east of Baghdad, was stored in a plastic container for the duration of the study. Samples of this water were analyzed chemically in the Al-Ahdab Oilfields and results are listed in **table 1.**

2.2 Coagulants

The chemical coagulants used in the present study were aluminum sulfate and calcium hydroxide. Aluminum sulfate (Alum) is selected as a primary coagulant, while calcium hydroxide (lime) is used as a coagulant aid. Alum is a white crystalline solid with the formula $Al_2(SO_4)_3.18H_2O$ with purity of 97.3%wt. Lime is a very fine white powder. It has the chemical formula of $Ca(OH)_2$, purity of 95%wt. The selected coagulants have been chosen in this work due to their physical and chemical properties which give their ability to remove turbidity on their molecular species from the bulk liquid. Also, they are of low cost and are locally available.

3. EXPERIMENTAL PROCEDURE

All coagulation experiments were conducted in six-place conventional jar-test apparatus. Six beakers with 1 liter volume of produced water are used at time of experiment. The study includes the effect of coagulant/ coagulant aid ratio, coagulant dose, pH, and sedimentation time on turbidity removal. Different combinations of coagulant dose (20, 40, 60, 80, 100, and 120 mg/l), pH (3, 4, 5, 6, 7, and 8), and sedimentation time (30, 60, 90, 120, 150, and 180 min) were tested. The pH was adjusted by adding drops of HCl (0.1M) or NaOH (0.1M) prior to the addition of coagulant. To simulate coagulation, flocculation, and sedimentation conditions, rapid mixing at 200 rpm was performed for 3 min, followed by slow mixing for 30 min at 30 rpm and final step (0 rpm) for 60 min settling time, **Degremont, 1979.** After completing the settling time, supernatant was withdrawn with a plastic syringe from near 3 cm below the liquid-air interface for analysis of turbidity and total suspended solids. All the experiments were carried out at ambient temperature of 20-25 C^o.

Total suspended solids (TSS) are that portion of the total solids that are retained on a filter paper (Cellulose nitrate membrane, approximately 0.45 mm pore size). Before sampling, filter papers were prepared by first soaking them in distilled water, drying them at 100 C^o, weighing and recording their weights. Now, a measured volume (100 ml) of produced water is passed through the filter. The filter containing the residue is then dried in an oven for one hour at 100 C^o. The sample is then cooled and weighed. The increase in weight represents TSS. Finally, TSS was calculated by using the equation below, **APHA, 1998.**

$$TSS\left(\frac{mg}{l}\right) = \frac{(A-B)}{C} \times 1000 \quad (1)$$

where A = final weight of the filter (mg), B = initial weight of the filter (mg), and C = volume of water filtered (l). This inexpensive TSS tells much about the produced water character and can be run in less than two hours with fairly inexpensive equipment.

4. RESULTS AND DISCUSSION

4.1 Evaluation of the Percentage Ratio of Coagulant/Coagulant Aid

Different doses of aluminum sulfate (alum) as a primary coagulant with the coagulant aid (lime) were added to the produced water with initial turbidity as 92 NTU, uncontrolled pH as 5.8, coagulant dose as 60 mg/l, and 60 min as sedimentation time. The results are shown in table 2. Examining this table, it is clear that there was an improvement in the turbidity removal when 25% lime were used as a coagulant aid in conjunction with 75% alum compared to alum alone and this can be regarded as the best coagulant. **Lin, et al., 1971,** showed that the addition of alum to water releases hydrogen ions and consequently lowers the pH. Unless the hydrogen ions can be removed, the formation of an effective floc, $Al(OH)_3$, is impossible. The hydrogen ions can be removed by the alkalinity in natural water or by the addition of lime. This finding is in agreement with **, Degremont, 1979** and **Kiely, 1997.** They mentioned that if there is insufficient alkalinity in the water with high turbidity, alkalinity is added by means of lime addition, even with small amount, to improve the alkalinity and optimize coagulation.

4.2 Effect of Coagulant Dosage

Coagulant dosage was one of the most important parameters that have been considered to determine the best condition for the performance of coagulant used (75%alum+25%lime) in coagulation/ flocculation process. The effect of coagulant dosage on the removal of turbidity is shown in **Fig. 1**. Coagulant dosage was varied from 0 to 120 mg/l while other parameters were kept constant at pH 5.8 and 60 min for sedimentation time. From **Fig. 1**, it can be seen that the best dose of coagulant was 80 mg/l and the removal efficiency of turbidity was 91.41%. It is noticed that turbidity values are decreasing for coagulant dosage level of 0 to 80 mg/l and gradually increasing for dosage level of 100 to 120 mg/l. This may be explained by: high dose of the coagulant in the suspension caused charge stabilization of colloid particles, due to the adsorption of counter ions (in this case was Al^{+3}). Increasing the dose of coagulant more than 80 mg/l raised the turbidity because the excess adsorption of the counter ions caused the charge of colloidal particles to become positive (i.e. re-stabilization of the colloidal particles). The results obtained in this study are similar to those reported by **Ghaly et al., 2007.** They reported that colloidal particles are negatively charged and upon addition of aluminum sulfate to wastewater, the Al^{+3} ions are attracted to these particles. At the point of complete charges neutralization, the colloids begin to agglomerate due to collisions between particles. If excess coagulant is added to the wastewater, the results are a reverse of the net charge on the colloidal particles (from negative to positive). Particle re-stabilization by charge reversal allowed greater amounts of smaller particles to remain in solution, thus increasing the total solids as well as the color intensity of the treated water.

4.3 Effect of pH

In the coagulation/ flocculation process, pH is very important as the coagulation occurs within a specific pH range. An optimum pH range, in which metal hydroxide precipitates occur, should be determined to establish best conditions for coagulation. In this study, a range of pH between 3 to 8 was selected. The results of the study showing the effect of pH on the removal of turbidity are presented in **Fig. 2**. To determine the best pH value, coagulant dosage was maintained at 80 mg/l and 60 min for sedimentation time. The best pH was determined at a value of 6 followed by 5 and 7 and the turbidity removal was 91.09% as shown in **Fig. 2**. It was found that the percentage of turbidity removal was increased at pH from 3 to 6 and then it declined for pH 7 to 8. The obtained results are in accordance with those obtained by **Degremont, 1979** and

Sadeddin et al., 2011. They indicated that aluminum salts work best in a pH range of 5.5-7.4. Outside this range, a higher concentration of dissolved aluminum is liable to be found.

4.4 Effect of Sedimentation Time

In this experiment, the sedimentation times were varied from 30 to 180 minutes. Other parameters were kept constant at pH 6 and 80 mg/l for coagulant dosage. The effect of sedimentation time on coagulation process is given in **Fig. 3**. From this figure, it can be seen that the turbidity decreased with increasing settling time and it reached equilibrium at 120 min. At this point, removal efficiency of turbidity was 97.72 %. Further increase in time had no effect on turbidity removal. This result explained that almost all flocs produced after the coagulation and mixing process have settled to the bottom of the sludge layer after 120 min. The settling process is mainly affected by the gravity where heavier flocs will settle faster than dispersed particle.

4.5 Turbidity versus Total Suspended Solids

Both turbidity and total suspended solids (TSS) are defined by the method used to measure them. Turbidity is an optical measurement; it depends on the number of particles in the sample and their shape and size. While TSS is a gravimetric measurement, it depends on the total mass of filterable material in the sample, **Rasmussen, 1995, Fig. 4**. The final relationship between turbidity and TSS at Al-Ahdab oilfields produced water was shown in **Fig. 5**. This figure confirms the existence of a strong linear relationship between turbidity readings and TSS concentrations. High coefficient of determination (R^2=0.972) value was obtained for this relationship. From the published NTU-TSS relationship, **Irvine, et al., 2002** and **Hannouche, 2011.** It is seen that it can vary considerably between different aquatic systems and even at different times for the same stream, so there is no universal correlation of turbidity and TSS.

5. CONCLUSIONS

The aluminum sulfate (alum) combination with coagulant aid (lime) provided higher removal efficiencies of turbidity compared to coagulation with alum alone. The added alum to water causes the release of hydrogen ions which lowers the pH.

The best conditions for turbidity removal using a jar test process can be obtained at 75% alum+25% lime coagulant ratio at coagulant dosage of 80 mg/l at pH 6 and 120 min for sedimentation time. This dose caused colloid particles to be charge stabilized, while increasing the dose increase the turbidity where re-stabilization occurs.

At these conditions, the NTU reading was reduced from 92 to 2.1. The TSS-turbidity relationship may be both site and time specific, so the relationship is normally unique for a particular catchment and within a particular period of time.

6. REFERENCES

- American Public Health Association, APHA, 1998, *Standard Methods for the Examination of Water and Wastewater*. 20th edition.

- Arthur D., Langhus G., and Patel C., 2005, *Technical Summary of Oil and Gas Produced Water Treatment Technologies*. Commissioner's environment produced water treatment Tech.

- Connachie, G. L., Folkard, G.K., Matawali, M. A. and Surtherland, J.P., 1999, *Field trials of appropriate hydraulic flocculation process*. J. Water Research, 33 (6), 1425-1434.

- Degremont, 1979, *Water Treatment Handbook*. 5th Ed; Distributed by Halsted Press N.Y.

- Eilbeck, W. J. and G. Mattock, 1987, *Chemical Processes in Waste Water Treatment*. England: Ellis Horwood Limited. Chapter 11.

- Ghaly, A.E., A. Snow and B.E. Faber, 2007, *Effective Coagulation Technology for Treatment of Grease Filter Wash Water*. American Journal of Environmental Sciences 3 (1), p: 19-29.

- Hannouche, G. Chebbo, G. Ruban, B. Tassin, B. J. Lemaire, and C. Joannis, 2011, *Relationship Between Turbidity and Total Suspended Solids Concentration Within a Combined Sewer System*. Water Science and Technology (64), 12.

- Irvine, K.N., E.L. Somogye, and G.W. Pettibone, 2002, *Turbidity, Suspended Solids, and Bacteria Relationships in the Buffalo River Watershed*. Middle States Geographer (35), p: 42-51.

- Kiely, Gerard, 1997, *Environmental Engineering*. Copyright, McGraw-Hill International Limited (UK).

- Lin, S. D., R. L. Evans, and D. B. Beuscher, 1971, *Algal Removal by Alum Coagulation*. Illinois State Water Survey, Urbana, Report of Investigation 68.

- Rasmussen, T.C., 1995, *Erosion and Sedimentation: Scientific and Regulatory Issues*. Report developed by Georgia Board of Regents scientific panel on evaluating the erosion measurement standard defined by the Georgia Erosion Sedimentation Act.

- Sadeddin, K., Naser A., and Firas, A., 2011, *Removal of Turbidity and Suspended Solids by Electro-Coagulation to Improve Feed Water Quality of Reverse Osmosis Plant*. Desalination Journal (268), p: 204-207.

- Smita, S. Borchate, G. S. Kulkarni, S. V. Kore, and V. S. Kore, 2012, *Application of Coagulation-Flocculation for Vegetable Tannery Wastewater*. International Journal of Engineering Science and Technology (4), p: 1944-1948.

- Tseng, T., Segal B.D., and Edwards M., 2000, *Increasing Alkalinity to Reduce Turbidity*. Journal of the American Water Works Association (92), p: 44-52.

- Uyak, V. and Toroz, I., 2007, *Disinfection by-Product Precursors Reduction by Various Coagulation Techniques in Istanbul Water Supplies*. Journal of Hazardous Materials (141) p: 320-328

Table 1. Analysis of produced water from Al-Ahdab Oilfields, Date: 2-3-2013.

Parameter	Value	Permissible Limit
pH	5.5-5.9	6.5-8.5
Turbidity (NTU)	92	5
TSS (mg/l)	2520	30
Density (kg/m^3)	1095	_

Table 2. The percentages of the coagulant doses**.**

Sample No.	Coagulants	Final Turbidity (NTU)	Removal Efficiency (%)
1	100 % alum + 0 % lime	54.4	40.87
2	75 % alum + 25 % lime	12.8	86.09
3	50 % alum + 50 % lime	37.2	59.57
4	25 % alum + 75 % lime	61.4	33.26
5	0 % alum + 100 % lime	73	20.65

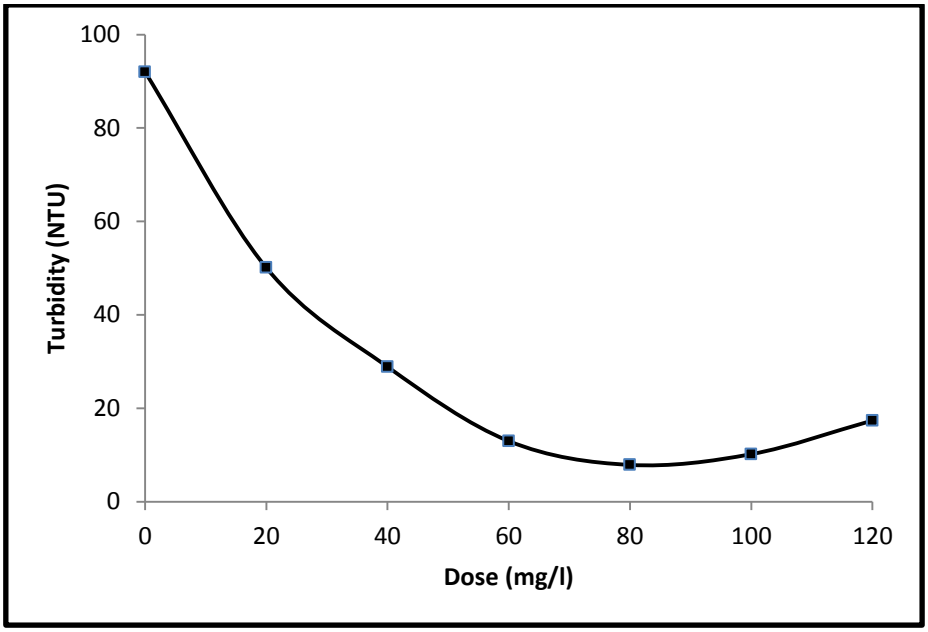

Figure 1. The effect of coagulant dosage on turbidity removal from produced water.

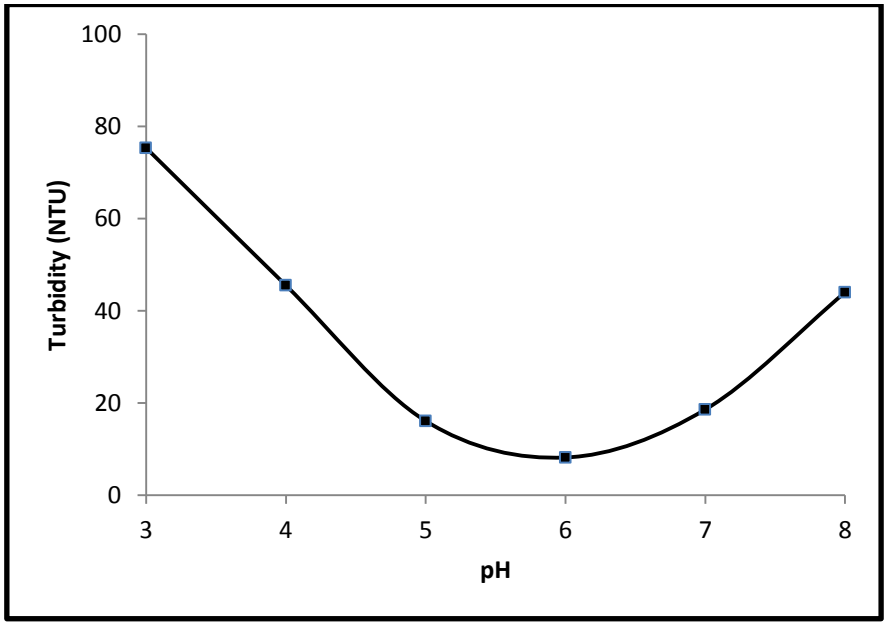

Figure 2. The effect of pH on turbidity removal from produced water**.**

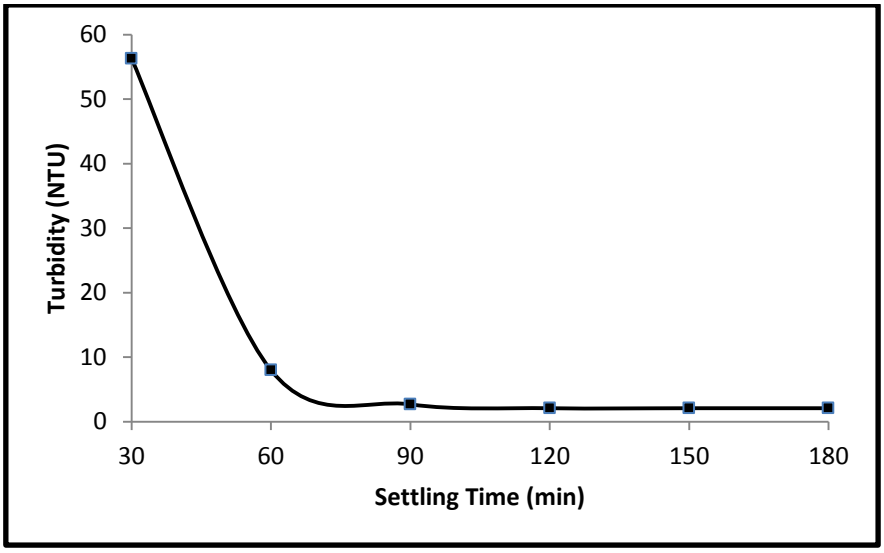

Figure 3. The effect of sedimentation time on turbidity removal from produced water.

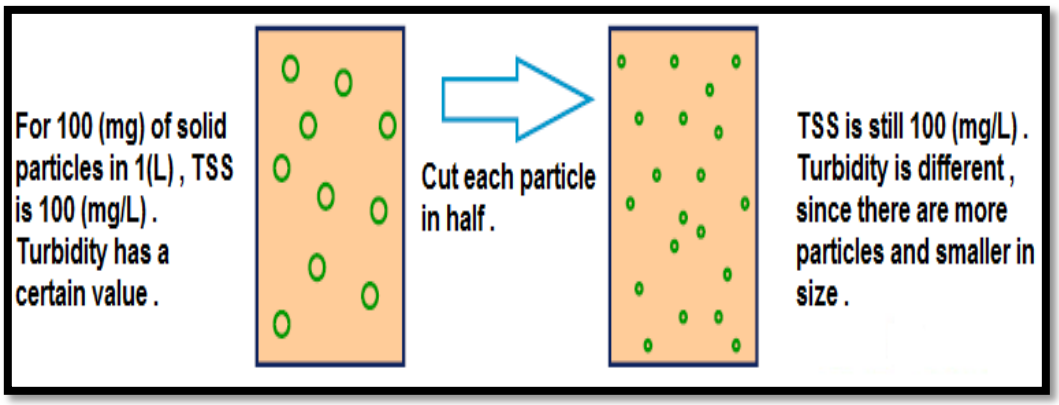

Figure 4. Turbidity compared to TSS.

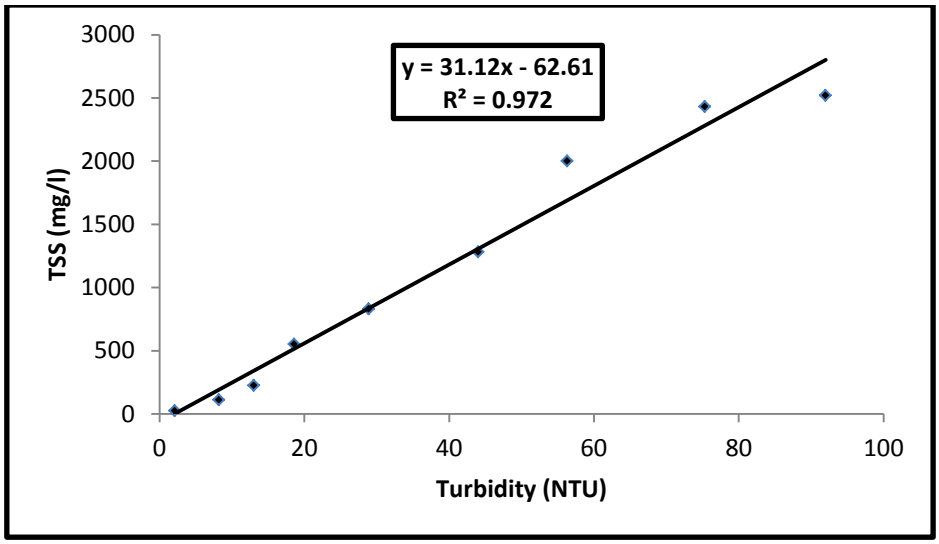

Figure 5. Turbidity-TSS relationship at Al-Ahdab oilfields produced water.

Entransy dissipation of Shell and Double Concentric Tube Heat Exchanger Calculations and Analysis

Asst. Prof. Dr. Basma Abbas Abdulmajeed
University of Baghdad – College of Engineering
Department of Chemical Engineering
Email: basma1957@yahoo.com

ABSTRACT

Shell-and-double concentric tube heat exchanger is one of the new designs that enhance the heat transfer process. Entransy dissipation is a recent development that incorporates thermodynamics in the design and optimization of heat exchangers. In this paper the concept of entransy dissipation is related to the shell-and-double concentric tube heat exchanger for the first time, where the experiments were studied at hot oil temperature of 80, 100 and 120°C, the flow rate of cold water was 0.667, 1, and 1.334 kg/m^3 respectively and the temperature of inlet cold water was 20°C. The entransy dissipation rate due to heat transfer and to fluid friction or pressure drop was studied.

Key Words: entransy, dissipation rate, heat exchanger, heat transfer enhancement, concentric tubes.

حسابات وتحليل منظومة المبادل الحراري ذو القشرة والانابيب المتداخلة المتمركزة باستخدام تبديد الانترانسي

أ.م.د. بسمة عباس عبد المجيد
قسم الهندسة الكيمياوية – كلية الهندسة - جامعة بغداد

الخلاصة

ان المبادل الحراري ذو القشرة والانابيب المتمركزة المتداخلة هو احد التصاميم الجديدة لتفعيل عملية انتقال الحرارة.ان عملية تبديد الانترانسي والتي توظف الثرموداينمك في عملية تصميم المبادلات الحرارية المثلى هو تطبيق حديث. في هذا البحث سوف يتم تطبيق مبادئ الانترانسي على المبادل الحراري الحراري ذو القشرة والانابيب المتمركزة المتداخلة ولاول مرة, حيث تمت دراسة التجارب عند درجة حرارة الزيت الساخن مساوية لـ 80, 100 و120°م و معدل جريان الماء البارد كان 0,667 و1 و1,334 كغم/م^3 و درجة حرارة الماء البارد الداخل مساوية لـ 20°م. تمت دراسة معدل تبديد الانترانسي نتيجة انتقال الحرارة والاحتكاك او انخفاض الضغط.

الكلمات الرئيسية: الانترانسي, معدل التبديد, مبادل حراري, تعزيز انتقال الحرارة, الانابيب المتمركزة

1. INTRODUCTION

A shell and double concentric tubes heat exchanger is a new invention in heat transfer devices that is used for transfer of internal thermal energy between three fluids at different temperatures (two hot flows and a cold flow H-C-H or opposite C-H-C). They are used in different industrial applications, where enhancement of heat transfer is needed in addition to increasing compactness. Accordingly, both weight and cost of the exchanger will be decreased to a good extent, **,Fadhil Abid A., 2013.**

The new heat exchangers differ in the use of double concentric tubes instead of the ordinary tubes used. The shell outside is the envelope of the double concentric tubes.

Principally, the second tube (inner tube) improves heat transfer through an additional flow passage and a larger heat transfer area per the same length of heat exchanger. In this new heat exchanger the application of two different streams leads to new heat transfer area which is equal to the heat transfer area of shell-and tube heat exchanger plus of inner tubes heat exchange area

First fluid (the same temperature level or the same nature as the third fluid) enters and is distributed between the shell and inner tubes. Whereas second fluid penetrates into annulus shape formed with the inner tubes and the second tube sheet.

Heat transfer enhancement is considered to have great role in the studies of the scientists since it affects the energy consumption all over the world. Studies led to different developments like heat transfer optimization and entransy dissipation for describing the heat transfer ability and irreversibility of heat conduction, respectively **,Zeng-Yuan et al., 2007.** and **,Mingtian, 2011.**

,Guo et al., 2007. defined a new physical quantity called entransy. They also defined heat transfer potential capacity and heat transfer potential capacity dissipation function **,Guo et al., 2003. and ,Chen, 2012.** By analogy between heat conduction process and electrical conduction process, a new term called entransy which can describe total heat transfer ability was introduced by **,Zeng-Yuan et al., 2007.**

,Guo et al., 2008. introduced an entransy dissipation number. They non-dimensionalized the entransy dissipation of heat exchanger. This can be used as thermodynamic figure to assess heat exchanger performance.

,Guo et al., 2010. defined an equivalent thermal resistance of a heat exchanger based on the entransy dissipation rate. They developed relationships between heat exchanger effectiveness and the thermal resistance which can be used to compare the irreversibility of a heat exchanger and its effectiveness.

,Xiaodong et al., in 2011. defined in their work the heat exchanger thermal resistance basing their work on entransy dissipation rate. They based the results on that the minimum entransy dissipation resistance corresponds to the highest heat transfer rate.

,Li Xuefang et al., in 2011. studied the optimization of a water-water counter current heat exchanger based on the entransy dissipation rate. They showed that increasing heat transfer area will reduce the irreversible dissipation in the studied heat exchanger.

,Mingtian, 2011. showed that entransy is a state variable which may be employed to describe the second law of thermodynamics.

,Mingtian, 2011. wrote a chapter studying the entransy dissipation theory and its application in heat transfer; convection and heat exchangers.

,Liu et al., in 2011. showed in a study that the considering the principle of entransy decrease in processes of heat transfer, that entransy would never increase when heat is transferred from higher to lower temperature in both equilibrium or non-equilibrium states.

,Xuetao, and ,Xingang in 2012. showed that for any thermodynamic process, it is found that some of net entransy flow from the heat sources is dissipated during process of heating or cooling of the working fluid and the other part is lost in doing work process.

,Jiangfeng and ,Mingtian, 2012. studied the optimization of heat exchanger using entransy dissipation theory and genetic algorithm.

,Chen, in 2012. summarized in his study entransy theory and its applications on heat conduction, heat convection, heat radiation, and heat exchanger design etc.

,Xuetao et al., in 2012. developed expressions of entransy dissipation, entransy dissipation based thermal resistance and entropy generation using the assumptions of incompressible fluids, ignored the influence of viscous dissipation on entransy and they assumed that there is no heat exchange between environment and the considered heat exchanger.

,Xuetao and ,Xingang, 2013. discussed the entransy expressions on thermodynamic laws. For the first law they showed that any thermodynamic system is in balance. The entransy expression for the second law of thermodynamics showed that entransy flow will not be transported from low temperature level to a higher one. Considering the third law of thermodynamics, the entransy expression showed that it is impossible to reach zero entransy for anybody.

,Xuetao and Xingang, 2013. used concepts of entropy generation and heat entransy loss to analyze the conversion of heat-work and heat transfer processes.

,Jia et al., 2014. studied the convective heat transfer optimization based on minimum entransy dissipation. Heat transfer is enhanced at relatively small flow resistance. This indicates that the investigated optimization method is useful in design of heat transfer enhancement.

,Puranik and ,Maheshwari, 2014. introduced a new heat exchanger design based on minimized entransy dissipation number which yields higher performance great savings in terms of energy and protection of environment.

,Kim and Kim, 2015. showed that the minimum entropy generation or the entransy dissipation does not represent the optimum performance for a counter-flow heat exchanger while the minimum entransy dissipation-based thermal resistance corresponds to the maximum heat transfer rate. It is found that the behavior of entropy generation is very similar to that of entransy dissipation.

The aim of the present research is the application, calculation and analysis of the concept of entransy dissipation rate to shell and double concentric tube heat exchanger at certain conditions.

2. THEORETICAL BACKGROUND

Entransy can be related to enthalpy by the following equations, **,Mingtian, 2011.**

$$dE = TdH \quad (1)$$

$$dH = \dot{m}\, cp\, dT \quad (2)$$

The shell and double concentric tube heat exchanger is assumed to work under adiabatic condition.

Entransy dissipation rate as a result of heat conduction in the considered heat exchanger can be written for the shell side as:

$$\dot{E}_1 = \int_{outside}^{inside} (\dot{m}\, T\, dH)_1 = \int_{outside}^{inside} (\dot{m}\, cp\, T\, dT)_1 = \frac{1}{2} (\dot{m}\, cp)_1 \left(T_{1,inside}^2 - T_{1,outside}^2\right) \quad (3)$$

while for the outer tube it can be written as:

$$\dot{E}_2 = \int_{outside}^{inside} (\dot{m}\, T\, dH)_2 = \int_{outside}^{inside} (\dot{m}\, cp\, T\, dT)_2 = \frac{1}{2} (\dot{m}\, cp)_2 \left(T_{2,inside}^2 - T_{2,outside}^2\right) \quad (4)$$

and finally for the inner tube side:

$$\dot{E}_3 = \int_{outside}^{inside}(\dot{m}\,T\,dH)_3 = \int_{outside}^{inside}(\dot{m}\,cp\,T\,dT)_3 = \frac{1}{2}(\dot{m}\,cp)_3\left(T_{3,inside}^2 - T_{3,outside}^2\right) \quad (5)$$

And the equation for the total entransy as a result of heat transfer is:

$$\dot{E}_T = \dot{E}_1 + \dot{E}_2 + \dot{E}_3 = \frac{1}{2}\left[(\dot{m}\,cp)_1\left(T_{1,inside}^2 - T_{1,outside}^2\right) + \right.$$

$$\left.\frac{1}{2}(\dot{m}\,cp)_3\left(T_{3,inside}^2 - T_{3,outside}^2\right)\right] \quad (6)$$

Since the hot oil is divided into two parts, one part flows in the shell side and the other part flows into the inner tubes, and since the temperature readings represent the inlet one of the hot oil while the outlet one represents the hot oil reading after mixing the two streams of hot oil, then the first two terms can be added together and equation (6) can be written as:

$$\dot{E}_T = (m\,cp)_1\left(T_{1,inside}^2 - T_{1,outside}^2\right) + \frac{1}{2}(\dot{m}\,cp)_3\left(T_{3,inside}^2 - T_{3,outside}^2\right) \quad (7)$$

Flow friction in heat exchanger causes also entransy dissipation rate. Assuming a finite pressure drop between inlet and outlet sides, and the flow is adiabatic and stationary. Then:

$$dE_p = -T\,dp/\rho \quad (8)$$

And the entropy dissipation rate due to friction is given by:

$$\dot{E}_p = \int_{inside}^{outside}\dot{m}\frac{T}{\rho}dp \quad (9)$$

Replacing the temperature with the logarithmic mean temperature difference, assuming incompressible fluid:

$$\dot{E}_p = \frac{\dot{m}\ \Delta\mathrm{p}\ \Delta T_{lm}}{\rho} \quad (10)$$

where: $\Delta p = p_{inside} - p_{outside}$

Considering the shell and double concentric heat exchanger studied, the entransy dissipation rate due to friction is given by the following equation:

$$\dot{E}_p = \left(\frac{\dot{m}\ \Delta\mathrm{p}}{\rho}\right)_1 \frac{T_{1,outside} - T_{1,inside}}{lnT_{1,outside} - lnT_{1,inside}}$$

$$+\left(\frac{\dot{m}\ \Delta\mathrm{p}}{\rho}\right)_2 \frac{T_{2,outside} - T_{2,inside}}{lnT_{2,outside} - lnT_{2,inside}} + \left(\frac{\dot{m}\ \Delta\mathrm{p}}{\rho}\right)_3 \frac{T_{3,outside} - T_{3,inside}}{lnT_{3,outside} - lnT_{3,inside}} \quad (11)$$

As mentioned above, the first two terms of equation (11) can be added to give the following equation:

$$\dot{E}_p = 2\left[\left(\frac{\dot{m}\ \Delta p}{\rho}\right)_1 \frac{T_{1,outside} - T_{1,inside}}{lnT_{1,outside} - lnT_{1,inside}}\right] + \left(\frac{\dot{m}\ \Delta p}{\rho}\right)_3 \frac{T_{3,outside} - T_{3,inside}}{lnT_{3,outside} - lnT_{3,inside}} \quad (12)$$

The total entransy dissipation rate due to both heat transfer and fluid friction can be written as:

$$\dot{E}_{total} = \dot{E}_T + \dot{E}_p \quad (13)$$

The entransy dissipation number can be introduced as the heat exchanger performance criteria, where:

$$\dot{E}_T^* = \frac{\dot{E}_T}{\dot{Q}(T_{1inside} - T_{3\ inside})} \quad (14)$$

where, $T_{1\ inside}$ and $T_{3\ inside}$ represent the maximum hot inlet temperature and the minimum cold inlet temperature, respectively.

According to **Li Xuefang et al in 2011**, eq. (14) can be written in another form as:

$$\dot{E}_T^* = \frac{\dot{E}_T}{\varepsilon(m\ cp)_1(T_{1\ inside} - T_{3\ inside})} \quad (15)$$

where, $\varepsilon = \frac{actual\ heat\ transfer\ rate}{maximum\ possible\ heat\ transfer\ rate}$

3. EXPERIMENTAL WORK

The laboratory unit of the shell and double concentric tube heat exchanger was built in the laboratories of Chemical Engineering Department, College of Engineering, University of Baghdad. It included: the heat exchanger, tanks with their heating coils to heat the oil, water tank, measuring instruments and control panel of temperature, flow rate and pressure drop. The heat exchanger was designed to perform counter currently, where the hot oil passed through the concentric tubes and the shell, while the cold water passed through the new construction or the annulus formed between the concentric tubes. The heat exchanger unit was built in the laboratories of Chemical Engineering Department, College of Engineering, University of Baghdad.

The new heat exchanger design was conducted according to Kern method. The volumetric flow rates were 4 m^3/hr and 8.35 m^3/hr for the hot oil and water respectively. The hot oil inlet temperature to the heat exchanger was 80ºC to 120ºC, while for water the inlet and outlet temperatures was 20ºC.

The experimental parameters studied were: temperature, flow rate of hot oil, and pressure drop. The temperatures studied were: 80ºC to 120ºC with an increase of 20ºC for each stage. For each temperature, the volumetric flow rate of hot oil was changed from 0.822 kg/m^3 to 0.274 kg/m^3. For cold water, the change in volumetric flow rate of water was 40l/min to 80l/min with an increase of 20l/min for each stage.

The test section was a shell- and - double concentric tube heat exchanger with dimensions of 1.3 m in length and 1.08 m effective tube length.

The shell and double concentric tube heat exchanger was designed for counter flow configuration. The heat exchanger constituted of: a bundle of 16 carbon steel tubes of 20 mm inside diameter and 25 mm outside diameter was used; the tubes are distributed as a triangular 30° tube pattern. The clearance between two adjacent tubes is 6.25 mm, with the tubes pitch of 31.25 mm. A second bundle of 16 carbon steel tubes of 6 mm inside diameter and 10 mm outside diameter, were added concentrically in each of the mentioned tubes. Plate of carbon steel with 8 mm thickness was used to construct the shell. The shell inner diameter is 203 mm, and the shell outer diameter is 220 mm. Baffles of thickness 6 mm were spaced by a distance of 100 mm. The free section left was of 25%. Two fluids were used to complete the cycle of the heat exchanges. The first one which passed through the shell side and the inner tubes side is forty stock oil (lube oil) from Dorra Refinery, while the other counter current stream is water. Figure (1) shows the concentric tubes arrangement of the heat exchanger studied.

The parameters to be measured during the test were:

1. The inlet and outlet temperatures of the tube side (inner and annulus) and shell side.
2. The inlet and outlet pressures of the tube (inner and annulus) side and shell side.
3. The flow rates of the tube side and the shell side.

The cold and hot oil are switched at the same time and the required flow rate was set.

After reaching the steady state conditions, the flow rate of cold water in the annulus is fixed, and the hot oil temperature is set by a thermostat. The range of hot oil temperature studied is 120-80°C with a step change of 20°C. The flow rate of hot oil is regulated. The temperatures of water are recorded with the variation in flow rate. The inlet and outlet pressures are also measured. The procedure was repeated with the change in flow rate of cold water.

4. RESULTS AND DISCUSSION

Table (1.a) to **table (3.c)** give the results of equation (7) for different inlet oil temperature, constant flow rate of cold water and inlet temperature of cold water.

Plotting the entransy dissipation rate of **table (1.a)** to **table (3.c)** against the outlet temperature of the hot stream, an increase in the entransy dissipation rate is pronounced with the temperature as shown in **Fig. 2** to **Fig. 10**.

Fig. 2 to **Fig. 10** shows that there is almost a unique trend, where an increase at the beginning, a maximum value and finally a decrease is noticed. This is in accordance with an increase in the heat transfer process with the flow of the hot oil in both the inner tubes and the shell counter-currently with the cold water in the annulus. It must be known that the entransy is dissipated due to the irreversibility of the heat transfer process. Also, it should be noted that increasing or improving the heat transfer performance of a heat exchanger normally corresponds to an increase in its heat transfer area and to a reduction in its cost due to the decrease in its mass or compactness. The newly used heat exchanger provides all the above mentioned parameters. From figures 2 to 10 it can be deduced that the higher the entransy dissipation rate the smaller is the reversibility in the heat exchanger. This was in agreement with **,Jiangfeng, and Mingtian, 2012.**

The hot oil flow rate was plotted vs. entransy dissipation rate in Fig.11. The dissipation rate shows the same trend, where a maximum is noticed for a certain value of flow rate. According to **,Li Xuefang et al., in 2011.** the reduction in the irreversible entransy dissipation rate is gained by increasing the heat transfer area with the minimum possible flow rate.

Using Eq.(12), the entransy dissipation rate due to friction effect or pressure drop across the heat exchanger is shown in Fig.12. It is shown that a small difference is found for all the experiments.

Comparing the values of entransy dissipation rate due to heat transfer with that due to pressure drop shows that the last can be neglected. This proves that heat transfer plays the great role in calculation of entransy dissipation rate. These findings were in agreement with **,Jiangfeng and ,Mingtian, 2012.** viewpoint. Thus it is important to optimize the heat exchanger design according to the heat transfer process.

It is must be noticed that to get the most optimum thermodynamically performance of a process, it is very important to minimize the entransy dissipation rate. Thus working in the range before maximum values in figures 2 to 11 will give such phenomena.

Entransy dissipation number can be calculated from Eq.(14). The results are represented in Fig. 13. The figure showed that entransy dissipation number values ranged from 3 to more than 9. The figure also showed that the values of entransy dissipation number decreased with the increase in heat transfer rate for the cases studied (80°C hot oil inlet temperature, 20°C cold water inlet temperature and three values of cold water flow rate; 0.667, 1 and 1.334 kg/s). According to **,Guo JiangFeng et al., 2009.** the decrease in the entransy dissipation number leads to an increase in the effectiveness of the heat exchanger. Or, it can be said that increasing the entransy dissipation number will increase the effectiveness of the heat exchanger. Considering the thermodynamics point of view of this process, entransy dissipation number can be used to assess the performance and effectiveness of such heat transfer process.

5. CONCLUSIONS

A study was made to analyze the idea of entransy dissipation rate on a shell and double concentric tubes heat exchanger. The study included both entransy dissipation rate due to heat transfer and that due to friction or pressure drop. It was found that the first played the greatest role in the calculations in comparison to that of friction or pressure drop.

The study also showed that there was a decrease in the value of entransy dissipation number with the increase in heat transfer rate, which emphasize the increase in the effectiveness of heat exchanger.

6. REFERENCES

- Fadhil A. Allawi, 2013, *Shell and Double Concentric Tubes Heat Exchanger calculations and Analysis*, An M. Sc. Thesis submitted to the College of Eng., University of Baghdad.

- Chen LinGen, 2012, *Progress in Entransy Theory and its Application*, Chinese science Bulletin, Dec. 2012, vol. 57, No. 34: 4404-4426.

- Guo Z,Y, Cheng X T, Xia Z, Z, *Least Dissipation Principle of Heat Transport Potential Capacity and its Application in Heat Conduction Optimization*, Chinese science Bulletin, vol. 57, 406-410.

- Guo JiangFeng, Cheng Lin and Xu MingTian, 2009, *Entarnsy Dissipation Number and its Application to Heat Exchanger Performance Evaluation*, Chinese science Bulletin, 54: 2708-2713

- Guo JiangFeng and Xu MingTian, 2012, *The Application of Entransy on Theory in Optimization Design of Heat Exchanger*, Applied Thermal Engineering, 36: 227-235.

- Guo Z Y, Zhu Y, Liang X G., 2007, *Entransy – A Physical Quantity Describing Heat Transfer Ability*, Int. J. Heat Mass Transfer, 50: 2545-2556.

- Guo Z Y, Liu X B., Tao W.Q., Shah R K., 2010,*Effectiveness – Thermal Resistance Method for Heat Exchanger Design and Analysis*, Int. J. Heat Mass Transfer, 53: 2877-2884.

- Kim, K.H. and Kim, S. W., 2015, *Entransy Dissipation Analysis for Optimal Design of Heat Exchangers*, J. of Automation and Control Engineering Vol. 3, No. 2, 87-91.

- Liu W., Liu Z C, Jia H., Fan A W., Nakayama A., 2011, *Entransy Expression of the Second Law of Thermodynamics and its Application to Optimization in Heat Transfer Process*, Int. J. of Heat Mass Transfer, 54:3049-3059

- Mingtian Xu, 2011, *The Thermodynamic Basis of Entransy and Entransy Dissipation*, Energy, 36: 4272-4277.

- Mingtian Xu, 2011, *Developments in Heat Transfer*, A book by Marco A., InTech, Chapter 14, 247-272.

- Sushant Puranik1, Govind Maheshwari, 2014, *Application of Entransy Dissipation Number as Performance Parameter for Heat Exchanger*, International Journal of Engineering Trends and Technology (IJETT) – Volume 12 Number 6, 282-285.

- Xiaodong, Q. and Zhixin L., 2011, *Analysis of Entransy Dissipation in Heat Exchangers*, Int. J. of Thermal Sciences, 50: 608-614.

- XueFang, L, Guo, J., Mingtian X., and Cheng L., 2011, *Entransy Dissipation Minimization for Optimization of Heat Exchanger Design*, Chinese Science Bulletin, vol. 56, no. 20: 2174-2178.

- Xuetao C., Qinzhao Z., and Xingang, L., 2012, *Analyses of Entransy Dissipation, Entropy Generation and Entransy-Dissipation-based Thermal Resistance on Heat Exchanger Optimization*, Applied Thermal Engineering, 38: 31-39.

- Xuetao C., and Xingang, L., 2012, *Entransy Loss in Thermodynamic Processes and its Application*, Energym 44: 964-972.

- Xuetao C., and Xingang, L., 2013, *Discussion on the Entransy Expressions of the Thermodynamic Laws and their Applications*, Energy, 56: 46-51.

- Xuetao C., and Xingang, L., 2013, *Analyses of Entropy Generation and Heat Transfer Loss in Heat Transfer and Heat-Work Conversion*, Int. J. of Heat Mass Transfer, 64: 903-909.

- Zeng-Yuan G, Hong-Ye Z. and Xin-Gang L., 2007, *Entransy-a Physical Quantity Describing Heat Transfer Ability*, Int. J. of Heat Mass Transfer, 50: 2545-2556.

NOMENCLATURE

Cp = specific heat, J/Kkg
E = Entransy
$\dot{E}_P$ = Entransy Dissipation Rate due to friction or pressure drop, WK
$\dot{E}_T$ = Entransy Dissipation Rate due to heat transfer, WK
$\dot{E}_{total}$ = Total entransy dissipation, WK
$\dot{E}_T^*$ = Entransy dissipation number
$\dot{m}$ = Mass flow rate, kg/s
$\dot{Q}$ = Heat transfer rate, J/s
T = Temperature, K
$T_{1inside}$ = Hot oil inlet temperature, K
$T_{1,outside}$ = Hot oil outlet temperature, K
$T_{3inside}$ = Cold water inlet temperature, K
$T_{3inside}$ = Cold water outlet temperature, K
Δp = Pressure drop, Pa
ρ = Density, Kg/m^3
ε = Heat exchanger effectiveness

Table (1.a) Entransy dissipation rate for hot oil inlet temperature of 80˚C, 0.667 kg/m^3 flow rate of cold water and 20˚C inlet temperature of cold water.

m_1, kg/m^3	$T_{3outside}$, K	$T_{1outside}$, K	Entransy dissipation rate*10^{-6}
0.822	300	322	25.33
0.685	299.5	321	26.17
0.548	299	317	23.27
0.411	298	314	18.71
0.274	297	309	13.75

Table (1.b) Entransy dissipation rate for hot oil inlet temperature of 100˚C, 0.667 kg/m^3 flow rate of cold water and 20˚C inlet temperature of cold water.

m_1, kg/m^3	$T_{3outside}$, K	$T_{1outside}$, K	Entransy dissipation rate*10^{-6}
0.822	302	331.5	20.52
0.685	301	329	21.02
0.548	300	328	18.01
0.411	299	325	14.24
0.274	298	320	11.19

Table (1.c) Entransy dissipation rate for hot oil inlet temperature of 120˚C, 0.667 kg/m^3 flow rate of cold water and 20˚C inlet temperature of cold water.

m_1, kg/m^3	$T_{3outside}$, K	$T_{1outside}$, K	Entransy dissipation rate*10^{-6}
0.822	305	335	11.73
0.685	303	332	12.73
0.548	302	329.5	11.3
0.411	301	328	8.315
0.274	300.5	324	5.28

Table (2.a) Entransy dissipation rate for hot oil inlet temperature of 80˚C, 1 kg/s flow rate of cold water and 20˚C inlet temperature of cold water.

m_1, kg/m^3	$T_{3outside}$, K	$T_{1outside}$, K	Entransy dissipation rate*10^{-6}
0.822	301.5	330	26.8
0.685	300	326	27.55
0.548	299	324	25.5
0.411	298	322	19.61
0.274	297	316	14.69

Table (2.b) Entransy dissipation rate for hot oil inlet temperature of 100˚C, 1 kg/s flow rate of cold water and 20˚C inlet temperature of cold water.

m_1, kg/m^3	$T_{3outside}$, K	$T_{1outside}$, K	Entransy dissipation rate*10^{-6}
0.822	299.5	321	17.01
0.685	298.5	318	18.14
0.548	297	314	15.55
0.411	296.5	312	12.18
0.274	295.5	307	9.55

Table (2.c) Entransy dissipation rate for hot oil inlet temperature of 120˚C, 1 kg/s flow rate of cold water and 20˚C inlet temperature of cold water.

m_1, kg/m^3	$T_{3outside}$, K	$T_{1outside}$, K	Entransy dissipation rate*10^{-6}
0.822	304	333	10.25
0.685	302	330	11.78
0.548	300.5	326	12.15
0.411	299.5	323	9.74
0.274	298	318	7.56

Table (3.a) Entransy dissipation rate for hot oil inlet temperature of 80˚C, 1.334 kg/s flow rate of cold water and 20˚C inlet temperature of cold water.

m_1, kg/m^3	$T_{3outside}$, K	$T_{1outside}$, K	Entransy dissipation rate*10^{-6}
0.822	299	320	28.07
0.685	297.5	316	28.79

0.548	297	314	23.85
0.411	296	311	19.54
0.274	295	306	14.84

Table (3.b) Entransy dissipation rate for hot oil inlet temperature of 100˚C, 1.334 kg/s flow rate of cold water and 20˚C inlet temperature of cold water.

M_1, kg/m^3	$T_{3outside}$, K	$T_{1outside}$, K	Entransy dissipation rate*10^{-6}
0.822	301	329	16.07
0.685	299.5	326	17.6
0.548	298.5	323	14.66
0.411	297	319	13.47
0.274	296	315	9.92

Table (3.c) Entransy dissipation rate for hot oil inlet temperature of 120˚C, 1.334 kg/s flow rate of cold water and 20˚C inlet temperature of cold water.

m_1, kg/m^3	$T_{3outside}$, K	$T_{1outside}$, K	Entransy dissipation rate*10^{-6}
0.822	302	332	10.32
0.685	301	329	10.69
0.548	300	325	10.63
0.411	299	322	8.46
0.274	297	317	7.53

Figure 1 The concentric tubes arrangement.

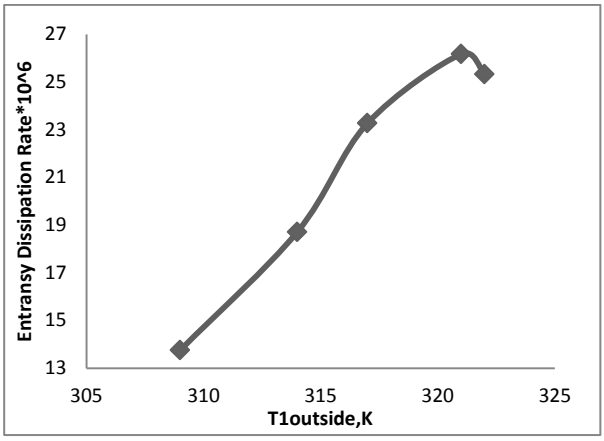

Figure 2. Entransy dissipation rate vs. $T_{1outside}$ for 0.667 kg/s flow rate and 20˚C inlet temperature of cold water.

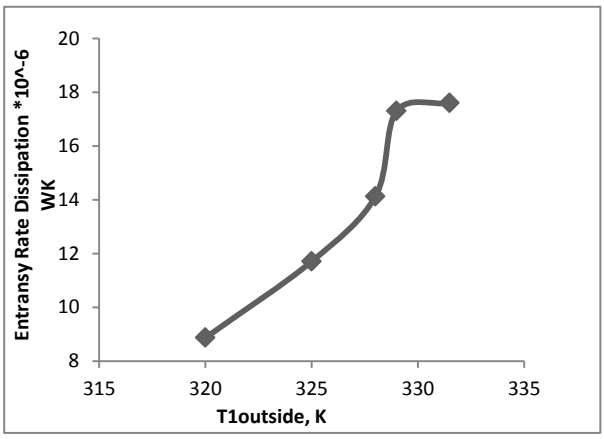

Figure 3. Entransy dissipation rate vs. $T_{1outside}$ for 0.667 kg/s flow rate and 20˚C inlet temperature of cold water.

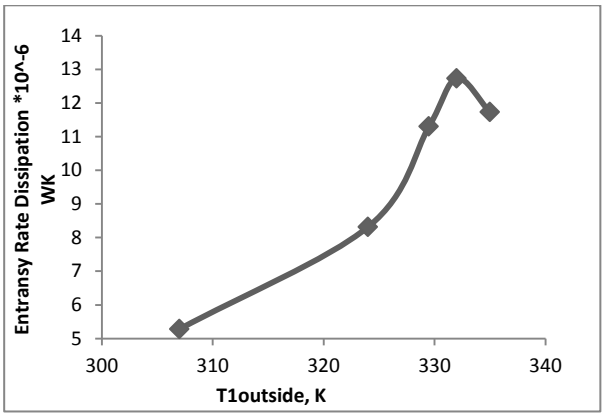

Figure 4. Entransy dissipation rate vs**.** $T_{1outside}$ for 0.667 kg/s flow rate and 20˚C inlet temperature of cold water.

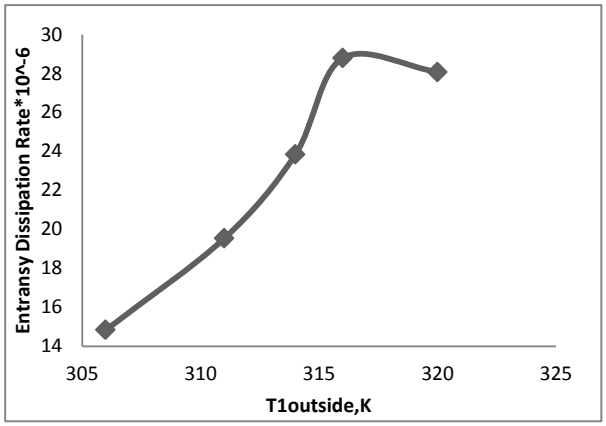

Figure 5. Entransy dissipation rate vs. $T_{1outside}$ for 1 kg/s flow rate and 20˚C inlet temperature of cold water.

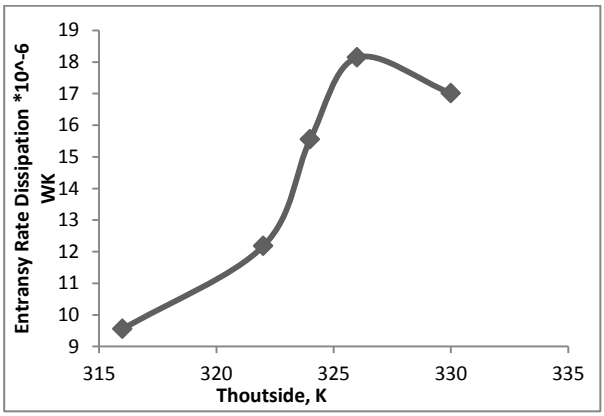

Figure 6. Entransy dissipation rate vs. $T_{1outside}$ for 1 kg/s flow rate and 20˚C inlet temperature of cold water.

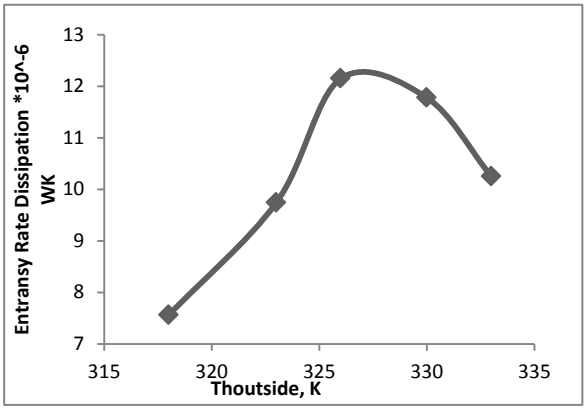

Figure 7. Entransy dissipation rate vs. $T_{1outside}$ for 1 kg/s flow rate and 20˚C inlet temperature of cold water.

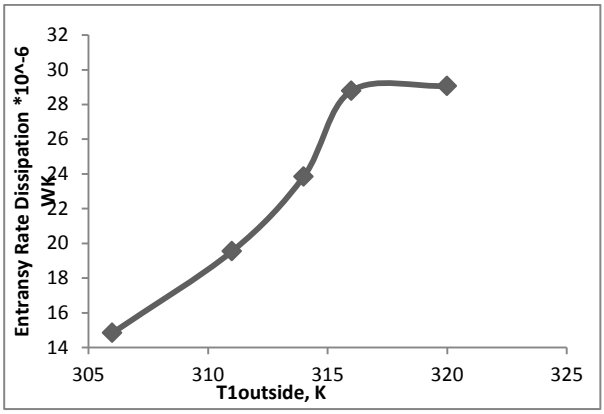

Figure 8. Entransy dissipation rate vs. $T_{1outside}$ for 1.334 kg/s flow rate and 20˚C inlet temperature of cold water.

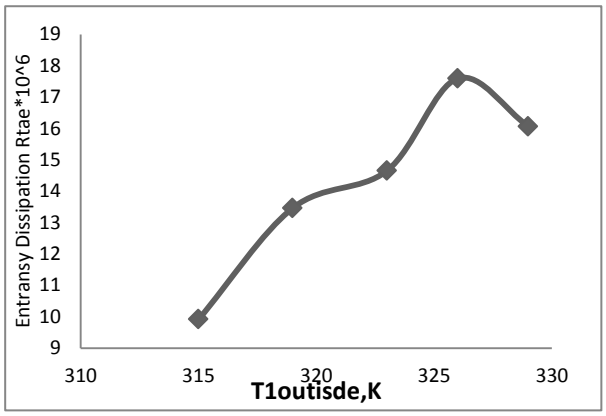

Figure 9. Entransy dissipation rate vs. $T_{1outside}$ for 1.334 kg/s flow rate and 20˚C inlet temperature of cold water.

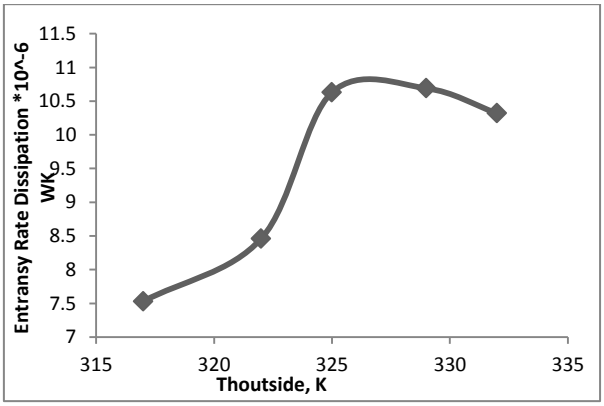

Figure 10. Entransy dissipation rate vs. $T_{1outside}$ for 1.334 kg/s flow rate and 20˚C inlet temperature of cold water.

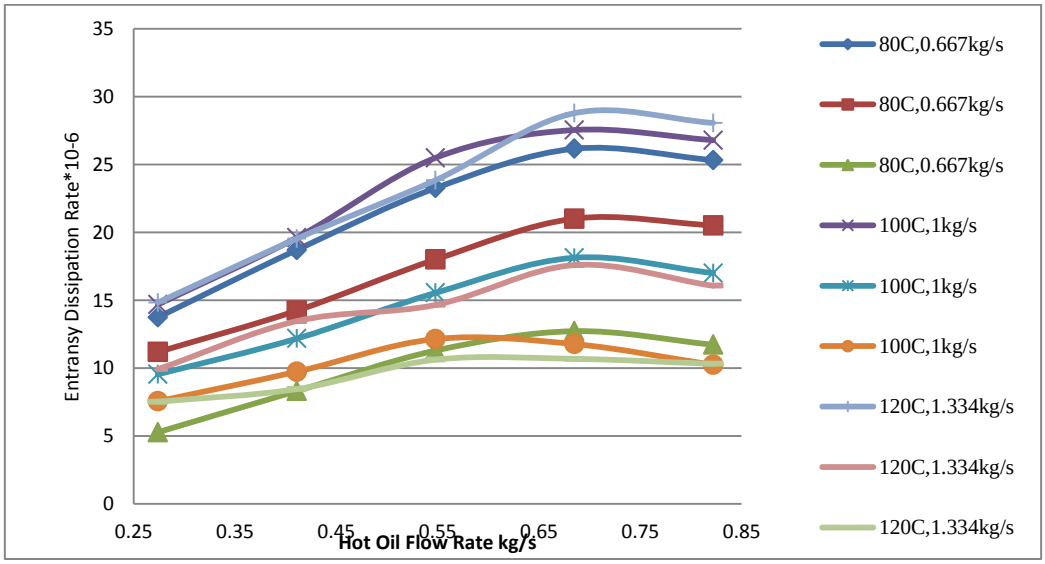

Figure 11. Entransy Dissipation Rate vs. Hot Oil Flow Rate.

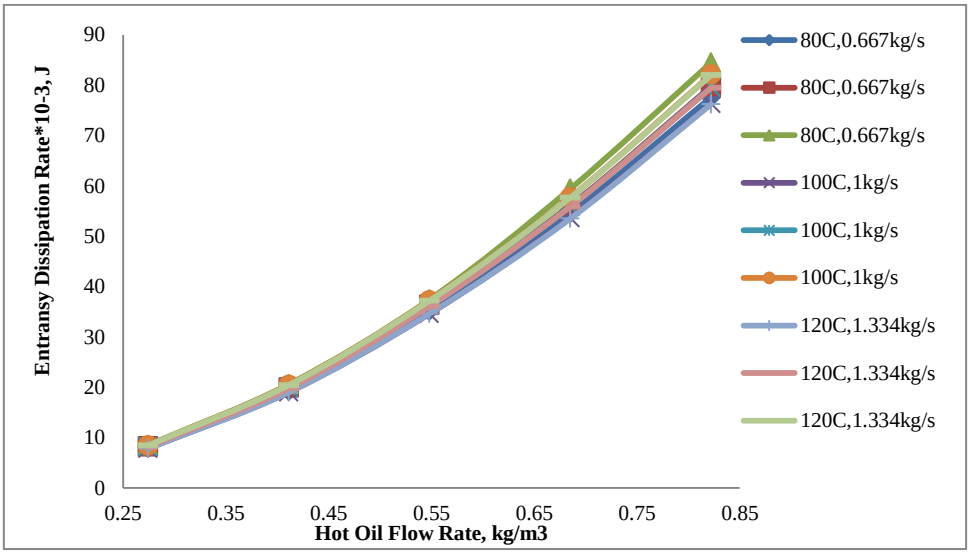

Figure 12. Entransy Dissipation Rate of friction factor vs. Hot Oil Flow Rate.

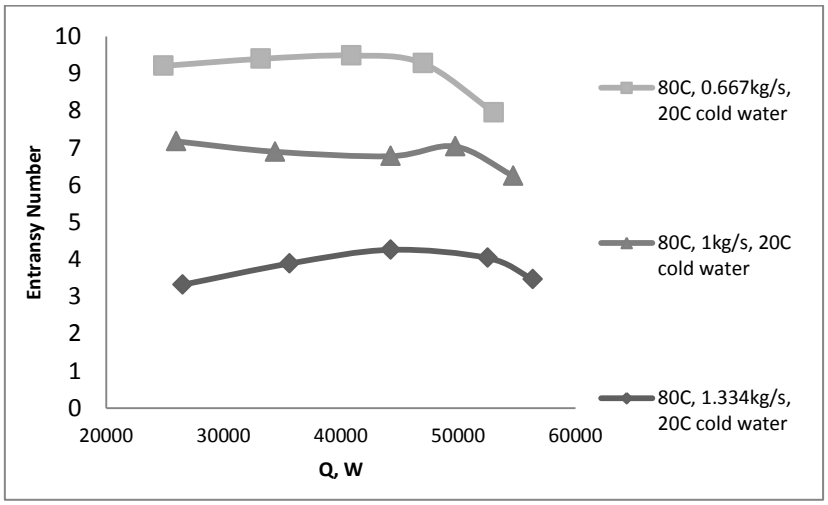

Figure 13. Entransy Dissipation number vs. Heat transfer rate.

Construction of Graduation Certificate Issuing System Based on Digital Signature Technique

Assist. Prof. Dr. Mohammed Issam Younis
Department of Computer Engineering
College of Engineering / University of Baghdad
younismi@coeng.uobaghdad.edu.iq

Assist. Lect. Hayder Faez Abdulkareem
Department of Computer Engineering
College of Engineering / University of Baghdad
haiderfaiz@ yahoo.com

Assist. Prof. Hamid Mohammed Ali
Department of Computer Engineering
College of Engineering / University of Baghdad
habdul_hussain@yahoo.com

ABSTRACT

With the development of computer architecture and its technologies in recent years, applications like e-commerce, e-government, e-governance and e-finance are widely used, and they act as active research areas. In addition, in order to increase the quality and quantity of the ordinary everyday transactions, it is desired to migrate from the paper-based environment to a digital-based computerized environment. Such migration increases efficiency, saves time, eliminates paperwork, increases safety and reduces the cost in an organization. Digital signatures are playing an essential role in many electronic and automatic based systems and facilitate this migration. The digital signatures are used to provide many services and solutions that would not have been possible by the conventional hand-written signature.

In the educational environment, the process of issuing the graduation certificates can no longer be restricted to the traditional methods. Hence, a computerized system for issuing certificates of graduation in an electronic form is needed and desired. This paper proposes a Graduation Certificates Issuing System (GCIS) based on digital signature technology. In doing so, this research highlights the state-of-the-art and the art-of-the-practice for some existing digital signature-based systems in the literatures. In addition, eight intertwined elected services are identified, namely: message authentication, entity authentication, integrity, non-repudiation, time stamping, distinguished signing authorities, delegating signing capability and supporting workflow systems. Moreover, this research examines nine existing systems, showing their merits and demerits in terms of these elected services. Furthermore, the research describes the architectural design using the Unified Modeling Language (UML) and provides the concrete implementation of the proposed GCIS. The GCIS is implemented using Visual Basic.Net programming language and SQL Server database management system.

Keywords: digital signature, graduation certificates issuing system, unified modeling language.

بناء نظام لإصدار وثيقة التخرج بالاعتماد على تقانة التوقيع الرقمي

أ.م.د. محمد عصام يونس
قسم هندسة الحاسبات
كلية الهندسة / جامعة بغداد

م.م. حيدر فائز عبد الكريم
قسم هندسة الحاسبات
كلية الهندسة / جامعة بغداد

أ. م. حامد محمد علي
قسم هندسة الحاسبات
كلية الهندسة / جامعة بغداد

الخلاصة

مع التطور العلمي الهائل لمعمارية الحاسوب وتقاناتها في السنوات الأخيرة، أصبحت التطبيقات مثل التجارة الإلكترونية، الحكومة الإلكترونية، الحوكمة الإلكترونية، والتمويل الإلكتروني منطقة للبحث العلمي النشط على نطاق واسع. وبالنتيجة أصبح لزاما الهجرة من البيئة الورقية إلى البيئة المحوسبة المستندة إلى الرقمية من أجل زيادة جودة وكمية المعاملات اليومية المنجزة. هذه الهجرة تزيد من الكفاءة، وتوفر الوقت، وتلغي المعاملات الورقية، وترفع درجة الأمان، وتقلل من التكلفة في المؤسسة. ومما يجدر الاشارة اليه أن التوقيعات الرقمية تلعب دورا أساسيا في العديد من الأنظمة الإلكترونية وتسهل هذه الهجرة. تستخدم التوقيعات الرقمية كوسيلة لتوفير العديد من الخدمات والحلول والتي من غير الممكن تحقيقها بواسطة التوقيعات اليدوية التقليدية.

إن عملية إصدار وثائق (شهادات) التخرج لا يمكن أن تبقى مقتصرة على الطرق التقليدية في البيئة التعليمية. وبالتالي، أصبح لزاما توفير نظام محوسب لإصدار وثائق التخرج في شكل الكتروني. على هذا النحو، يقترح هذه البحث بناء نظام لإصدار وثائق التخرج (GCIS) بالاعتماد على تقانة التوقيع الرقمي. وبالقيام بذلك، يتبنى هذا البحث تسليط الضوء على حالة بعض الأنظمة المستندة على التوقيع الرقمي وواقعها العملي. فضلا عن ذلك، يحدد هذا البحث ثمانية خدمات منتخبة ومتشابكة، هي: مصادقة الرسالة، مصادقة الكيان, النزاهة, عدم التنصل، ختم الوقت، سلطة التوقيع الجزئية (التوقيع حسب الصلاحية او المسؤولية)، وتفويض القدرة على التوقيع (التخويل بالتوقيع)، ودعم نظم سير العمل. وعلاوة على ذلك ، يسلط هذا البحث الضوء على تسعة من النظم القائمة ، ويبين مزايا وعيوب كل منها بالاعتماد على الخدمات المنتخبة الآنفة الذكر. أخيرا، يصف البحث التصميم المعماري باستخدام لغة النمذجة الموحدة (UML) وتوفر التنفيذ الملموس للنظام المقترح. ومن الجدير بالذكر, إن النظام المقترح تم تنفيذه باستخدام لغة البرمجة (Visual Basic.NET) ونظام إدارة قواعد البيانات (SQL Server).

الكلمات الرئيسية : التوقيع الرقمي، نظام إصدار وثائق التخرج، لغة النمذجة الموحدة.

1. INTRODUCTION

Organizations have been trying to move from a paper-intensive environment to a paper-free environment. Word processors have replaced the writing pad and pen, spreadsheet applications have replaced manual spreadsheets, and e-mails have supplanted handwritten letters. Organizations are moving away from the traditional, time consuming paper processes and searching for new and innovative technology to improve efficiency **,Zupan, 2006.** As digital technologies continue to develop rapidly, this impact on many daily tasks which rely on technology. Many of the paper-based documents are being gradually replaced by their electronic versions, such as e-Tickets, e-mail, online (internet) banking and e-Portfolios. These technologies are powerful, flexible and bring huge advantages **,Chen-Wilson, et al., 2011.**

Nowadays various applications such as banking, sale-purchase and stock trading are increasing day by day and emphasizing on electronic transaction to minimize the operational cost and increasing the services. This need has led to the development of the new notion of electronic document that can be generated, processed and stored in computers and transmitted over the net. The information transmitted over these documents can be susceptible and thus need to be protected from intruders and malicious third parties. Traditionally, in paper document this kind of protection is provided by the written signature and thus it authenticates the document for the communicating parties. For electronic documents, this facility is provided by means of digital signature. Using the digital signature algorithms can provide authenticity and validation to the electronic document **,Shukla, et al., 2012.** With the development of computer engineering and technology, e-commerce, e-government and e-finance are widely used. Digital signatures are playing an important role in many electronic and automatic based applications **,Wang and He, 2010.** Therefore, the migration from the paper-based systems to the electronic or digital-based systems emphasizes the need for the digital signature **,Fazlagic, 2010.**

Digital signatures can significantly benefit organizations by eliminating the last of the paper in the business cycle. The ability to instantly sign and seal documents and transactions electronically results in much shorter process cycle times, accelerated customer service and drastic cost savings. Digital signatures provide enhanced convenience for both the customer and the organization, while significantly reducing application processing time **,Zupan, 2006.**

The remainder of this paper is organized as follows: Section 2 highlights literature review. In addition, this section presents the problem statements and the motivation of this research work. Section 3 presents the additional elected services that must be provided by the digital signature beside the basic services. Section 4 gives the art-of-the-practice of related works. Section 5 gives the architectural design of the proposed system. Section 6 discusses the implementation issues. Section 7 gives a comparison of the proposed system against the existing works. Section 8 gives the conclusion. Finally, Section 9 gives recommendations for future works.

2. LITERATURE REVIEW

Since the introduction of the concept of "digital signature" by Diffie and Hellman in their classic paper "New Directions in Cryptography" **,Diffie, and Hellman, 1976,** this subject has been widely studied and employed in different systems. This section briefly describes the major developments.

Josang and AlFayyadh, 2008, proposed a method for WYSIWYS (What You See Is What You Sign) that ensures the integrity of digital documents and their digital signatures. This method can only be directly applied to documents written with traditional American Standard Code for Information Interchange (ASCII) characters. The WYSIWYS property articulates that the bit representation of digital documents must be visualized consistently and as intended to the signer by the digital signature system. **,Zefferer and Knall, 2010.** introduced a circular Resolution Database System (RDS). The circular RDS is based on the Austrian citizen card concept and makes use of qualified electronic signatures that provide means for secure authentication of users as well as for electronic signing of digital documents. **,Kang and Han, 2010.** proposed a Threshold Proxy Signature Scheme (TPSS). The TPSS uses a warrant, which is agreed and signed by the original signer and all proxy signers together. In a proxy signature

scheme, the original signer is allowed to authorize a designated person as his/her proxy signer, and then the proxy signer is able to sign on behalf of the original signer. Fazlagic and ,**Fazlagic, 2010.** proposed a Delegating Digital Signing Capability Mechanism (DDSCM) during a workflow process taking into account the need for verification of digital signature and document integrity after a document is archived. **,Zhou, et al., 2010.** proposed a Threshold Signature Scheme (TSS) with distinguished signing authorities. The proposed scheme not only has the property of threshold signature generation, but also has the property of threshold signature verification. Furthermore, the proposed scheme is a group oriented signature scheme with distinguished signing authorities, in which the signers do not have to sign the whole documents but only a part of the document. **,Liu, et al., 2011,** proposed a Multi-Proxy Signature Scheme (MPSS) with proxy revocation. The MPSSs are very useful tools when an original signer needs to delegate his/her signing capability to a group of proxy signers. The proxy revocation means the revocation of delegated rights for the situation where proxy signer or signer's key is compromised and the delegated rights are abused. It may also happen that the original signer wants to terminate the delegated rights before the expiration of the delegation period. **Chen and Lin, 2011,** proposed an Electronic Medical Record (EMR) system with a re-signing scheme which is used to make a going-expired digital signature been resigned in time, in keeping with the premise of not conflicting with the laws, morals and privacy while maintaining the security of the EMR system. **,Feng, et al., 2011.** proposed a Multi-Policy Threshold Signature Scheme (MPTSS) with distinguished signing authorities. In this scheme two groups can sign and verify each other, so the scheme is two-way signing and verifying. Moreover, the threshold values of the two groups can change with the security classification of the signing document and every discretionary signatory only signs a small part of the document instead of the whole one. **,Zhang, et al., 2012.** proposed a provably secure Certificateless Proxy Signature Scheme (CLPSS). A proxy signature scheme allows a proxy signer to sign messages on behalf of an original signer within a given context. The Certificateless Public key Cryptography (CL-PKC) has the advantages of no certificate management and no key escrow compared with traditional public key cryptography and identity-based public key cryptography respectively.

2.1 Problem Statements and Motivation

The processes of issuing the various documents are still in a paper form and have been done in a manually and routinely manner that does not fit with the technological progress and the current age requirements and variations. Moreover, using paper-based systems is a costly process and causes waste of precious time including the possibility of damaging and losing of paper documents. Furthermore, the archiving process for the increasing stacks of document papers would become very difficult to look after or sort out. The switching from paper based work to a fully computerized work is not without difficulties. As a result, many systems have been developed in the recent years. Eight intertwined elected services will be identified; namely: message authentication, entity authentication, integrity, non-repudiation, time stamping, distinguished signing authorities, delegating signing capability and supporting workflow systems.Useful works have been done in the literature as reviewed in the previous section. However, these systems are missing a number of services. Moreover, the combination

of all the elected services is missing in the benchmarked systems. This combination is a challenging process that stresses the need of a computerized workflow. Motivated by such challenge, this research aims to solve the manual work problems and provide the combination of the elected digital signature services mentioned before by adopting a system for issuing the graduation certificates in the educational environment.

3. DIGITAL SIGNATURE SERVICES

Digital signature services include message authentication, message integrity, non-repudiation and message confidentiality. A digital signature can directly provide the first three; for message confidentiality it is still a need for using encryption/decryption techniques. Also, a digital signature scheme can provide the entity authentication. However, ordinary digital signature schemes are not quite enough to satisfy some practical needs **,Hwang, et al., 2013.** Thus, there are other services related to digital signature include time stamping, distinguished signing authorities, delegating signing capability and supporting workflow systems.

3.1 Message Authentication

A digital signature scheme can provide message authentication (also referred to as data-origin authentication). Bob can verify that the message is sent by Alice because Alice's public key is used in verification. Alice's public key cannot verify the signature signed by Eve's private key **,Forouzan, 2010.** Digital signatures can be used to authenticate the source of documents or messages (i.e., authentication of a device, a message sent by the device and/or a person sending the message); by creating a digital signature of a message using the private key, which can be verified using the public key. The relationship of a public key to a user's private key allows a recipient to authenticate and validate a sender's message. As ownership of secret key(s) is bound to specific users, valid signatures guarantee that a document was signed by that user **,Ahmed, et al., 2012 and ,Singh, et al., 2012.**

3.2 Entity Authentication (Identification)

Entity authentication is a technique designed to let one party prove the identity of another party. An entity can be a person, a process, a client or a server. The entity whose identity needs to be proven is called the claimant; the party that tries to prove the identity of the claimant is called the verifier. Entity authentication is required when Alice gets cash from an automatic teller machine. Entity authentication happens in real time and authenticates the claimant for the entire duration of the session **,Forouzan, 2008.**

Entity authentication is the security process that validates the identity of the communicating party. In the simplest implementation, this takes the form of a password **,Banday, 2011.** The use of a password is the simplest and oldest method of entity authentication. In password authentication, the claimant proves his/her identity by demonstrating that he/she knows a secret, the password **,Forouzan, 2008.** Entity authentication can also be achieved using a digital signature. When a digital signature is used for entity authentication, the claimant uses his/her private key for signing and the verifier must use the public key of the claimant for the purpose of verification **,Forouzan, 2007.**

3.3 Message Integrity

The integrity of the message is preserved even if the whole message is signed because it is infeasible to get the same signature if the message is changed. The digital signature schemes use a hash function in the signing and verifying algorithms that preserves the integrity of the message **,Forouzan, 2007.** A valid digital signature can assure the recipient the origin and the integrity of a message **,Wu, et al., 2013.**

3.4 Non-repudiation

A trusted third party is used to solve many problems concerning security services. The digital signature with a trusted third party could be used for achieving non-repudiation service **,Wu, et al., 2013.** If in the future Alice denies that she sent the message, the center can show a copy of the saved message. If Bob's message is a duplicate of the message saved at the center, Alice will lose the dispute **,Forouzan, 2007.**

3.5 Time Stamping

One of the major drawbacks of digital signatures is the fact that there is no inherent certainty about date and time at which a document was signed. A signer may have included a time stamp with the signature. The document itself may also have a date mentioned on it. However, later readers cannot be certain the signer did, for example, backdate date and time of the signature. Trusted time stamping in addition to digital signatures is needed to prevent such cases of misuse **,Sageder, et al., 2008.** A time stamping service supports assertions of proof that a datum existed before a particular time. One of the major uses of time stamping is to time stamp a digital signature to prove that the digital signature was created before a given time **,Mir , and Banday, 2012.** In many situations, people need to certify that a document existed on a certain date. Thus, the digital signatures are improved by including the time stamps. In doing so, the date and time of the signature are attached to the message and signed along with the rest of the message **,Schneier, 1996.**

3.6 Distinguished Signing Authorities

For the sake of labor-division and responsibility sharing inherent in certain applications and the group works, every discretionary signatory within the group might be required to sign or read the partial document instead of the whole document **,Feng, et al., 2011.** Under this scenario, the document is divided into several parts and each signer signs only on the part which he is responsible for where each signer signs a partial document that he is responsible for **,Chien, 2005.** Each group member is responsible for his or her own signing of a partial document or message **,Yoon, and Yoo, 2006.** For example, a company releases a document that may involve the financial department, the marketing department and the program office. Each entity signs the partial message related to his work. Each signer signs the section message that he is responsible for **,Huang and Chang, 2005.**

3.7 Delegating Signing Capability

In the digital world, the original signer delegates its signing capabilities to another person. For example, a manager can delegate to his staff member the right to sign certain documents during his absence, who can sign documents as a proxy signer on behalf of the manager. In such digital schemes referred to as proxy signature schemes, the original signer is able to delegate his signing capability to a designated person. This concept is referred to as one-to-one proxy signature **,Fazlagic, 2010.** In a proxy signature scheme, an original signer can delegate his or her signing capability to a proxy signer and then the proxy signer can generate a valid signature on behalf of the original signer **,Liu, et al., 2011.** The simplest approach to achieve the main goal of a proxy signature scheme is for the designator (original signer) to give its secret key to the proxy signer, who can then use it to sign messages. In this case proxy signatures are just standard signatures, and can be verified the usual way. This scheme called full delegation in the literature **,Boldyreva, et al., 2012.**

3.8 Supporting Workflow Systems

Nowadays, information systems must be able to deal with a highly dynamic environment. Traditionally, workflow systems have been used by business organizations to support the execution of business processes. In workflow literature each business process can be separated into a set of well-defined and inter-related tasks. By controlling task execution the workflow system ensures sequential signing. Using this workflow functionality along with digital signature schemes provides a mechanism for multiuser document signing. Usually, definition of the workflow process predefines the order of signing the documents. Workflow systems must be able to handle digital signatures for different purposes. For example, workflow processes frequently need multiple signers to sign the same electronic document, in line with the organizational structure. Digital signature scheme also should support document verification during and after workflow process execution **,Fazlagic, 2010.**

4. RELATED WORK IN PRACTICE

This section gives the art-of-the-practice of the up-to-date digital signature-based systems. The following subsections contain a brief description of the components and features of these systems according to the elected digital signature services, namely: the message authentication, the entity authentication, the integrity, the non-repudiation, the time stamping, the distinguished signing authorities, the delegating signing capability and the supporting of workflow systems services.

4.1 Features of the What You See Is What You Sign (WYSIWYS) System

Based on the elected services, the WYSIWYS system provides the message authentication, the entity authentication, the integrity and the non-repudiation services. However, WYSIWYS does not support the time stamping, the distinguished signing authorities, the delegating signing capability and the workflow systems services **,Josang, and AlFayyadh, 2008.**

4.2 Features of the Circular Resolution Database System (RDS)

The circular RDS comprises features to create, publish and maintain electronic documents. The main objective of this system is to increase the security of basic operations like user authentication and the signing of digital documents. The circular RDS solution incorporates qualified electronic signatures for two purposes. On the one hand, the application of qualified electronic signatures is used to unambiguously and securely authenticate users by means of a citizen card based two-factor authentication. On the other hand, created and maintained resolutions are electronically signed in order to guarantee integrity and non-repudiation of the particular data **,Zefferer and Knall, 2010.** In addition, the entity authentication is supported in this system. The workflow service being one of the core components of the entire RDS is responsible for all tasks concerning the creation, signing and publishing of resolutions. However, the time stamping, the distinguished signing authorities and the delegating signing capability are not supported in this system.

4.3 Features of the Threshold Proxy Signature Scheme (TPSS)

The TPSS is a (t; n) threshold proxy signature scheme. In a (t; n) threshold proxy signature scheme, the original signer can authorize (n) members of a proxy group. Moreover, only the cooperation of (t) or more proxy members is allowed to generate the proxy signature. In the TPSS, a warrant agreed and signed by the original signer and all proxy signers together has been used. The computation complexity and communication cost of the scheme have nothing to do with the size of the proxy group. Moreover, the verification of proxy signature is divided into two steps, one is the verification of the warrant; the other is the verification of the proxy signature. Having these properties, the proposed TPSS has less computation and communication cost, compared with previously proposed schemes based on discrete logarithms. It is more efficient and secure scheme **,Kang, and Han, 2010.** The TPSS ensures the message authentication, the entity authentication (identities of the original signer and the proxy signers), the integrity of the massage, the non-repudiation and the delegating signing capability services. However, the TPSS does not support the time stamping, the distinguished signing authorities and workflow systems services.

4.4 Features of the Delegating Digital Signing Capability Mechanism (DDSCM) in Workflow Systems

The dynamic nature of business processes imposes the need for the workflow management system (WfMS) to be able to modify a process model at run-time to deal with exceptional situations and adjust to the changing business policies. A fully computerized workflow processes with a digital signature technology used to provide authenticity and the integrity of electronic documents throughout the document life cycle. The delegating digital signing capability service is achieved by using an appropriate proxy scheme integrated with the WfMS **,Fazlagic, 2010.** Furthermore, the time stamping and non-repudiation services are supported in this system. However, the service of distinguished signing authorities is not supported in this system.

4.5 Features of the Threshold Signature Scheme (TSS) with Distinguished Signing Authorities

In most signature schemes, the signer and the verifier of a signature may be a single person. However, when one message is exchanged between one organization and another organization, the message may require the approval or consent of several members. Under this scenario, the signature generation and verification require more than one consenting rather than by a single member. Threshold signature schemes are introduced to solve this problem **,Zhou, et al., 2010.** Based on elected services, the TSS with distinguished signing authorities provides the message authentication, the entity authentication, the integrity and the non-repudiation services. However, it does not support the time stamping, the delegating signing capability and the workflow systems services.

4.6 Features of the Multi-Proxy Signature Scheme (MPSS) with Proxy Revocation

In some cases, the original signer may delegate his or her signing power to a specified proxy group while ensuring individual accountability of each participant signer. The proxy signature scheme that achieves such purpose is called MPSS, and the signature generated by the specified proxy group is called multi-proxy signature for the original signer. The proxy revocation, i.e., the revocation of delegated rights is needed and it is important for the situation where proxy signer or signer's key is compromised and the delegated rights are abused **,Liu, et al., 2011.** The MPSS satisfies the message authentication, the entity authentication (the original signer and the proxy signers' identities), the integrity of the massage, the non-repudiation and the delegating signing capability services. However, MPSS does not support the time stamping, the distinguished signing authorities and workflow systems services.

4.7 Features of the Electronic Medical Record (EMR) System

The EMR is a digital format of the traditionally paper-based anamnesis (patient's record), which contains the complete medical case history of a patient such as his somewhat illness, current health problems and his chronic treatments. An electronic anamnesis is meant to make the patient's health information more conveniently accessible and transferable between different medical institutions and also easier to be kept quite a long time. In regard to the security purpose, all the EMRs are embedded with both of the PKI cryptography and the digital signature technique so as to ensure the records well-protected **,Chen, and Lin, 2011.** The digital signature that integrated to the EMRs system ensures the authentication, the data integrity and help to verify the non-repudiation of the content. In addition, the time stamping technique is supported in this system. However, the distinguished signing authorities, the delegating signing capability and the workflow systems services are not supported in this system.

4.8 Features of the Multi-Policy Threshold Signature Scheme (MPTSS) with Distinguished Signing Authorities

There are three trusted parties involved in the MPTSS: the system authority (SA), the document dispatcher (DD) and the signature collector (SC). SA is responsible for defining system public parameters and generating the private keys and the public keys for signing and verifying groups and their members. The tasks of DD are to divide the signing document into smaller subdocuments according to the significance of the document and choose the signatories within

the signing group for signing these subdocuments. The responsibilities of SC are to collect and verify individual signatures generated by the signatories, to check whether the contents of the whole document have been signed by these discretionary signatories, and to construct a group signature from the individual signatures **,Feng, et al., 2011.** The MPTSS with distinguished signing authorities provides the message authentication, the entity authentication, the Integrity and the non-repudiation services. However, it does not support the time stamping, the delegating signing capability and the workflow systems services.

4.9 Features of the Certificateless Proxy Signature Scheme (CLPSS)

CL-PKC does not use public key certificates. It successfully solves the key escrow problem. In CL-PKC, a third party called Key Generation Center (KGC) is used to help a user to generate his private key. CL-PKC eliminates the need of certificates and does not suffer from the key escrow problem. Therefore, it is interesting to introduce proxy signatures into CL-PKC. Compared with proxy signature schemes in traditional public cryptography, CLPSS can eliminate the certificate verification and burdensome certificate management. Hence, CLPSS supports true non-repudiation **,Zhang, et al., 2012.** The CLPSS ensures the message authentication, the entity authentication, the Integrity of the massage and the delegating signing capability (proxy signature scheme with delegation by warrant) services but it does not support the time stamping, the distinguished signing authorities and workflow systems services.

5. THE ARCHITECTURAL DESIGN OF THE GRADUATION CERTIFICATES ISSUING SYSTEM (GCIS)

The proposed GCIS performs different functions (activities); these functions are executed by specific users (actors). Therefore, the design of the GCIS will be described by using the UML diagrams to represent the interaction between the actors and the GCIS functions. The UML is a very helpful tool in developing a specific structure according to specific requirements. Based on the elected services related to the digital signature mentioned, the architectural design of the proposed GCIS will be constructed by the use case diagrams.

The use case diagram specifies the functionality that the system has to offer from the perspective of users and defines what should take place inside the system. In addition, this diagram uses "actors" to represent the roles that users can play, and it also utilizes "use cases" to represent what users can do with the system. Thus, the use case diagram consists of two parts **,Al-Tameemi, 2010.**

1. Actor(s): It represents someone or something that acts in the system (i.e., human beings who will interact with the system). The classes of actors capable of using the system are presented in the next section.
2. Use case(s): It is a special sequence of related transactions performed by an actor and the system in a dialogue. The use cases specify all interactions within the system.

Fig. 1 shows the use case diagram of the proposed GCIS and the use cases related to each user.

6. THE IMPLEMENTATION OF THE GCIS

Before going into implementation details, it is necessary to mention that the Visual Studio 2008 (Visual Basic.Net) with the .Net framework 3.5 is used to:

1. Construct the GUIs of the proposed GCIS to allow users to interact with the system.
2. Implement the cryptographic algorithms with regard to the digital signature (RSA digital signature scheme) and the hash function (SHA-512) in addition to the encoding and decoding techniques (UTF-8). It should be mentioned that these cryptographic algorithms are invoked by an industrial standard APIs' built in the "Microsoft .Net" framework.
3. Access and manipulate the data or records stored in the tables of the GCIS within the SQL Server database.

6.1 The Login GUI

The users of the GCIS gain access to the resources of the system through the login GUI. For the purpose of entity authentication (identification) service, each user has a username and password. The users can login by entering a valid username and password as show in **Fig. 2**. The delegated user check box in the login GUI is checked only by the delegated signers for login process, so as distinguishing them from the original signers.

6.2 The Administration GUI

This GUI is used for generating and updating the RSA key pair for the users of the GCIS and to activate the delegating signing capabilities service. **Fig. 3** shows the main administration GUI. The administrators is responsible for accomplishing the tasks related to this GUI.

6.3 The Student's Information GUI

There are two users (with stdinfo1 and stdinfo2 usernames) responsible for inserting (data entry) and updating the main students' information. The GCIS support the share access to the system's resources. In addition, the processes of the system could be performed simultaneously by multi-user due to adopting the client/server paradigm. Therefore, inserting and updating processes could be performed by stdinfo1 and stdinfo2 simultaneously without any conflict. **Fig. 4** shows the data entry mode of the student's information GUI for a certain graduated student.

6.4 The Student's Degrees

There are two users (with stddeg1 and stddeg2 usernames) responsible for inserting and updating the students' degrees. After the login process the student's degrees main GUI will appear which indicates that there are a certain number (between the square brackets) of students' records ready for the inserting and/or updating degrees processes (four students' records are ready for degrees inserting process in our case study), as shown in **Fig. 5**.

6.5 The Checking Process

When the data entry process of the student's information and degrees records complete successfully then the checkers of the GCIS will be ready for accomplishing the checking processes in order to make sure that there are no mistakes exist in the students' information and degrees records. The checking processes could be done in parallel (i.e., simultaneously) by eight checkers; two checkers for each class. The checkers are responsible for reviewing the student's information, the student's degrees for the subjects, the attempt of each subject and the year related to the specific class. **Fig. 6** shows the details of the checking GUI.

6.6 The Examination Board / Registration Unit Processes

When the checking process is finished successfully for all the graduated students, then several processes should be performed by the examination board/registration unit before issuing the graduation certificates in their final form. **Fig. 7** shows the main examination board/registration unit GUI and the processes related with it. Examination Board / Registration Unit Employees perform the following activities:

1- Automatically, calculating the final averages and the ranks for the graduated students.
2- Editing the syllabus for each class including the subjects' IDs, the subjects' names in English and Arabic languages, and the number of units for each subject.
3- Specifying the types of the required graduation certificates for each student as part of the issuing process. These types include: the certificate of graduation and the transcript of records in Arabic and English languages.
4- Printing the paper copies of the achieved graduation certificates. A soft copy for the finished graduation certificates will be available as a PDF file in addition to the HTML and ASP formats.

6.7 The Final Graduation Certificates Issuing and Signing Processes

After completing the pervious steps, all the required information for issuing the graduation certificates will be available. Therefore, the graduation certificates in their final form will be ready for signing. The signing process will be performed by the following signers (arranged according to the signing process sequence): the examination board member, head of the examination board, head of the department, the registers, the assistant dean, the dean, the issuer (performs the process of inserting the graduation certificate's number and date), and the manager of the higher studies and certifications, respectively.

As in real word, the order of signers should be respected. This fact is taken into account within the internal design of the system. The verification process will be performed automatically for the digital signature of the previous signer. In case of an invalid signature, the signing process will be aborted until fixing the problem. Otherwise, in case of a valid signature, the graduation certificate will appear to the current signer for the reviewing and signing purposes, as shown in **Fig. 8**.

7. COMPARISON OF THE GCIS WITH THE EXISTING DIGITAL SIGNATURE-BASE

Table.1 demonstrates the digital signature services of the GCIS compared with the existing systems and schemes.

8. CONCLUSIONS

In this research, a number of existing systems and schemes based on digital signature have been studied in terms of the elected services. Based on that, Graduation Certificates Issuing System (GCIS) has been proposed. The proposed GCIS overcomes the drawbacks in the existing systems and schemes. The proposed GCIS has been implemented by using Visual Studio 2008 (Visual Basic.Net) with .Net framework 3.5, SQL Server 2005 database and Visual Paradigm

for UML 8. The proposed GCIS has been compared with the other digital signature based systems. The comparison showed the advantages of the proposed GCIS over the existing systems and schemes. In this paper, the desired elected services have been accomplished as shown below.

8.1 Message Authentication (Data-Origin Authentication) Service

The system provides a message authentication service through the verification processes for the digital signatures of the signers. This service is reflected in the GCIS through employing the cryptographic digital signature algorithms (RSA digital signature scheme). When the user (singer) signs data with digital signature (using his/her private key) someone else (other users) can verify this signature (using the associated signer's public key), and can prove that the data originated from the original user (singer) himself not from other user.

8.2 Entity Authentication (Identification) Service

The system provides the entity authentication service through utilizing the username and password for user (signer). Thus, the identity of each user (signer) will be validated or proven. This service is employed for the purpose of login process in order to gain access to the system's resources.

8.3 Integrity Service

The system employed the digital signature algorithm for the purpose of signing and verification processes. The digital signature schemes imply the using of the one way hash function to provide the integrity service. Thus, any unauthorized change for the content of the data records will be detected and that will ensure that the received data are exactly as signed by the original signer.

8.4 Non-repudiation Service

Since the system is employing the client/server paradigm, a trusted database server in association with the digital signature technology has been used for providing the non-repudiation service. Thus, the users of the system will not be to deny their activities within the processes of the system.

8.5 Time Stamping Service

The system provides time stamping services through using a stored procedure within the main database to return the current system date and time of the main server. This time stamp will be appended to the data record and digitally signed along with it. Thus, the time stamp service has been accomplished. In addition, the conflicts of the clients' computers time stamps have been avoided.

8.6 Distinguished Signing Authorities Service

The system provides the distinguished signing authorities service for the purpose of labor-division, responsibility sharing, saving efforts and time. This service is exactly reflected in the checking process within the system, in which the student's degrees record has been checked by

separated groups of checkers (two checkers for each class). Thus, the signers (checkers) do not have to check and sign the whole student's degrees record but only a part of it.

8.7 Delegating Signing Capability Service

The system provides the delegating signing capability due to changing or absence of the original signer or for any other reason; therefore, another user (signer) will be delegated to sign the final graduation certificates. This service is exactly reflected in the system through filling the delegation form to designate another user (signer) for signing purposes instead of the original signer.

8.8 Supporting Workflow Systems Service

This system is divided into intertwined processes; the execution of each process is dependent on the previous process, which means it could not execute a certain process until completing the process which is related on. This service is reflected in the system, for example the student's degrees inserting process could not be performed until finishing the inserting process of the student's information.

9. REFERENCES

- Ahmed M., Sazzad T. M. S., and Mollah M. E., 2012, *Cryptography and State-of-the-art Techniques*, International Journal of Computer Science Issues (IJCSI), Vol. 9, Issue 2, No. 3., PP. 583-586.

- Al-Tameemi, Z. F. A., 2010, *Design and Implementation of a Scalable Automated RFID Based Attendance System with Scheduling Technique*, M.Sc. Thesis, School of Electrical and Electronic Engineering, University of Science Malaysia, Penang, Malaysia.

- Banday, M. T., 2011, *Easing PAIN with Digital Signatures*, International Journal of Computer Applications (IJCA), Vol. 29, No. 2, PP. 46-56.

- Boldyreva, A., Palacio A., and Warinschi B., 2012, *Secure Proxy Signature Schemes for Delegation of Signing Rights*, Journal of Cryptology, Vol. 25, Issue 1, PP. 57-115.

- Chen, T., and Lin F. Y. S., 2011, *Electronic Medical Archives: A Different Approach to Applying Re-signing Mechanisms to Digital Signatures*, Journal of Medical Systems, Vol. 35, Issue 4, PP. 735-742.

- Chen-Wilson, L., Gravell A. M., and Argles D., 2011, *Giving You back Control of Your Data Digital Signing Practical Issues and the eCert Solution*, Proceedings of the World Congress on Internet Security (WorldCIS) , London, UK , PP. 93-99.

- Chien, H., 2005, *Comments on ID-based Multi-signature with Distinguished Signing Authorities*, Journal of Applied Mathematics and Computation, Vol. 170, Issue 2, PP. 1284-1289.

- Diffie, W., and Hellman, M. E., 1976, *New Directions in Cryptography*, Proceedings of the IEEE Transactions on Information Theory, Vol. 22, Issue 6, PP. 644-654.

- Fazlagic, S., 2010, *Delegating Signing Capability in Workflow Systems*, Proceedings of the 2nd IEEE International Conference on Computer Engineering and Technology (ICCET), Chengdu, China, Vol. 4, PP. 324-327.

- Feng, W., You-sheng, Z., Li-ze G., Shi-hui, Z., and Yi-xian Y. , 2011, *Multi-policy Threshold Signature With Distinguished Signing Authorities*, The Journal of China Universities of Posts and Telecommunications, Vol. 18, Issue 1, PP. 113-120.

- Forouzan, B. A., 2008, *Cryptography and Network Security*, Special Indian Edition, The McGraw-Hill Companies, Inc.

- Forouzan, B. A., 2007, *Data Communications and Networking*, Fourth Edition, The McGraw-Hill Companies, Inc.

- Forouzan, B. A., 2010, *TCP/IP Protocol Suite*, Fourth Edition, The McGraw-Hill Companies, Inc.

- Hwang, M., Lee C., and Tzeng, S., 2013, *A New Proxy Signature Scheme for a Specified Group of Verifiers*, Information Sciences, Vol. 227, PP. 102-115.

- Huang, H., and Chang C., 2005, *Multisignatures with Distinguished Signing Authorities for Sequential and Broadcasting Architectures*, Journal of Computer Standards and Interfaces, Vol.27, Issue 2, PP. 169-176.

- Josang, A., and Alfayyadh, B., 2008, *Robust WYSIWYS: A Method for Ensuring that What You See Is What You Sign*, Proceedings of the 6th Australasian Information Security Conference (AISC 2008), Wollongong, Australia, PP. 53-58.

- Kang, B., and Han, J., 2010, *A More Practical and Efficient Threshold Proxy Signature Scheme*, Proceedings of the 2nd IEEE International Conference on Education Technology and Computer (ICETC), Shanghai, China, Vol. 5, PP. 202-205.

- Liu, Z., Hu Y., Zhang, X., and Ma, H., 2011, *Provably Secure Multi-proxy Signature Scheme with Revocation in the Standard Model*, Special Issue of Computer Communications on Information and Future Communication Security, Vol. 34, Issue 3, PP. 494-501.

- Mir, F. A., and Banday, M. T., 2012, *Authentication of Electronic Records: Limitations of Indian Legal Approach*, Journal of International Commercial Law and Technology, Vol. 7, Issue 3, PP. 223-232.

- Sageder, S., Sametinger, J., and Wiesauer, A., 2008, *Case Study: Using Digital Signatures for the Archival of Medical Records in Hospitals*, Proceedings of the 3rd IEEE International Conference on Risks and Security of Internet and Systems (CRiSIS'2008), Tozeur, Tunisia, PP. 213-220.

- Schneier, B., 1996, *Applied Cryptography: Protocols, Algorithms, and Source Code in C*, Second Edition, John Wiley & Sons.

- Shukla, S., Gupta, D. L., and Malviya, A. K., 2012, *A Comparative Study of Cryptosystems with Elliptic Curve Cryptography Using Digital Signature*, International Journal of Computer Technology and Applications (IJCTA), Vol. 3, Issue 1, PP. 9-16.

- Singh, K., Kharbanda, I., and Kaur, N., 2012, *Security Issues Occur in Cloud Computing and There Solutions*, International Journal on Computer Science and Engineering (IJCSE), Vol. 4, No. 5, PP. 945-949.

- Wang L. and He M., 2010, *Improved Efficient Forward Secure Signature Scheme*, Proceedings of the IEEE International Conference on E-Business and E-Government (ICEE), Guangzhou, China, PP. 1338-1341.

- Wu, W., Zhou, J., Xiang, Y. and Xu, L., 2013, *How to Achieve Non-Repudiation of Origin with Privacy Protection in Cloud Computing*, Journal of Computer and System Sciences, Vol. 79, Issue 8, PP. 1200-1213.

- Yoon, E. and Yoo, K., 2006, *Cryptanalysis of Two Multisignature Schemes with Distinguished Signing Authorities*, Proceedings of the IEEE International Conference on Hybrid Information Technology (ICHIT'06), Cheju Island, South Korea, Vol. 1, PP. 492-495.

- Zefferer, T. and Knall, T., 2010, *An Electronic-signature Based Circular Resolution Database System*, Proceedings of the ACM Symposium on Applied Computing

(SAC'10), Sierre, Switzerland, PP. 1840-1845.

- Zhang, L., Zhang, F. and Wu, Q., 2012, *Delegation of Signing Rights Using Certificateless Proxy Signatures*, Information Sciences: an International Journal, Vol. 184, Issue 1, PP. 298-309.

- Zhou, Y., Wang, F., Xin, Y., Luo S., Qing, S. and Yang, Y., 2010, *A Novel Threshold Signature Scheme with Distinguished Signing Authorities*, Proceedings of the 3rd IEEE International Conference on Broadband Network and Multimedia Technology (IC-BNMT), Beijing, China, PP. 728-732.

- Zupan, A., 2006, *Digital Signature as a Tool to Achieve Competitive Advantage of Organization*, M.Sc. Thesis, Faculty of Economics and International Center for Promotion of Enterprises (ICPE), Ljubljana, University of Ljubljana.

Table 1. Comparison between the proposed GCIS and the related systems.

✓	Implemented service	Digital signature elected services							
×	Not implemented service								
Digital signature-based systems		Message authentication	Entity authentication	Integrity	Non-repudiation	Time stamping	Distinguished signing authorities	Delegating signing capability	Supporting workflow systems
WYSIWYS **(Josang, and AlFayyadh, 2008)**		✓	✓	✓	✓	×	×	×	×
Circular RDS **(Zefferer, and Knall, 2010)**		✓	✓	✓	✓	×	×	×	✓
TPSS **(Kang and Han, 2010)**		✓	✓	✓	✓	×	×	✓	×
DDSCM in Workflow Systems **(Fazlagic, 2010)**		✓	✓	✓	✓	✓	×	✓	✓
TSS with Distinguished Signing Authorities **(Zhou, et al., 2010)**		✓	✓	✓	✓	×	✓	×	×
MPSS with Proxy Revocation **(Liu, et al., 2011)**		✓	✓	✓	✓	×	×	✓	×

EMR System **(Chen and Lin,2011)**	✓	✓	✓	✓	✓	×	×	×
MPTSS with Distinguished Signing Authorities **(Feng, et al., 2011)**	✓	✓	✓	✓	×	✓	×	×
CLPSS **(Zhang, et al., 2012)**	✓	✓	✓	✓	×	×	✓	×
The Proposed GCIS	✓	✓	✓	✓	✓	✓	✓	✓

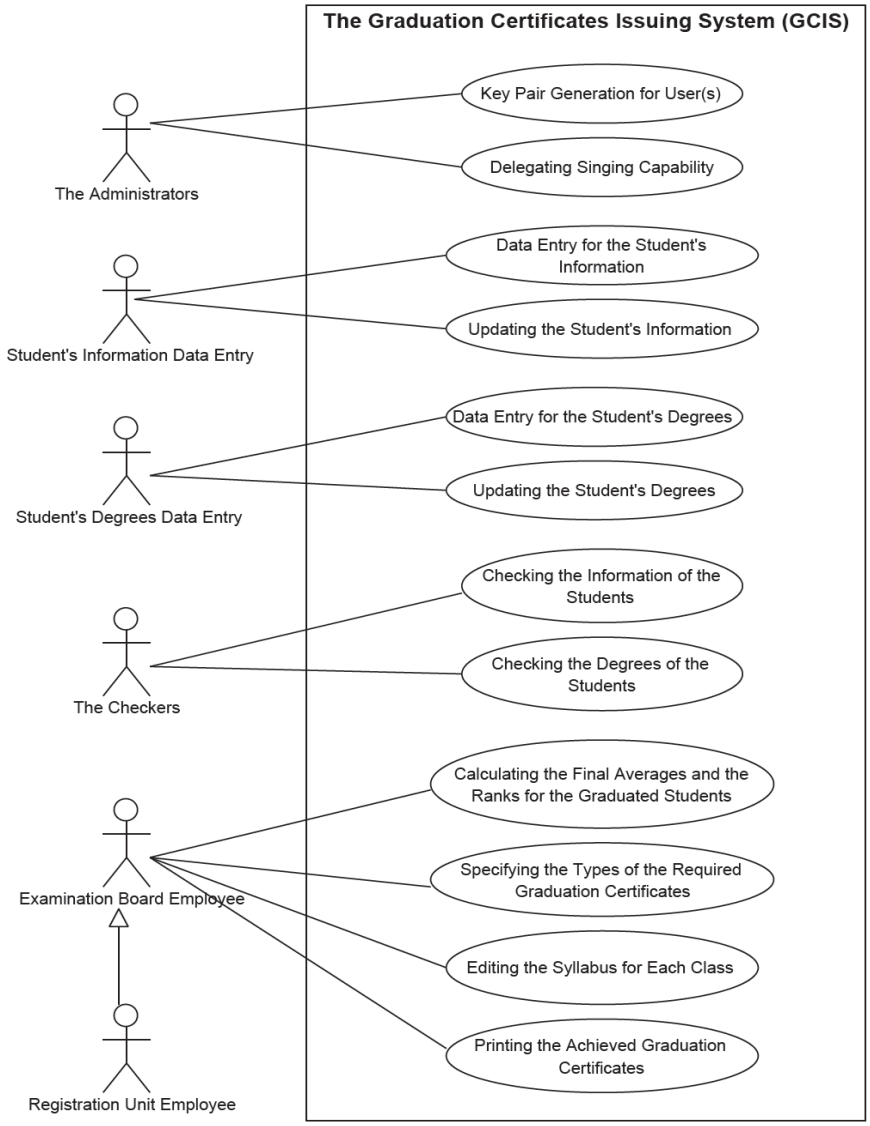

Figure 1. The use case diagram of the GCIS.

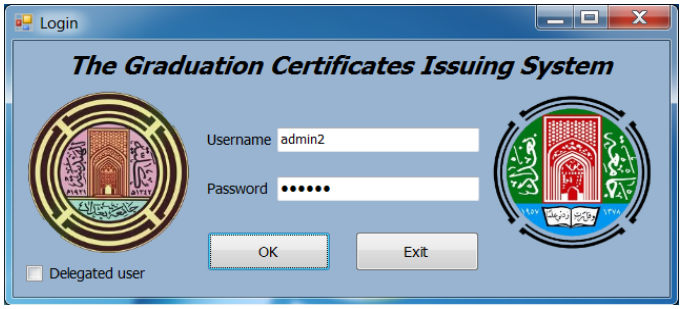

Figure 2. The login GUI of the GCIS.

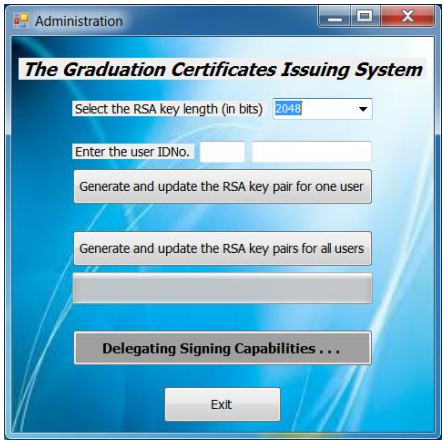

Figure 3. The administration GUI.

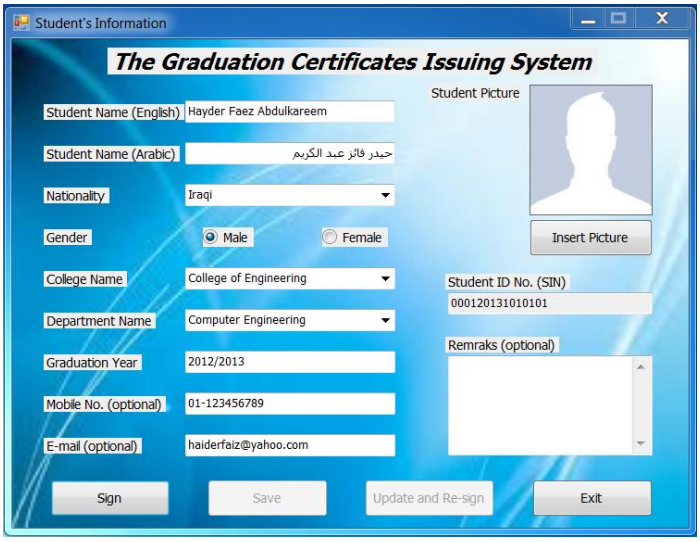

Figure 4 The student's information GUI.

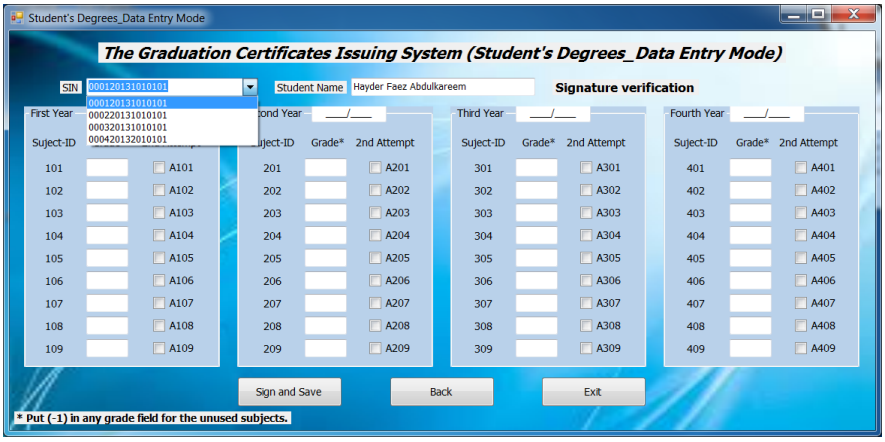

Figure 5. The student's degrees GUI.

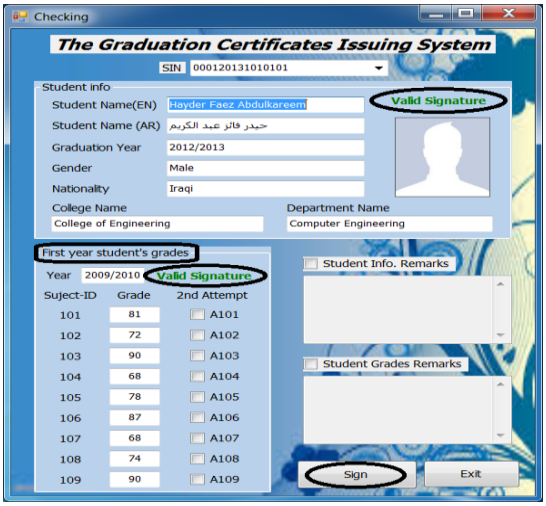

Figure 6. The checking process with valid signatures and no mistakes.

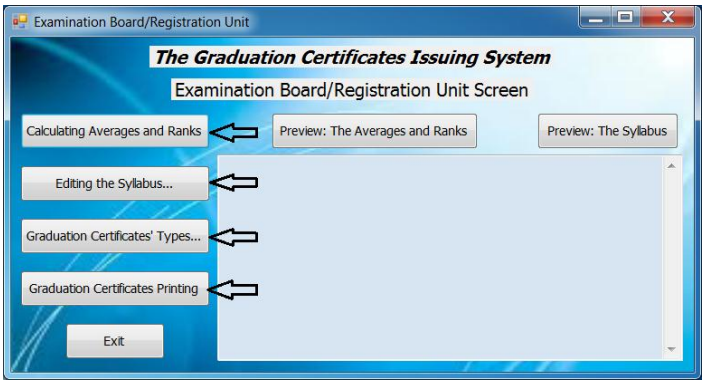

Figure 7. The main examination board/registration unit GUI.

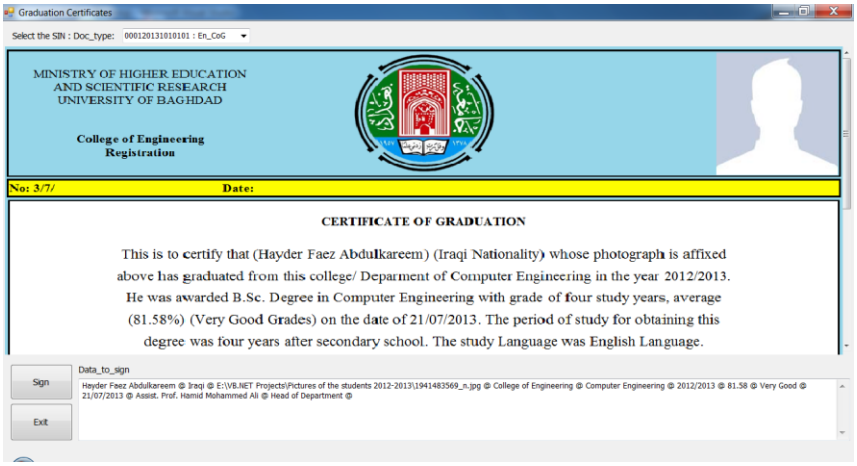

Figure 8. The final graduation certificates issuing and signing GUI.

Using Nanoparticles for Enhance Thermal Conductivity of Latent Heat Thermal Energy Storage

Baydaa Jaber Nabhan
Mech. Eng. Dept.
College of Engineering
AL-Mustansiriya University
E-mail:Baydaa1971@yahoo.com

ABSTRACT

Phase change materials (PCMs) such as paraffin wax can be used to store or release large amount of energy at certain temperature at which their solid-liquid phase changes occurs. Paraffin wax that used in latent heat thermal energy storage (LHTES) has low thermal conductivity. In this study, the thermal conductivity of paraffin wax has been enhanced by adding different mass concentration (1wt.%, 3wt.%, 5wt.%) of (TiO_2) nano-particles with about (10nm) diameter. It is found that the phase change temperature varies with adding (TiO_2) nanoparticles in to the paraffin wax. The thermal conductivity of the composites is found to decrease with increasing temperature. The increase in thermal conductivity has been found to increase by about (10%) at nanoparticles loading (5wt.% and 15^{o}C).

Key words: phase change materials (PCM), LHTES, thermal conductivity, TiO_2.

استخدم جزيئات نانوية لتحسين الموصلية الحرارية لخزين من الطاقة الحرارية الكامنة

المدرس المساعد بيداء جابر نبهان
قسم الهندسة الميكانيكية
كلية الهندسة
الجامعة المستنصرية

الخلاصة

المواد متغيرة الطور(PCM) مثل شمع البرافين يستطيع خزن او تحرير كمية كبيرة من الطاقة عند درجة حرارة تغير الطور من الصلب الى السائل. لذلك يستخدم شمع البرافين في خزن الطاقة الحرارية كطاقة كامنة الا انه يمتلك موصلية حرارية واطئة. وقد تم في هذه الدراسة تحسين الموصلية الحرارية لشمع البرافين بأضافة نسب كتلية مختلفة (1 wt.%,3wt. %,5wt. %) من الجزيئات النانوية (TiO_2) اوكسيد التيتانيوم . وقد وجد ان درجة حرارة تغير الطور تتغير مع اضافة (TiO_2) الى شمع البافين. كما لوحظ ان الموصلية الحرارية للمركبات تقل بزيادة درجة الحرارة وان الموصلية الحرارية تزداد مع زيادة النسبة الكتلية لجزيئات النانو (TiO_2) وبنسبة (10%) عند (5wt.% و 15^{o}C).

الكلمات الرئيسية: المواد متغيرة الطور, خزن الطاقة الحرارية كطاقة كامنة,الموصلية الحرارية, اوكسيد التيتانيوم.

1. INTRODUCTION

Thermal energy can be stored when a change in internal energy of a material as sensible and latent heat. And it will be important energy management with emphasis on efficient use and conversation of the waste heat and solar energy .Energy storage plays important role in conserving the over demand of energy. **,Abhat, 1983,** gave a useful classification of the substances used for thermal energy storage as shown in **Fig.1**.

In sensible heat storage, thermal energy is stored based on the specific heat capacity of the material. Here the temperature of the material varies and does not undergo any phase transformation during charging or discharging cycles, for example: water, copper, cast iron **,Garg and Prakach, 2002.** And in latent heat storage system the process of storing and retrieving the thermal energy is based on the latent heat of fusion, where storage medium undergoes a phase transformation. The heat stored during the phase change process of the material is called latent heat. As the source temperature increases the chemical bonds of the material breaks up which leads to the transformation from one phase to other, **Sharma, et al., 2009.** Here the temperature is almost constant with less temperature swing. Latent heat storage materials can be classified based on temperature, phase transition and compounds used to: Organic PCMs and inorganic PCMs. A phase change material PCM which contains carbon atom is known as organic PCM, so phase change materials PCMs is a kind of very important latent heat energy storage materials with the general chemical formula (C_nH_{2n+2}) are categorized under paraffin, where the heat of fusion and melting point increases with the increasing value of carbon atom number, **Abhat, 1980.** Paraffin having 5 to 15 carbon atoms is liquid at room temperature, and those with more carbon atoms are waxy solid. PCMs have wide applications in many fields, such as refrigeration and air-conditioning systems, solar energy systems, heating and cooling of building. It has attracted great interest in recent years , **,Qinbo He, et al., 2012.** Few of the advantages of using organic PCM are no tendency to segregate, chemically stable, high heat of fusion, no tendency of sub-cooling and compatible with all containers except plastic at high temperature. Some of the demerits are low thermal conductivity, sometime flammable and mildly corrosive, **Garg, and Prakach, 2002.**

Many researchers have carried out similar studies for the heat transfer performance of nanofluids. For example, **Lee and Choi, 1996,** had tried to use nanofluids and miniature heat exchangers constitute efficient cooling system. In recent years, nanofluids have been employed to enhance the heat transfer in PCMs for energy storage, due to its desirable properties of high thermal conductivity. **Xie HQ, et al., 2002,** revealed that the thermal conductivity of Al_2O_3 nanofluid was higher than that of the base fluid and increased with increasing nanoparticle concentration level. The enhanced thermal conductivity ratio decreases with an increase in PH value, from (PH 2.0 to PH 11.5). They also found that the thermal conductivity of nanofluids varied with particle size and the optimal particle size for thermal conductivity enhancement was (60nm). **Khodadadi and Hosseinizadeh, 2007,** studied the phase change process of Cu-H_2O nanofluids by using numerical simulation method. The nanofluids shows the preferable thermal energy storage characteristic, the heat release rate is high than that of pure water. **Wu et al., 2009,** investigated the thermal properties of (Al_2O_3-H_2O) nanofluid they concluded that the supercooling degree was reduced by 70.9% with suspending 0.2 wt.% Al_2O_3 nanoparticles in water. **Ho and Gao, 2009,** studied the effective thermophysical properties, such as latent heat of fusion, density, dynamic viscosity and thermal conductivity of n-octadecane PCM embedded with Al_2O_3 nanoparticles with the composition of 5%

and 10%. Prepared by emulsifying alumina by means of non-ionic surfactant. The change in the values of melting temperature, freezing temperature and latent heat of fusion is given in **Table 1.**

Shin and Banerjee, 2011 studied the high-temperature silica-nanofluids for soler thermal storage application, the specific heat capacity of the nanofluid was enhanced by (14.5%). **Qinbo He, et al., 2012,** investigated the thermal properties of TiO_2 nanoparticles in saturated $BaCL_2$ aqueous solution, they concluded that the thermal conductivities of nanofluids PCMs is enhanced by (12.76%) at (-5^{o}C) with volume fraction (1.13%).

Parameshwaran, et al., 2013, investigated the performance of organic ester by incorporating silver nanoparticles in terms of latent heat capacity, thermal conductivity, and heat storage and release capabilities. Report shows, latent heat capacities decreased by (7.88%) in freezing and (8.91%) in melting whereas thermal conductivity of composite PCMs increased from (0.284 to 0.765 W/m.K). **Alhamdo, et al., 2013** studied thermal conductivity enhancement of paraffin and natural waxes composites by employing four different high conductivity additives in filtrated within waxes. It was found that for copper network (CN) composite with (6%) additives, the charging and discharging time decreased by (26.4%) and (30.3%) respectively, than that of pure wax and the thermal conductivity enhanced by (2.57) times than of pure wax.

The aim of this work is to present a method to enhance the thermal conductivity of paraffin wax as PCM by adding different mass concentration of nanoparticle (TiO_2).

2. THEORETICAL FORMULATION

Generally paraffin based PCMs have low thermal conductivity, during the discharge the thermal energy from liquid PCM is released and a layer of solid PCM develops on the container wall. Thermal resistance of this layer increases with increasing thickness, thus diminishing heat transfer rate **,Sharma, and Sagara, 2005.** To overcome this problem nanoparticle (TiO_2) has been added into the PCM, due to its bigger specific surface area and with small size surface energy. The experimental temperature records have been used in theoretical formulation. The following assumptions and boundary conditions were used in the modeling:

1.The study case is transient state because the temperature is changing over the time.

2. The inlet of the test section defined as velocity inlet with velocity magnitude of 7m/sec and constant temperature for the heat transfer fluid of 76^{o}C (during charging) and 12^{o}C (during discharging).

3. The outlet portion of the test section was considered outflow boundary. This is intended to use with incompressible flow.

Fig. 2 shows a physical representation of the numerical model. The governing conservation equations are as follows **, Alhamdo, et al., 2013.**

- Continuity equation: $\nabla \vec{u} = 0$ (1)
- Momentum equation:

$$\rho_{wf} \cdot \frac{\partial u}{\partial t} = -\nabla P + \mu \nabla^2 \vec{u} \quad (2)$$

Where P: Pressure gradient

- Energy equation:

The enthalpy of a material is **,Alhamdo, et al., 2013.**

$$H=H_{sensible}+H_{latent} \quad (3)$$

$$\& \ H_{sensible}=H_{ref}+\int_{T_{ref}}^{T} C_p dT \quad (4)$$

Where: H_{ref} = Reference enthalpy, kJ/kg.
T_{ref}= Reference temperature, ^{o}C.

The latent heat content can be written by latent heat of the material and L:

$$H_{latent}=\beta.L \quad (5)$$

Where β: Liquid fraction and can be defined as:

$$\beta=0 \qquad if\ T\leq T_{solidus}$$
$$\beta=1 \qquad if\ T\geq T_{liquidus}$$

$$\beta=(T-T_{solidus})/(T_{liquidus}-T_{solidus}) \qquad if\ T_{solidus}<T<T_{liquidus} \quad (6)$$

The energy equation is written as **,Alhamdo, et al., 2013.**

$$\frac{\partial}{\partial t}(\rho H)+\nabla.(\rho\vec{u}H)=\nabla.(K\nabla T)+S \quad (7)$$

Where *S*: Dissipation function. This function includes the energy transformed into heat due to the fluid shear stress.

The thermal conductivity is an important property of PCMs because the rate of energy storage or release is highly depended on the thermal conductivity of materials. PCMs are used for thermal energy storage in environments with temperature variation. Therefore, it is important to know the thermal conductivity of the PCMs in both solid and liquid states of the temperature range of interest. Many theoretical works had carried out to estimate the thermal conductivities of the composite. The equation used to calculate the thermal conductivities of the composite given by, **,Bhattachary, et al., 2004.**

$$k_C=\varphi_v*k_P+(1-\varphi_v)*k_f \quad (8)$$

Where k_C , k_P and k_f are thermal conductivities of the composite, nanoparticle and the matrix respectively. The relationship between volume fraction φ_v and weight fraction φ_w **,Bhattachary, et al., 2004.**

$$\varphi_v=(m_P*\rho_c)/(m_c*\rho_p)=\varphi_w*(\rho_c/\rho_p) \quad (9)$$

The mass fraction associated with volume fraction of the samples is shown in **Table 2. Table 3.** shows the properties of nanoparticle (TiO_2) and PCM.

3. EXPERIMENTAL TEST RIG

Fig. 3 shows the experimental test rig. Experimental test rig consists of the components required as shown schematically in **Fig. 4** such as, the flow unit which contain refrigerated air operates by a three phase electric motor, the heating unit which contain three electrical helical heaters (600 Watt, each) used for heating the test section and the duct section which has a square section (15x15) cm^2 with a length of (210 cm) the test section placed at the last (60cm) of the duct. (120) spherical capsules filled with (25g) of PCM have been packed inside the test section. The test rig insulated by using a layer of glass wool.

4. MEASUREMENT INSTRUMENT

Temperature and air velocity were measured by measuring devices. Thermocouples of (T type) were used to measure the temperatures of PCM and air at five different locations along the axial direction in the test section and recorded by using digital thermometers. Five special spherical capsules having thermocouples are locate at the center line of the test section at axial location of (X/L = 0, 0.25, 0.5, 0.75 and 1). Thermal camera (Ti32) was used to measure the surface temperature of the test capsules, as shown in **Fig.5**. A digital vane-type anemometer was used to measure the average air velocity at the inlet and outlet of the section. The measurement test is carried out at A/C laboratory in Mech. Eng. Dept. /College of Engineering/AL-Mustansiriya University.

5. RESULTS AND DISCUSSION

In the present study, the results of improvement of thermal conductivity of PCM for thermal storage of charging and discharging process are presented here.

Fig. 6 shows photograph images, thermal images of PCM and changes in thermo- physical properties with respect to different weight% of nanoparticle TiO_2 at 60^oC and after 15 minute, also it shows three dimensional images and the temperature distribution. It can be noted, the melting process occurs faster with increasing mass fraction of nanoparticles TiO_2 compared to that of pure paraffin because of the high surface energy with so small size to nanoparticles

Fig.s 7, 8 and 9 show the temperature distribution of the PCM along the axial direction of the test section at (X/L=0, 0.25, 0.5, 0.75 and 1) with flow rate of (7m/s). It can be observed for charging process, at (X/L = 0) the PCM melt faster than the other locations because it absorb most the energy carried by the heat transfer fluid, where the flow over the capsules mentioned along the test section, this energy decreased gradually until the last PCM capsules in the end section have less energy to melt. The heat transfer processes between the PCM and heat transfer fluid enhanced and become more active by (11.5%) in the adding mass fraction (5 wt. %) of nanoparticle TiO_2, because the thermal resistance becomes smaller.

In discharge process a reveres process take place to release the energy absorbed. It can be noted that the first capsules solidify faster than the others, and the solidification occur faster than the melting, due to low thermal resistance of liquid PCM. The adding different mass fraction of nanoparticle TiO_2 in PCM enhanced the heat transfer process between PCM and heat transfer fluid.

Fig. 10 shows the temperature distribution of the PCM with different weight fraction of nanoparticle (TiO_2) during charging and discharging processes. It can be noted, nanoparticle (TiO_2) was added into PCM to improve thermal storage performance. Thermal storage (charging) and release rate (discharging) were increased by (0.95) times and (1.5) times respectively at (50^oC), as compared with the PCM without nanoparticle (TiO_2).

Fig. 11 shows the latent heat at different mass fraction of TiO_2 nanoparticle. As can be seen the latent heat of fusion of composite PCMs decreases with increasing mass fraction by (4%). The decrease can be attributed to two reasons: The first is that the nanoparticle specific heat is lower than the PCM specific heat which decreases the overalls thermal absorptance of the composite PCM. The second reason is that the nanoparticles change the molecular arrangement of the PCM crystals which affects on the ability to melt which eventually affect the latent heat of fusion. Hence the thermal property of system is affected **,Cai et al., 2008.**

Fig. 12 depicts the enhanced thermal conductivity (K) as a function of mass fraction of nanoparticles TiO_2 at three test temperatures. It seen that thermal conductivity decreases by (0.17%) with increasing temperature, but it increases with increasing loading of the nanoparticles TiO_2. When the mass fraction is (5 wt. %) and temperature is (15^oC) thermal conductivity is increased to (10%). However, the enhancement of thermal conductivity may be due to the dynamic viscosity.

6. CONCLUSIONS

In the present work, the following conclusions have been found:

1. The heat transfer process has been found to enhance by (11.4%) with adding mass fraction of (5 wt. %) nanoparticle TiO_2.
2. The solidification is found to occur faster than the melting due to low thermal resistance.
3. Thermal storage and release rate were found to increase by about (0.95) and (1.5) respectively times at (50^oC) as compared with the PCM without nanoparticles loading.
4. Increasing of nanoparticle TiO_2 concentration leads to a decrease in PCM latent heat of fusion by (4%), but with significant increase in composite PCM thermal conductivity.
5. Thermal conductivity decreases with increasing temperature by (0.17%), on the other hand, it increases with increasing of nanoparticle TiO_2 loading by (10 %) at mass fraction (5 wt.%) and temperature is (15^oC).

REFERENCES

- Abhat, ,A., 1980, *Review Physical Application*, Solar Energy 15, pp.477-501.
- Abhat, A., 1983, *Low Temperature Latent Heat Thermal Energy Storage: heat storage materials*, Solar Energy 30, pp. 313-332.
- Al hamdo, M, H., Bdoiwi B, A.and Hasan A, H. ,2014, *Transient Response of Different Highly Conductive PCM Composites*, Springer proceedings in physics, vol. 155, pp.253-264.
- Bhattacharya, P., Saha S., Yadav A., Phelan P. and Prasher R.,2004, *Brownian Dynamics Simulation to Determine the Effective Thermal Conductivity of Nanofluids*, Journal of Applied Physics 95(11):64, pp. 92-94.
- Cai, Y. Wei Q, and Huang F, 2008, *Preparation and Properties Studies of Halogen-Free Flame Retardant form-Stable Phase Change Materials Based on Paraffin/High Density Polyethylene Composites*, Appl Energy 85:7, pp.65-75.
- Garg, HP, and Prakach J., 2002, *Soler Energy Fundamentals and Applications*, New Delhi: Tata McGraw-Hill.
- HO, CJ.Gao JY., 2009, In Commune Heat Mass transfer 36:4, pp.67-70.
- Khodadadi, JM., and Hosseinizadeh SF., 2007, *Nanoparticle-Enhanced Phase Change Materials (NEPCM) with Great Potential for Improved Thermal Energy Storage*,Int Commune Heat Mass, 34:5, pp.34-43.
- Lee, S., and Choi SUS., 1996, *Application of Metallic Nanoparticle Suspensions in Advanced Cooling System*, New York ASME, vol. 72, pp. 27-34.
- Parameshwaran, R., Jayavel R. and Kalaiselvam S.J., 2013, *Therm anal Calorim*, 306, pp.4-9.
- Qinbo, H.,Shuangfeng W.,Mingwei T. and Yudong L.,2012, *Experimental Study on Thermo Physical Properties of Nanofluids as Phase-Change Material (PCM) in Low Temperature Cool Storage*, Energy cnnversion and management 64, pp. 199-205.
- Sharma, A., Tyag V, Chen CR. and Buddhi D, 2009, *Renew Sustain Energy Rev*, 13:3, pp. 18-45.
- Sharma, S.D.and Sagara K., 2005, *Latent Heat Storage Materials and Systems: a Review*, International Journal Green energy, 2, pp.56-62.
- Shin, D. and Banerjee D., 2011, *Enhancement of Specific Heat Capacity of High-Temperature Silica-Nanofluids Synthesized in Alkali Chloride Salt Eutectics for Solar Thermal Energy Storage Applications*, Int J Heat Mass Transfer 54:10, pp.64-70.

- Wu, S., Zhu D. and Li X., 2009, *Thermal Energy Storage Behavior of Al_2O_3-H_2O Nanofluids*, Thermochim Acta 483:7, pp.3-7.
- Xie, HQ., Wang JC., Xi TG., Liu Y.,Ai F. and Wu QR., 2002, *Thermal Conductivity Enhancement of Suspensions Containing Nanosized Alumina Particles*, Journal of Applied Physics 91(7):45, pp.68-72.

NOMENCLATURE

Cp= specific heat at constant pressure, kJ/kg.^{o}C.
D= diameter of capsule, m.
H= specific enthalpy, kJ/kg.
K=thermal conductivity, W/m.^{o}C.
L= length of test section, m.
M=mass, kg.
U= velocity, m/s.

GREEK SYMBOLS

∇= gradient, dimensionless.
μ=dynamic viscosity, N.s/m^2.
φ_v=particle volume fraction, %vol.
φ_w= particle weight fraction, %wt.

Table 1. Variation in melting, freezing temperatures and latent heat of fusion as a function of different weight % of Al_2O_3 nanoparticle, **Ho and Gao, 2009.**

Mass fraction of nanoparticles (wt.%).	Melting temperature (^{o} C)	Freezing temperature (^{o} C)	Latent heat of fusion (kJ/kg)
0	26.5	25.1	243.1
5	26	25	225.6
10	26.3	25.3	212.3

Table 2. The wt. % associated with vol. % of the nanoparticle sample at 20^0C.

wt.%	vol.%
1	2.57
3	2.68
5	2.798

Table 3. The properties of nanoparticle TiO_2 and PCM.

	Density (kg/m^3)	Thermal conductivity (W/m.K)	Specific heat (J/kg.K)	Melting temperature (^{0}C)
TiO2 (dp=10 nm)	4230	8.4	710	---
PCM (paraffin wax)	785	0.214	2871	62-68

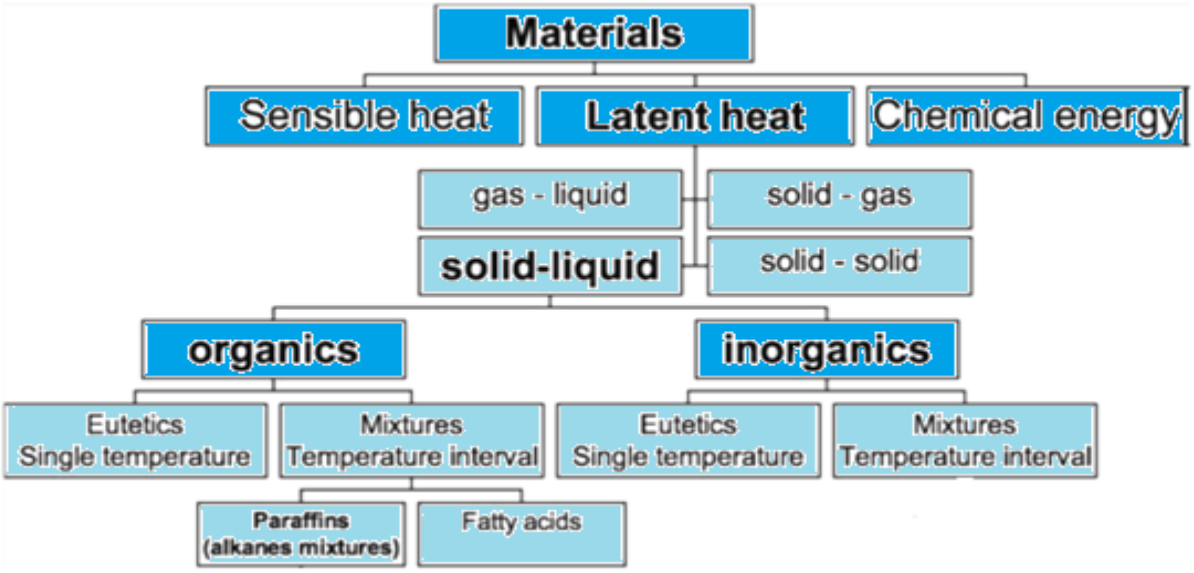

Figure. 1 Classification of energy storage materials, **Abhat, 1983.**

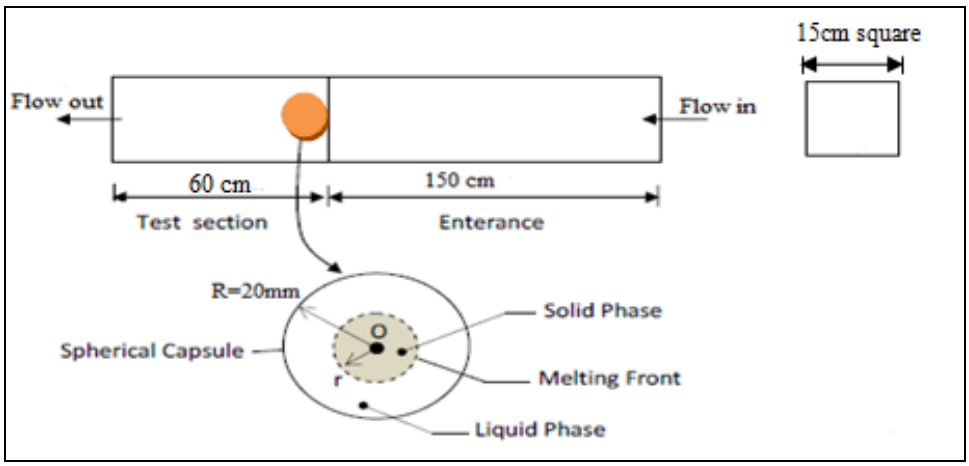

Figure. 2 Schematic diagram of the numerical model.

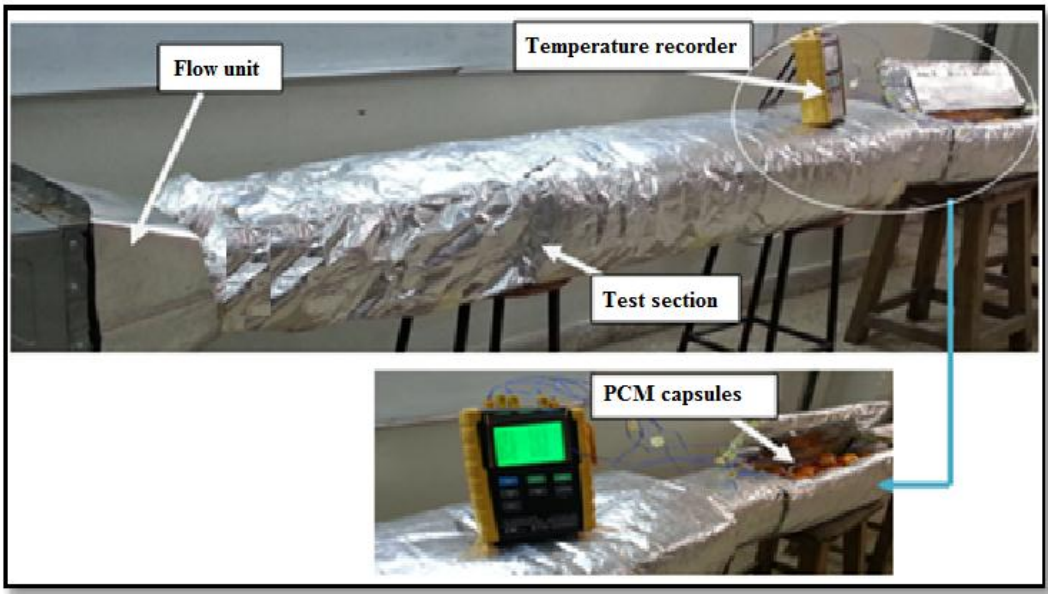

Figure. 3 Experimental test rig.

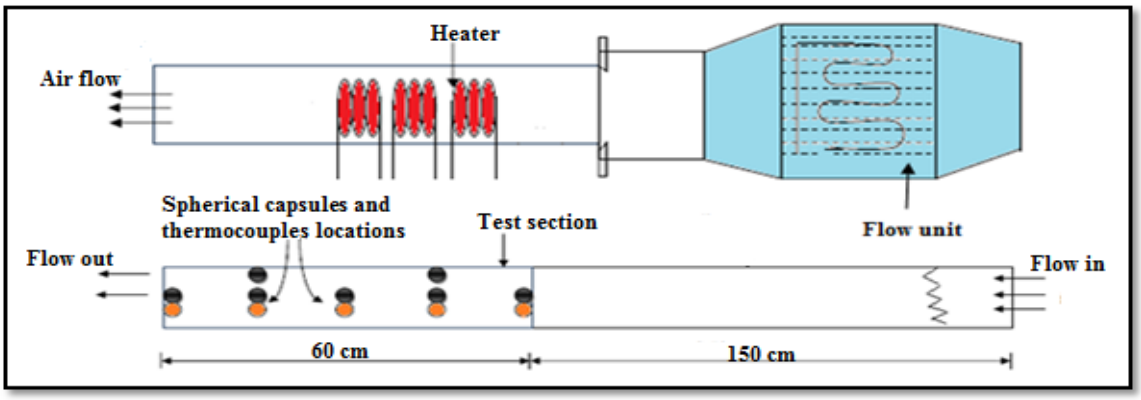

Figure. 4 Schematic diagram of the experimental apparatus.

Figure. 5 Thermal camera.

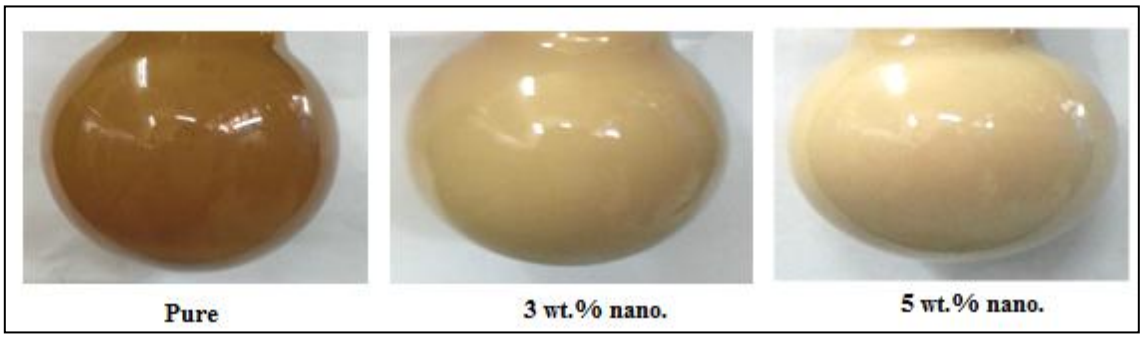

(a)

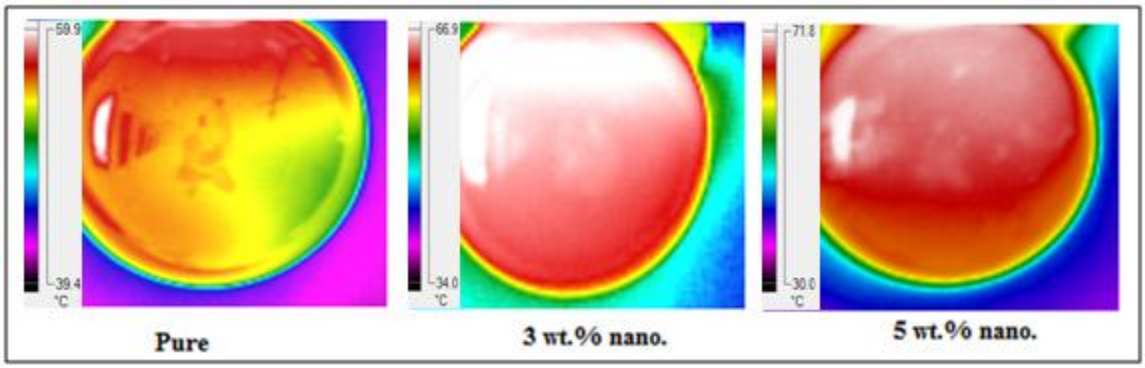

(b)

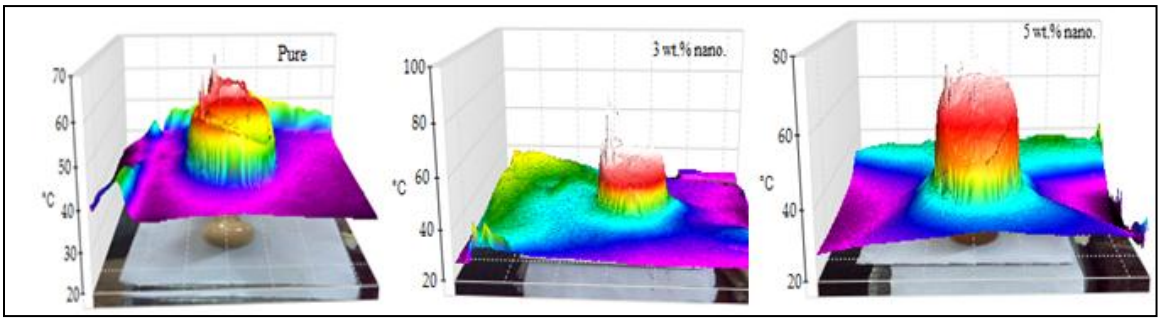

(c)

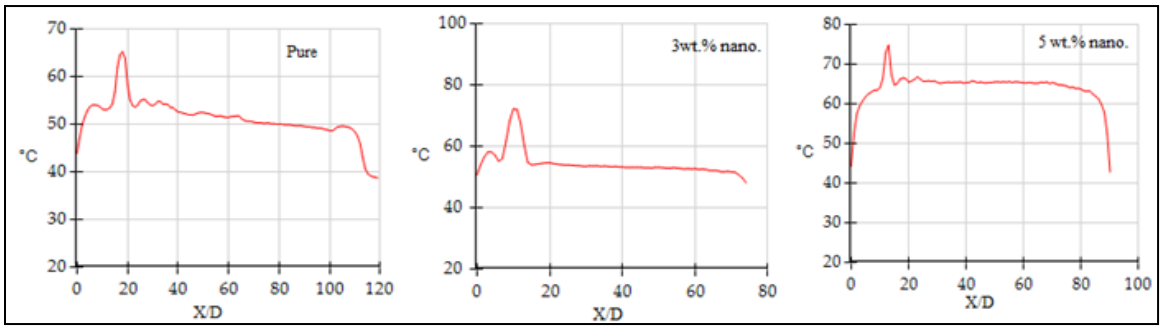

(d)

Figure. 6 (a) Photograph images (b) Thermal images of PCM at different weight% of nanoparticle TiO_2 at 60^{o}C and after15 minute, (c) 3-Dimantion images and (d) Temperature distribution.

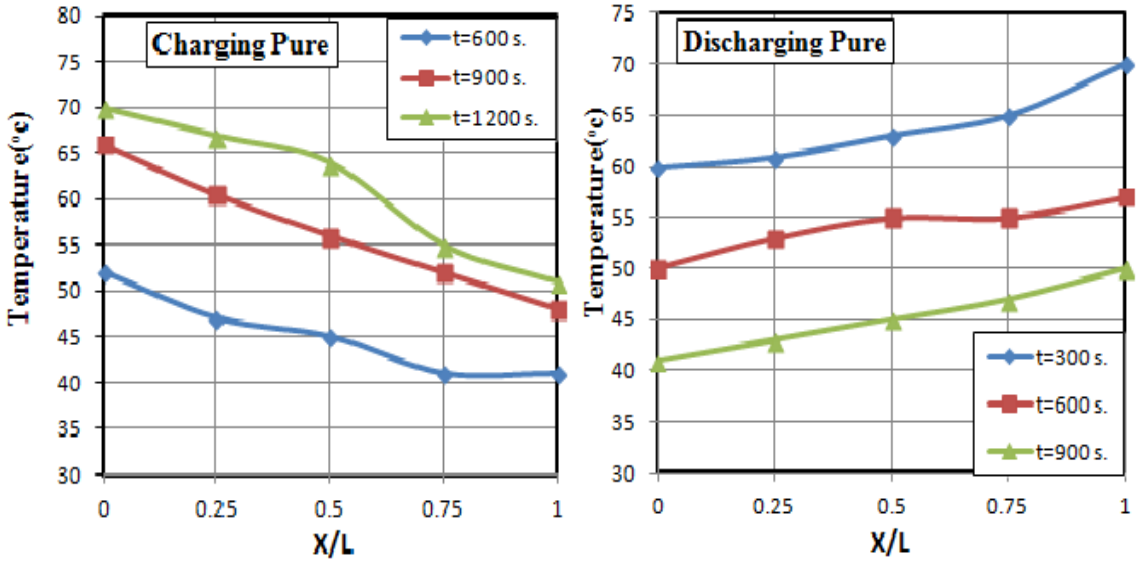

Figure. 7 Distribution the temperature of PCM along the axial direction of the test section during charging and discharging processes.

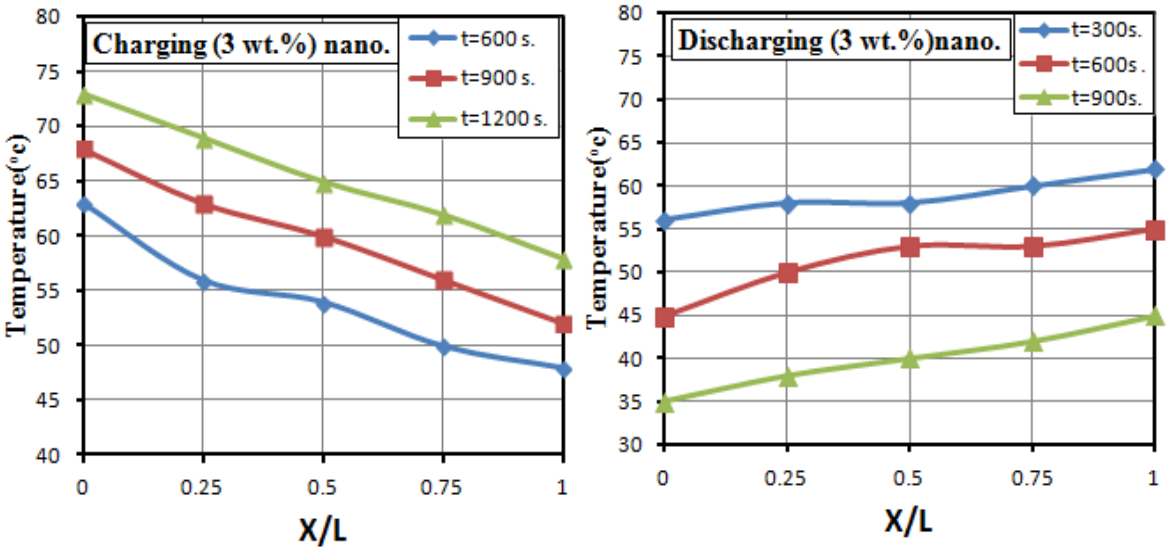

Figure. 8 Distribution the temperature of PCM with (3 wt. %) nano along the axial direction of the test section during charging and discharging processes.

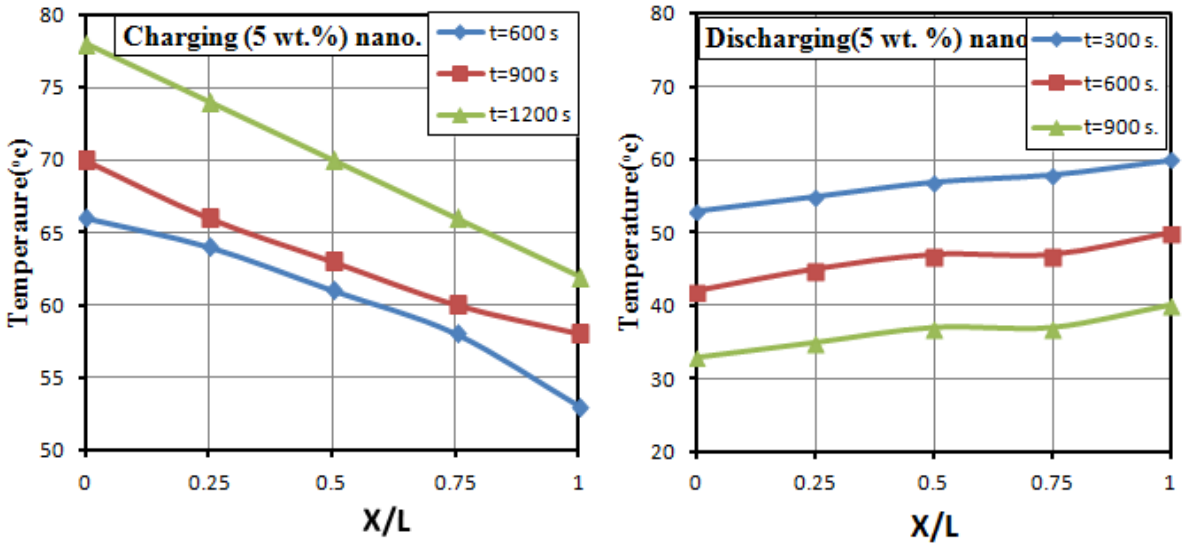

Figure. 9 Distribution the temperature of PCM with (5 wt. %) nano along the axial direction of the test section during charging and discharging processes.

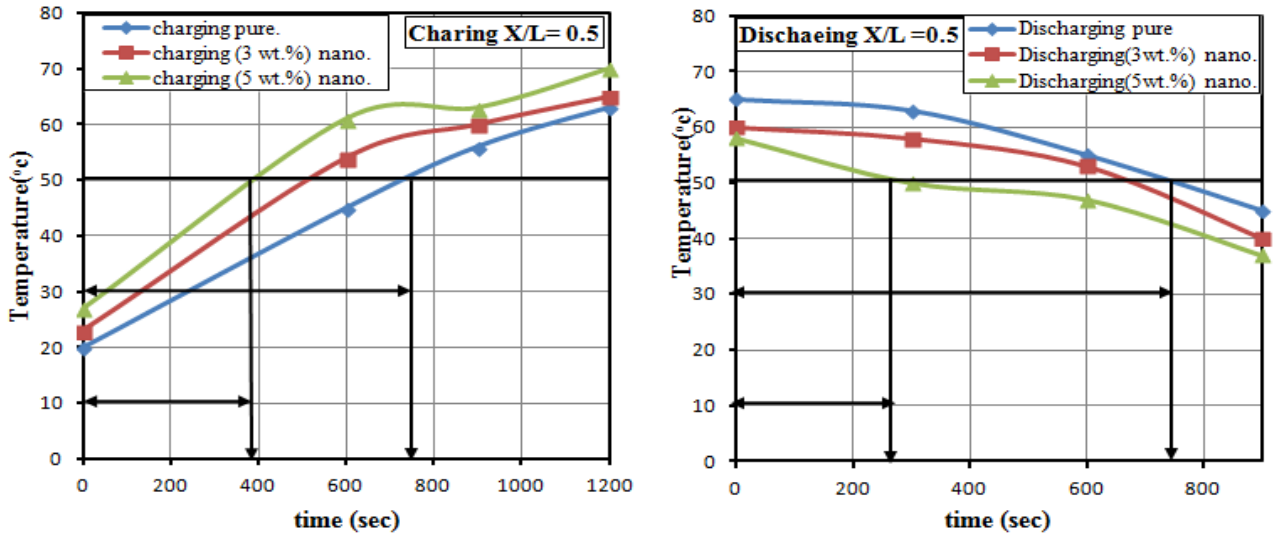

Figure. 10 Distribution the temperature of PCM with different weight fraction of nanoparticles along the axial direction of the test section during charging and discharging processes at X/L of (0.5).

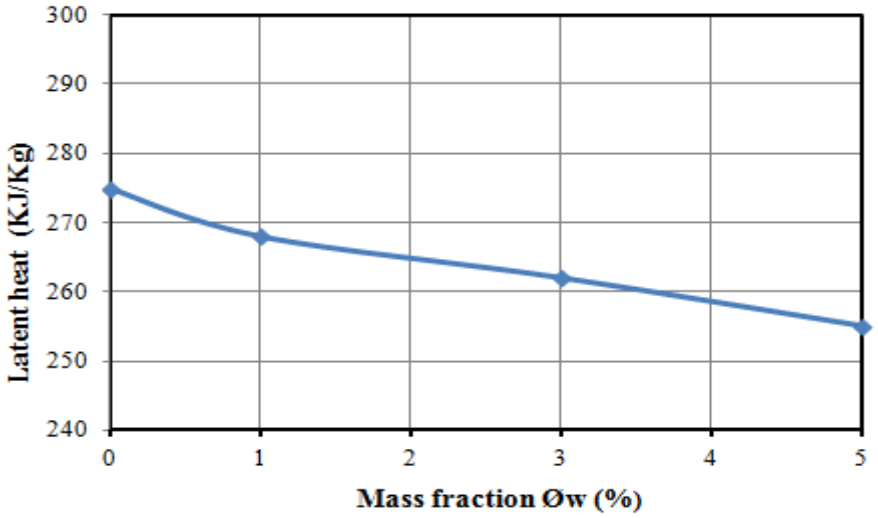

Figure. 11 Effect mass fraction of nanoparticles on the latent heat of fusion of composite PCMs.

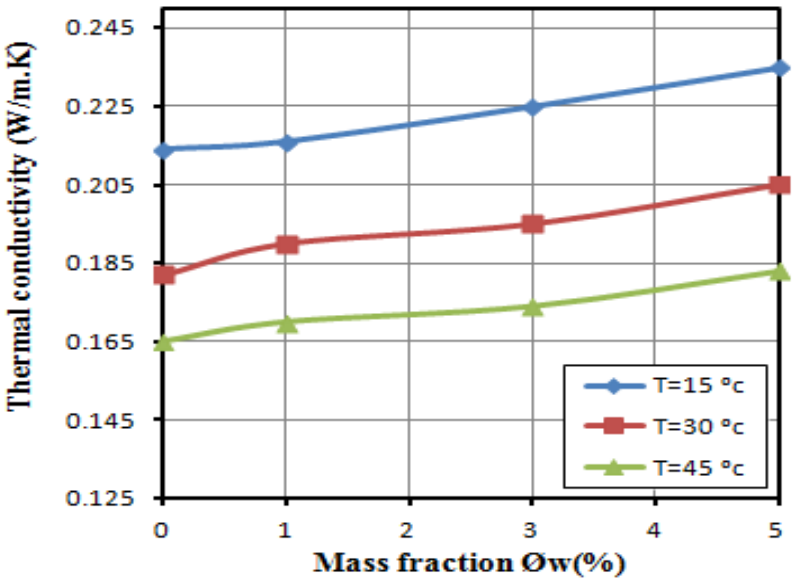

Figure. 12 Effect mass fraction of nanoparticles on the thermal conductivity at different temperatures.

Mechanical Properties Of AA 6061-T6 Aluminum Alloy Friction Stir Welds

Asmaa M. Abdullah
Lecture Assistant
Haweeja Technical Institute
E-mail:asmaamuneam@ymail.com

Abstract

The different parameters on mechanical and microstructural properties of aluminium alloy 6061-T6 Friction Stir-Welded (FSW) joints were investigated in the present study. Different welded specimens were produced by employing variable rotating and welding speeds. Tensile strength of the produced joints was tested at room temperature and the efficiency was assessed, and it was 75% of the base metal at rotational speed 1500 rpm and weld speed 50 mm/min. Hardness of various zones of FSW welds are presented and analyzed by means of brinell hardness number . Besides to these tests the bending properties investigated and showed good results in some specimen and not in another. The mamximum stress was 240 N/mm^2 at rotational speed 1500 rpm and weld speed 50 mm/min , while the maximum stress at 1250 rpm and 75 mm/min was 94 N/mm^2 . Hardness results showed lower values in heat affected and nugget zones than the base metal with improving of hardness at 1500 rpm, 75 mm/min .

Key words: friction stir welding , 6061 T6, mechanical properties.

الخواص الميكانيكية لسبيكة المنيوم 6061 T6 ملحومة بطريقة اللحام المزج الإحتكاكي

أسماء منعم عبدالله
مدرس مساعد
معهد تقني حويجة

الخلاصة

تضمن البحث دراسة الخواص الميكانيكية لعدة سرع خطية ودورانية لسبيكة المنيوم لحمت بطريقة لحام المزج الإحتكاكي.وقد صنعت عدة عينات لهذه السرع المختلفة (السرعة الخطية والدورانية),تم إجراء إختبار الشد بدرجة حرارة الغرفة وقد كانت قيمة كفاءة اللحام 75% من المعدن الأساس وكذلك تم إجراء إختبار الصلادة بطريقة برينل . إضافة لهذه الإختبارات تم إجراء إختبار الحني أيضاً لدراسة متانة منطقة اللحام والتي أظهرت نتائج جيدة عند بعض السرع و لم تظهر عند بعضها الآخر فعند سرعة دورانية 1500 دورة\دقيقة وخطية 50 ملم\دقيقة كانت قيمة أعلى إجهاد 240 نت\ملم^2 بينما كان اعظم إجهاد عند 1250 دورة\دقيقة سرعة دورانية و75 ملم\دقيقة سرعة خطية كان قد بلغ 94 نت\ملم^2 , نتائج الصلادة اظهرت نقصان بقيمة الصلادة في مركز اللحام وفي المنطقة المتأثرة بالحرارة عنه في المعدن الأساس بينما كان هنالك تحسن في نتائج الصلادة عند السرعة 1500 دورة\دقيقة و75 ملم\دقيقة.

الكلمات الرئيسية: لحام المزج الاحتكاكي ,6061 T6 ,الخواص الميكانيكية

1.INTRODUCTION

Friction stir welding (FSW) has proven to be an effective joining technique for a variety of different materials, including metals and polymers. Metals with low melting temperatures such as aluminum and copper were among the first to be joined by this technique using a steel tool **Heidarzadeh et al., 2012.** Friction-stir welding (FSW) is a solid-state joining process utilizing a rotating tool consisting of a pin and tool shoulder that applies severe plastic deformation and frictional heating into the joining materials. The benefits and uniqueness of the FSW have been well established for many light-weight metals and alloys that have difficulties in joining by the conventional fusion welding methods. The frictional heat and severe plastic deformation involved in the FSW, **Wanchuck et al.,2008.** Aluminum alloys are important for the fabrication of components and structures which require high strength, low weight or electric current carrying capabilities to meet their service requirements. Among all aluminum alloys, AA 6061 alloy plays

major role in the aerospace industry in which magnesium and silicon are the principal alloying elements. It is widely used in the aerospace applications because it has good formability, weldability, machinability, corrosion resistance and good strength compared to other aluminum alloys. When using the conventional arc welding techniques, long butt or lap joints between AA 6061 and other aluminum alloys are particularly difficult to make without distortion because of high thermal conductivity and special welding procedures and high levels of welder skill are generally required. AA 6061 Aluminum alloy cannot be TIG welded without filler wire because it leads to solidification cracking due to its chemistry The mechanical properties of the alloys are affected not only by their chemical composition but also by their condition, e.g. annealed, cold worked, precipitation hardened. The work pieces are secured against the vertical, longitudinal and lateral forces, which will try to lift them and push them apart during the process **Indira, 2011.** This highly plasticized material provides for some hydrostatic effect as the rotating tool moves along the joint, which helps the plasticized material to flow around the tool. The plasticized weld material then coalesces behind the tool as the tool moves away show **Fig.1**.

The basic concept behind FSW is simple: The non-consumable rotating tool with a specially designed pin and shoulder is inserted into the abutting edges of the two parts to be joined and traversed along the line of joint ,**Mohamadreza et al., 2011.** The FSW process mechanism and the tool geometry are shown in **Fig. 2, Adamowski et al, 2007.**

The tool is plunged into the part at a specified spindle speed and plunge rate until the shoulder makes contact with the material to be joined. Following a brief dwell period, the rotating tool advances along the weld path at a specified traverse rate and spindle rotation speed. The combination of heat input and tool geometry cause the material along the boundaries of the weld region to deform and mix together to form a solid joint **,Thomas and Robert, 2009.** Aluminum alloys of 2xxx, 6xxx and 7xxx series have been considered for substantial use in these industries. This ensues from their desirable strength to weight ratio, excellent formability, appropriate weldability and acceptable corrosion resistance. Depending on the specific application, corrosion behavior is a significant factor of a welded joint ,**Fahimpour et al., 2012.** As a result, the FSW shows a unique grain structure influenced by the severe thermo-mechanical deformation, recovery, and/or recrystallization at elevated temperatures during welding.

2. EXPERIMENTAL PROCEDURE

2.1 Material

Wrought 6061-T6 aluminum sheets having 4 mm thickness defined by code B0209-04 ASTM standard were welded together by FSW method .The plates were cut and machined into rectangular welding specimens of 200 mm × 100 mm cross-section. A schematic diagram of FSW plate dimensions is shown in **Fig.3**

Chemical composition and the mechanical properties of base metals are presented in **Tables 1 and 2** respectively. The initial joint configuration was obtained by securing the plates in position using mechanical clamps. The direction of welding was normal to the rolling direction. Single pass welding procedure was used to fabricate the joints. Trial experiments were carried out to find the working limits of welding parameters. The welding parameters used to fabricate the joints are presented in **Table 3**.

2.2 Tool

A CNC perpendicular milling machine used to weld the plates, and cylindrical tool steel X38 with (16mm) shoulder diameter and (5mm) pin diameter with plunging depth equal to 3.9 mm as shown in **Fig. 4**.
Welding system fixed at the machine with clamps and fixtures made of carbon steel as in **Fig.5**

2.3 Welding Parameters
The friction stir welding parameters was listed in **Table 3.** All welds were produced using the same tool, but varying rotational and welding speed. Two welded samples were produced for each weld parameter, in order to have samples for mechanical testing.

3. MECHANICAL TESTS
To the marked welding parameters tensile, bending and hardness tests done to the welding results as follow:

3.1 Tensile Test
It done at room temperature by using testometric apparatus and specimen dimensions ASTM E8 as shown in **Figs. (6- A** and **B**)

3.2 Hardness Test
A brinell hardness number method used to observe and determine the hardness value under 187.5 kg_f load for six welding test specimens at seven points (five in welding region and two at the base metal) . A brinell hardness number test was used to investigate the hardness of the welded joints at 60 sec time loading.

3.3 Bending Test
Root and face bend tests were used as an important tool to understand the ductility and toughness of friction stir welds bending, bending, the specimens are show in F**ig. 7.** The dimensions of bending specimen are 10 mm width and 100 mm length.

4. RESULTS AND DISCUSSIONS
Many types of defects can be observed from the overall cross-sectioned samples, like flash, voids and tunnel defects, flash defects could be seen in **Fig. 9**. Most of the as-welded specimens are free of tunnel defects as shown by eye that no defected line was noted long the welding line. This indicates that tunnel defects can be fully vanished in a relative broad parameter range. With the increasing of the shoulder diameter, So, it can be considered that, using a welding tool with a relative bigger shoulder is helpful to vanish tunnel defects in FSW **,Lei et al.,2012.** The parametric boundaries investigated in the present study have been defined based on previous experience in welding of the non- reinforced alloy 6061 **, Raghu et al., 2008.**

4.1 Tensile Results
In all cases the samples failed in NZ and the results are presented in **Fig. 10**. This can be attributed to the decreased heat input and relative limited softening of the HAZ **,Vladvoj et al.,2005** and because of the loss of strength (under matching). The stirring of the tool has a substantial influence on the reinforcement particle distribution and shape. It breaks off the sharp edges of the bigger particles and rounding them up at the same time. This action results in smaller, round particles in the nugget **,Raghu et al., 2008.** From **Fig.8,** the results were different according the parameters and the value of the ultimate tensile stress was 75% of the base metal at

rotational speed 1500 rpm and weld speed 50 mm/min. yield and ultimate tensile values of welded samples are shown in **Table 4**.

4.2 Hardness Results

Fig. 11, represents the hardness diagram of the joint FSW. The hardness of both the heat affected zone (HAZ) and the nugget zone (NZ) are lower than that of base metal (BM),but at speed 1500 rpm and 75 mm/min there is improving in the weld nugget zone and heat affected zone in spite of the still of high properties in the base metal ,also a difference between HAZ, NZ properties , the difference between HAZ (heat affected zone) and NZ (nugget zone) is attributable to the grain refinement in NZ (nugget zone) , caused by intensive stirring. The softest points of the joints correspond to the failure locations in tensile tests, should be noted that a local material softening occurs in the weld because of the thermal action of the welding process; in particular a localized softening in the NZ (nugget zone) is observed. Note that results will show increasing in hardness from center to the parent metal and the lowest value is observed in the nugget zone **,Adamowski and Szkodo, 2007.** The results of hardness due to the welding process and to the tool pin action, a reduction of the density of such particles is observed with the utilized instrument **, Barcellona et al., , 2006 .**

4.3 Bending Results

Some FS welded aluminium alloy 6061-T6 samples did not fail in bend test at 1500 rpm and 50 mm/min speed and 2000 rpm and 50 mm/min. The parts have been tested utilizing a customized bending test with the aim of highlighting their behavior it showed a very good bending results they stay successful in high load without failing it ensure the high quality of welding at some parameters, bending results are shown in **Figs.12** and **13**.

5. CONCLUSIONS

1. FSW was successfully at medium rotation and weld speed .
2. Reducing the plunging depth and the weld speed that will decrease the flash defects.
3. By softening the tool surface and the shoulder and pin surfaces voids could be reduced or not appears in weld results.
4. Hardness drop was observed in the weld region. The softening was mostly evident in the heat affected zone on the advancing side of the welds. This zone corresponds to the failure location in tensile tests **,Raghu et al., 2008.**
5. The material flow around the off-center features is more complicated than the conventional centered pin. It appears that higher temperature allow better material flow and joint strength with the new tool **,Mishra et al., 2007 .**
6. Some FSW welded aluminium alloy 6061-T6 samples did not fail in bend test at 1500 rpm and 50 mm/min speed .
7. The efficiency of welded metal is 75 % of the base metal at 1500 rpm and 50 mm/min.

REFERENCES

- Barcellona, G. Buffa, L. Fratini and D. Palmeri , 2006. *On Microstructural Phenomena Occurring in Friction Stir Welding of Aluminium Alloys* , Journal of Materials Processing Technology, pp 340–343.

- Heidarzadeh H. Khodaverdizadeh ، A. Mahmoudi, and E. Nazari , 2012.*Tensile Behavior of Friction Stir Welded AA 6061-T4 Aluminum Alloy Joints* , Elsevier, Vol. 37, , pp166–173.

- Dr.Ayad M. Takhakh and Asmaa M. Abdullah ,2012. *The Optimization Conditions of Friction Stir Welding (FSW) for Different Rotational and Weld speeds*, College of Engineering Journal (NUCEJ), Vol.15 No.2, 2012 pp.187 – 196.

- Raghu Babu, K. G. K. Murti and G. Ranga Janardhana, 2008. *An Experimental Study on the Effect of Welding Parameters on Mechanical and Microstructural Properties of AA6082-T6 Friction Stir Welded Butt Joints*, Engineering and Applied Sciences VOL. 3, ARPN Journal of,NO. 5. ISSN 1819-6608,PP 68-64.

- Indira Rani M., Marpu R.N. and A.C.S.Kumar, 2011. *A Study of Process Parameters of Friction Stir Welded AA 6061 Aluminum Alloy in O and T6 Conditions*, journal of engineering and applied scinces, vol. 6, No.2, Issn 1819-6608.

- Adamowski ,C. Gambaro , E. Lertora , M. Ponte ,and M. Szkodo, 2007. *Analysis of FSW welds Made of Aluminium Alloy AW6082-T6*, International Scientific Journal, Vol. 28, Issue 8, PP 453-460.

- Adamowski a and M. Szkodo, 2007. *Friction Stir Welds (FSW) of Aluminium Alloy AW6082-T6* , Journal of Achievements in Materials and Manufacturing Engineering ,VOL. 20 ,ISSUES 1-2 .

- Lei Cui, Lei Cui, Xinqi Yang ,Guang Zhou, Xiaodong Xu,and Zhikang Shen,2012. *Characteristics of Defects and Tensile Behaviors on Friction Stir Welded AA6061-T4 T-joints* , Materials Science and Engineering: A ,Elsevier ,Vol. 543, , PP 58–68.

- Mohamadreza Nourani, Abbas S. Milani and Spiro Yannacopoulos, 2011. *Taguchi Optimization of Process Parameters in Friction Stir Welding of 6061 Aluminum Alloy* , A review and case study, Engineering, vol.3, pp 144-155.

- Mishra,R.S. Freeney,T.A. and Webband ,2007. *Friction Stir Spot Welding of 6016 Aluminum Alloy* , TMS (the minerals, metals & materials society).

- Thomas Oakes and Robert G. Landers , 2009 .*Design and Implementation of a General Tracking Controller For Friction Stir Welding Processes*, University of Science and Technology,PP 5576-5581.

- Fahimpour,V. Fahimpour,V ، Sadrnezhaad,S.K and Karimzadeh,F., 2012. *Corrosion Behavior of Aluminum 6061 Alloy Joined ByFfriction Stir Welding and Gas Tungsten Arc Welding Methods*, Materials & Design Vol. 39, PP 329–333. .

- Vladvoj Očenášeka, Margarita Slámováa, Jorge F. dos Santosb,and Pedro Vilaça, 2005. *Microstructure and Properties of Friction Stir Welded Aluminum Alloys* , Hradec nad Moravicí,PP 1-8.

- Wanchuck Woo, leventa Balogh, Tamas Ungar, Hahu Choo, and Zhili Feng,2008. *Grain Structure and Dislocation Density Measurements in a Friction-Stir Welded Aluminum Alloy Using X-ray Peak Profile Analysis*, Materials Science and Engineering: A, Elsevier, Vol. 498, Issues 1–2, pp 308–313.

Table 1. Chemical compositin of 6061 alloy **, Fahimpour et al., 2012.**

Alloy	Cu	Mg	Mn	Fe	Si	Cr	Ti	Pb
6061	0.19	1.07	0.12	0.64	0.65	0.21	0.02	0.05

Table 2. Mechanical properties of base metal 6061 T6 alloy **,Adamowski et al., 2007.**

σyield Mpa	σultimate Mpa	E %	VHN
235	283	22	100

Table 3. Welding parameters.

Samples	Rotaiting speed rpm	Weld speed mm/min	Plunging depth mm	Reheating time Sec
F1	1250	50	3.9	60
F2	1250	75	3.9	60
F3	1500	50	3.9	60
F4	1500	75	3.9	60
F5	2000	50	3.9	60
F6	2000	75	3.9	60

Table 4. Yield and ultimate tensile results of welding samples.

Samples Of welding	Ultimate tensile stress N/mm^2	Yield stress N/mm^2
F1	198	59
F2	115	34
F3	215	64
F4	125	37
F5	150	45
F6	201	60

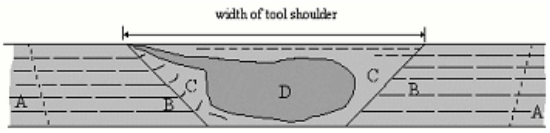

Figure 1. FSW regions **,Indira, 2011.**
A: unaffected material.
B: heat affected zone HAZ.
C: thermo-mechanical affected zone TMAZ.
D: nugget zone NZ.

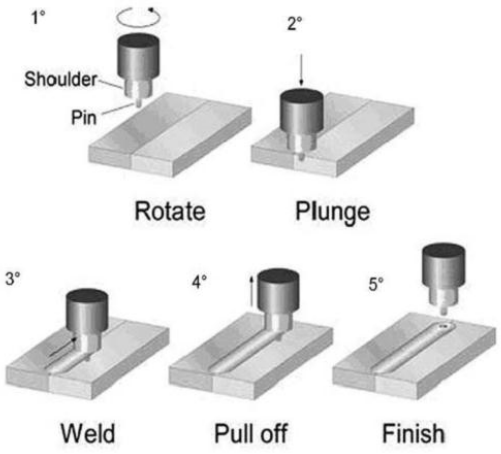

Figure 2. Schematic representation of FSW process **,Adamowski et al., 2007.**

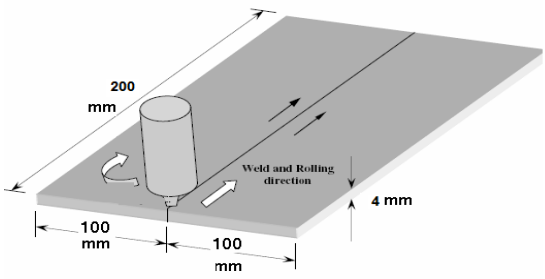

Figure 3. FSW plates dimensions.

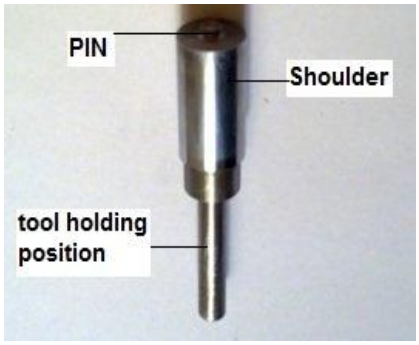

Figure 4 . Welding tool dimensions.

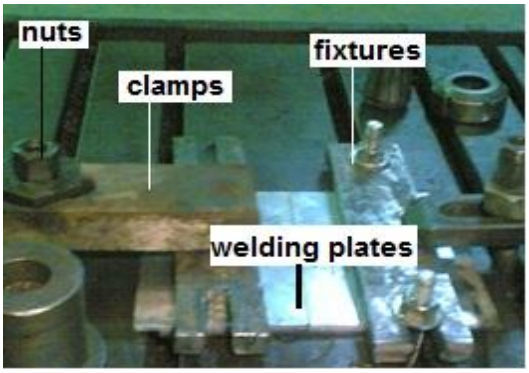

Figure 5. Welding clamping and fixtures system.

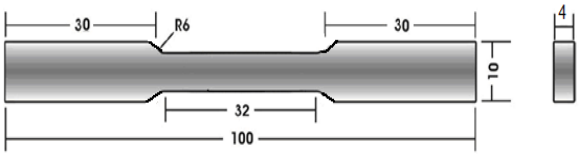

(A)

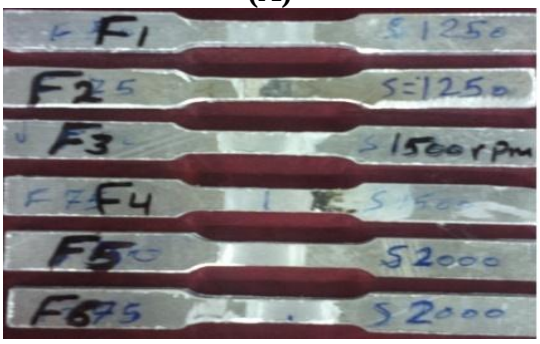

(B)

Figure 6. Tensile test specimen dimensions before test**.**

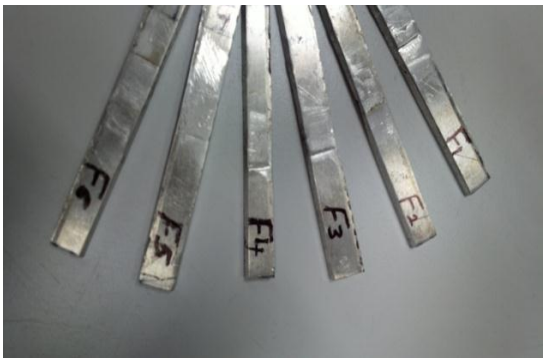

Figure 7. Bending test specimen.

Figure 8. Tensile specimen after test.

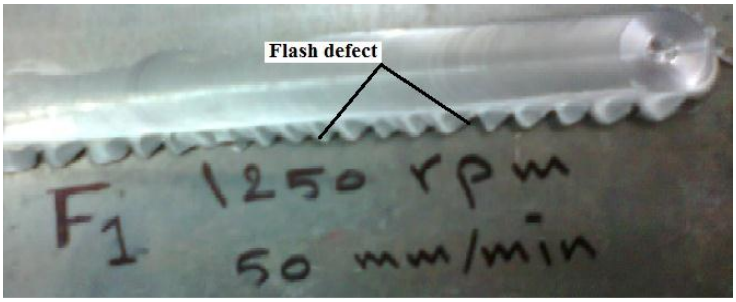

Figure 9. Flash defects at 1250 rpm, 50 mm/min.

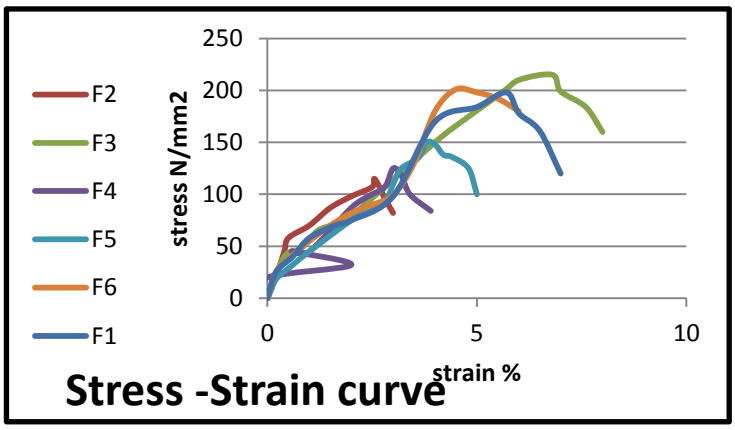

Figure 10. Tensile test results.

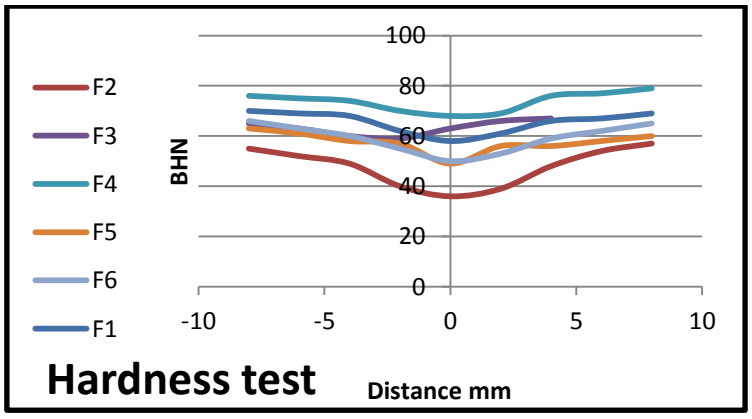

Figure 11. Hardness test.

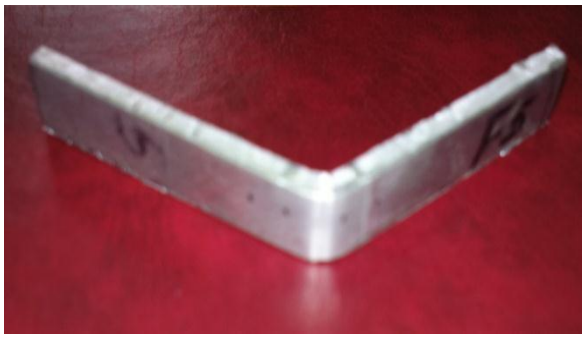

Figure 12. Bending sample result at 1500 rpm , 50 mm/min.

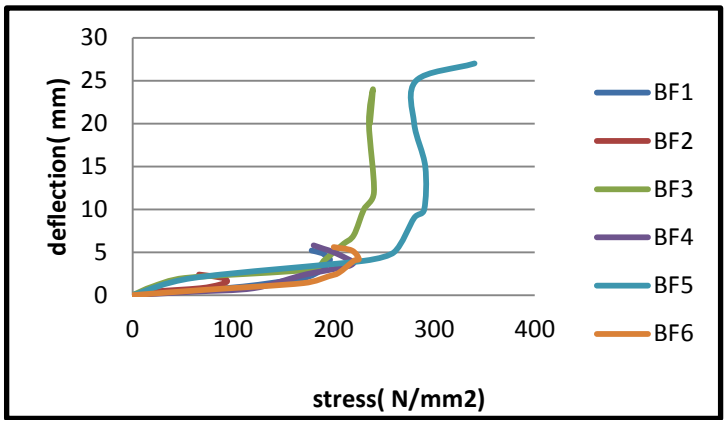

Figure 13. Bending results curve.

Coagulation - Flotation Process for Removing Oil from Wastewater Using Sawdust+ Bentonite

Ass. Prof. Dr. Abeer Ibrahim Alwared
College of Engineering / University of Baghdad
abeerwared@yahoo.com

Noora Saad Faraj
College of Engineering / University of Nahrain
nano_8098@yahoo.com

ABSTRACT

In many industries especially oil companies in Iraq consumed large quantities of water which will produce oil-contaminated water which can cause major pollution in agricultural lands and rivers. The aim of the present work is to enhance the efficiency of dispersed air flotation technique by using highly effective and cost-efficient coagulant to treat gas oil emulsion. The experimental work was carried out using bubble column made of Perspex glass (5cm I.D, 120cm height). A liquid was at depth of 60cm. Different dosage of sawdust +bentonite at ratio of 2:1 (0.5+ 0.25; 1+ 0.5 and 2+1) gm and alum at concentration (10,20and30mg/l) at different pH (4 and 7) were used to determine optimum dosages of coagulant. Jar test experiment showed that optimum dosage of (sawdust +bentonite) was (1+0.5gm) and alum concentration was 30 mg/l at pH=4.

The present study was conducted to evaluate the effect of various parameters pH (3, 4,7and 9); air flow rate (300, 500, 1000, and 1500 cc/min); initial oil concentration (300 up to 1000 ppm); concentration of Sodium dodecylsulphat surfactants ,SDS (25, 75and 150mg/l); and the effect of the addition coagulant (sawdust + bentonite at ratio 2:1) and alum (30mg/l) in the removal efficiency of oil from wastewater by coagulation –flotation process.

The study showed that the removal efficiency of COD, oil content and turbidity were related to the initial oil concentration; additive concentration of SDS and dosage of coagulants. It was found that the flotation rate increases when using coagulants, the fastest removal rate was obtained when pH 4 and also the higher removal efficiency achieved was for flotation (87%) and (95.7%) sawdust +bentonite; (97%) for alum in coagulation – flotation process.

Key words: oily wastewater; sawdust+ bentonite; alum; coagulation -flotation

التخثير والتعويم لازالة الزيت من المياه الملوثه باستعمال نشارة الخشب + البنتونايت

أ.م. د. عبير ابراهيم موسى
كلية الهندسة – جامعة بغداد
abeerwared@yahoo.com

نوره سعد فرج
كلية الهندسة – جامعة النهرين
nano_8098@yahoo.com

الخلاصة

في العديد من الصناعات وخاصة شركات النفط في العراق تستهلك كميات كبيرة من المياه والتي سوف تنتج عنها مياه الملوثة بالنفط ويمكن أن يسبب تلوث كبير في الأراضي الزراعية والأنهار.

الهدف من هذا العمل هو تعزيز كفاءة تقنية تعويم الهواء باستخدام مواد مخثرة فعالة للغاية و رخيصة لعلاج مستحلب زيت الغاز . تم تنفيذ العمل التجريبي باستخدام عمود التعويم المصنوع من زجاج البرسبيكس (قطره الداخلي 5 سم وارتفاعه 120 سم) . تم تثبيت ارتفاع السائل عند 60 سم .

تم استخدام جرعات مختلفة من خليط نشارة الخشب +البنتونايت وبنسبة 2 :1 (0.5+0.25 و 1+0.5 و 2+1) غرام وتراكيز مختلفة من الشب (10 و 20 و30) ملغم/لتر وعند قيم مختلة من الدالة الحامضيه (4 و 7) باستعمال اختبار الجرة وكانت افضل جرعة من المادة المخثرة نشارة الخشب + طين البنتونايت (1 +0.5 غرام) وافضل تركيز للشب وكان 30 مليغرام / لتر عند دالة حامضية = 4.

تم دراسة تاثير عوامل مختلفة الدالة الحامضية (3و4و7 و 9) ،ومعدل تدفق الهواء(300 و 500و 1000 و 1500 سم ^{3} / دقيقة) ،والتركيز الأولي النفط (300 حتى 1000 ملغم /لتر)، وتركيز المواد الخافضة للشد السطحيSDS(25 و75 و 150 ملغم/لتر) ، و تأثير المواد المخثرة نشارة الخشب + طين البنتونايت (1+0.5غرام) و الشب 30 ملغم /لتر في عملية التخثير والتعويم.

بينت الدراسة أن كفاءة إزالة COD ، محتوى الزيت و العكورة تزيد عند اضافة مادة ال SDS والمواد المخثرة وعند زيادة التركيز الاولي للزيت ، تم الحصول على ان اسرع إزالة كانت عند دالة حامضية = 4 كما وتم التوصل الى ان أعلى كفاءة إزالة لأفضل ظروف في عمود التعويم فقط (87%) وفي لتخثير والتعويم كانت(95.7%) عند استخدام لنشارة الخشب + طين البنتونيت و(97 ٪) عند استخدام الشب .

الكلمات الرئيسية : مياة ملوثة بالزيت ، نشارة الخشب + طين البنتونايت ، الشب ، التخثير و التعويم

1. INTRODUCTION

The threat of oil pollution increases with the expansion of oil exploration and production activities, as well as the industrial growth around the world. The study on the treatment of oily wastewater is a critical issue to the environmental protection as oil caused problems to the wastewater treatment facilities **,Wahi et al., 2013.**

Oil is one of the important contaminants in water and causes the wastewater problems in environments. In practice, this can form various types of oily wastewaters; for instance, soluble oil in water, emulsion with or without surfactants or floating film **,Painmanakul et al., 2009.**

Major spills, such as pipeline, tanker or storage tank accidents, create an acute problem of pollution. On the other hand, continuous low-level inputs are rarely noticed, and pose a serious threat to the environment as contamination accumulates. Therefore, diesel hydrocarbons create a world-wide problem of contaminated water and soil that require decontamination.

Diesel causes eye and skin irritation in humans, but otherwise its effects on humans are considered to be poorly investigated **,Muzyka et al., 2002.**

Standards and regulation were adopted for discharge of oily wastewater into surface water or sewage systems. These regulations may vary from country to country, and even within a country itself. Environment Canada (1976 b) has established a discharge limit for oil and grease of 15 mg/L at federal establishment. The allowable oil concentration for discharge into water bodies

are 2 to 10 mg/L and 5 mg/L in Germany and Switzerland, respectively. The allowable hydrocarbons and its derivatives discharge into water bodies about 3 mg/L in Iraq **,Iraqi preservation law, Law No. 2, 2001.**

Flotation separation is a primary water treatment process. Numerous studies on the potential of using flotation unit to remove oily emulsions have been reported by **Weltz et al., 2007 ,Xiao et al., 2007 and ,Painmnakul et al., 2009.**
Gas flotation units work by introducing small gas bubbles into the wastewater being treated. The gas bubbles acquire a small electronic charge, opposite that of the oil droplets. As the gas bubbles rise through the oily wastewater, oil attaches to the bubbles **,Bradley, 1990 and Arnold and Stewart, 2008.** Flotation units use two distinct methods for producing small gas/air bubbles needed to contact with water: pressurized gas/air injection and induced gas/air **,Cline, 2000.**

Flotation units typically serve as a preliminary step for water treatment in removal of suspensions and emulsion due to small differences in the density of continuous phase and of particulate phase. Flotation is an alternative as it has high efficiency as well as low operating cost **,Rubio et al., 2002.**

Generally, flotation separation can be divided into two types: (1) dispersed air flotation and (2) dissolved air flotation, (DAF).

Coagulation is the addition of chemicals and the provision of mixing so that particles and some dissolved contaminants are aggregated into larger particles that can be removed by solids removal processes such as sedimentation, dissolved air flotation, rapid filtration or membrane filtration **Fig.1** illustrates the process of coagulation, flocculation and flotation **,Dempsey, 2006.**

Saatci et al., 2001, studied the efficiency of treating vegetable oil factory wastewater by using the DAF coagulation with lime and alum; their analyses have shown that COD concentration of wastewater depends on its oil and grease content. This means that COD load could be importantly decreased with a decrease in oil and grease concentration.

The efficiency of wastewater treatment increased depending on the reduction of pH. And they concluded that the amount of sludge produced was reduced to 58 % compared to lime treatment and it was shown that clay could be an alternative to lime.

Soletti et al., 2005. studied the effect of ferric sulfate Fe $(SO_4)_3$ on pH values in dissolved air flotation of oily wastewater treatment by flotation column and obtained increase in coagulant concentration decrease pH value and enhance removal efficiency.

Welz et al., 2007. investigated the flotation of oil from wastewater in a laboratory scale mechanically agitated flotation cell and explores the effect of chemical factors (coagulant and flocculants) on flotation performance based on coagulant and flocculants dosages of (0.5 mg/l) when using $Al_2(SO_4)_3$ and 1.5mg/l when using lime. They found that the effect of coagulant dosage is more economical with the use of $Al_2 (SO_4)_3$ is the further justified due to lower cost as well as lower dosage and higher efficiency.

Mohammed and Zain-al-albideen 2007, studied the effect of coagulant (alum, clay) on removal efficiency of oily wastewater treatment by dissolved air flotation. They found that the removal efficiency of oil increase with alum until reaching the optimum dosage (25, 40, 70) ppm for initial oil concentration (30, 58, 136) ppm respectively, and the over dosage causes a decrease in the oil removal efficiency, but the other coagulant (clay) having higher removal

efficiency of oil the optimum dose of it was (2.5, 5, 9) ppm for the same initial oil concentration, but disadvantage of higher amount of sludge caused.

The removal of oil emulsion in wastewater had also been studied by **Painmanakul et al., 2009,** by utilizing the induced air flotation on the study of the effect of bubble hydrodynamic such as bubble size and addition of chemical coagulant (alum) to induced air flotation process and chemical dosage for the treatment of oily wastewater. They reported optimum pH value between the values of 8-10.This research study showed some similarity with the study of **,Xiao et al., 2007,**though the former used induced air flotation while the latter used DAF.

AlMaliky et al., 2009, studied oil and grease removal from two types of industrial wastewaters; Sweets and Dairy Industries wastewater by induced air flotation. Their results have shown that (3-5 l/min.) air flow rates are the optimal for having separation efficiencies between (77%- 80%) for effluent of Sweets industry, and (66%- 70%) for effluent of Dairy industry. The addition of (0.5 g/l) alum has proved significant influence on oil/ water separation efficiency, which could reach the values of (96%- 99%), using the air flow rates mentioned above, for Dairy and Sweets industrial effluents respectively. **Sulaymon and Mohammed, 2010.** studied the effect of coagulant $Al_2(SO_4)_3.17H_2O$and surfactant on separation efficiency of the emulsified kerosene in water in bubble column. The results indicate that the rate of the flotation enhanced when using SLES (sodium laurel ether sulfate) where the surface tension was reduced which leads the improvement of the separation efficiency, and found that adding $Al_2 (SO_4)_3.17H_2O$ and SLES together have a high coagulant effect than individually.**Tansel and Pascual, 2011,** investigated the removal of emulsified fuel oils from brackish and pond water by dissolved air flotation (DAF) with and without use of coagulants and they concluded that coagulant addition initially increased the petroleum hydrocarbon (PHC) removal by about 5–15%. **SEIN, 2011,** concluded that dispersed air flotation (DIAF) unit was efficient as a primary water treatment process in treating synthetic wastewater containing suspended solids and oily emulsions, also the addition of alum (coagulant) and anionic polymer (flocculent) is necessary to improve flotation via destabilization of colloids and agglomeration of destabilized particles. Oil and grease removal required a more agitated system compare to total suspended solid (TSS) and turbidity removal which suggest that a more turbulent system had a beneficial rather than disruptive effect on oil flotation. **Fu and Chung, 2011,** concluded that the use of a mixture of bentonite and sawdust, with sawdust being the vast majority, is highly effective for the coagulation of oil in water, giving coagulation efficiency 92% or above.

Sawdust by itself sinks in water. However, the coagulated aggregates float on water when sawdust is used with the bentonite. These aggregates are sheet-like, with the oil–bentonite–sawdust serving as a continuous matrix and apparently no upper limit to the aggregate sheet size. Without sawdust, the aggregates sink in water and the coagulation efficiency is only37%. The sawdust functions as a fibrous framework for the attachment of the coagulating oil and bentonite, thus facilitating floating aggregate formation and the subsequent removal of the aggregates. **Mohammed et al., 2013,** studied experimentally the use of induced air flotation (IAF) to treat the oily wastewater of Iraqi North Oil Company and they showed that the removal efficiency of oil was increased with increasing initial oil concentration, it reached up to 76 %. While it became 89%when using stirrer.The experimental results were translated to a computer program to predicate empirical correlation.**Vasseghian et al., 2013,** investigated the efficiency of Dissolved Air Flotation (DAF) for the treatment of refinery wastewater. The effect of several parameters on flotation efficiency namely, saturator pressure, and coagulant dose, on COD removal was examined experimentally. Experiments were done by using poly aluminum

chloride coagulant (PAC) at pressures 2bar up to 5bar and in three doses 15mg/l ،20mg/l and 25mg/l. The data obtained from COD experiments using neuro-fuzzy systems have been modeled. The correlation coefficient (R^2), root mean square error (RMSE) and sum of square error (SSE) of predicted values by using euro-fuzzy systems are obtained 0.9991, $6.35\times10^{-3}$and 4.04×10^{-5} respectively, which shows the high accuracy of neuro-fuzzy systems.
The aim of the present study is to studying the enhancement of oil removal by induced air flotation using sawdust +bentonite clay as coagulant.

2. EXPERIMENTAL WORK

2.1Gas Oil

Commercial gas oil was used in this study as the model pollutant**.** Gas oil was analyzed in Petroleum Research and Development Center/Ministry of Oil; the chemical compositions are as follows: 62.5% Paraffin's; 18.7% Aromatics and 18.8% Naphthenes.

The functional groups present in gas oil were detected by FTIR analysis; **Fig 2**. The physical properties of gas oil were shown in **Table 1.**

2.2 Materials

- Surfactant type Sodium dodecylsulphat (SDS) from Fisher Scientific was used as anionic collectors and is a white powder material with a chemical structure of ($C_{12}H_{25}OSO_3Na$), molecular weight 288.38 g/mol.
- pH adjustment was done by using (NaOH molecular weight is 40 gm/mole and purity of 100%, HCl molecular weight is 98.08gm/mole and purity of 100%).
- Sawdust was 100% recycled from solid wastes. It is collected, cleaned, milled, and then sieved to obtain grain sizes of (0.6-1) mm in diameter (effective diameter ,de =0.63mm , uniform coefficient,Uc =1.5).
- Bentonite clay Ca-Montmorillonite % (70min) CEC (65min)-pass from sieve 0.075mm (98%min) (Ministry of Industry and Minerals, Iraqi Geological Survey).
- Aluminum sulfate (Alum): commercial alum was used in the experiments, it is a white dry powder, has a formula of ($Al_2(SO_4)_3.18H_2O$) and molecular weight of (594.4 gm/mole).

2.3 Apparatuses

2.3.1 Flotation column

The experiments were performed into a cylindrical Perspex glass flotation column with the dimensions (5 cm inner diameter and 120 cm in height), samples were drawn from tap of 0.2 cm inside diameter, at the middle of column, and the column was operated in a semi- batch mode (batch wastewater, continuous air). **Figs.3** and **4** show a schematic and photographic diagram of experimental apparatus.

2.3.2 Jar test

The sedimentation jar test (Aztec environmental control LTD) was used to simulate conventional clarification, coagulation, flocculation and sedimentation steps. It consists of six beakers (volume of 1L) and stirrers, which could be adjusted to the same stirring conditions for all the beakers. The beakers were filled with 1L of sample and the coagulant was added simultaneously to all beakers.

2.4 Experimental Procedure

- The oil emulsion was prepared with the desired concentrations (300 up to 1000 ppm) by injection the required volume of oil into specific volume of distilled water. Agitation was achieved by bubbling air into the solution for half hour in a tank. The drop oil sizes distribution were found by using microscope type (novex) and the mean drop diameter was found to equal to 20μm
- After oil emulsion was prepared at different concentrations, SDS surfactant (25, 75 and 150 mg/l) was added then poured gently at the top of the column, air was fed to the column at different velocity (0.25, 0.424, 0.849 and 1.273cm/s) by rotameter and then samples were taken at different time intervals 10, 20, 30 and 40 min. pH was adjusted to a desired value using HCL or NaOH.

- Jar test constituted the preliminary test to determine optimum dosage of coagulant for (sawdust + bentonite at ratio 2:1 (Fu and Chung, 2011) (0.5+ 0.25; 1+ 0.5 and 2+1) gm , and alum concentration (10, 20, 30 mg/l) and determine its optimum pH from (pH=4 and pH=7) for optimum removal efficiency of oily wastewater.

The jar test speed was set to be 300 rpm for at least 1 min to mix the synthetic wastewater then coagulation was allowed to take place for at least 25 min or until the suspended solids form colloids. Jar test was stopped when coagulation was completed.

- Optimum dosages of coagulant will be added to oil emulsion at its best conditions , then it will be stirrer at speed 300 rpm for 1 min , then it will allowed to take place, coagulated oil emulsions were drained into the flotation tank, then the flotation process was allowed to take place for 40 minutes.

2.5 Analysis

2.5.1 Chemical oxygen demand (COD)

Chemical Oxygen Demand of samples was analyzed by using COD photometer apparatus. The appropriate amount of sample (2ml) was introduced into commercially available digestion solution (MR-Rang: 150-1500mg/L) containing potassium dichromate, sulfuric acid and mercuric sulfate. The mixture was then incubated for 120 min at 150^{o}C in a COD reactor (model RD-125, Lovibond Company, Germany). After oxidation is complete, the COD concentration was measured colorimetrically at 605 nm using a DR/2010 spectrophotometer.

2.5.2 Oil content

Oil content analysis was carried out using the oil content analyzer based on infrared analysis. It includes a single-beam, fixed wavelength, non- dispersive infrared filter-based spectrophotometer. Infrared radiation from a tungsten lamp is transmitted through a cylindrical, quartz curette containing a sample extract. The radiation which passed through the extract enters a detector containing a filter that isolates analytical wavelength in the 3400- to 3500-nanometer range (Model: HORIBA OCMA-350).

2.5.3 Turbidity

The turbidity of the samples was measured using turbidity meter **(laviboind meter with NTU unit).**

3. RESULTS AND DISCUSSION

3.1 Effect of pH

The effect of pH plays an important role in the removal of oil emulsion by flotation method. Different values of pH were examined in this study (3, 4,7and 9) keeping the other parameters constant (initial oil concentration 500 mg/l, flow rate 500cc/min and SDS= 20mg/l).By plotting the concentration ratio (C/Co) versus time at various pH values, **Fig.5** , it can be seen from this figure that concentration ratio(C/Co) of COD; oil content and turbidity decreases suddenly at the beginning of the run then the ratio began to increase slowly with time and it was found that the highest removal is achieved at pH= 4, which suggests that the repulsion between bubble and oil particle is lost and that adhesion between them is promoted.

3.2 Effect of Initial Oil Concentration

Different concentrations of initial gas oil concentrations (300, 500,700 and 1000) mg/L were studied keeping other parameters constant (pH=4, air flow rate 500cc/min and SDS= 20mg/l).By plotting the concentration ratio(C/C_o) versus time at various initial gas oil concentration, **Fig. 6**.

It can be seen from this figure that concentration ratio(C/C_o) of COD , oil content and turbidity increases with increasing initial oil concentration that because when the initial concentration of oil increased the contact of air bubble and oil droplet was increased , this result are in agreement with the results of **,Mohammed et al., 2013.**

3.3 Effect of Air Flow Rate on the Removal Efficiency

Different air flow rates were studied (300, 500, 1000, and 1500 cc/min) that is at gas velocity equal to 0.25 , 0.424 , 0.849 and 1.273cm/s respectively , with keeping the other parameters constant (pH=4, initial oil concentration=1000ppm and SDS= 20mg/l) in order to show the effect of air flow rate on the concentration ratio.

This effect is shown in **Fi g.7**. by plotting (C/Co) versus time at different airflow rate and from this figure, it can be seen that as gas flow rate increased, the concentration ratio increased, This is because increasing gas flow rate causes early bubble detachment, large fluid activities (stress) at the bottom section and bubble coalescence and (mostly) break up. This results in a large number of small bubbles which facilitates collision with oil **,Sulaymon and Mohammed, 2010.**

3.4 Effect of Surfactant

The removal rate of oil from water was studied at different of SDS surfactant concentrations (20, 75, 150 mg/l) in order to show the effect of adding anionic surfactant on the removal rate of oil. **Fig. 8** shows the effect of (SDS) concentration on the concentration ratio of (COD, oil content and turbidity).

The explanation of this improvement is that surfactant reduces surface tension and reduces the bubble diameter and increases the coalescence of larger diameter droplets which are more easily removed, that result is in agreement with **,Gregory and Zebal,1990.** They concluded that chemical pre-treatment of oil-water emulsions is based on the addition of chemicals that destroy the protective action of the emulsifying agent, overcoming the repulsive effects of the electrical double layers to allow the finally sized oil droplets to form larger droplets through coalescence.

3.5 Effect of Coagulant

In order to study the effect of natural coagulant on the removal efficiency of gas oil emulsion by flotation process,(sawdust +bentonite) at its optimum dosage (1+0.5gm) was added to flotation process and compare the results with alum at concentration 30mg/l, **Fig. 9**, it can be seen from this figure that there is slight difference between natural coagulant (sawdust+ bentonite) and alum, higher removal efficiency achieved was 87% for flotation only and 95.7%; 97% for sawdust +bentonite and alum respectively in coagulation – flotation process.

4. CONCLUSIONS

1. The emulsified oil with concentration (300-1000 ppm) can be removed by dispersed air flotation; higher removal rate was achieved at 40 minutes, and it was increased with increasing flow rate.
2. The best removal efficiency by dispersed air flotation was 87% at pH 4
3. In coagulation – flotation process ,the use of a mixture of bentonite and sawdust with sawdust being the vast majority for the coagulation of oil emulsion, increase the removal efficiency to 95.7% while when using alum ,the removal efficiency was 97%.

5. RECOMMENDATIONS

1. Utilization of other types of coagulant and using industrial or domestic wastewater for comparison purposes in terms of removal efficiency of oil emulsion.
2. Studying the oily wastewater treatment by fibrous coalescer process
3. Using two or three columns in order to enhance the removal efficiency.
4. Studying the effect of temperature.
5. Studying other bubble rise characteristics gas hold up trajectory and drag coefficient produced acceptable and consistent results

REFERENCES

- Al Maliky, S.J. , Al Ajawi, H. A., and Al Bayati, N. A., 2009, *Study of Induced Air Flotation for the removal of Oils from the effluents of Sweets and Dairy Industries* , The Iraqi Journal For Mechanical And Material Engineering, Special Issue (C) , Pp. 535-542.

- Cline, J.T., 2000, *Survey of Gas Flotation Technologies for Treatment of Oil and Grease"*, Presented at the 10th Produced Water Seminar, Houston, Pp.19-21.

- Dempsey, B. A., 2006, *Coagulation Characteristics and Reactions*, Interface Science in Drinking Water Treatment, Pp. 5-23.

- Fu, Y. and Chung, D.D.L., 2011, *Coagulation of Oil in Water using Sawdust, Bentonite and Calcium Hydroxide to form Floating Sheets*, Applied Clay Science, Vol.53, Pp. 634–641.

- Gregory, R., and Zabel,T.,1990, *Water Quality and Treatment*,4th Edition, New York, P.7 .

- Mohammed, T J. , Mohammed, S .S. and khalaf, Z. , 2013, *Treatment of Oily Wastewater by Induced Air Flotation*, Eng. And Tech. Journal, Vol. 31, Part (A), no.18, Pp. 88-99.

- Mohammed, T. J., Zain-al-albideen,E. H., 2007, *Treatment of Oily Wastewater for the North of Oil Company by Flotation Process*, 7th Egyptian Syrian conference on petroleum and Chem. Eng., Pp. 29-31.

- Muzyka, V., S. Bogovski, A. Viitak, and T. Veidebaum, 2002, *Alterations of Heme Metabolism in Lymphocytes and Metal Content in Blood Plasma as Markers of Diesel Fuels Effects on Human Organism*, Science of the Total Environment, Vol. 286, Pp.73-81.

- Painmanakul , P. , Kongkorn , K. , and Chawaloesphonsiyam N. ,2009 , *Treatment of Oily Wastewater by Fibrous Coalescer Process : Stage Coalescer and Model Prediction*, World Academy of Science , Engineering and Technology , Vol. 34, Pp. 317-322.

- Rubio, J., Souza, M.L. and Smith, R.W., 2002,*Overview of Flotation as Wastewater Treatment Technique*, Minerals Engineering, Vol. 15, Pp.139-155.

- Saatci, Y., Hasar, H., Cici, M., 2001, *Treatability of Vegetable Oil Industry Effluents through Physical -Chemical Methods*, Fresenius Environmental Bulletin, Vol.10, no. 2, Pp. 854 – 858.

- Sein, L.O., 2011, *Removal of Total Suspended Solids and Oil and Grease using Flotation Unit*, Project Report, University Tunku Abdul Rahman.

- Soltti, HV, Carralho, P.H.L, quitela, 2005,*Coconut industry wastewater treatment using dissolved air flotation*, department of Engenharia-University of federal de Alagoas.

- Sulaymon A. H. and Mohammed A., A., 2010, *Separation and Hydro dynamic Performance of Air –Kerosene System by Bubble Column*, International Journal of Chem. Reactor Eng. Vol., 8 Article A48.

- Tansel, B. and Pascual, B., 2011, *Removal of Emulsified Fuel Oils from Brackish and Pond Water by Dissolved Air Flotation with and without Polyelectrolyte use: Pilot-Scale Investigation for Estuarine and Near Shore Application*s, Chemosphere, Vol. 85 ,Pp. 1182–1186.

- Vasseghian, Y, Ahmadi, M. ,Gholami, R. and Aghaali, S., 2013, *COD Removal Prediction of DAF Unit Refinery Wastewater by Using Neuro- Fuzzy Systems (ANFIS) (Short Communication)*, Journal of Chemical and Petroleum Engineering, University of Tehran, Vol. 47, no.1, Pp.61-70.

- Wahi, R. , Chuah, L.A. , Choong, T.S. Y. , Ngaini, Z., and Nourouzi, M.M., 2013, *Oil Removal from Aqueous State by Natural Fibrous Sorbent: An overview*, Separation and Purification Technology, Vol. 113, Pp. 51–63.

- Welz, M., Baloyi, N. and Deglon, D., 2007, *Oil Removal from Industrial Wastewater using Flotation in a Mechanically Agitated Flotation Cell*, Available on website http://www.wrc.org.za.

- Xiao-bing Jiong-tian, Yong-tian, Cun-ying, Xiao-hua, 2007, *Separation Oil from Wastewater by Column Flotation"* Journal of China University of Mining and Technology, Vol. 17, no.4, 0546-0551.

Table 1. Physical properties of the gas oil.

Density(Kg/m^3)	**0.84**
Viscosity(Kg/m.sec)	**4.04**
API	**35.1**
Surface tension(N/m)	**0.0283**

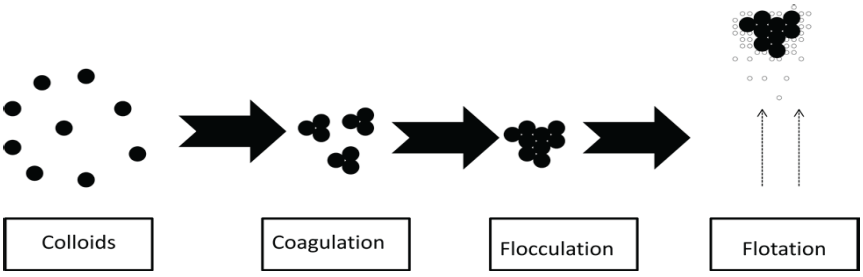

Fig.1 Process of coagulation, flocculation and flotation **,Dempsey, 2006.**

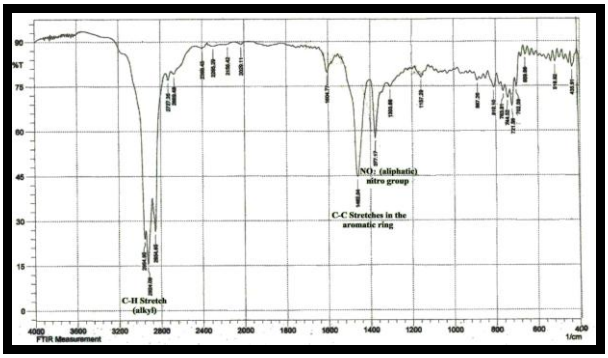

Fig.2 The functional groups of gas oil detected by FTIR analysis **,Ibn-Sina labs.**

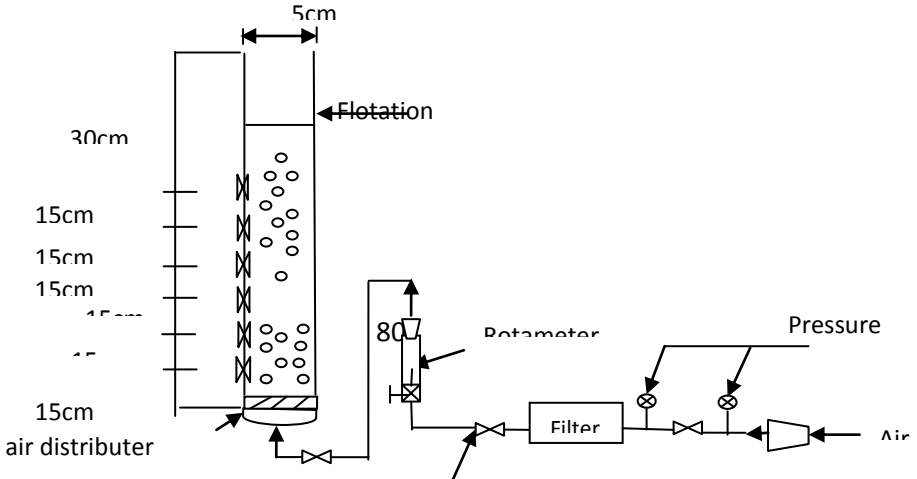

Fig.3: Schematic diagram for the experimental apparatus.

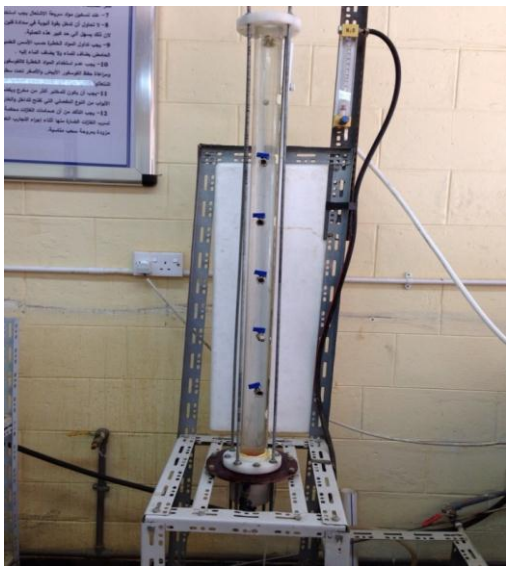

Fig.4:: Photographic diagram for the experimental apparatus

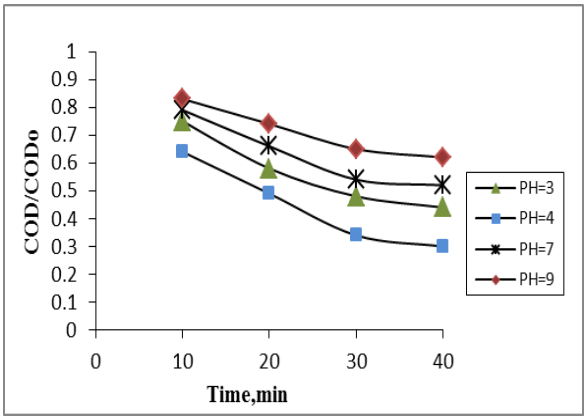

(a)Effect of pH on concentration ratio of COD

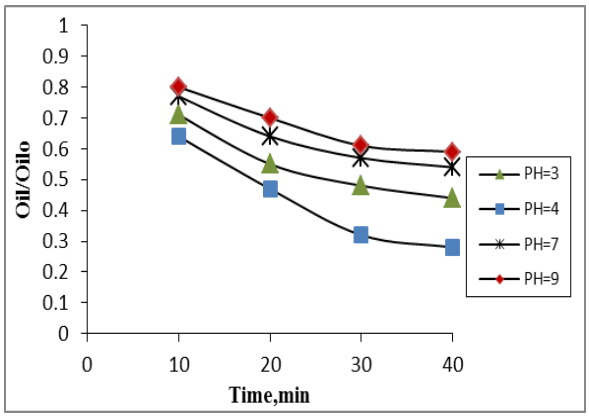

(b) Effect of pH on the concentration ratio of oil content

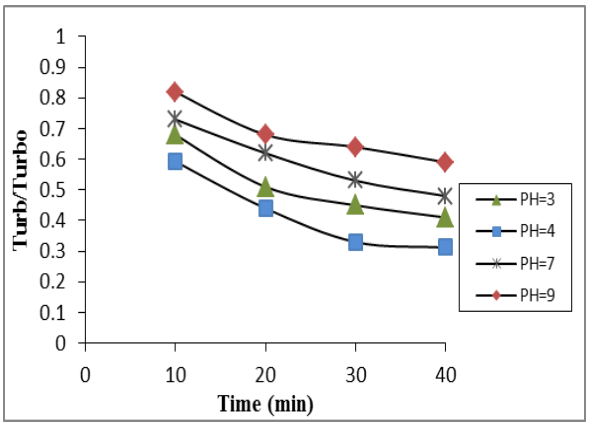

(c) Effect of pH on the concentration ratio of turbidity

Fig.5 Effect of pH on the concentration ratio at different time intervals at initial oil concentration 500mg/l, flow rate 500 cc/min and SDS=20mg/l.

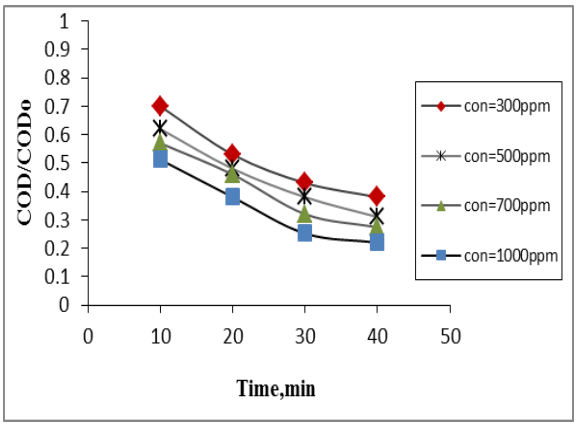

(a)Effect of the initial oil concentration on the COD ratio

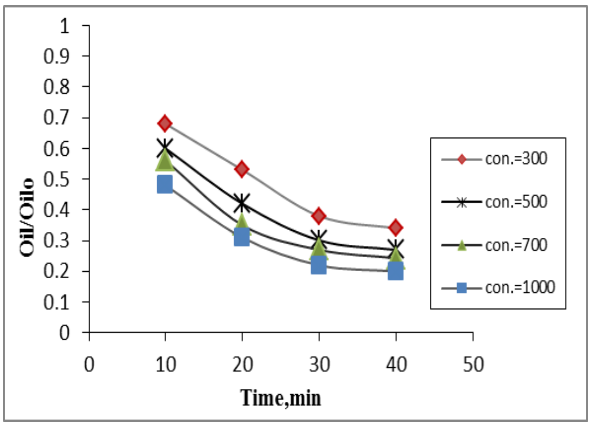

(b) Effect of the initial oil concentration on the oil content ratio

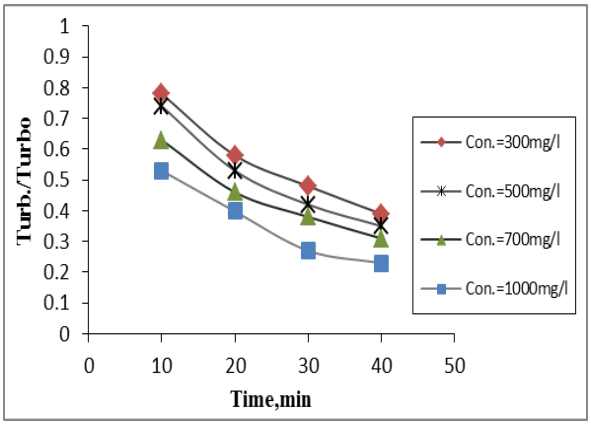

(c) Effect of the initial oil concentration on the turbidity ratio

Fig.6: Effect of the initial oil concentration on the concentration ratio at different time intervals at pH 4, flow rate 500 cc/min and SDS=20mg/l.

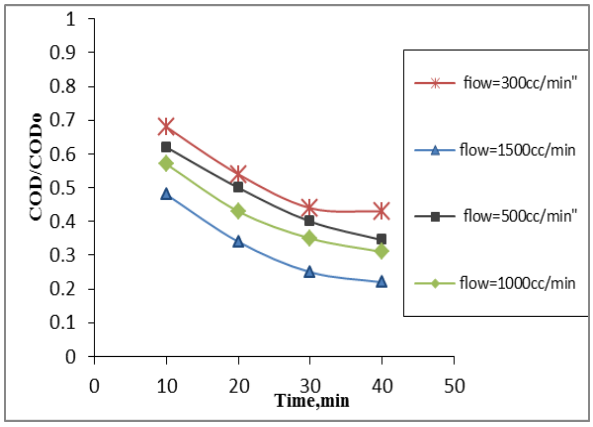

(a) Effect of the flow rate on the COD ratio

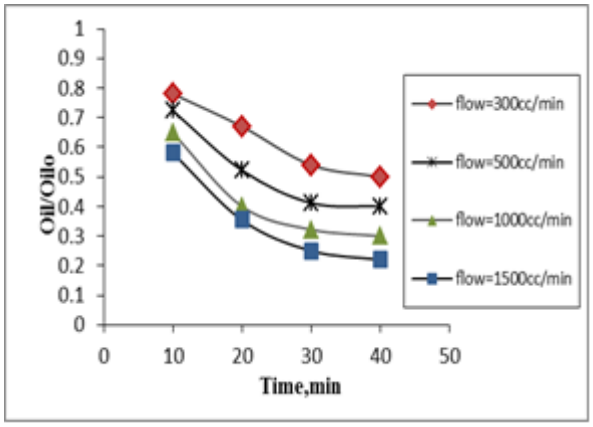

(b) Effect of the flow rate on the oil content ratio

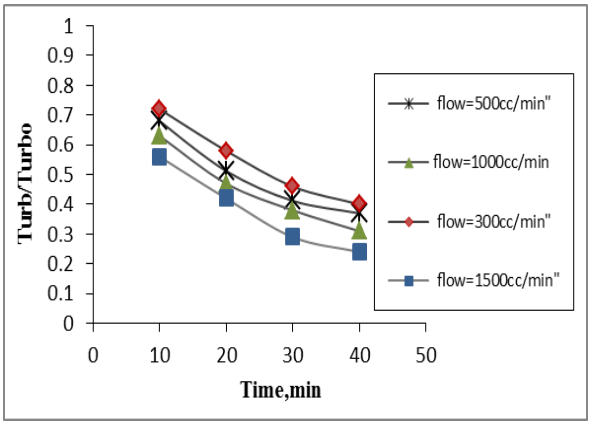

(c) Effect of the flow rate on the turbidity ratio

Fig 7: Effect of flow rate on the concentration ratio at different time intervals , initial oil conc. =1000mg/l, pH=4 and SDS=20mg/l.

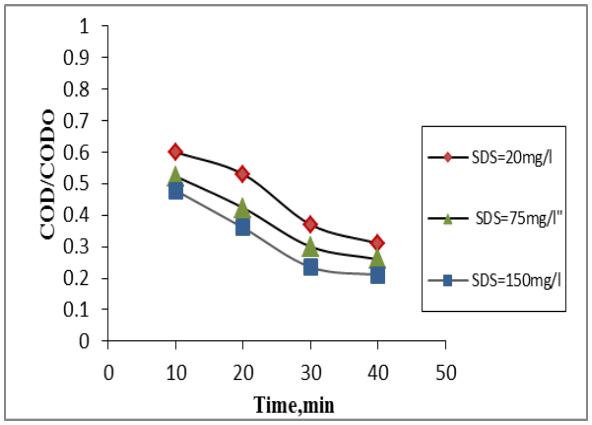

(a)Effect of the SDS on the COD ratio

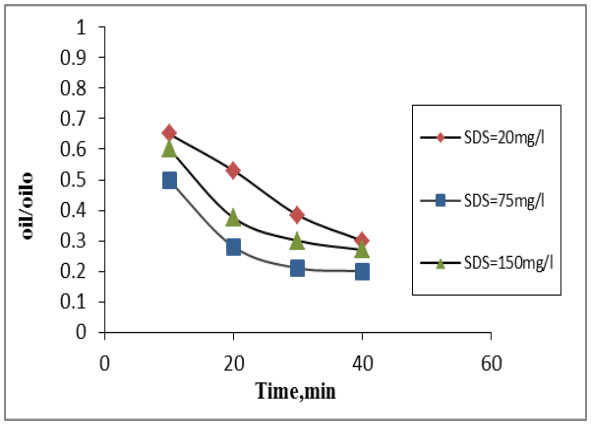

(b) Effect of the SDS on the oil content ratio

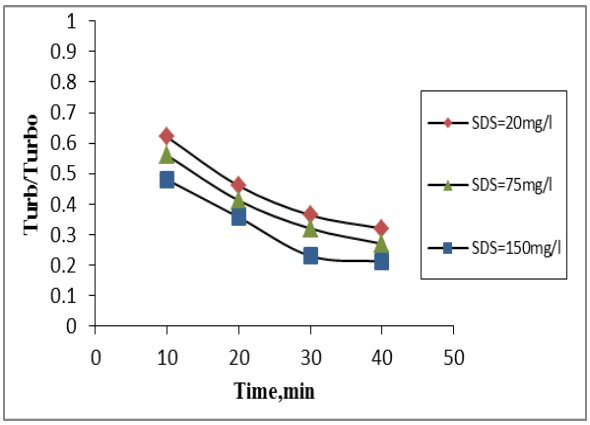

(c) Effect of the SDS on the turbidity ratio

Fig.8: Effect of SDS on the concentration ratio at different time intervals at initial oil conc. =1000mg/l, pH=4 and flow rate=1500cc/min.

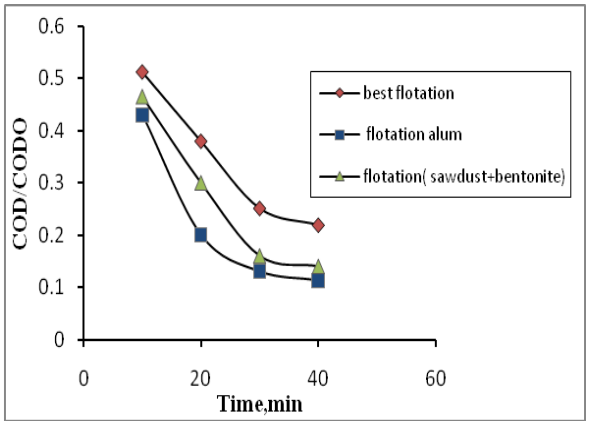

(a) Effect on the COD ratio

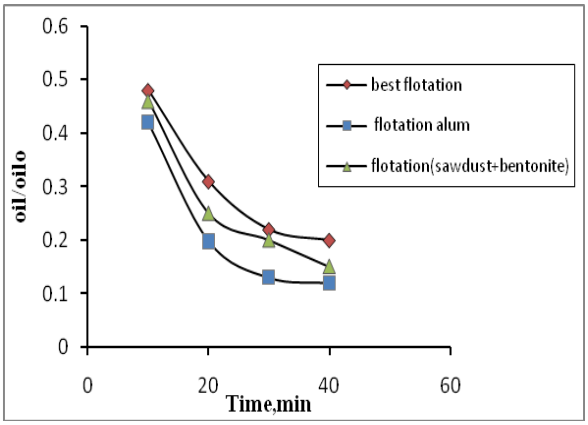

(b) Effect on the oil content ratio

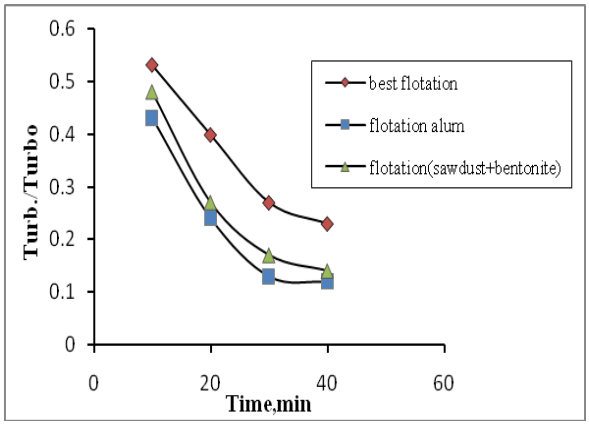

(c)Effect on the turbidity ratio

Fig.9: Effect of coagulant on the concentration ratio at different time intervals , initial oil conc. =1000mg/l, pH=4 and flow rate=1500cc/min and SDS=150mg/l.

Variation of Compression Index and Swelling Index with Degree of Saturation in Unsaturated Soils

Ala Nasser Aljorany
Professor
College of Engineering-University of Baghdad
Email:Ala Nasir Aljorany@gmail.com

Abdul Kareem Esmat Zainal
Assistant Professor
College of Engineering-University of Baghdad
Email: kareem_esmat@yahoo.com

Mustafa Yasen Namah
Student at Department of Civil Engineering
College of Engineering-University of Baghdad
Email:mutafayasen679@yahoo.com

ABSTRACT

The variation of compression index C_c and swelling index C_s with the degree of saturation S was studied on unsaturated and fully saturated soils for different degrees of saturation (100%, 91%, 85%, 75%, 60%). Several mathematical equations were found to describe these relationships, these equations can be used to predict settlement during the consolidation process in unsaturated and fully saturated soils.

Key words: unsaturated soils, soil compressibility, compression index, swelling index.

تغير معامل الانضغاط و معامل الانتفاخ مع تغير درجة التشبع في الترب غير المشبعة

أ. د. علاء ناصر الجوراني
استاذ في قسم الهندسة المدنيه جامعة بغداد

أ.م. د. عبدالكريم عصمت زينل
استاذ مساعد في قسم الهندسة المدنية جامعة بغداد

مصطفى ياسين نعمه
طالب في قسم الهندسة المدنية جامعة بغداد

الخلاصة

تم دراسة تغير معامل الانضغاط و معامل الانتفاخ في الترب غير المشبعة والمشبعة كليا لعدد من درجات التشبع (100% , 91% , 85% , 75% , 60%) وتم ايجاد عدد من المعادلات التي تمثل العلاقات بين تلك المعاملات و درجات التشبع المختلفة, ويمكن لهذا المعادلات ان تستخدم لتخمين الهبوط الحاصل في التربة خلال عملية الانضمام في الترب غير المشبعة والترب المشبعة .

الكلمات الرئيسية: الترب غير المشبعة، انضغاطية التربة، معامل الانضغاط، معامل الانتفاخ.

1. INTRODUCTION

The general field of soil mechanics can be subdivided into the portion dealing with saturated soils and the portion dealing with unsaturated soils. The differentiation between saturated soils and unsaturated soils becomes necessary due to basic differences in the material nature and engineering response. An unsaturated soil has more than two phases, and the pore-water pressure is negative relative to pore-air pressure, **Fredlund and Rahardjo, 1993.**

Any soil near the ground surface, present in an environment where the water table is below the ground surface, will be subjected to negative pore-water pressures and possible reduction in degree of saturation.

In recent years, with growing interest in the field of partially saturated soil, and the development of powerful numerical techniques, a number of literatures have been published.

Researchers have dealt with partially saturated soils in many categories.

Mainly, those could be put as: –

1. Partially saturated soil physics and properties,
2. Partially saturated soil constitutive relations and volume change prediction,
3. Partially saturated soil consolidation,
4. Partially saturated soil strength,
5. Heat and mass transfer in partially saturated soil, and
6. Laboratory and field-testing of partially saturated soil.

Consolidation in general for both fully saturated and partially saturated soils is concerned with volume change and with time as the excess pore-water pressure dissipates **,Biot, 1941, Fredlund, and Hasan, 1979, Lloret, and Alonso, 1980, ,Fredlund, 1982 ,Chang and Duncan, 1983,Dakshanamurthy et al., 1984 ,Fredlund and Rahardjo, 1986 and Zainal, 2000.**

A series of Oedometer tests were conducted to determine the compressibility of soil samples with different degrees of saturation.

The objectives of this study are:

1- The variation of the compression index C_c with different degrees of saturation.
2- The variation of the swelling index C_s with different degrees of saturations.
3- The variation of settlement with different degrees of saturation.

2. EXPERIMENTAL WORKS

Tests were conducted to obtain the physical properties of the clayey silt soil used for this study; all the results (Physical properties) are shown in **table. 1** then a series of Oedometer tests were conducted for different degrees of saturations (100%, 91%, 85%, 75%, and 60%), the results of settlement with loading and unloading were obtained to be investigated.

3. RESULTS OF TESTS

Oedometer tests were conducted according to ASTM D2435 (Non-observance of fully saturated sample) specifications to determine the variation of volume change described as void ratio (e) vs. the logarithm of the incremental loading to calculate the value of the compression index (Cc) and the value of swelling index (Cs) of the soil.

The same procedure was conducted for various values of degree of saturation namely (100%, 91%, 85%, 75%, and 60%). These values represent different air content states **,Smith and Smith, 1988.**

1. Fully saturated state where S=100% represents no air in the voids.
2. Partially saturated where S=91% represents air as occluded bubbles in the voids where there is no continuous path for the air through the voids.
3. Partially saturated where S=85% represents air that has continuous path in the voids as well as water phase.
4. Partially saturated where S=75% represents air that has continuous path in the voids but not for the water phase.
5. Partially saturated where S=60% represents air that has continuous path in the voids but not for the water phase where the soil approaches minimum value of relative permeability of water phase.

The standard procedure was conducted on the fully saturated sample. For the other sample where the degree of saturation is less than 100%, all the procedure steps were conducted except the soaking of the sample to maintain the degree of saturation as it is, so the deformation of the soil sample is determined for the degree of saturation of the sample.

The results for the soil samples with different degrees of saturation are shown in **table 2.** The table shows the load increment as the first field, other fields show the variation of the void ratio (e) in response to the applied load for different degrees of saturation.

Fig. 1 shows the results for the fully saturated soil sample (S=100%) showing the loading and the unloading conditions. Three lines are drawn in **Fig**. **1**, (Line 1) is the line connecting the Oedometer actual readings, (Line 2) is the unloading line to determine C_s, and (Line 3) is the Virgin line to determine C_c from the curve.

The same presentation of lines 1, 2 and 3 are also valid for **Fig. 2** which have the same details about Oedometer tests for the various degrees of saturation 91%, 85%, 75%, and 60% respectively.

Fig. 3 shows the variation lines for unloading conditions respectively; also describing different degrees of saturation, 100%, 91%, 85%, 75%, and 60% respectively.

4. DISCUSSION

The results of these tests obtained were analyzed thoroughly, and many relationships were obtained trying to describe the effect of the variation of the compression index C_c and the variation of the swelling index C_s with the degree of saturation S. these variations are shown in **table 3.**

Fig. 4 shows the variation of C_c with the degree of saturation, this relationship can be described by finding the best fit curve from the data shown in **Table 2.** There were two best fit curves found to describe the relationship between compression index C_c and the degree of saturation S as percentage (%), the first equation is a polynomial equation of the second degree and can be described as:

$$C_c = 2.8322\times10^{-5}S^2 - 2.1032\times10^{-3}S + 0.18857 \quad (1)$$

with $R^2 = 0.99744$

And the second equation is an exponential equation and can be described in Eq.(2) with $R^2 = 0.99708$.

$$C_c = 2.2926336\frac{e^{(0.02436263S)}}{S} \quad (2)$$

The two equations were extended to cover the range of degree of saturation down to 40%, the two equations can still give very good prediction of the variation of compression index C_c with degree of saturation S; though Eq. (2) was found to give more significant results for lower degrees of saturation, hence it is recommended to be used for prediction.
However, and for simplicity, a linear relationship can also be used to describe the variation between the compression index C_c and the degree of saturation without much loss of accuracy as can be seen in **Fig. 4** The mathematical relation is shown in Eq. (3), with $R^2 = 0.9765$.

$$C_c = 0.0024S + 0.0148 \quad (3)$$

Fig. 5 shows the variation of the swelling index C_s with the degree of saturation. Swelling index C_s has almost the same value for a particular soil (Suzuki et al., 2011), fig. 5 also shows that the best fit line has a slope of almost zero value (9×10^{-5}), average value is calculated to be 0.059775 and an average deviation of 0.001425, is defined as "the average of the absolute deviations of data points from their mean", and is shown in Eq. (4).

$$\frac{1}{n}\sum|x - \bar{x}| \quad (4)$$

where:
n= number of data points
x=data point, and
$\bar{x}$ = average

All this can tell that there is no loss of significant in using constant value for the value of C_s which represents the slope of the unloading curve.

5. VARIATION OF SETTLEMENT WITH THE DEGREE OF SATURATION.

It is noted from **Fig. 6** that the settlement increases with the increase of the degree of saturation for the same loading that was used for all tests. **Table 4** shows the variation of settlement ratio (s/H) which is the settlement normalized by dividing the settlement value (s=ΔH mm) by the height of the ring used (H=19 mm), and the value (s/H) is obtained for each degree of saturation.
The variation is shown in **Fig. 6** where the minimum value of settlement ratio is found at the lower degree of saturation and the maximum value of settlement ratio is found at the higher degree of saturation.
This is believed to be due to particles rearrangement caused by more lubrication provided by the presence of more water at higher degrees of saturation hence giving more settlement, and vice versa where less water provides more friction which resists settlement. This behavior is similar to the soil behavior in "wet of optimum" and "dry of optimum" sides of the compaction curve respectively.
From **Table 4,** we can also obtain the ratio of maximum over minimum value (max./min.) of s/H for each loading case, the variation is shown in **Fig. 7**.
Examining these values reveals that the variation is close and an average value (max./min. = 1.63244) i.e.($\Delta H_{s=100}/\Delta H_{s=60}$=1.63244) can be taken as a suggested value for settlement ratio calculations, (e.g. if settlement for 1 m layer of fully saturated soil was found to be 5 cm

(s/H=0.05) then for 60% saturation of the same soil and also for 1 m layer, the settlement ratio is 0.05/1.63244=0.03 and the settlement is 3 cm.). This ratio is a good aid in estimating the settlement value at any degree of saturation less than 100% by only knowing the settlement value of the fully saturated soil sample. **Fig. 8** shows the best fit lines obtained from the curves of **Fig. 7** while **Table 5** shows their equations and the correlation coefficient squared.

For practical purposes of shallow foundation design usually q_{all} net for Iraqi soil which is approximately between 25 kPa to 100 kPa, it is recommended to use equations related to number 2, 3, and 4 **Table 5** where these loading conditions are most common and cover most Iraqi soil types either soft soils in southern parts or stronger soil in northern parts. These equations give more accurate values of settlement ratio which can be used to predict settlement in unsaturated soils.

As an example, the loading of 100 kPa is discussed more thoroughly, and this procedure can be implemented to any loading case.

Three types of best fit lines are found to have the highest coefficient of regression. These suggested equations are ordered from highest coefficient of regression to the lowest as shown in **Fig. 9**

1) Polynomial of the second degree

$$\frac{s}{H} = 0.000027S^2 - 0.003132S + 0.173022 \quad (5)$$

$R^2 = 0.990775$

2) Exponential relationship

$$\frac{s}{H} = 0.040036e^{0.011574S} \quad (6)$$

$R^2 = 0.949194$

3) Linear relationship

$$\frac{s}{H} = 0.001210S + 0.005647 \quad (7)$$

$R^2 = 0.918432$

For simplicity, the linear relationship is recommended to be used for prediction of the settlement without much loss of accuracy.

6. CONCLUSIONS

1. The settlement increases with the increase of the degree of saturation for the same loading that was used in all tests.
2. The compression index (C_c) variation with degree of saturation (S) can be expressed as an exponential relationship with very good accuracy (R^2=0.99), and as a second degree polynomial (also R^2=0.99); and for simplicity, it can be expressed as a linear relationship without too much loss of accuracy (R^2=0.98).
3. The swelling index value (Cs) is approximately constant for unloading curve for different degrees of saturation as expressed in the present work and previous work of (Suzuki et al., 2011).

4. The settlement ratio which can be expressed as ($\Delta H_{s=n}/\Delta H_{s=100}$ = constant) (n=any degree of saturation) can be approximated as a constant value for a specific soil, then this ratio can be used to predict settlement for any degree of saturation depending on the settlement of the fully saturated soil.
5. The variation of (s/H) with the degree of saturation for a specific loading can be expressed as linear relationship with very good approximation as best fit line gives good accuracy as shown in the **Table 5** and **Fig. 8** an even more accurate expressions are found.

REFERENCES

- Barden, L., Anthony O. Madedor, and Geoffrey R. Sides, 1969, *Volume Change Characteristics of Unsaturated Clay*, Journal of the Soil Mechanics and Foundations Division, ASCE, Vol. 95, No. SM1, Jan., pp 33–50.

- Biot, M. A., 1941, *General Theory of Three–Dimensional Consolidation*, Journal of Applied Physics, Vol. 12, No. 2, pp. 155–164.

- Chang, C. S., and J. M. Duncan, 1983, *Consolidation Analysis for Partly Saturated Clay Using an Elastic–Plastic Effective Stress–Strain Model*, International Journal for Numerical and Analytical Methods in Geomechanics, Vol. 7, pp 39–55.

- Dakshanamurthy, V., Fredlund, D.G. and Rahardjo, H.,1984.*Coupled Three Dimensional Consolidation Theory Of Unsaturated Porous Media*, Proceedings of the fifth International Conference on Expansive Soil, Adelaide, South Australia, May 1984.

- Fredlund, D. G., and Jamshed Hasan, 1979, *One–Dimensional Consolidation Theory: Unsaturated Soils*, Canadian Geotechnical Journal, 16, pp. 521–531.

- Fredlund, D. G., and Morgenstern, N. R. (1976). *Constitutive Relations for Volume Change in Unsaturated Soils*, Canadian Geotechnical Journal, Vol. 13, No.(3), pp. 261–276.

- Fredlund, D.G.,1982,*Consolidation of Unsaturated Porous Media*, Proceedings, Symposium on Mechanics of Fluid in Porous Media-New Approaches in Research, NATO Advance Study Institute, Newark, DL.

- Fredlund, DG, and Rahardjo, H, 1986, *Unsaturated Soil Consolidation Theory and Laboratory Experimental Data*, Consolidation of Soils: Testing and Evaluation, ASTM STP 892, R. N. Yong and F. C. Townsend, Eds., ASTM, Philadelphia PA, pp. 154-169.

- Fredlund, D. G., H. Rahardjo, 1993, *Soil Mechanics for Unsaturated Soils*, John Wiley & Sons.

- Lloret, A., and, Alonso E.E.,1980,*Consolidation of Unsaturated Soils Including Swelling and Collapse Behavior*, Géotechnique 30, No. 4, pp. 449–477.

- Matyas, E. L., and Radhakrishna H.S.,1968, *Volume Change Characteristics of Partially Saturated Soils*, Géotechnique, 18, pp. 432–448.
- Smith, G. N., and Smith, Ian G. N., 1998, *Elements of Soil Mechanics*, Blackwell Science Ltd.
- Suzuki, H., R. Tsutsumi, and Y. Okano,2011,*Properties of Compression of Unsaturated Clay and Examination of Effective Stress, By Collapse Test*, PP.185-189.

  Proceedings of The 5th Asia Pacific Conference On Unsaturated Soils, Pattaya, Thailand, 14-16 NOVEMBER 2011 PP.185-189.
- Zainal , A. E. (2002). *Solution of Some Problems of Partially Saturated Soils Using the Finite Element Method*, Ph.D. thesis, University of Baghdad .

Table 1. The physical properties tests.

No.	Property	symbol	Value	Specific. standard test
1	Field water content	w_n	34%	ASTM D2216
2	Field mass density	ρ_{wet}	1.92 gm/cm^3	ASTM D854
3	Specific gravity	G_s	2.8	ASTM D854
4	Initial void ratio	e_o	0.95	$e_o = (G_s/\rho_d) - 1$
5	Plastic limit	P.L.	30	ASTM D4318
6	Liquid limit	L.L.	44	ASTM D4318
7	Plasticity index	P.I.	14	P.I = L.L – P.L
8	Liquidity index	L.I.	0.714	L.I. = (L.L – w_n)/ P.I
9	Sand	S	10%	>0.06 mm
10	Silt	M	50%	0.06>M>0.002 mm
11	Clay	C	40%	<0.002 mm
12	Soil classification	ML	low Plasticity silt	ASTM D422

Table 2. Results of Oedometer tests.

load (kPa)	(e) at S=100%	(e) at S=91 %	(e) at S=85%	(e) at S=75%	(e) at S=60%
12.5	0.863	0.878	0.889	0.895	0.9
25	0.824	0.838	0.856	0.868	0.878
50	0.768	0.796	0.819	0.827	0.823
100	0.692	0.724	0.753	0.769	0.788
200	0.608	0.666	0.704	0.728	0.746

400	0.512	0.571	0.643	0.669	0.695
800	0.425	0.475	0.56	0.573	0.616
1600	0.328	0.395	0.417	0.491	0.554
12.5	0.458	0.523	0.541	0.606	0.676

Table 3. Compression index C_c and swelling index C_s.

S%	**Cc**	**Cs**
100	0.2607	0.0617
91	0.2345	0.0607
85	0.212	0.0588
75	0.1905	0.0546
60	0.1644	0.0579

Table 4. Variation of settlement / height ratio with degree of saturation S%.

Load (kPa)								
S %	12.5	25	50	100	200	400	800	1600
100	0.04463	0.06442	0.09305	0.13242	0.17526	0.22442	0.26894	0.318947
91	0.03684	0.05747	0.07894	0.11578	0.14578	0.19473	0.24315	0.28452
85	0.03157	0.04736	0.06736	0.10105	0.12631	0.15789	0.20031	0.27336
75	0.02821	0.04221	0.06315	0.09305	0.11368	0.14421	0.19315	0.23467
60	0.02563	0.03689	0.06473	0.08305	0.10421	0.13078	0.17105	0.20310

Table 5. Load cases and best fit line equations, and correlation coefficients.

No.	Load kPa	Best fit Line equation	R^2
1	12.5	s/H = 0.0005 S - 0.0044	0.8741
2	25	s/H = 0.0007 S - 0.0078	0.9212
3	50	s/H = 0.0007 S + 0.0172	0.6999
4	100	s/H = 0.0012 S + 0.0056	0.9184
5	200	s/H = 0.0017 S - 0.008	0.8718
6	400	s/H = 0.0023 S - 0.0213	0.8700
7	800	s/H = 0.0024 S + 0.0157	0.8830
8	1600	s/H = 0.0029 S + 0.0244	0.9858

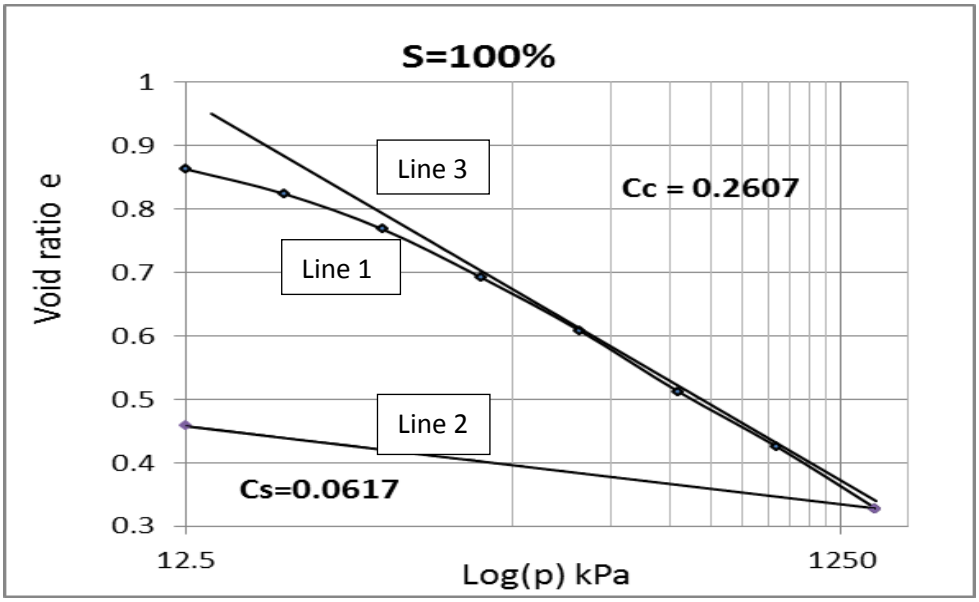

Figure 1. e –log (p) curve at S=100%.

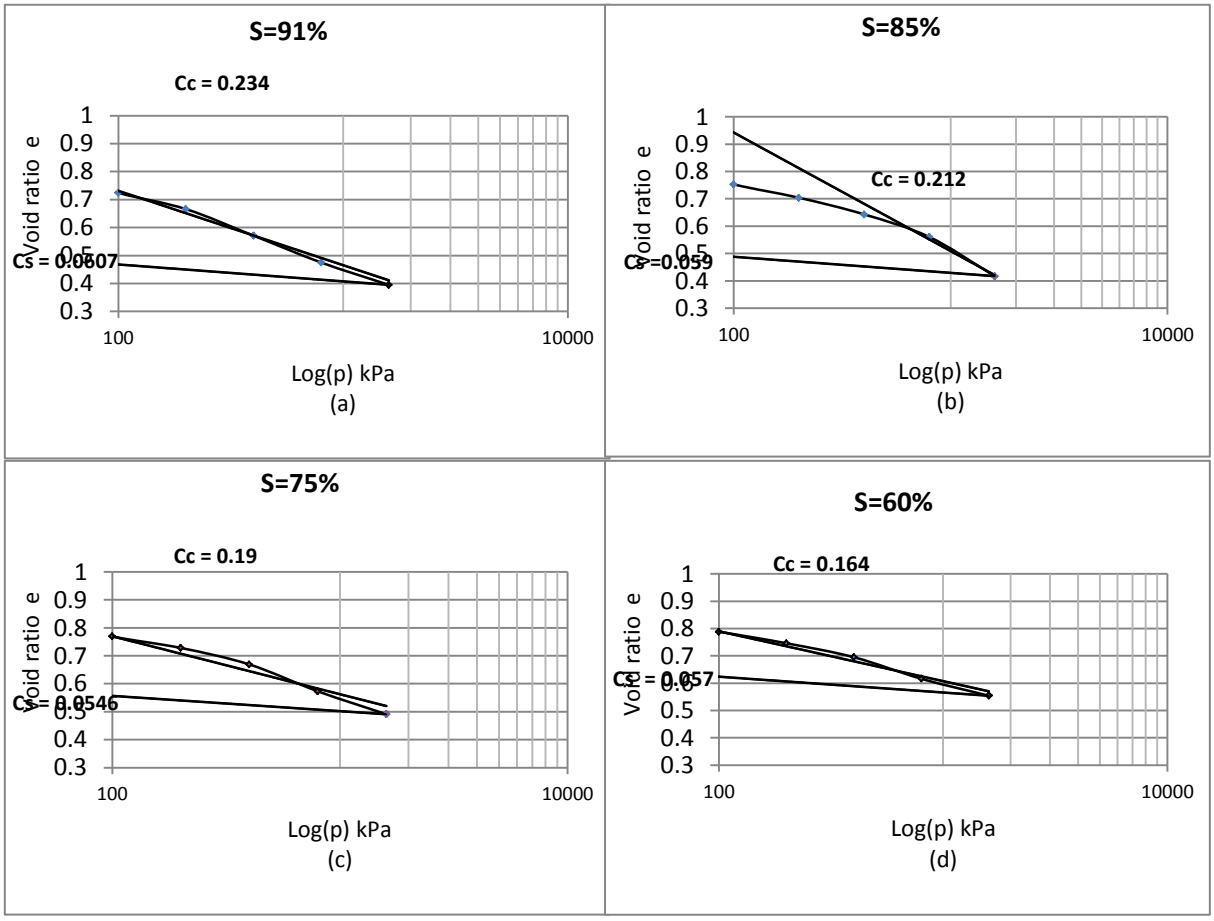

Figure 2. e – log (p) curve at S=91%,85%,75%,60% respectively.

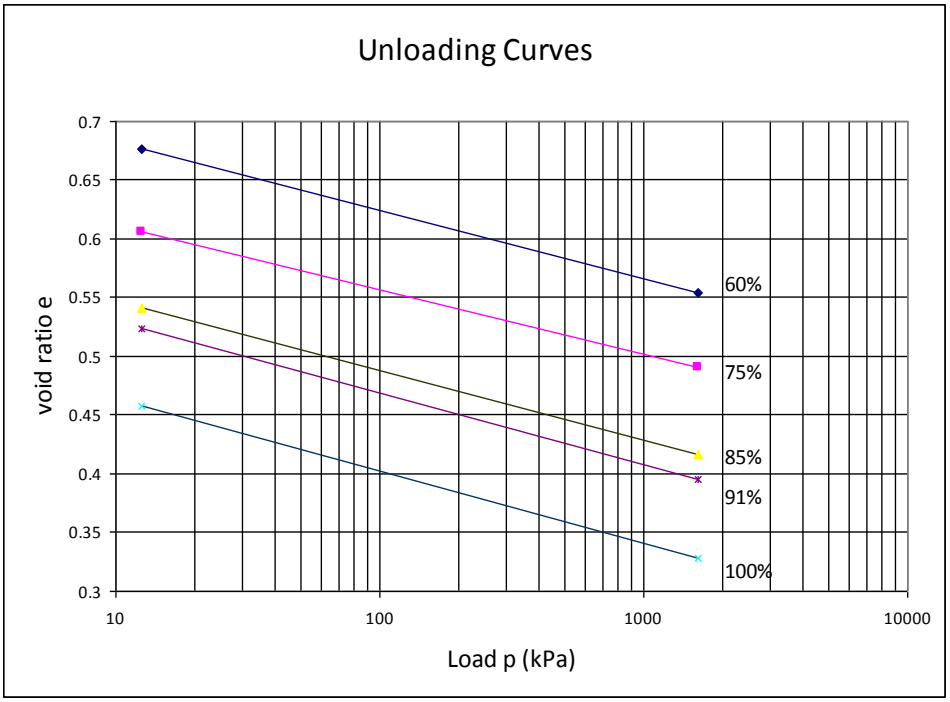

Figure 3 e-log(p) for unloading condition for different degrees of saturation.

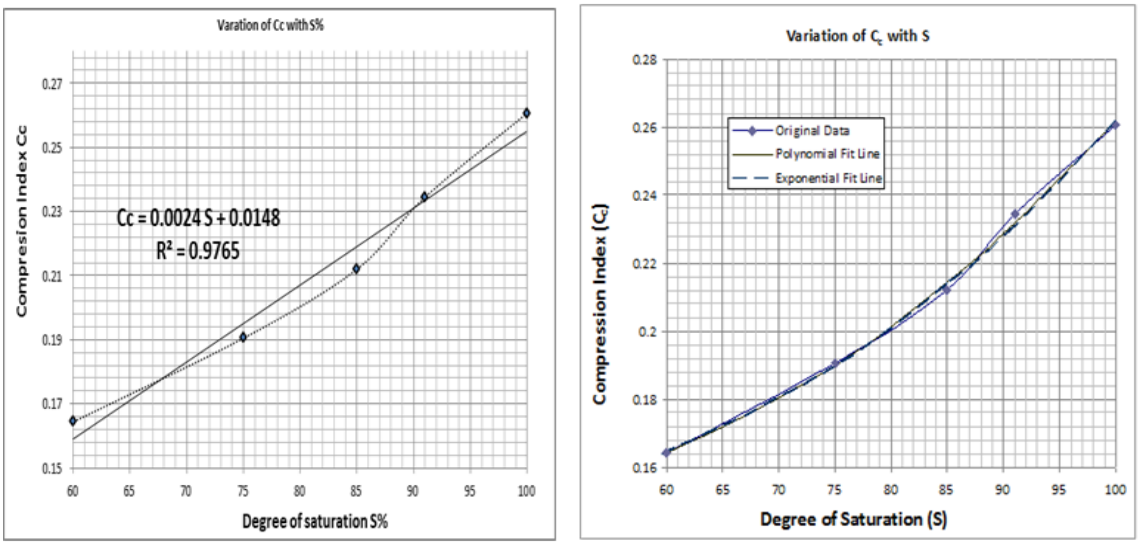

Figure 4 Variation of compression index C_c with degree of saturation S% .

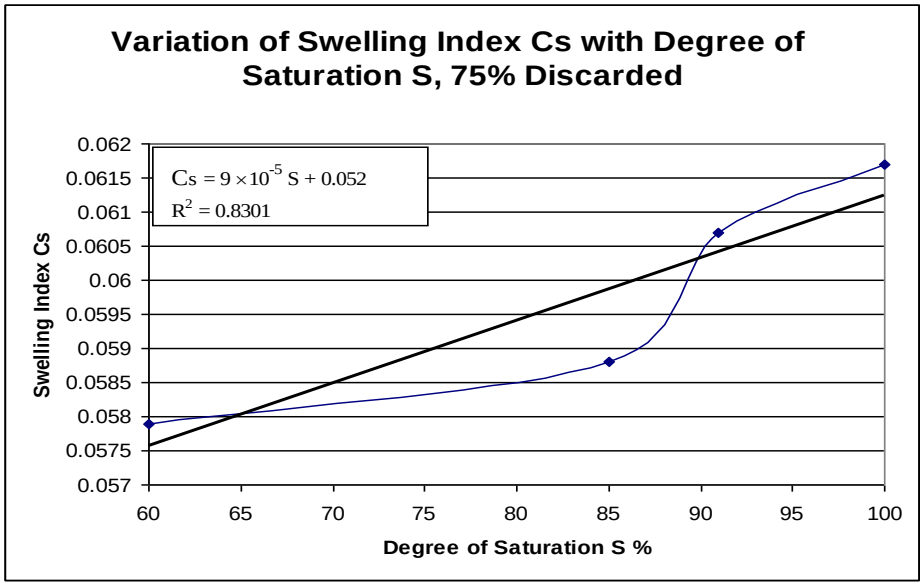

Figure 5. Variation of swelling index C_s with degree of saturation S%.

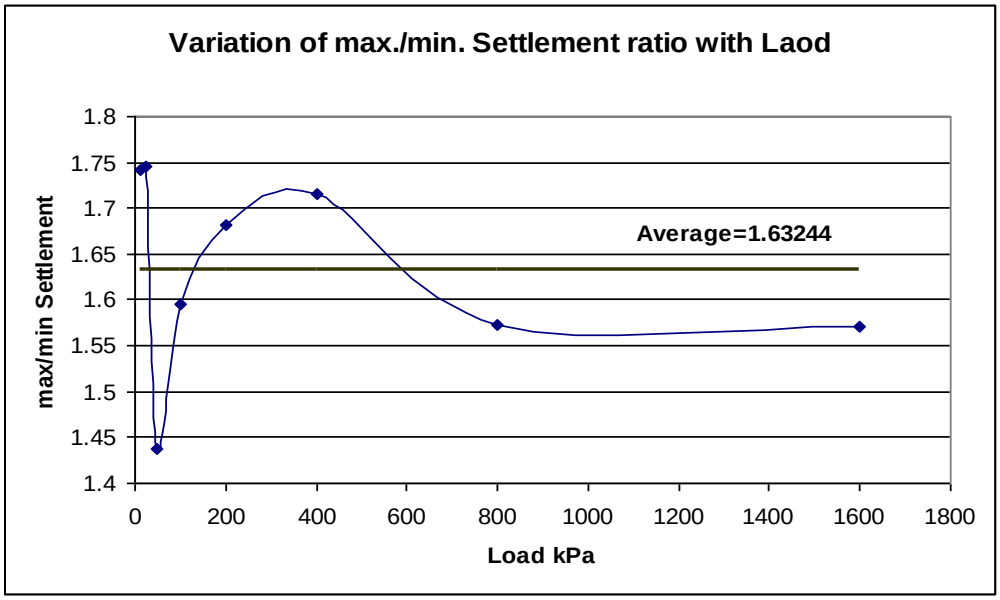

Figure 6. Variation of max./min. settlement ratio with load.

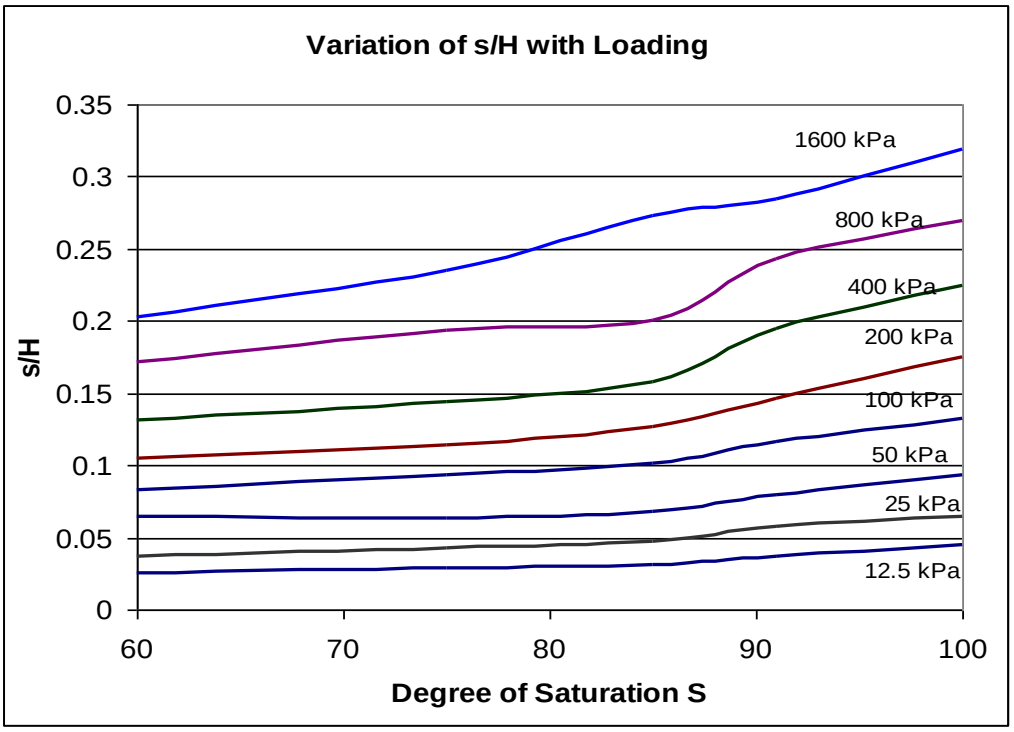

Figure 7. Variation of s/H with degree of saturation S% for each load.

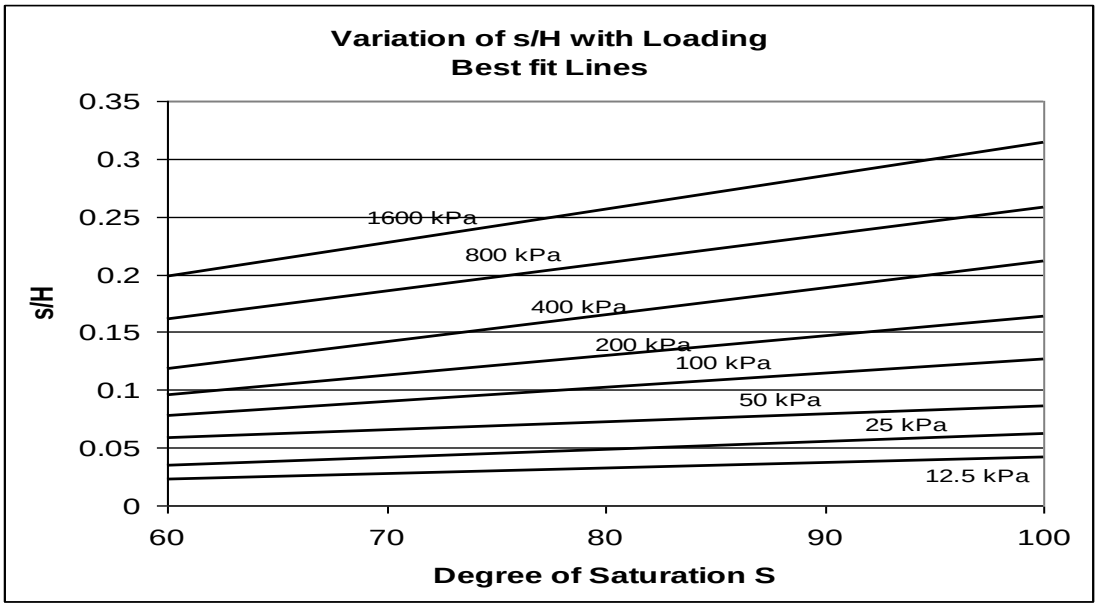

Figure 8. Best fit lines for s/H for different loading cases of variation with degree of saturation S%.

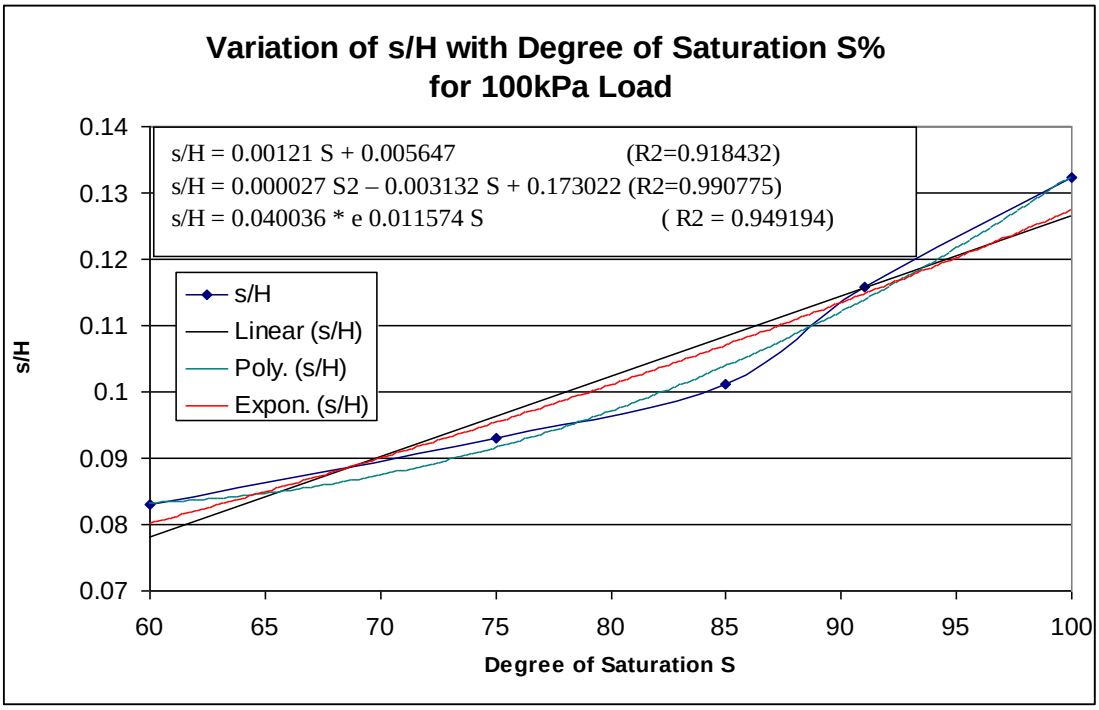

Figure 9. Variation of s/H with degree of saturation S% for 100 kPa load.

Unity Sliding Mode Controller Design for Active Magnetic Bearings System

Safanah M. Raafat
Assistant Professor
Control & Systems Eng. Dept.
University of Technology
E-mail: smraafat@uotechnology.edu.iq

Shibly Ahmed Al-Samarraie
Assistant Professor
Control & Systems Eng. Dept.
University of Technology
E-mail: dr.shiblyahmed@yahoo.com

Ali M. Mahmood
Lecturer
Control & Systems Eng. Dept.
University of Technology
E-mail: alimmj81@yahoo.com

ABSTRACT

Active Magnetic Bearings (AMBs) are progressively being implemented in a wide variety of applications. Their exclusive appealing features make them suitable for solving traditional rotor-bearing problems using novel design approaches for rotating machinery. In this paper, a linearized uncertain model of AMBs is utilized to develop a nonlinear sliding mode controller based on Lyapunov function for the electromechanical system. The controller requires measurements of the rotor displacements and their derivatives. Since the control law is discontinuous, the proposed controller can achieve a finite time regulation but with the drawback of the chattering problem. To reduce the effect of this problem, the gain of the unite vector term is evaluated as a function to state variables. As a result the proposed discontinuous controller regulates the state to the origin in a finite time in spite of the uncertainty in system model and the presence of external disturbances. These results are demonstrated via numerical simulations. In addition the chattering in system response in these results is within the acceptable range.

Keywords: active magnetic bearings (AMB), finite time regulation, linearized uncertain model, sliding mode controller, matching conditions.

تصميم مسيطر منزلق أحادي لمنظوظة محامل مغناطيسية فعالة

الاستاذ المساعد الدكتورة سفانة مظهر رأفت
قسم هندسة السيطرة والنظم
الجامعة التكنولوجية

الاستاذ المساعد الدكتور شبلي أحمد السامرائي
قسم هندسة السيطرة والنظم
الجامعة التكنولوجية

المدرس علي مجيد محمود
قسم هندسة السيطرة والنظم
الجامعة التكنولوجية

الخلاصة

إن تطبيق المحامل المغناطيسية الفعالة هي في تصاعد مستمر في الكثير من المجالات. إن صفات المحامل المغناطيسية المميزة يجعلها مناسبة كحل مبتكر لمشكلة محامل اللأعمدة الدوارة للمكائن. في هذه الورقة البحثية تم إستخدام نموذج خطي لمنظومة المحامل المغناطيسية الفعالة وذلك لإشتقاق قانون المسيطر المنزلق الاخطي بالإعتماد على دالة Lyapunov والذي يتطلب قياس إزاحات الجزء الدوار ومشتقات هذه الإزاحات. إن كون المسيطر هو غير مستمر هذا يضمن الوصول الى سطح الإنزلاق بزمن محدد بعدها الإنزلاق الى الهدف حسب دالة الExponential وهو الأمر الذي يتسبب بحدوث مشكلة الإرتجاج. للتقليل من تأثير الإرتجاج تم حساب معامل المسيطر المنزلق كدالة لمتغيرات الحالة. كنتيجة سيكون المسيطر المنزلق قادرا على قيادة متغيرات الحالة الى نقطة الأصل على الرغم من وجود الشك في النموذج الرياضي (التغير في معاملات النموذج الرياضي). لإختبار وتأكيد صحة التصميم تمت محاكات نموذج منظومة المحامل المغناطيسية عدديا. بالإضافة لذلك وجد الإرتجاج في إستجابة المنظومة ضمن المستوى المقبول.

الكلمات الرئيسية: المحامل المغناطيسية الفعالة، التعديل بزمن محدد، النموذج الخطي الغير دقيق، المسيطر المنزلق النمط، شرووط المواءمة.

1. INTRODUCTION

Active magnetic bearings (AMBs) are noncontact support bearings for rotating machinery. Using a pair of electromagnets at opposite sides of the rotor, it balances the attractive magnetic forces of the electromagnetic actuators in order to center the rotating element in the control axis. This allows the rotor to float in the bearing air gap and the machine to operate without frictional losses. Additionally, the contactless operation of the AMBs eliminates the need of lubrication of the bearing components, allowing them to operate cleanly and virtually maintenance free for long periods of time **,Yoon, et. al., 2013.**

Recently, there is a remarkable interest in industrial applications of active magnetic bearings (AMB), as in jet engines, compressors, pumps and flywheel systems that afford non-contacting support of rotors, eliminating distresses due to friction, wear, power consumption, and lubrication typical of standard bearings. AMB systems as electromagnetic devices have other exclusive abilities such as: high rotor speed, weight reduction, precise position control and active damping as described by **,Polajzer and Dolinar, 1999 and Motee and Queiroz, 2002.**

Nevertheless, magnetic bearings are highly nonlinear and inherently unstable. The non-linearity of the active magnetic bearing system is due to the relationship between forces that are generated in the electromagnetic actuator, the coil's current and the air gap between the rotor and the stator. These nonlinearities bound control effectiveness and the region of stable performance as shown in **,Hung, 1995.** The requirements of high speed, low vibration, zero friction, and clean environment are essential for smooth AMB operation. In addition **,Zhang, et. al., 2002** showed that a controller with high robustness to uncertainty was vital. Also **,Habib and Hussain, 2003** showed that the open loop unstable characteristic of the magnetic bearings required feedback control to ensure the normal operation of AMB systems.

Abdul, 2007 advanced PD-like Fuzzy Logic Controller (FLC) had been designed for AMB system stabilization. An intelligent approach to estimate uncertainty bound was introduced by **,Buckner, 2002** and applied to sliding mode controller design. **Sivrioglu and Nonami, 1996** a robust H_∞ controller was developed for high speed machining applications. Robustness against uncertainties and variations in operating conditions can be achieved as long as the uncertainty weighting function and performance weighting function are well tuned. However, the determination of these weighting functions were critical and usually very hard. Many works focused on developing strategies that can automate the selection of suitable weighting function. An automatic weight selection is developed to shape the sensitivity and complementary weighting functions,**Nair et. al., 2009**. Some other works **Cao, et. al., 2004 ,Arredondo and Jugo, 2007 and Zdzislaw, and Mystokowski, 2007** implemented *ad hoc* procedure for the selection of the weighting functions. Based on the approach of **Buckner, 2002** a confidence interval neural network was developed by **Choi et. al., 2006 ,Gibson et. al., 2003 and Gibson et. al., 2005** to adaptively estimate the uncertainty bounds for robust controller design. **Raafat, et. al., 2011** an intelligent estimate of uncertainty weighting function was presented for robust H_2 /H_∞ controller design. *v*- gap metric was utilized to validate the estimated uncertainty bounds for improved robust stability.

The variable structure system was presented by **Utkin, 1977** and indicated that variable structure control is unaffected to parameters perturbations and external disturbances. Recently, some applications have been developed using sliding mode control and adaptive control. For MIMO case the sliding mode control is designed based on hierarchy procedure as given by **Utkin, 1992.** As an alternative procedure design a unit control method is proposed for the MIMO system which preserved the sliding mode robustness with respect to the uncertainty in system parameters and to the external disturbances. The control law is designed using Lyapunov function where the root of this approach may be found in papers by **Gutman and Leitmann, 1976 and ,Gutman, 1979.**

In the present work the sliding mode control algorithm is employed to design a robust control system to AMB based on the unit control approach in the presence of model uncertainty and disturbances.

The paper is organized as follows. In section 2, the dynamics of AMB system with a flexible rotor is described. In section 3, a unity sliding mode controller with pole placement control is developed. Simulation results are presented in section 4. Conclusions are provided in section 5.

2. DYNAMIC MODELING OF THE AMB SYSTEM

In AMB systems, more than one actuator can be used in order to control the rotor levitation along several degrees-of-freedom (DOF). In this case, actuators are usually assembled as pairs facing each-other. This allows attracting the rotor in two opposite directions along one axis. Typically, the basic components of an AMB are: electromagnets, iron core, winding, rotor, position sensor, controller and power amplifier, as shown in **Fig.1**. The control objective is to manipulate the coil current $i(t)$ so that the vertical position of the rotor $x(t)$ tracks the desired trajectory. AMB are usually available in many configurations like radial bearings, in which the main purpose is to guarantee the levitation even in case of total failure of an actuator axis.

2.1 Theoretical Model

The force generated by an electromagnetic actuator **Fig.1** can be derived using magnetic circuit analysis and conservation of energy technique **,Schweitzer, 1994.**

$$f_{em} = \frac{1}{4}\mu_0 N^2 A_g \frac{i^2}{x^2} \quad (1)$$

The resulting nonlinear magnetic force Eq. (1) is proportional to the square of the coil current $i$and inversely proportional to the square of the air gap between the actuator and the rotor$x$. μ_0 is the permeability of free space ($4\pi.10-7H/m$), $N$is the number of turns in the coil, and A_g is the area of the air gap **,Schweitzer, 1994.** In order to develop a model based control of the system in **Fig.2**, the electromagnetic force Equation (1) is linearized about a nominal operating point and an accurate dynamical model was formulated **,Choi et. al., 2006.** The linearized system dynamics for the AMB system were obtained using a Lagrangian analysis of **Fig.2**, then they were represented using a state vector x composed of the rotor displacements and their time derivatives.

$$\dot{x} = Ax + Bu \quad (2)$$

$$y = Cx \quad (3)$$

Where **,Choi et. al., 2006.**

$$x = \begin{bmatrix} z_M \\ \dot{z_M} \end{bmatrix},\ A = \begin{bmatrix} 0 & I \\ M_B^{-1}K_s & -M_B^{-1}G_B \end{bmatrix},\ B = \begin{bmatrix} 0 \\ M_B^{-1}K_i \end{bmatrix},\ C = \begin{bmatrix} I \\ 0 \end{bmatrix}^T,\ M_B = T_F^{-1}MT_z,$$

$$G_B = T_F^{-1}GT_z, M = \begin{bmatrix} m & 0 & 0 & 0 \\ 0 & l_y & 0 & 0 \\ 0 & 0 & m & 0 \\ 0 & 0 & 0 & l_y \end{bmatrix}, \qquad G = \Omega \begin{bmatrix} 0 & 0 & 0 & 0 \\ 0 & 0 & 0 & -I_z \\ 0 & 0 & 0 & 0 \\ 0 & I_z & 0 & 0 \end{bmatrix}$$

$$, T_F = \begin{bmatrix} 1 & 0 & 0 & 0 \\ l_a & -l_b & 0 & 0 \\ 0 & 0 & 1 & 1 \\ 0 & 0 & -l_a & l_b \end{bmatrix},\ z_M = \begin{bmatrix} x_a \\ x_b \\ y_a \\ y_b \end{bmatrix},\ T_z = \frac{1}{l_a + l_b} \begin{bmatrix} l_b & l_a & 0 & 0 \\ 1 & -1 & 0 & 0 \\ 0 & 0 & l_b & l_a \\ 0 & 0 & -l_a & l_b \end{bmatrix},$$

$$K_s = \begin{bmatrix} k_s & 0 & 0 & 0 \\ 0 & k_s - k_c & 0 & 0 \\ 0 & 0 & k_s & 0 \\ 0 & 0 & 0 & k_s - k_c \end{bmatrix}, \text{ and } \qquad K_i = \begin{bmatrix} k_i & 0 & 0 & 0 \\ 0 & k_i & 0 & 0 \\ 0 & 0 & k_i & 0 \\ 0 & 0 & 0 & k_i \end{bmatrix}$$

with system parameters $m = 1.549\,kg,\ I_x = I_y = 2.39 \times 10^{-2} kg.m^2,\ I_z = 10^{-4} kg.m^2,\ l_a = 0.153\,m,\ l_b = 0.170\,m,\ k_s = -96.5 \times \frac{10^3 N}{m},\ k_i = 29.9 \frac{N}{A},\ k_c = 2.6 \times \frac{10^3 N}{m}$ and $\Omega = 627.0\,rad/sec$ (nominal speed: $6.0\,krpm$). The resulting continuous-time model is unstable, with eigenvalues

$$\lambda = -471 \pm 3.6i, 471 \pm 3.6i, -351 \pm 0.006i,\ 351 \pm 0.006i. \tag{5}$$

3. SLIDING MODE CONTROLLER DESIGN

This section proposes a unity sliding mode control strategy for the AMB system. A detailed study of the sliding mode control algorithm is presented in the presence of matched uncertainties and external disturbance with the AMB model.

3.1 Representation of Uncertainties

Starting by rewriting Eq. (2) to include the parametric uncertainties and disturbance effect

$$\dot{x} = Ax + \Delta Ax + Bu + \Delta Bu + d(t) \tag{6}$$

where $x \in \mathcal{R}^n,\ A\ \&\ \Delta A \in \mathcal{R}^{n \times n},\ u \in \mathcal{R}^m$ and $B\ \&\ \Delta B \in \mathcal{R}^{n \times m}$. Here ΔA and ΔB refer to the matched uncertainty in the matrices A and B respectively. In addition $d(t)$ is an external disturbance satisfies the matching condition. Namely

$$d(t) = B\delta(t) \tag{7}$$

Since (A, B) is a controllable pair, then the following control signal is proposed:

$$u = u_o - Kx \tag{8}$$

where $K \in \mathcal{R}^{m\times n}$ is chosen such that the matrix

$$A_o = A - BK \tag{9}$$

is Hurwitz with the desired characteristic roots. Consequently Eq. (6) becomes:

$$\dot{x} = A_o x + \Delta A x + B u_o + \Delta B u + d(t) \tag{10}$$

Now let the uncertainty in matrix A and B can be written as

$$\Delta A = B A_\delta \text{ and } \Delta B = B B_\delta \tag{11}$$

Then the bracket $\{\Delta A x + \Delta B u + d(t)\}$ can be written as:

$$\Delta A x + \Delta B u + d(t) = B\{A_\delta x + B_\delta u + \delta(t)\} = B\{(A_\delta - B_\delta K)x + B_\delta u_o + \delta(t)\} \tag{12}$$

Assumption: The matched uncertainty A_δ and B_δ and external disturbance $\delta(t)$ are bounded. Accordingly

$$\|(A_\delta - B_\delta K)x + B_\delta u_o + \delta(t)\| \le \alpha\|x\| + \beta\|u_o\| + \varepsilon \tag{13}$$

where $\|A_\delta - B_\delta K\| < \alpha$, $\|B_\delta\| < \beta$,$\|\delta(t)\| < \varepsilon$, and α,$\beta$, ε are positive constants.

Detailed formulation of the derivation of uncertainties is provided in Appendix A.

3.2 Unit Control Design

The objective of this section is to demonstrate a design method for discontinuous control enforcing sliding mode in some manifold without individual selection of each component of control as a discontinuous state function. The approach implies design of control based on a Lyapunov function selected for a nominal system. The control is to be found such that the time derivative of the Lyapunov function is negative along the trajectories of the system with perturbations caused by uncertainties in the plant model and environment conditions **,Utkin et. al., 2009.**

From previous discussion, the unit control signal u_o is proposed as

$$u_o = -\gamma(\|x\|)\frac{B^T \nabla V}{\|B^T \nabla V\|} \tag{14}$$

where $\|\cdot\|$ is the Euclidean norm, and hence the control law in Eq. (8) becomes:

$$u = -\gamma(\|x\|)\frac{B^T \nabla V}{\|B^T \nabla V\|} - Kx \tag{15}$$

Since the system $\dot{x} = A_o x$ is asymptotically stable, then by the converse theorem as given **by Khalil, 2002** there is a Lyapunov function with a positive definite matrix *P*

$$V = x^T P x \tag{16}$$

such that $\dot{V} < 0$, $\forall x \neq 0$. To this end, differentiate V with respect to time, to get:

$$\dot{V} = \nabla V^T\{A_o x + \Delta A x + B u_o + \Delta B u + d(t)\} = \nabla V^T A_o x + \nabla V^T B u_o + \nabla V^T\{\Delta A x + \Delta B u + d(t)\} \quad (17)$$

The unite vector gain $\gamma(\|x\|)$ is evaluated such that $\dot{V}$ is negative definite. As a result, $\dot{V}$ is rewritten as follows:

$$\dot{V} = \nabla V^T A_o x + \nabla V^T B u_o + \nabla V^T B\{\Delta A x + \Delta B u + d(t)\} \quad (18)$$

Now let us consider the following:

$$\frac{(\nabla V^T B)(B^T \nabla V)}{\|B^T \nabla V\|} = \frac{\|B^T \nabla V\|^2}{\|B^T \nabla V\|} = \|B^T \nabla V\|,$$

$$\nabla V^T A_o x = 2x^T P A_o x = -x^T Q x \leq 0$$

and

$$\nabla V^T B\{(A_\delta - B_\delta K)x + B_\delta u_o + \delta(t)\} \leq \|\nabla V^T B\|\|(A_\delta - B_\delta K)x + B_\delta u_o + \delta(t)\|$$
$$\leq \|B^T \nabla V\|(\alpha\|x\| + \beta\gamma + \varepsilon)$$

then Eq. (18) becomes:

$$\dot{V} \leq -x^T Q x - \gamma\|B^T \nabla V\| + \|B^T \nabla V\|(\alpha\|x\| + \beta\gamma + \varepsilon)$$
$$\leq -\gamma\|B^T \nabla V\| + \|B^T \nabla V\|(\alpha\|x\| + \beta\gamma + \varepsilon) = -\|B^T \nabla V\|\{\gamma - \alpha\|x\| - \beta\gamma - \varepsilon\}$$
$$= -\|B^T \nabla V\|\{\gamma(1-\beta) - \alpha\|x\| - \varepsilon\}$$

Now for

$$\gamma(\|x\|) = \frac{1}{(1-\beta)}\{\alpha\|x\| + \varepsilon + k\},\ k > 0 \quad (19)$$

then $\dot{V}$ becomes;

$$\dot{V} \leq -k\|B^T \nabla V\| < 0\ ,\ \forall\|x\| \neq 0 \quad (20)$$

This implies that the trajectory reaches the sliding surface in a finite time and remains on the sliding surface for all future time.

Note that the finite reaching time is a consequence of the unit vector term $\frac{B^T \nabla V}{\|B^T \nabla V\|}$ in the control law (Eq. (15)), and the reaching time is directly related to the magnitude of the gain $\gamma(\|x\|)$ **,Khalil, 2002.**

Eventually for the system dynamics in Eq.(6) the control law is given by

$$u = -Kx - \gamma(\|x\|)\frac{S}{\|S\|} \quad (21)$$

where S is the switching function vector given by

$$S = [s_1 s_2 \ \dots \ s_m]^T = B^T \nabla V = B^T 2Px = Gx$$

$G = 2B^T P \in \mathcal{R}^{m \times n}$, and $\gamma(\|x\|)$is as in Eq. (19). In addition the norm of the vector S which appears in the unit vector is given by (the induced inner product norm);

$$\|S\| = \sqrt[2]{S^T S} \tag{23}$$

Due to the presence of a discontinuous term in the control law ($\frac{S}{\|S\|}$ in Eq. (21)), the chattering behavior will be induce in system response. Many methods have been developed to eliminate the chattering problem, as in the case of replacing the discontinuous term by an approximate continuous form as for example the saturation function (see **,Utkin, et. Al., 2009).** The price paid to eliminate the chattering effect by approximating the discontinuous term is that the state will be only regulated to a region near the origin. The size of this region depends on the approximation form.

As an alternative solution to the chattering problem with preserving the finite time reaching property is by reducing the amplitude of the switching term in the control law. In the present work the amplitude of the switching term $\gamma(\|x\|)$ is taken as a function to the state rather than a constant value. This will help in reducing the chattering around the origin where $\gamma(\|x\|)$ will be equal to $\frac{(\varepsilon+k)}{(1-\beta)}$.

In the following section the unity sliding mode control law as given in Eq. (21) is applied to design a robust nonlinear control for the AMB system with considering both the uncertainty in system model and the effect of the external disturbances.

4. SIMULATION RESULTS

According to the plant description in section 2.1 and using Eqs. (2) and (3), simulation of the AMB is developed. MATLAB is used to simulate the AMB controlled system. The first experiment was accomplished using the following linear state feedback control equation: $u = -Kx$, where K is 4×8 matrix selected to satisfy that Eq. (9) is Hurwitz with the desired characteristic roots. Accordingly let the following set of closed loop poles are selected as:

$$p = [-1.0 \ -2.0 \ -3.0 \ -4.0 \ -2.0 \ -5.0 \ -6.0 \ -7.0]$$

Figure 3 shows the resulted states response of the controlled AMB system. The disturbance effects due to noise variations are not considered in this case. Subsequently, the controller can effectively regulate the system as shown in **Fig.4**.

Then, the uncertainty and disturbance effects are included in the simulation by considering Eq. (6), using the same previously designed state feedback controller. The applied disturbance is given by:

$$d = d_r[0.0 \ 0.0 \ 0.0 \ 0.0 \ 0.001 \ 0.002 \ 0.003 \ 0.002]^T$$

where d_r is uniformly distributed pseudorandom number. The transients of the system are drastically affected, as shown in **Fig. 5.**We allowed ±10% parameter variations for the matrices A and B and further assumed 10% to 35% magnitude changes in the $\delta(t)$ term. Consequently, the matrices A_δ and B_δ are calculated by equations (A-5) and (A-8) respectively (Appendix A). The parameter variations constitute ΔA and ΔB is assumed to have only matched uncertainty. The external disturbance is a random variable with zero mean and unit variance which is assumed to have only matched disturbance in the simulation. Accordingly, the parameters, β and ε will be equal to 1.7129, 0.2105 and 0.6393 respectively. The parameter k is set to 0.01 as a positive value in order that $\dot{V}$ becomes negative definite (Eq. (20)). In the same time k is selected small to reduce chattering that induced due to a high gain value of the discontinuous term $\gamma(\|x\|)$. The control signals are shown in **Fig.6**. The evaluated coefficients of Svector (Eq. (23)), can be seen in **Fig.7** while **Fig.8** presents the resulted norm of S. It is clear that the linear state feedback controller cannot overcome the effects of uncertainties and presence of disturbance. Therefore, further improvement is required to be applied, as described in section (3); the term unity control is included as described in Eq. (21). The switching gain $\gamma(\|x\|)$, which is responsible for reject the uncertainty in system parameters and the external disturbance effects, varies continuously from 0.9876 and to less than 0.014 rapidly in less than 9 minutes, which reflects the effectiveness of the added term to the control signal.

Fig. 9 presents the transient response of the system while **Fig.10** presents the control signals. **Fig.11** presents the norm of the S function. **Fig.11** also reveals the objective of the proposed controller in regulating the switching function vector to the origin in finite time. Here the time required to reach the origin is about 15 seconds. Further decrease in the reaching time can be gotten by increasing the gain γ of the unit control according to Eq.(21). Then to further explore the robustness of the developed controller, another larger value of disturbance is applied as:

$$d = d_r[0.0 \quad 0.0 \;\; 0.0 \quad 0.0 \;\; 0.020 \quad 0.040 \;\; 0.030 \quad 0.040]^T$$

The transient response of the system is shown in **Figs.12** and **13** show the control signals. The norm of the S function is given in **Fig.14**. It is clear that the new controller can effectively overcome the disturbance effects. Robust performance is also guaranteed in this case as proved in section (3.2).

5. CONCLUSIONS

This paper presents a derivation for a unity sliding mode controller design for a linear uncertain MIMO system subjected also to external disturbances. The proposed control is robust with respect to the uncertainty in system model and to the matched external disturbances since it was derived based on making the derivative of a candidate positive definite Lyapunov function negative definite. The developed unity sliding mode control was effectively derives the uncertain AMB system model to robust stability and performance conditions under the existence of matching condition. The simulation results, which are carried out for ±10% parameter variations for the matrices A and B and 10% to 35% magnitude changes in the disturbance term $\delta(t)$, clearly demonstrated the robustness and the effectiveness of the proposed unity sliding mode controller. In addition the results show that the effect of the chattering problem in sliding mode control is reduced via the use of a variable switching gain $\gamma(\|x\|)$ which has its minimum value at the origin.

REFERENCES

- Abdul Somad F.,2007, *System Identification and Control of Magnetic Bearing Systems*, School of Electrical Engineering, Master Thesis, Victoria University.
- Arredondo and Jugo J.2007, *Active Magnetic Bearings Robust Control Design based on Symmetry Properties*. Proceedings of the 2007 American Control Conference, USA, July 11-13.
- Buckner G. D., 2002, *Intelligent Bounds on Modeling Uncertainty: Applications to Sliding Mode Control*, IEEE Trans. On system, man, and Cybernetics-part c, applications and reviews, 32(2), 113-124.
- Cao G., Fan S. and Xu G.2004, *The Characteristics Analysis of Magnetic Bearing Based on H-infinity Controller*. Proceedings of the 51th World Congress on Intelligent Control and Automation. Hangzhou, P.R. China, June 15-19.
- Choi H.,.Buckner G.D, and Gibson N.S., 2006, *Neural Robust Control of High-Speed Flexible Rotor Supported on Active Magnetic Bearings.* in Proc. Of the 25th American Control Conference, Minneapolis, Minnesota, USA, June 14-16, the AACC and IEEE.
- Gibson, N.S., Choi H. & Buckner G.D., 2003, *H_∞control of Activemagnetic Bearings Using Artificial Neural Network Identification of Uncertainty*. System, Man, Cybernetics, 2003.IEEE International Conference, 2, 1449-1456.
- Gibson, N.S., Buckner,G.D, Choi H. and Wu, F., 2005, *Confidence Interval Networks for Bounding Model Uncertainty: Experimental Evaluations on an Active Magnetic Bearing System*. IEEE Mid-summer workshop on soft computing in industrial applications, Helsinki University of Technology, Espoo, Finland, June 28-30.
- Gosiewski Z. and Mystokowski A., 2007, *Robust Control of Active Magnetic Bearing Suspension: Analytical and Experimental Study*. Mechanical systems and Signal Processing.
- Gutman S, and Leitmann G., 1976, *Stabilizing Feedback Control for Dynamic Systems with Bounded Uncertainties*. IEEE Conf. Decision Control .94–99.
- Gutman S., 1979, *Uncertain Dynamic Systems: A Lyapunov Min-Max Approach*. IEEE Trans Automatic Control AC-24:437–449.
- Habib, M. M. and Hussain J. I., 2003, *Control of Dual Acting Magnetic Bearing Actuator System Using Fuzzy Logic*. IEEE International Symposium on Computational Intelligence in Robortics and Automation, Kobe, Japan, IEEE.
- Hung, J. Y. 1995, *Magnetic Bearing Control Using Fuzzy Logic*. IEEE Transactions on Industry Applications. 31(6), 1492-1497.

- Khalil H. K., 2002, *Nonlinear Systems*.3rd Edition, Prentise Hall, USA.
- Motee, N. and Queiroz M. S. D., 2002, *Control of Active Magnetic Bearing.Proc.Ofthe 41st IEEE Conference on Decision and Control*, Las Vegas, Nevada, USA, IEEE.
- Nair S.S., Vaidyan M. V. and Joy M. L.2009,*Generalized Design and Disturbance Analysis of Robust H infinity Control of Active Magnetic Bearings*. IEEE/ASME International Conference on Advanced Intelligent Mechatronics Suntec Convention and Exhibition Center Singapore, 1124-1129. July 14-17.
- Polajzer, B., and Dolinar, D., 1999, *Modeling and Control of Horizontal-Shaft Magnetic Bearing System*. IEEE, 1051-1055.
- Raafat S.M., Akmeliawati R., and Logow A., 2011, *Intelligent Estimation of Uncertainty Bounds of An Active Magnetic Bearings Using ANFIS*. ICIEM 2011, China.
- Schweitzer G., Bleuler H. and Traxler A. 1994, *Active Magnetic Bearings*..Hochschul verlag AG der ETH Zürich.
- Sivrioglu S. and Nonami K., 1996, *LMI Approach to Gain Scheduled H_∞Control beyond PID Control for Gyroscopic Rotor-Magnetic Bearing System*. Proceedings of the 35th FA19 Conference on Decision and Control, Kobe, Japan, 3694-3699.
- Utkin V. I., 1977, *Variable Structure Systems with Sliding Modes*. IEEE Trans Automat Contr..22:212–222.
- Utkin V. 1., 1992, *Sliding Modes in Optimization and Control*. Springer-Verlag, New York.
- Utkin V. I., Guldner J., and Shi J., 2009, *Sliding Mode Control in Electro-mechanical Systems*, CRC Press. Taylor & Francis Group.
- Yoon S. Y., Lin Z., and Allaire P. E., 2013, *Control of Surge in Centrifugal Compressors by Active Magnetic Bearings.* Springer-Verlag London.
- Zhang, H., and Lin Z., 2002, *A Convex Optimization Approach to Robust Controller Design for Active Magnetic Bearing Suspension Systems*.8th International Symposium on Magnetic Bearing, Mito, Japan.

Appendix A: Computing the Uncertainty Matrices

1) $\Delta A = BA_\delta,\ \Delta A \in \mathcal{R}^{n\times n}, B \in \mathcal{R}^{n\times m}\ and\ A_\delta \in \mathcal{R}^{m\times n}$

Let ΔA be written as:

$$\Delta A = \begin{bmatrix} O & O \\ \Delta A_{21} & \Delta A_{22} \end{bmatrix} \quad (A.1)$$

where $O, \Delta A_{21}$ and $\Delta A_{22} \in \mathcal{R}^{m\times m}, m = n/2$. Also let B andA_δ be written as follows:

$$B = \begin{bmatrix} O \\ B_{21} \end{bmatrix}, \quad O \quad \text{and} \quad B_{21} \in \mathcal{R}^{m\times m} \quad (A.2)$$

$$A_\delta = [A_{\delta 11} \quad A_{\delta 12}], \quad A_{\delta 11} \text{and} A_{\delta 12} \in \mathcal{R}^{m\times m} \quad (A.3)$$

Now $\Delta A = BA_\delta$ becomes:

$$\begin{bmatrix} 0 & 0 \\ \Delta A_{21} & \Delta A_{22} \end{bmatrix} = \begin{bmatrix} 0 \\ B_{21} \end{bmatrix} [A_{\delta 11} \quad A_{\delta 12}] = \begin{bmatrix} 0 & 0 \\ B_{21}A_{\delta 11} & B_{21}A_{\delta 12} \end{bmatrix} \quad (A.4)$$

where the matrix B_{21} is an invertable matrix ($det(B_{21}) \neq 0$). Therefore

$$\left.\begin{aligned} A_{\delta 11} &= B_{21}^{-1}\Delta A_{21} \\ A_{\delta 12} &= B_{21}^{-1}\Delta A_{22} \end{aligned}\right\} \quad (A.5)$$

2) $\Delta B = BB_\delta$, $\Delta B \in \mathcal{R}^{n\times m}$, and $B_\delta \in \mathcal{R}^{m\times m}$, Let ΔB be written as:

$$\Delta B = \begin{bmatrix} 0 \\ \Delta B_{21} \end{bmatrix}, \quad 0 \text{ and} \Delta B_{21} \in \mathcal{R}^{m\times m} \quad (A.6)$$

and with the aid of Eq. (A.2), we can write $\Delta B = BB_\delta$ as:

$$\begin{bmatrix} 0 \\ \Delta B_{21} \end{bmatrix} = \begin{bmatrix} 0 \\ B_{21} \end{bmatrix} B_\delta = \begin{bmatrix} 0 \\ B_{21}B_\delta \end{bmatrix} \quad (A.7)$$

Solving for B_δ

$$B_\delta = B_{21}^{-1}\Delta B_{21} \quad (A.8)$$

Then, by taking

$$\beta = \|B_\delta\|_2 \quad (A.9)$$

and

$$\alpha = \|A_\delta\|_2 + \|B_\delta K\|_2 \quad (A.10)$$

where $\| \quad \|_2$ refer to the 2-norm. Therefore $\gamma(\|x\|)$ will be evaluated from

$$\gamma(\|x\|) = \frac{1}{(1-\beta)}\{\alpha\|x\| + \varepsilon + k\}, \; k > 0 \quad (A.11)$$

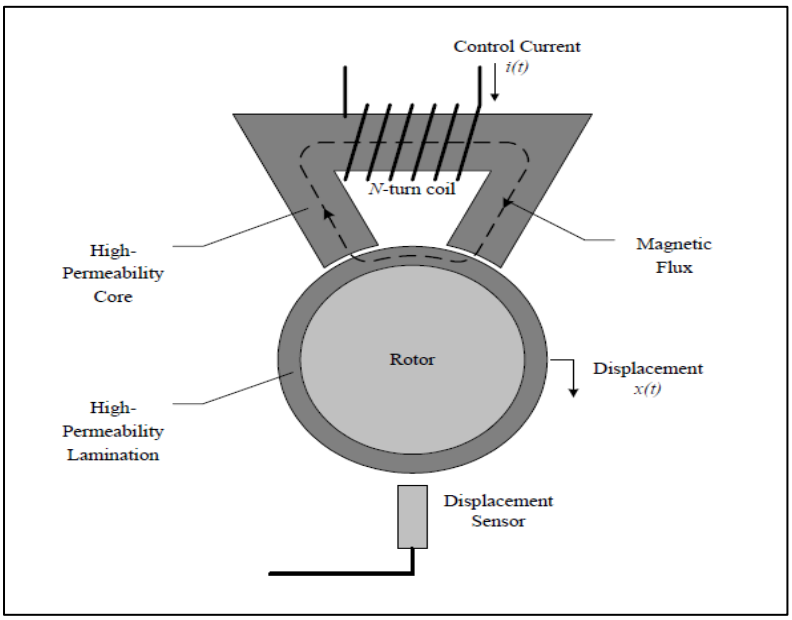

Figure1. AMB operating principals **,Gibson et. al., 2003.**

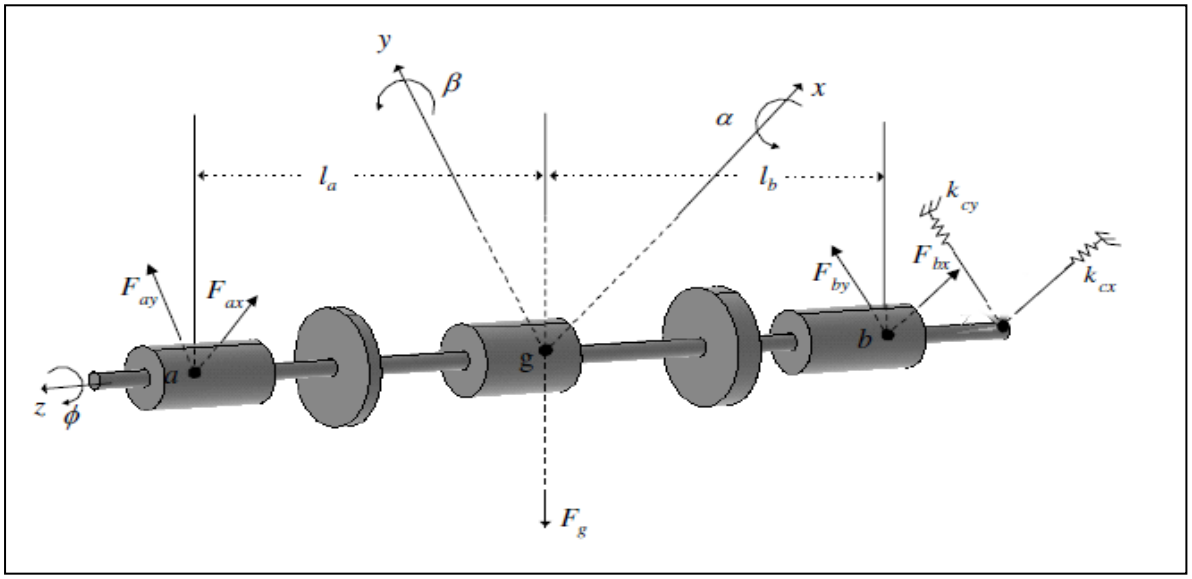

Figure 2. Generalized rigid rotor supported by two radial bearings **,Choi et. al., 2006.**

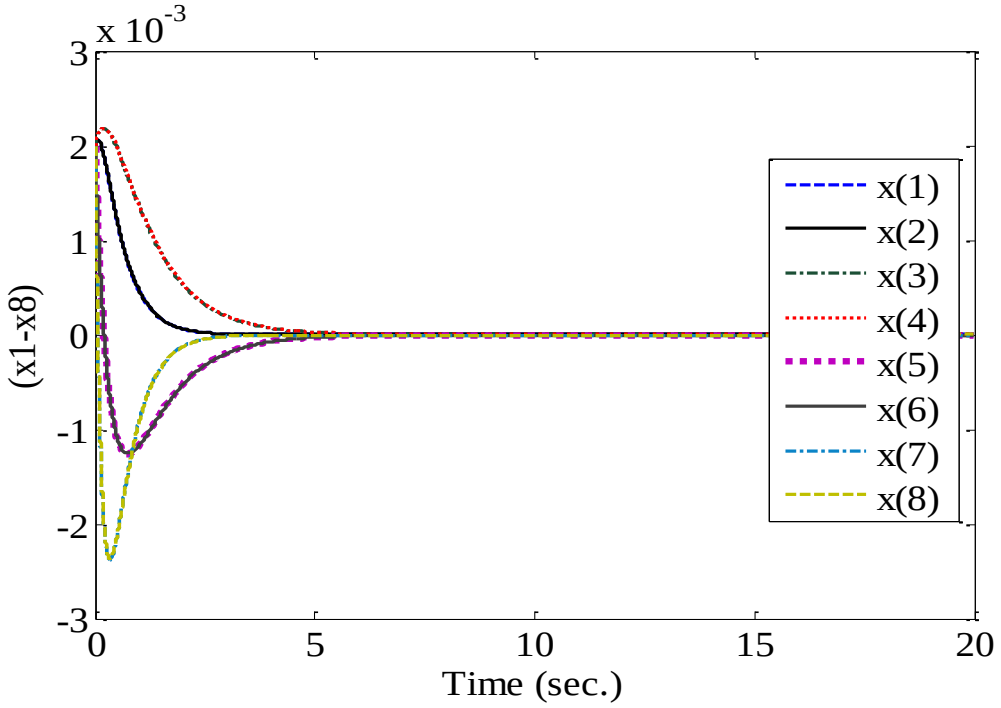

Figure 3. The transient responses of the AMB system under pole placement control, x(0)=2*10^{3}states x(1)-x(8).

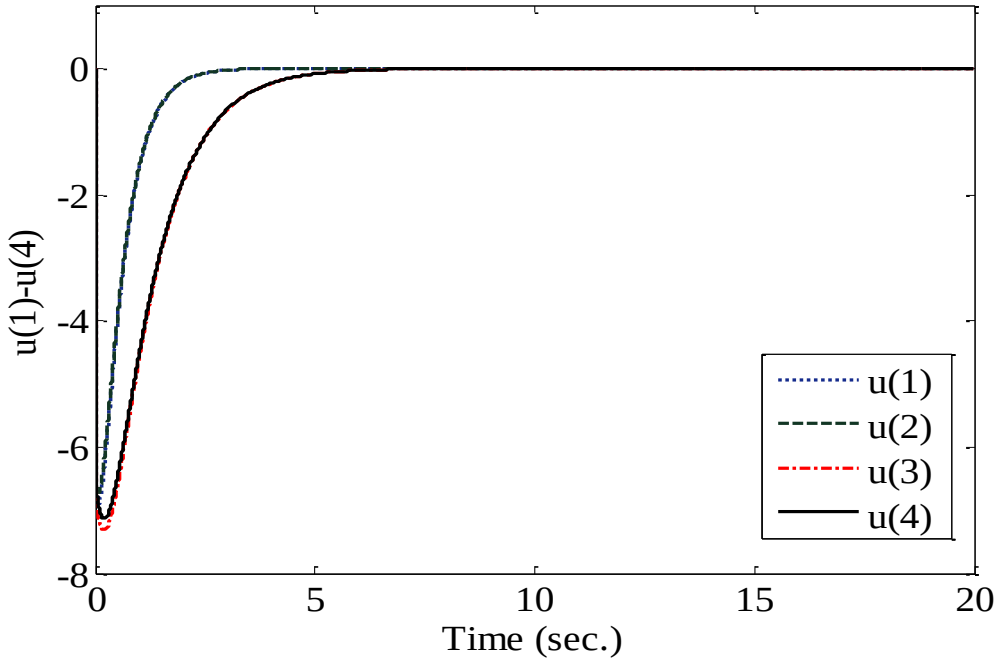

Figure 4. The control signals u(1)-u(4).

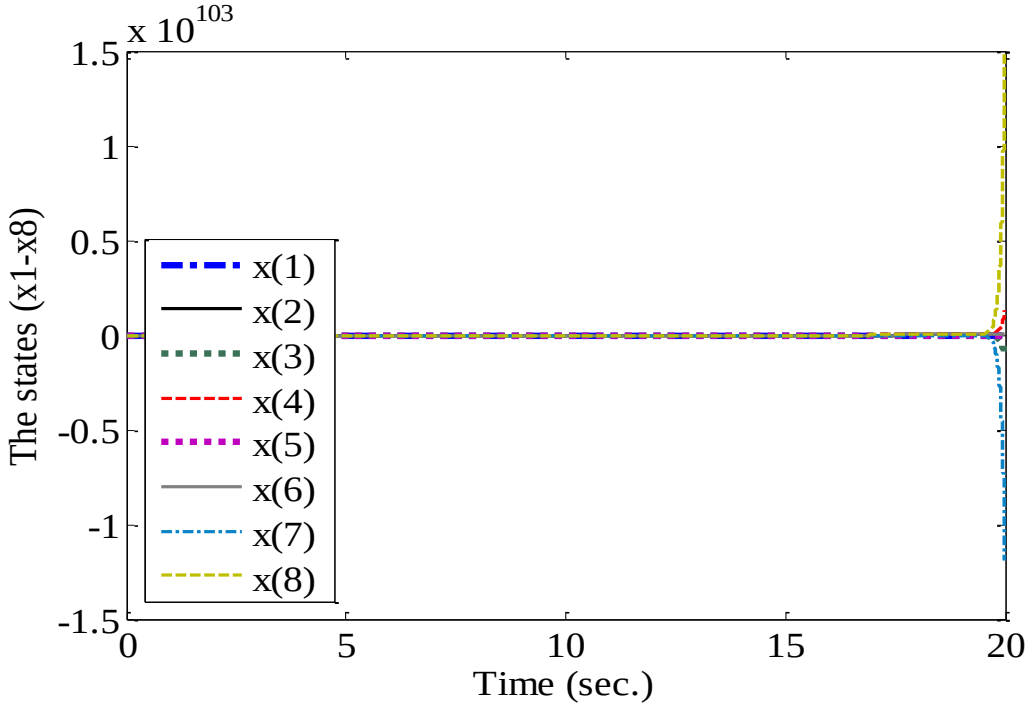

Figure 5. The transient responses of the disturbed AMB system under pole placement control, $x(0)=2*10^{-3}$.Disturbance of Eq. (28) is applied.

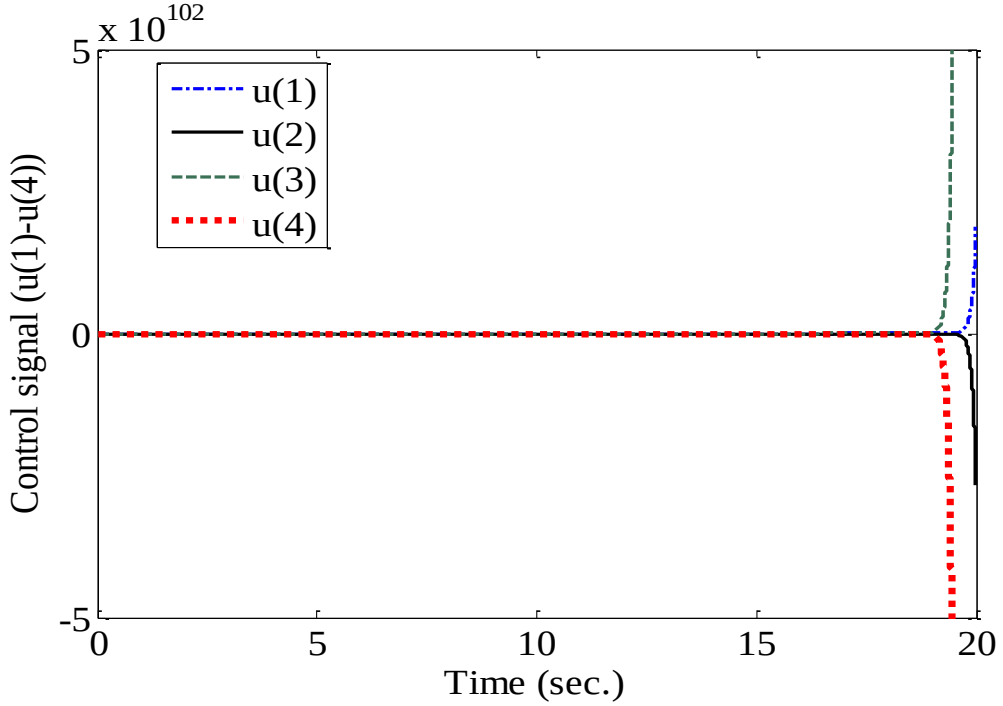

Figure 6. The control signals u(1)-u(4).

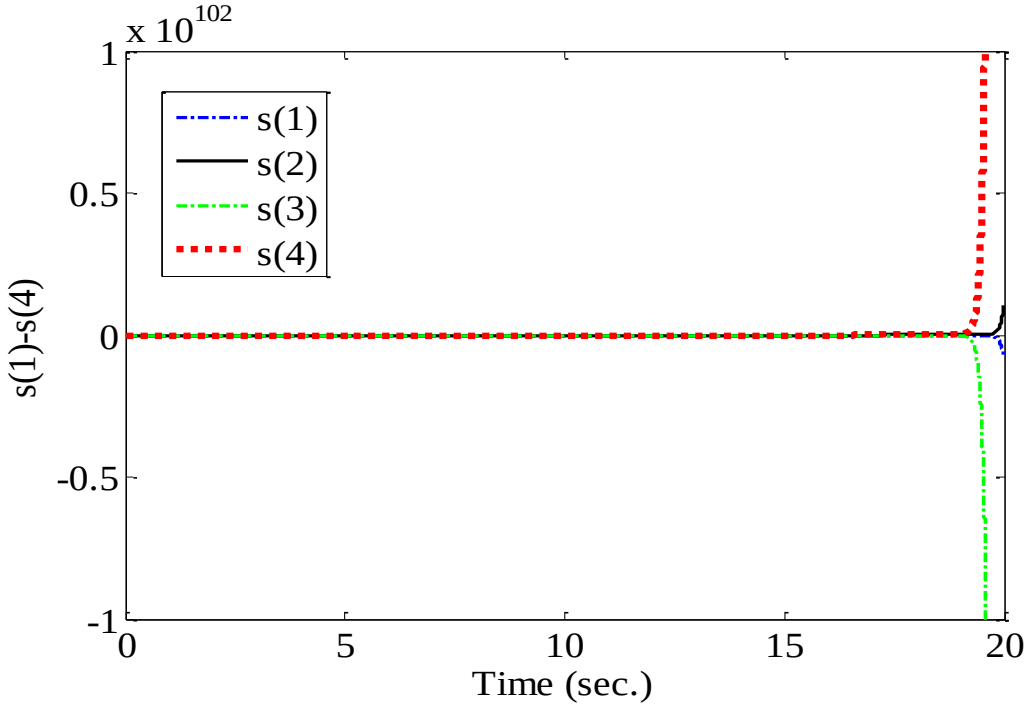

Figure 7. The evaluated function S.

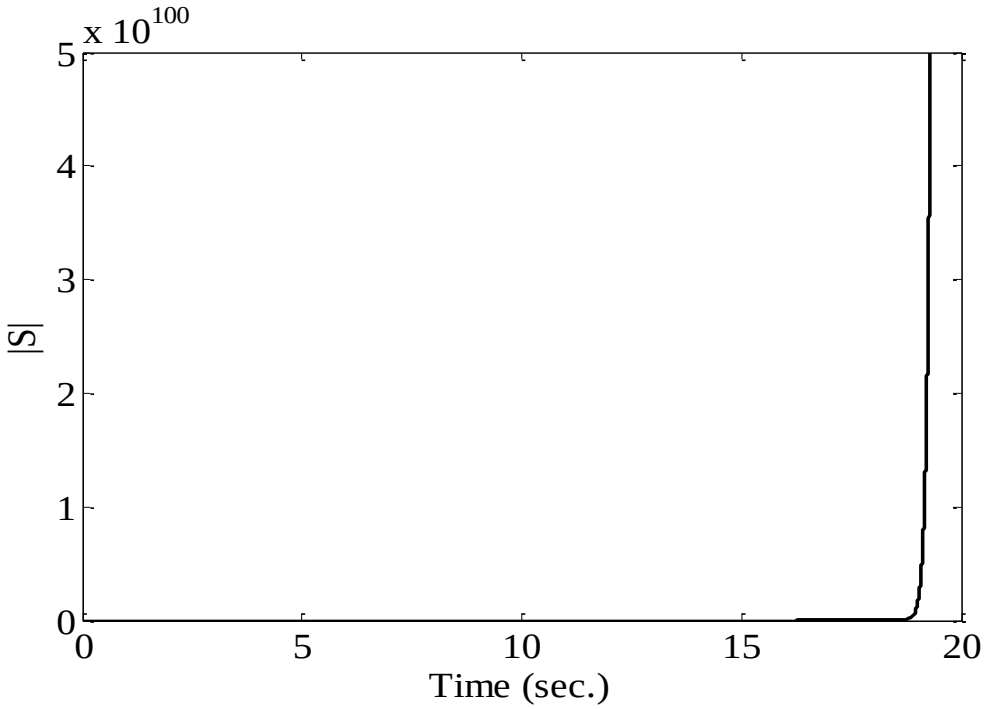

Figure 8. The resulted norm (S).

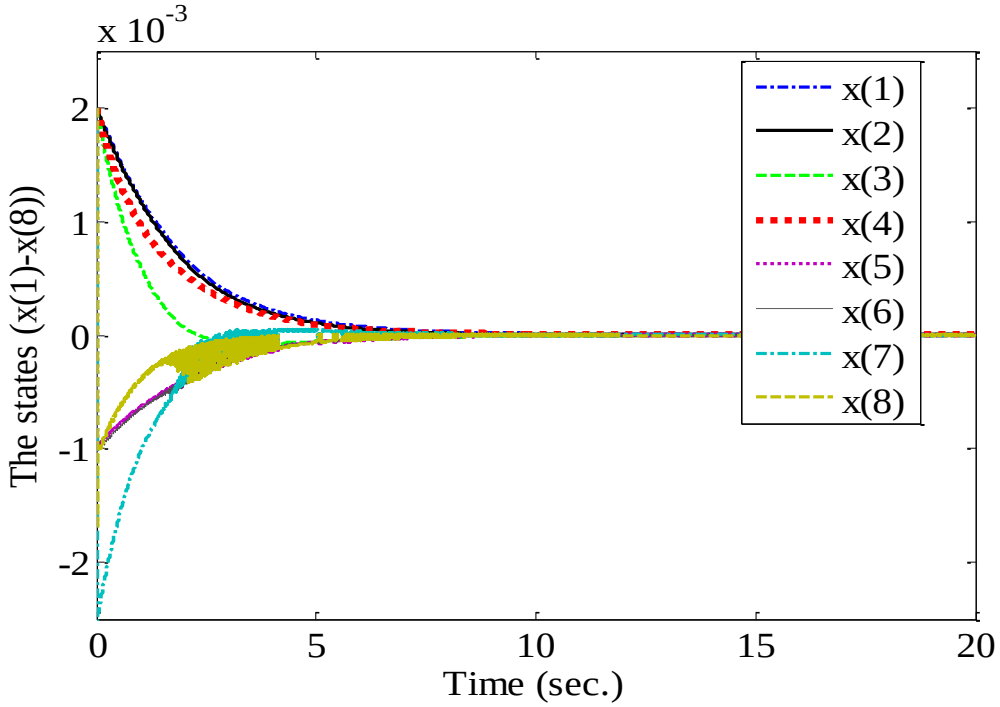

Figure 9. The transient responses of the disturbed AMB system under pole placement and unity control, $x(0)=2*10^{-3}$. Disturbance of Eq. (28) is applied.

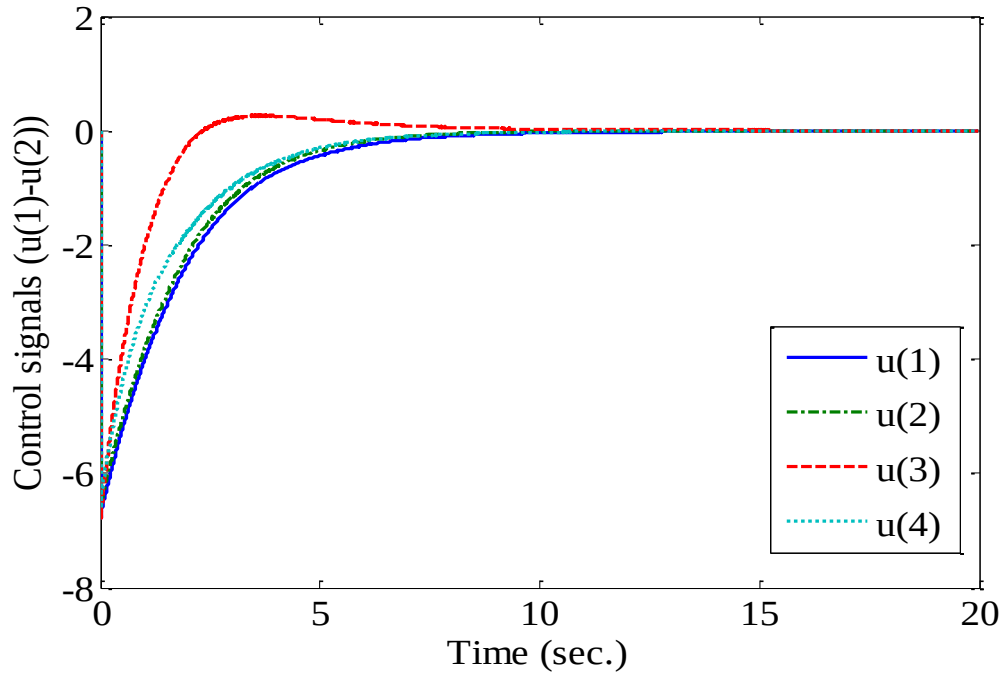

Figure 10. The control signals u(1)-u(4).

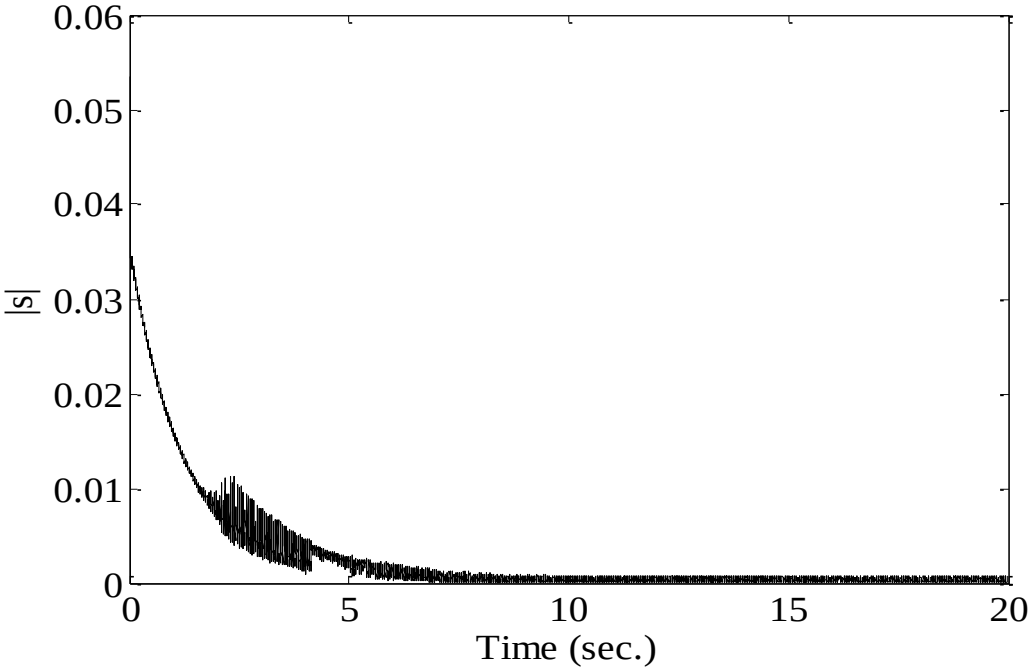

Figure 11. The norm |S|

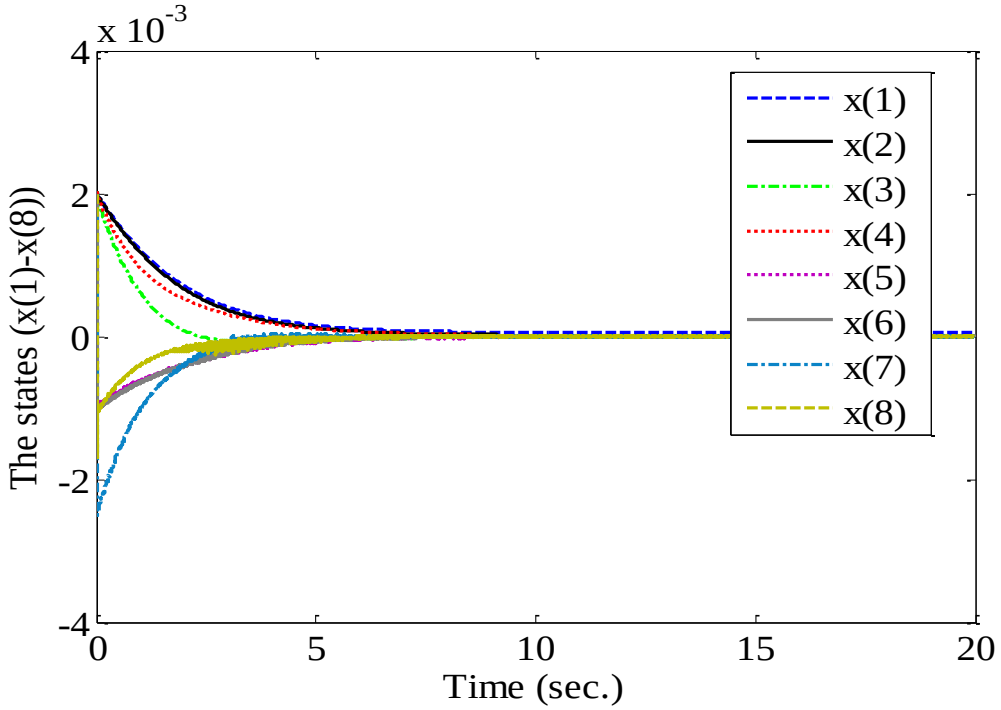

Figure 12. The transient responses of the disturbed AMB system under pole placement and unity control, $x(0)=2*10^{-3}$. Disturbance of Eq. (29) is applied.

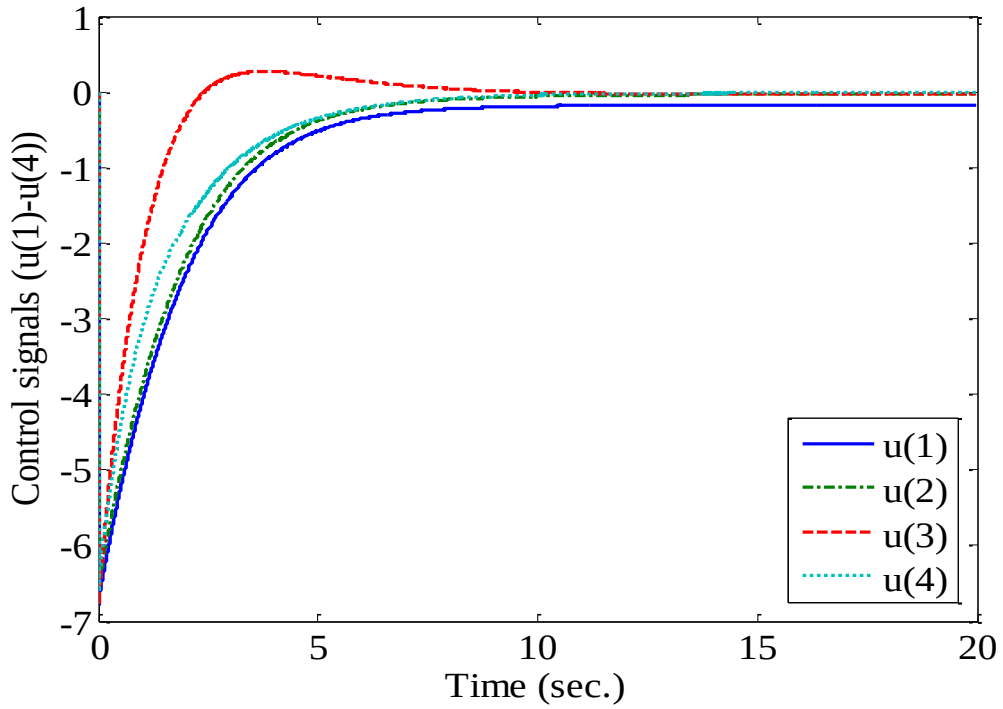

Figure 13. The control signals u(1)-u(4).

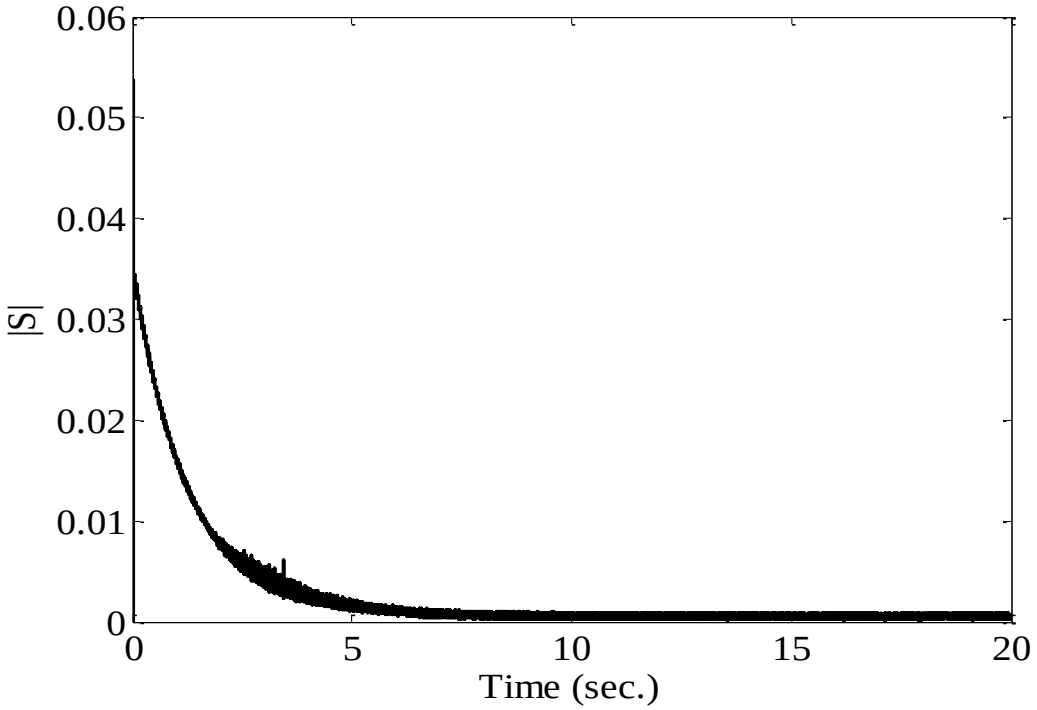

Figure 14. The norm |S|

Theoretical Investigations on the Structural Behavior of Biaxial Hollow Concrete Slabs

Prof. Dr. Nazar Kamel Ali Oukaili
Department of Civil Engineering
College of Engineering
University of Baghdad
Email: dr_nazar12000@yahoo.com

Lect. Hassan Hamoudi Yasseen
Department of Civil Engineering
College of Engineering
University of Baghdad
Email: hassanbayati@ymail.com

ABSTRACT

This paper presents a numerical analysis using ANSYS finite element program to simulate the reinforced concrete slabs with spherical voids. Six full-scale one way bubbled slabs of (3000mm) length with rectangular cross-sectional area of (460mm) width and (150mm) depth are tested as simply supported under two-concentrated load. The results of the finite element model are presented and compared with the experimental data of the tested slabs. Material nonlinearities due to cracking and crushing of concrete and yielding of reinforcement are considered. The general behavior of the finite element models represented by the load-deflection curves at midspan, crack pattern, ultimate load, load-concrete strain curves and failure modes shows good agreement with the experimental data.

Keywords: finite element analysis, one way slabs, prestressed concrete slabs, bubbled slabs, spherical voids.

تحريات نظرية على السلوك الانشائي للبلاطات الخرسانية المجوفة بمحورين

أ.د. نزار كامل علي العقيلي
قسم الهندسة المدنية
كلية الهندسة / جامعة بغداد

م. حسن حمودي ياسين
قسم الهندسة المدنية
كلية الهندسة / جامعة بغداد

الخلاصة

في هذا البحث تم استخدام التحليل العددي (طريقة العناصر المحددة ببرنامج ANSYS) لتمثيل البلاطات الخرسانية المسلحة ذات الفراغات الكروية الداخلية. تم تمثيل ستة بلاطات ذات الاتجاه الواحد بابعاد (٣٠٠٠ملم) طولا وذات مقطع مستطيل بابعاد (٤٦٠ملم) للعرض و(١٥٠ملم) للارتفاع. هذه البلاطات تم فحصها كبلاطات بسيطة الاسناد تحت نقطتي تحميل. تم استعراض النتائج النظرية ومقارنتها مع النتائج العملية للبلاطات المفحوصة. اخذ بنظر الاعتبار السلوك اللاخطي للمواد نتيجة لتشقق وسحق الخرسانة وخضوع حديد التسليح. اظهرت النتائج النظرية ان السلوك العام للنماذج المبنية بطريقة العناصر المحددة والمتمثلة بمنحي الحمل - الهطول عند منتصف العتبة، شكل التشققات، الحمل الاقصى، منحي الحمل- انفعال الخرسانة، وانماط الفشل، توافق جيدا مع النتائج العملية.

الكلمات الرئيسية: تحليل العناصر المحددة, البلاطات ذات الاتجاه الواحد, البلاطات الخرسانية المسبقة الشد, البلاطات المتفقعة, الفراغات الكروية.

1. INTRODUCTION

The wide application of the finite element method coupled with the availability of high-speed electronic digital computers has put the method in extensive use. Concrete structures may exhibit nonlinear behaviour due to material or geometric nonlinearities. The material nonlinearity is due to cracking of concrete, crushing of concrete, yielding of reinforcement and nonlinear stress-strain response of concrete, while the geometric nonlinearity is caused when the structure experiences large deformations, **ANSYS Help, 2009**.

Various attempt have been made in the past to reduce the weight of concrete slabs, without affecting their flexural strength. Not all the internal concrete can be replaced though, since aggregate interlock of the concrete is important for shear resistance, concrete in the top regions of the slab is necessary to form the compression block for flexural resistance, and concrete in the tension zones of the slab needs to bond with reinforcement to make the reinforcement effective for flexural resistance. Also the top and bottom faces of the slab need to be connected to work as a unit and insure the transfer the stresses, **Marais, 2009.** The dominant advantage of slabs with internal spherical voids is that it uses (35%) less concrete than normal solid slabs. The plastic spheres replace the non-effective concrete in the centre of the section, thus reducing the dead load of the structure by removing unused heavy material. Also leads to less structural steel since the need for reinforcement diminishes. The building foundations can be designed for smaller dead loads as well. On site construction time can be shortened since slabs with internal spherical voids can be precast, in relation to savings in material and time, cost reductions are also typical with this system as shown in **Fig.1**, **BubbleDeck, Lighter Flat, 2006.**

2. EXPERIMENTAL PROGRAM

2.1 Characteristics of the Tested Slabs

Six full-scale one way structural concrete bubbled slabs of (3000mm) length with rectangular cross-sectional area of (460mm) width and (150mm) depth were tested as simply supported under two-concentrated loads, in which each specimens contain (80) plastic spheres of (100mm) diameter with ratio of (D/H=0.67) and (26.40%) reduction in self weight/m^3 as shown in **Fig. 2.** The variables studied are given in **Table.1 ,Oukaili and Yasseen, 2014.** Load (P) is applied by means of hydraulic jack which acted on the slabs as two symmetrical concentrated loads (with ratio of shear span (a) to effective depth (d), a/d=6.88) (see **Fig. 3**). For all specimens, deflection at midspan, first cracking load, ultimate load and concrete strains are recorded and measured at various stages of loading.

2.2 Material Properties

The specimens constructed using a concrete with a compressive strength of approximately (40 MPa). The concrete produced in the laboratory using normal Portland cement, fine aggregate, and crushed coarse aggregate of (10mm) maximum nominal size. Seven-wire strand of (12.7mm) nominal diameter (grade 270, low relaxation, confirming to **ASTM A416/ A416M-06** used as

flexural reinforcement, at a prestressing level of (70%) of the ultimate strength (1860 MPa). In addition, different diameters (12mm, 10mm and 6mm) of steel bars used in this study as flexural and shear reinforcement. The plastic spheres were made by embodying high density polypropylene (HDPE) from recycled plastic with diameter (100mm).

3. FINITE ELEMENT ANALYSIS

3.1 Modeling of Material Properties

3.1.1 Concrete

The concrete is assumed to be homogeneous and initially isotropic. The compressive uniaxial stress strain relationship for the concrete model is obtained by using the following equations to compute the multilinear isotropic stress- strain curve for the concrete as shown in **Fig. 4, Desayi and Krishnan, 1964.**

$$f_c = E_c \varepsilon \qquad for\ 0 \le \varepsilon \le \varepsilon_1 \tag{1}$$

$$f_c = \frac{E_c \varepsilon}{1+(\frac{\varepsilon}{\varepsilon_o})^2} \qquad for\ \varepsilon_1 \le \varepsilon \le \varepsilon_o \tag{2}$$

$$f_c = f_c' \qquad for\ \varepsilon_o \le \varepsilon \le \varepsilon_{cu} \tag{3}$$

$$\varepsilon_o = \frac{2f_c'}{E_c} \tag{4}$$

The modulus of elasticity, E_c, can be calculated with a reasonable accuracy from the empirical formula, **ACI 318M-14**.

$$E_c = 0.043(w)^{1.5}(f_c')^{0.5}$$

For the normal weight concrete based on a dry unit weight (2200-2500 kg/m^3), E_c can be permitted to be taken as, **ACI 318M-14**.

$$E_c = 4700\sqrt{f_c'}$$

Poisson's ratio (v) of concrete has been observed to remain approximately constant and ranges from about (0.15 to 0.22) up to a stress level of 80% of f_c', **,Neville, 1987.**

3.1.2 Reinforcing Steel

Ordinary Reinforcement: For all practical purposes, steel exhibits the same stress-strain curve in compression as in tension. The steel stress-strain relation exhibits an initial linear elastic portion, a yield plateau, a strain hardening range in which stress again increases with strain and, finally, a range in which the stress drops off until fracture occurs. The extent of the yield plateau is a function of the tensile strength of steel. For computational convenience it even often suffices to idealize the one dimensional stress-strain relation for steel, as shown in **Fig. 5 ,Kwak, 1990.**

Prestressing Strands: The multi-linear curve option is useful to define stress-strain curve of prestressing strand elements. Coordinates for each point on the curve are derived using the equations available in **PCI Manual for the Design Handbook** (**PCI, 2010)** for low relaxation strands of grade (270 ksi) (1860 MPa) which have been summarized below and plotted in **Fig. 6**.

For the elastic segment of the curve when ($\varepsilon_p < 0.0085$), stress in the LINK8 element (f_p) is calculated from the following linear equation:

$$f_p = 28500\varepsilon_p \quad \text{(ksi)} \qquad (5)$$

While for the plastic segment ($\varepsilon_p > 0.0085$), the stress in strand elements (f_p) is calculated from the following expression:

$$f_p = 270 - \frac{0.04}{\varepsilon_p - 0.007} \quad \text{(ksi)} \qquad (6)$$

where f_p and ε_p are the strand stress and corresponding strain at any arbitrary point on the curve.

3.2 Element Types

SOLID65 is used for the 3-D modelling of solids with or without reinforcing bars (rebar). The solid is capable of cracking in tension and crushing in compression. The element is defined by eight nodes having three degrees of freedom at each node: translations of the nodes in x, y, and z-directions. This 8-node brick element is used, in this paper, to represent the concrete. The element is defined by the isotropic material properties. The geometry, node locations, and the coordinate system for this element are shown in **Fig. 7**.

LINK8 is a spar (or truss) element which used to model the steel reinforcement. The 3-D spar element is a uniaxial tension-compression element with three degrees of freedom at each node: translations of the nodes in x, y, and z-directions. The geometry, node locations, and the coordinate system for this element are shown in **Fig. 8**.

SOLID45 is defined with eight nodes having three degrees of freedom at each node; translations in x, y, and z directions. SOLID45 is used to model the steel plate which existed under point load (applied load) and supports in order to avoid stress concentration problems. The geometry, node locations, and the coordinate system for this element are shown in **Fig. 9 ,ANSYS Help, 2009.**

3.3 Real Constant and Material Properties

The real constants for all materials used in constructing the model of reinforced concrete bubbled slabs are described and listed in **Table 2.** Parameters needed to define the material models for the first specimen are given in **Table 3.**

3.4 Modeling of Bubbled Slab

ANSYS program create the solid slab, solid spheres, plates, and supports as volumes. By taking advantage of the symmetry of both slab geometry and loading, one quarter of the entire model slab is used for the element analysis. The model is (1500mm) in length, with a cross-section of (150mm

x 230mm) for solid slab. Due to symmetry, only one loading plate and support plate are needed. The loading and support plates are (230mmx 150 mm x 10mm). Twenty solid spheres with radius of (50mm) are created and moved to the correct positions inside the block of solid slab and by subtract command, subtracting all the solid spheres from the solid slab, the voids will be formed in the center of cross-section. The combined volumes of the slab, spheres, plates and supports, are shown in **Fig. 10**. LINK8 elements are used to create the upper and lower welded wire meshes of (3mm) diameter in addition to the flexural and shear reinforcement see **Fig. 11**.

3.5 Meshing of Bubbled Slab

Using of a triangular mesh with tetrahedron volume is necessary to obtain good results from the SOLID65 element. Therefore, the mesh is set up in such manner that triangular elements are created see **Fig. 12**. Also, the volume free command is used to mesh the steel plate and support. This properly sets the width and length of elements in the plates to be consistent with the elements and nodes in the concrete portions of the model.

3.6 Loads and Boundary Conditions

Rollers are used to show the symmetry condition at the internal faces. Moreover, a single line support is placed under the centerline of the support position to allow rotation of the support while vertical movement is restricted; when the loaded slab starts to displace download, rotation of the support should be permitted. The single line of external forces is applied to the centerline of steel plate to reduce the stress concentration caused by the applied force and result in early cracking.

4. COMPARISON OF EXPERIMENTAL AND ANALYTICAL RESULTS

4.1 Load-deflection Relationship

Figs. 14 through **17** show load-deflection curves of the bubbled slabs of the present finite element analysis and experimental results.

It can be observed that, the present finite element model performs satisfactorily and it predicts the real behavior of the bubbled slab. However, the finite element load-deflection curves in the linear stage are somewhat stiffer than the experimental responses for slab (BD1), while, the analytical load-deflection curves of slabs (BD2, BD4 and BD5) well match the test data. For bubbled slabs (BD6 and BD7), the finite element load-deflection curves in the linear stage are somewhat stiffer than that of the experimental responses. After first cracking, the stiffness of the modeled elements is slightly higher than that of the experimental specimens. There are several reasons that may cause the higher stiffness in the finite element models. First, micro-cracks produced by drying shrinkage and handling which are present in the concrete to some degree. They would reduce the stiffness of the actual specimens, while the finite element models do not include micro-cracks. Second, the perfect bond between the concrete and reinforcing steel is assumed in the finite element analysis, but the assumption would not be true for the actual specimens. As bond slip occurs, the composite action between the concrete and reinforcing steel begins to diminish. Thus, the overall stiffness of the actual specimens could be lower than what the finite element models predict, due to factors that are not incorporated into the models.

The load-deflection response at midspan for the bubbled slabs with prestress steel is essentially bilinear with a transition curve at the cracking load. This is due to the linear characteristics of the prestressing strands that do not show any yield plateau.

The contours representing the deflected shapes of the specimen BD7 due to prestressing force and ultimate load is shown in **Fig. 18**.

4.2 First Cracking and Ultimate Loads

The first cracking and ultimate loads obtained in analysis by (ANSYS) program are compared with experimental results for all the bubbled slabs. The values are given in **Table 4**.

In finite element analysis, it is found that, the first cracking load (P_{cr}) is formed at (39.8%, 53%, 55.5%, 69%, 63% and 69.8%) of the ultimate load (P_u) of bubbled slabs (BD1, BD2, BD4, BD5, BD6 and BD7), respectively. Based on the finite element analysis, the first cracking loads for all models are almost higher than those from experimental results.

The average value of the ratio of the experimental load at first cracking to the corresponding load observed in the analytical results is found be (0.91) with a standard deviation of (0.084). While, at ultimate load the average and the standard deviation become (0.95 and 0.073) respectively.

4.3 Load-Concrete Strain Relationship

Figs. 19 and **20** show the distribution of concrete strains at the ultimate load in the longitudinal x-direction, along the bubbled slabs (BD1) and (BD4), respectively. It is noted that, the maximum compressive strains for (BD1) are at the upper fibers of the cross-section at midspan, while, for prestressed bubbled slab (BD4), they are located at the support region at the level of prestressing steel, this is due to the assumption of the perfect bond between the concrete and prestressing steel in the finite element analysis. But, the maximum tensile strains for all bubbled slabs are located in the region occupied by the spherical voids.

The compressive and tensile strains data for concrete collected from the experimental test of bubbled slabs are compared with the results obtained from the finite element analysis. It is noted that, the analytical load-concrete strain curves in the linear stage are somewhat stiffer than the experimental responses, after this stage, the strains in the concrete calculated by ANSYS are higher than those from the experimental results especially in the bottom fibers as shown in **figures 21** and **22**.

The analytical results show that, there is a significant increase in concrete strain of bubbled section occupied by the spherical voids in comparison with solid section (between two voids) for the bubbled slab.

4.4. Crack Pattern and Failure Mode

In finite element analysis, it is observed that, the first flexural cracking initiates at (39.8%-69%) of the ultimate load, and at this stage of loading, the tensile stress in concrete reaches the modulus of rupture, and crack appears in the zone of maximum tensile stress. As the load increases, flexural-shear cracks appear in shear span. Flexural failure mode for bubbled slab (BD1) is shown as circles

at midspan and spread toward the top fiber of bubbled slab in compression zone as shown in **Fig. 23**.

For prestressed bubbled slabs (BD2, BD4, BD5, BD6 and BD7), the first flexural cracks are observed as circles in the tension face of the bubbled slabs at midspan. As the load is increased, these cracks spread horizontally to the support and vertically to the top fiber of slabs, and when load increases, web-shear or flexural-shear cracks form diagonally in the voids region resulting in shear failure, as shown clearly in **Fig. 24** for bubbled slab (BD6).

5. CONCLUSION

Based on the analytical results, the following conclusion may be drawn:

1- The general behavior of the finite element models represented by the load-deflection curves at the midspan of the bubbled slabs shows good agreement with the experimental results. However, the finite element models show slightly more stiffness than the test data in both the linear and nonlinear ranges. The effects of bond slip and micro-cracks that occur in the experimental slabs which are excluded in the finite element models are contributing to the higher stiffness of the finite element models.

2- First cracking and ultimate loads for most models calculated by the finite element analysis are almost higher than those from the experimental data.

3- The variation of strain over the depth of cross-sections due to the incremental load for the finite element models, shows good agreement with the test data. Also, The analytical results show that, there is a significant increase in concrete strain of bubbled section occupied by the spherical voids in comparison with solid section (between two voids).

4- The crack patterns at the first cracking and ultimate loads obtained by the finite element models correlate well with the observed failure modes of the experimental slabs.

REFERENCES

- ACI Committee 318, 2014, *Building Code Requirements for Structural Concrete (ACI 318M-14) and commentary*, American Concrete Institute, Farmington Hills, 524pp.
- ANSYS, 2005, *ANSYS Help*, Release 10.0, Copyright.
- ASTM A416/ A416M, 2006, *Standard Specification for Steel Strand, Uncoated Seven-Wire for Prestressed Concrete*, ASTM International.
- BubbleDeck, 2006, *Lighter Flat Slab Structures with BubbleDeck*, www.BubbleDeck-UK.com.
- Desayi, P. and Krishnan, S.,1964, *Equation for the Stress-Strain Curve of Concrete*, Journal of the American Concrete Institute, Vol. 61, No. 3, pp. 345-350.

- Kwak, H.G. and Filippou F.C., 1990, *Finite Element Analysis of Reinforced Concrete Structures under Monotonic Loads***,** Report No. UCB/SEMM-90/14 Structural Engineering, Mechanics and Materials Department of Civil Engineering University of California.

- Marais, C. C., 2009, *Design Adjustment Factors and Economical Application of Concrete Flat-Slabs with Internal Spherical Voids in South Africa,* M.Sc Thesis, University of Pretoria.

- Neville, A.M., and Brooks, J.J., 1987, *Concrete Technology*, Longman Scientific and Technical, U.K, 438 pp.

- Oukaili, N., and Yasseen, H., 2014, *Effect of Prestressing Force on Performance of Polymer Bubbled Deck Slabs*, The 7th International Conference on FRP Composites in Civil Engineering (CICE 2014), Vancouver, Canada, pp. 1-6

- Precast/Prestressed Concrete Institute (PCI), 2010, *Design Handbook,* Sixth Edition, Precast/Prestressed Concrete Institute, Chicago, 736 pp.

NOMENCLATURE

Δ_u = ultimate deflection, mm

ε_{cu} = ultimate compressive strain

f_c' = the cylinder compressive strength of concrete, MPa

f_c = stress at any strain ε, MPa

ε_1 = strain corresponding to $(0.3f_c')$

ε_o = strain at the ultimate compressive strength f_c'

w_c = the air-dry unit weight of concrete, kg/m³

Table 1. Summary of test data **,Oukaili and Yasseen, 2014.**

Specimen	Thickness of Specimen, mm	Sphere Diameter, mm	Distance c/c of Spheres, mm	D/H	Type of Reinforcement	Number of Bars and / or Strands	Number of Spheres
BD1	150	100	115	0.67	Non-prestressed	2φ12 mm	80
BD2					Partially Prestressed	6φ12 mm & 2φ12.7 mm	

BD4					**Partially Prestressed**	**2φ12 mm & 2φ12.7 mm**	
BD5					**Fully Prestressed**	**2φ12.7 mm**	
BD6					**Partially Prestressed**	**2φ12 mm & 3φ12.7 mm**	
BD7					**Fully Prestressed**	**3φ12.7 mm**	

Table 2. Real constant.

Real Constant set	**Element Type**	**Constant**			
1	**SOLID65**		**Real Constant for Rebar 1**	**Real Constant for Rebar 2**	**Real Constant for Rebar 3**
		Material number	**0**	**0**	**0**
		Volume ratio	**0**	**0**	**0**
		Orientation angle	**0**	**0**	**0**
2	**LINK8**	**Cross-sectional area, mm**	**99.6**	**Strand Φ 12.7mm**	
		Initial strain, mm/mm	**0.0056**		
3	**LINK8**	**Cross-sectional area, mm**	**113.09**	**Steel Φ 12mm**	
		Initial strain, mm/mm	**0**		
4	**LINK8**	**Cross-sectional area, mm**	**78.53**	**Steel Φ 10mm**	
		Initial strain, mm/mm	**0**		
5	**LINK8**	**Cross-sectional area, mm**	**7.06**	**Steel Φ 3mm**	
		Initial strain, mm/mm	**0**		
6	**LINK8**	**Cross-sectional area, mm**	**28.27**	**Steel Φ 6mm**	
		Initial strain, mm/mm	**0**		
7	**SOLID45**			**Steel Plate**	

Table 3. Material properties.

Material model number	**Element type**	**Material properties**

1	SOLID65	**Linear i otropic**
		Ex 27583MPa
		PRXY 0.2

Multilinear isotropic

	Strain	Stress, MPa
Point 1	0.00046	12.93
Point 2	0.0008	15.98
Point 3	0.0015	29.74
Point 4	0.0020	35.83
Point 5	0.0029	43.10

Concrete

ShrCf-Op	0.2
ShrCf-Cl	0.8
UnTensSt	4.31MPa
UnCompSt	43.1MPa
BiCompSt	0
HydroPrs	0
BiCompSt	0
UnTensSt	0
TenCrFac	0

Material model number	Element type	Material properties
2	LINK8 Strand Φ 12.7mm	**Linear isotropic** Ex: 197500MPa PRXY: 0.3 **Multilinear isotropic** Point 1: Strain 0.0085, Stress 1657 MPa Point 2: Strain 0.009, Stress 1724 MPa Point 3: Strain 0.0095, Stress 1751 MPa Point 4: Strain 0.010, Stress 1770 MPa Point 5: Strain 0.015, Stress 1827 MPa Point 6: Strain 0.020, Stress 1860 MPa
3	LINK8 Steel Φ 12mm	**Linear isotropic** Ex: 200000MPa PRXY: 0.3 **Bilinear isotropic** Yield Stss: 442MPa Tang Mod: 0MPa
4	LINK8 Steel Φ 10mm	**Linear isotropic** Ex: 200000MPa PRXY: 0.3 **Bilinear isotropic** Yield Stss: 483MPa Tang Mod: 0MPa
5	LINK8 Steel Φ 3mm Meshes	**Linear isotropic** Ex: 200000MPa PRXY: 0.3 **Bilinear isotropic** Yield Stss: 546MPa Tang Mod: 0MPa
6	LINK8 Steel Φ 6mm Stirrup	**Linear isotropic** Ex: 200000MPa PRXY: 0.3 **Bilinear isotropic** Yield Stss: 598MPa Tang Mod: 0MPa

7	SOLID45	Linear isotropic	
		Ex	200000MPa
		PRXY	0.3

Table 4. Comparison of experimental and analytical results.

Specimen	Experimental				Finite Element Analysis				$P_{cr}(EXP)/P_{cr}(FEM)$	$P_u(EXP)/P_u(FEM)$
	Camber, mm	P_{cr}, kN	P_u, kN	Δ_u, mm	Camber, mm	P_{cr}, kN	P_u, kN	Δ_u, mm		
BD1	0	14	43.5	14.90	0	16.5	41.5	13.84	0.85	1.05
BD2	2.16	54	92	21.54	2.00	56.5	106.5	18.97	0.95	0.86
BD4	2.30	46	86	20.00	2.00	51.5	92.75	19.75	0.89	0.92
BD5	2.45	40	78	16.05	2.10	51	73.87	17.42	0.78	1.05
BD6	3.98	65	98	19.42	3.00	66.5	105.25	16.66	0.97	0.93
BD7	4.40	61	94	14.60	3.40	66.5	95.25	13.49	0.91	0.98

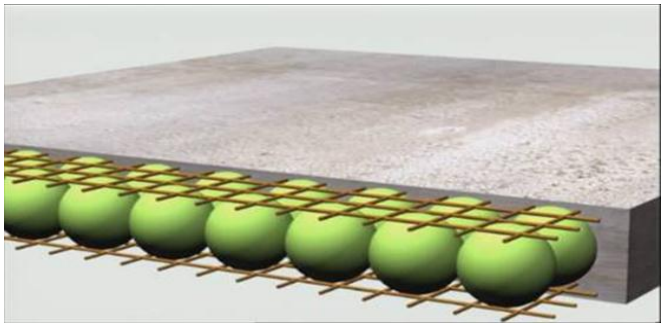

Figure 1. BubbleDeck floors system.

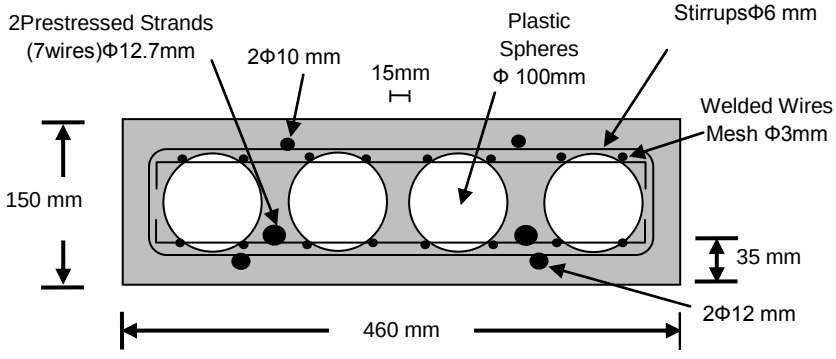

Figure 2. Reinforcement details.

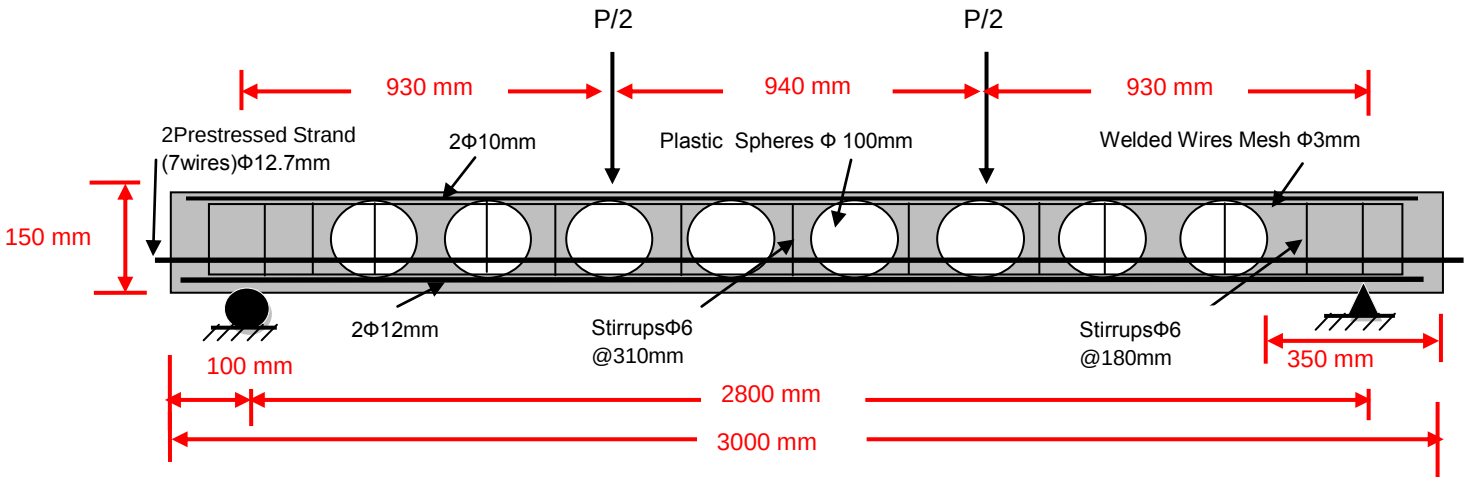

Figure 3. Full-scale model under loading.

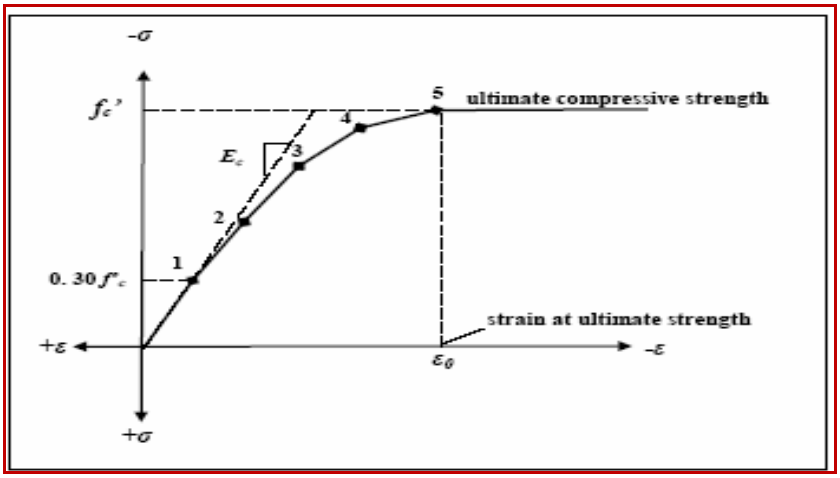

Figure 4. Simplified compressive uniaxial stress-strain curve for concrete.

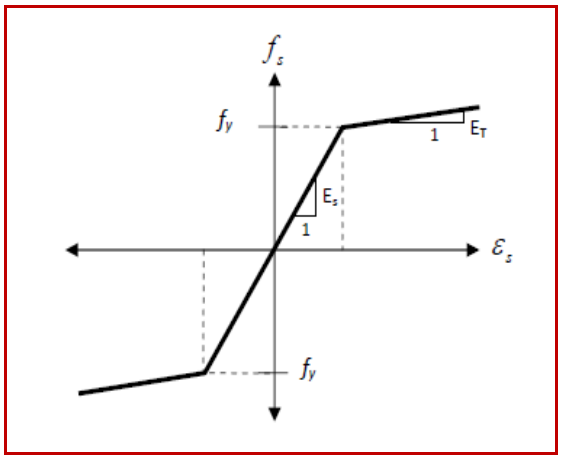

Figure 5. Steel stress-strain relation.

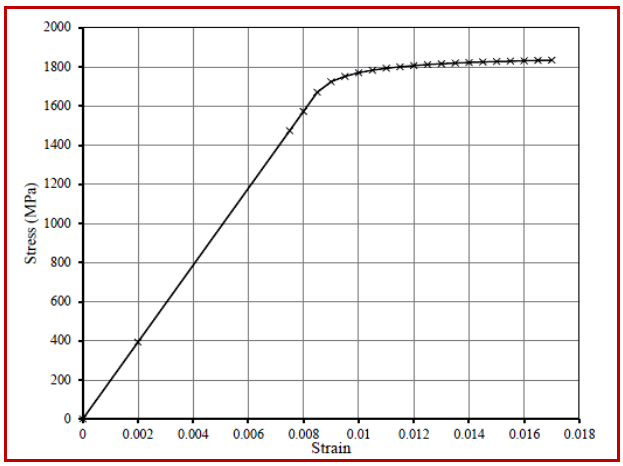

Figure 6. stress-strain curve for strand.

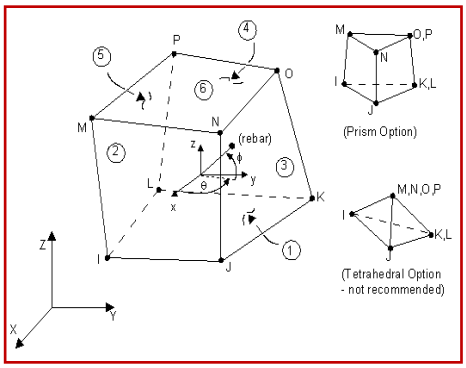

Figure7. SOLID65 element.

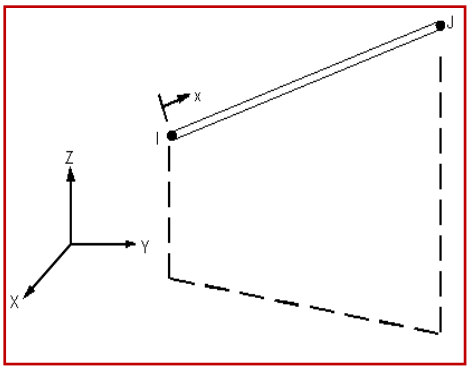

Figure 8. LINK8 element.

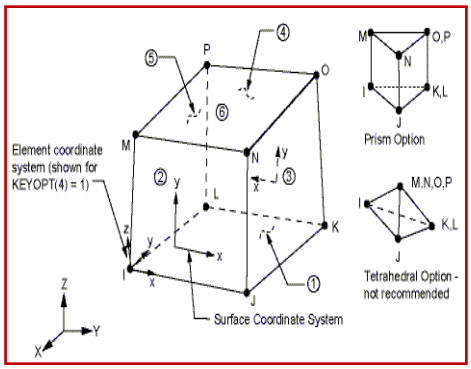

Figure 9. SOLID45 element.

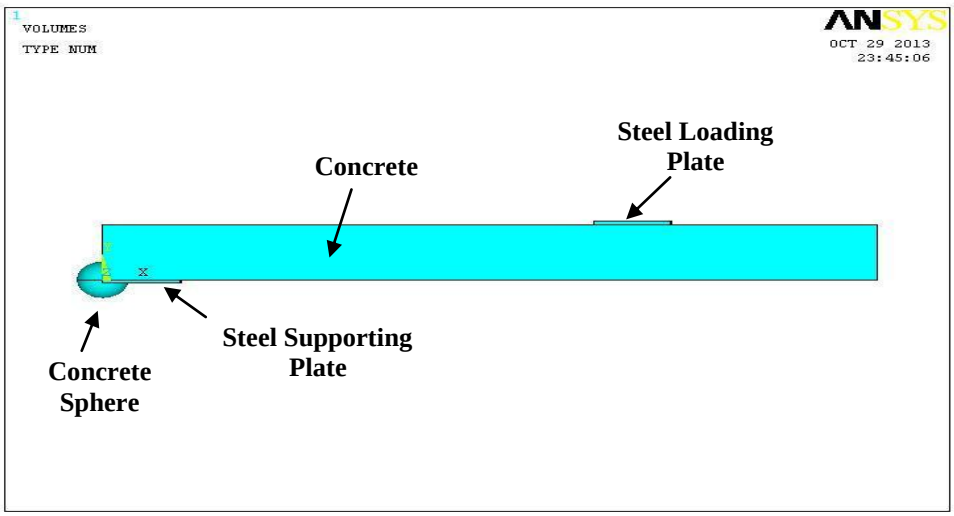

Figure 10. Modeling of concrete bubbled slab, steel supporting plate and steel loading plate.

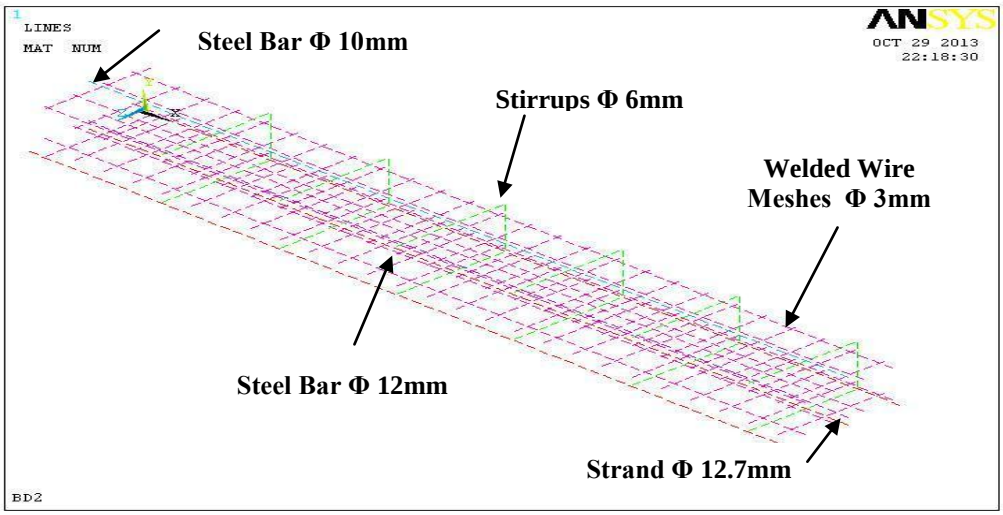

Figure 11. Modeling of flexural and shear reinforcement.

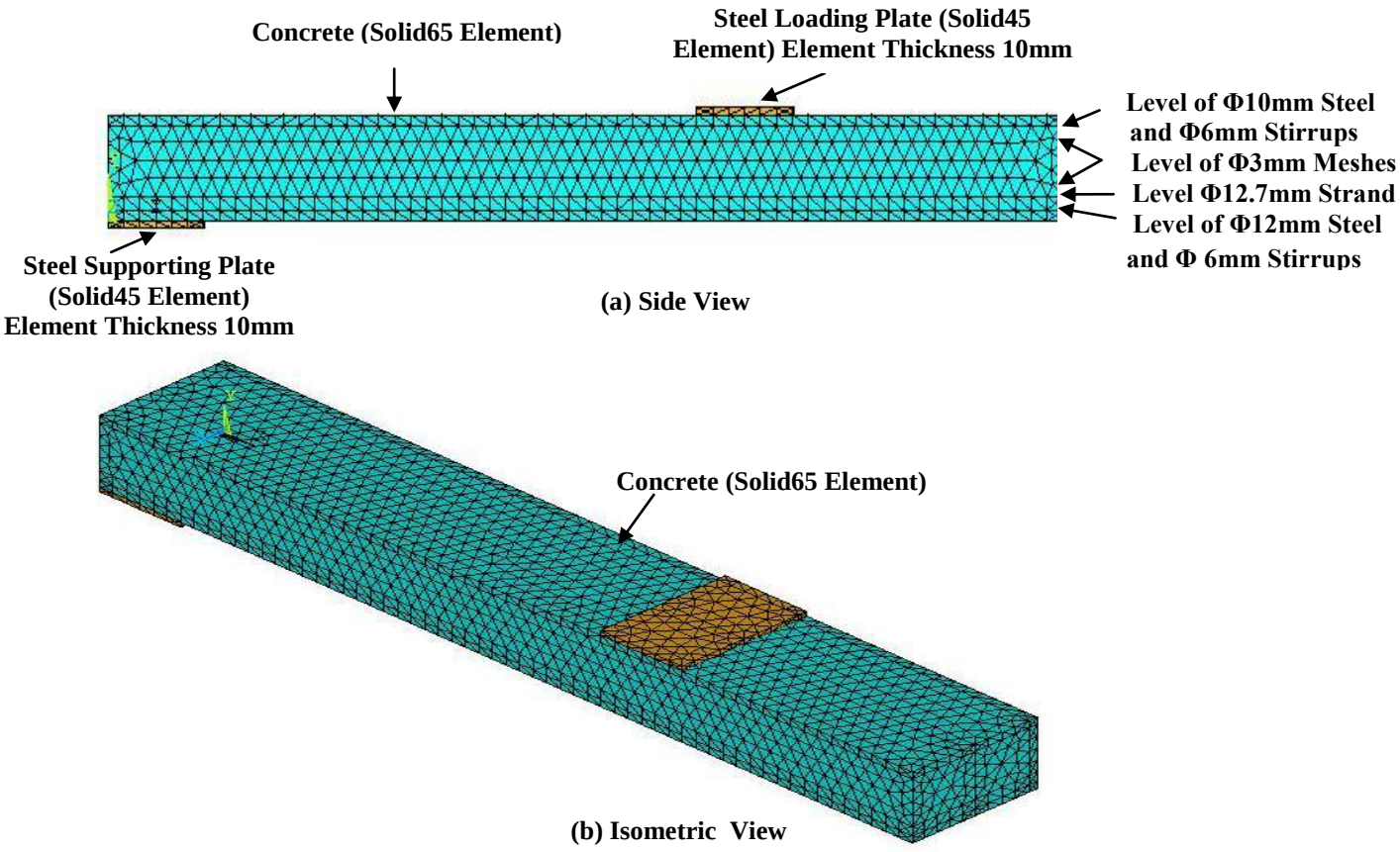

Figure 12. Meshing of concrete, support and plate.

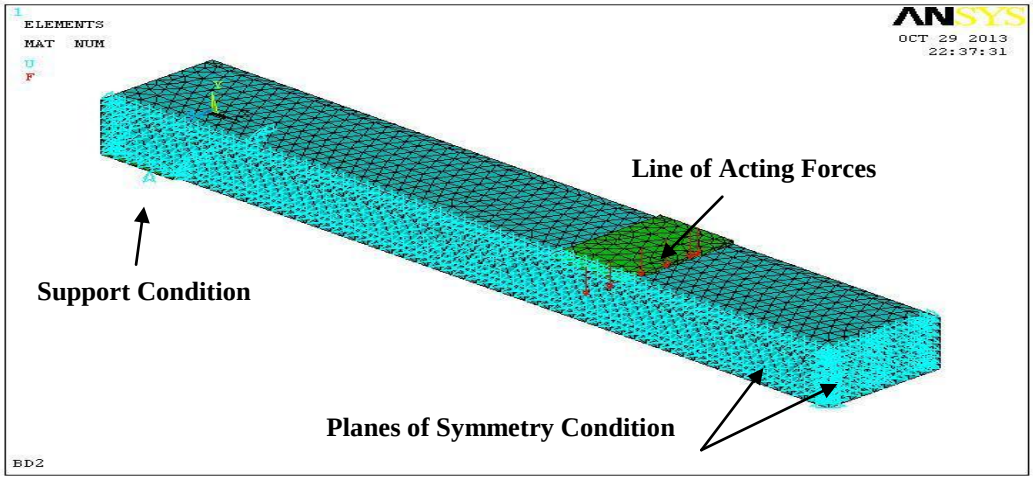

Figure 13. Loads and boundary conditions.

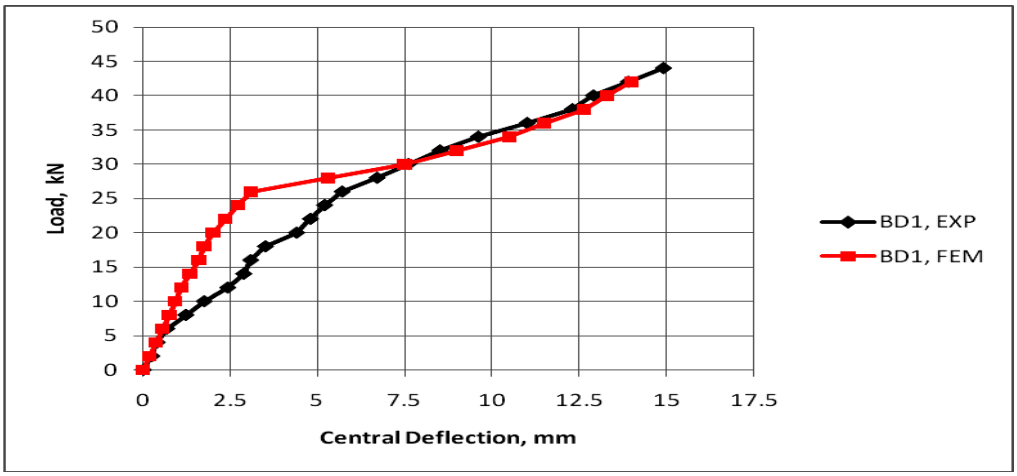

Figure 14. Comparison of experimental and analytical load-central deflection curves for BD1.

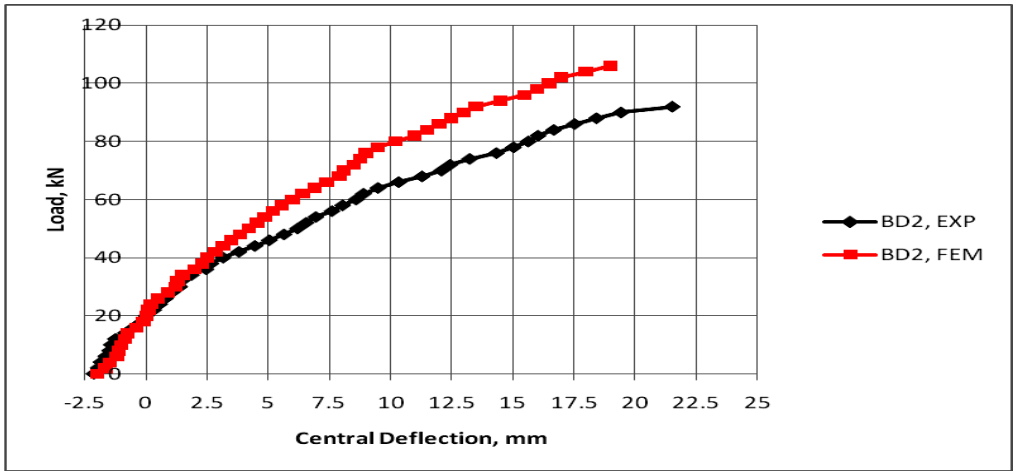

Figure 15. Comparison of experimental and analytical load-central deflection curves for BD2.

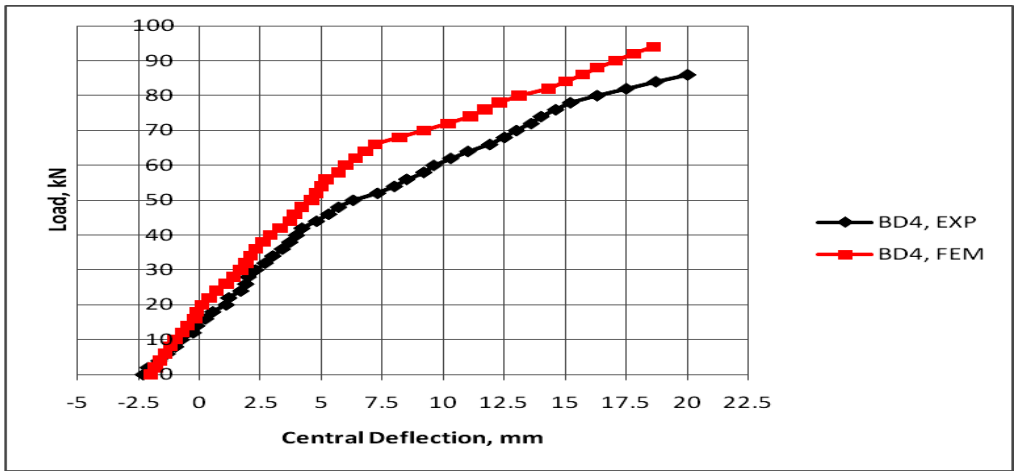

Figure 16. Comparison of experimental and analytical load-central deflection curves for BD4.

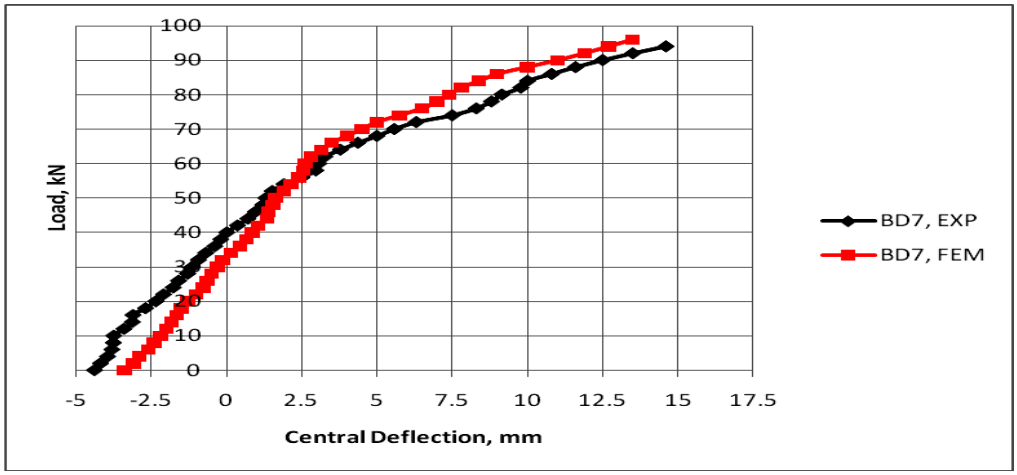

Figure 17. Comparison of experimental and analytical load-central deflection curves for BD7.

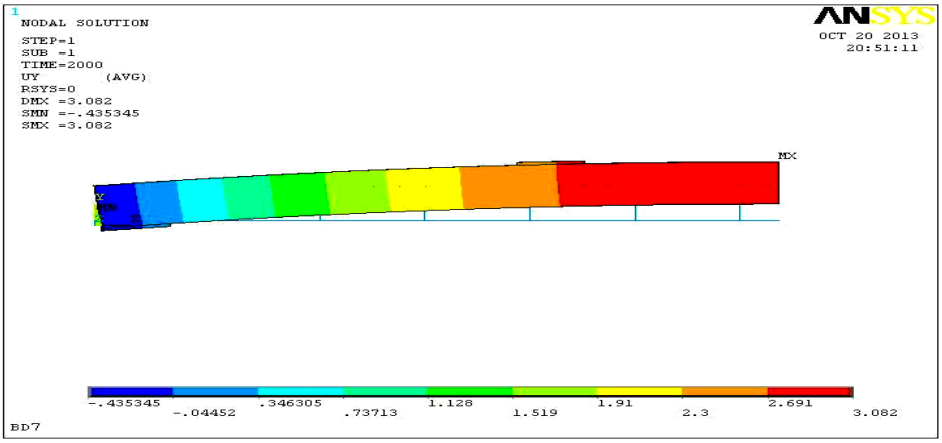

(a) Deflected shape due to prestressing force.

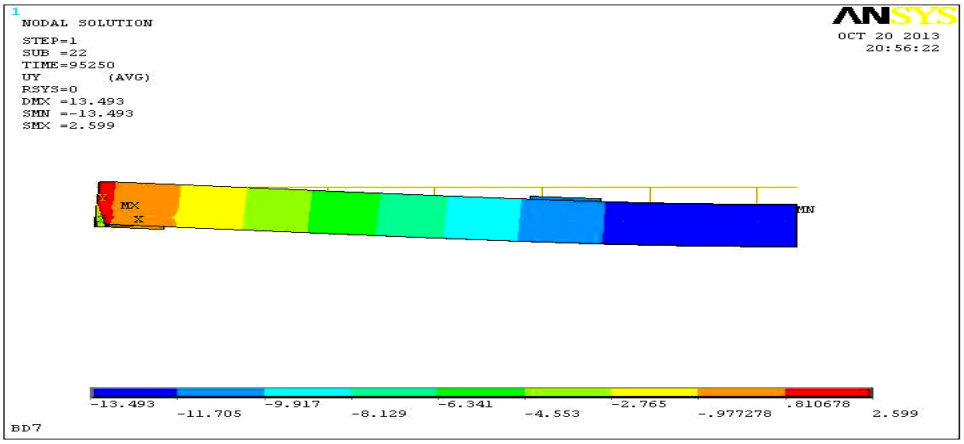

(b) Deflected shape at failure.

Figure 18. Deflected shape for BD7.

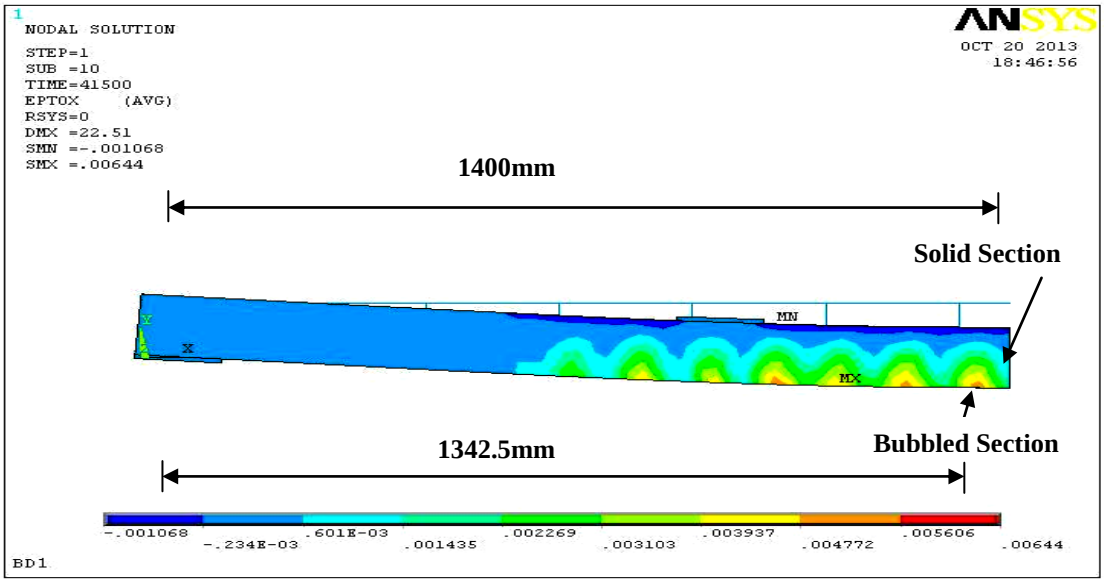

Figure 19. Strain contour for BD1 at ultimate load.

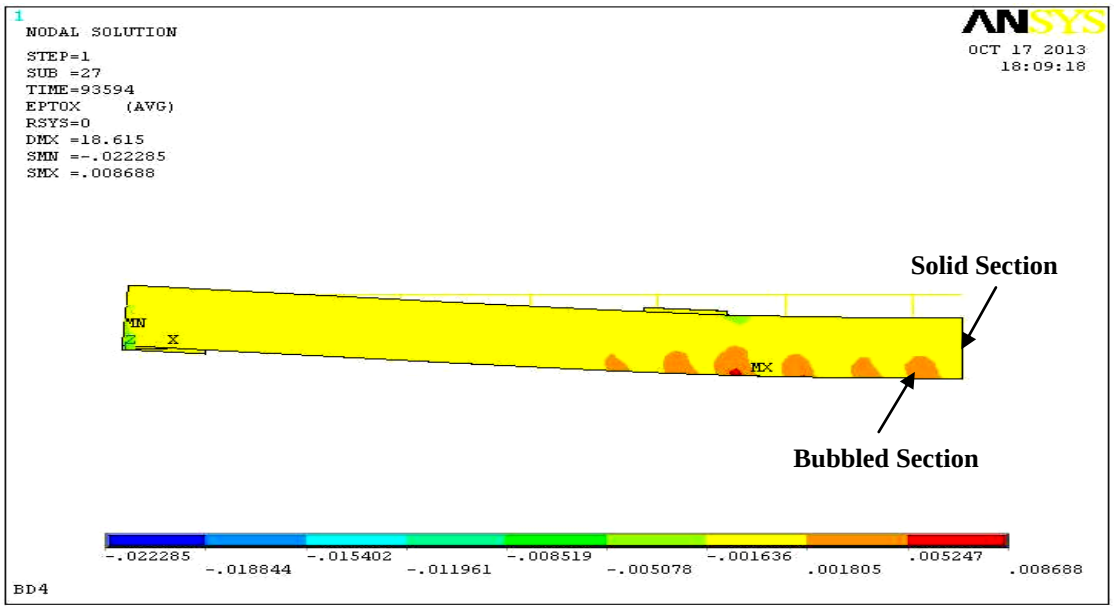

Figure 20. Strain contour for BD4 at ultimate load.

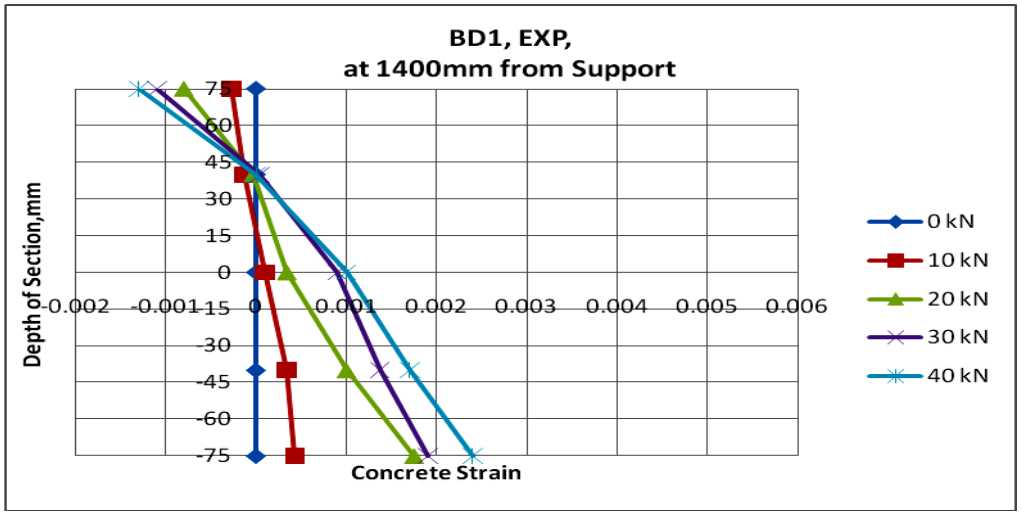

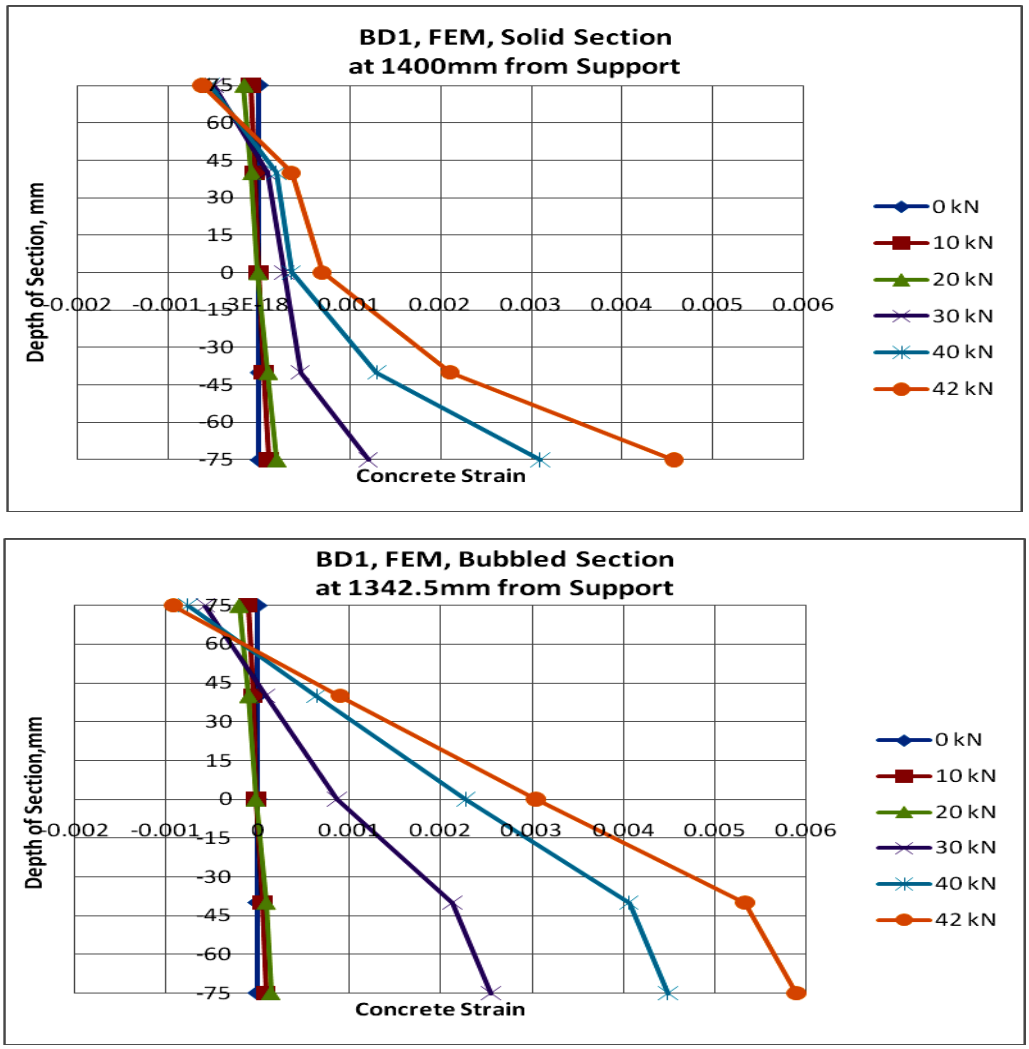

Figure 21. Comparison of experimental and analytical load-concrete strain curves for BD1.

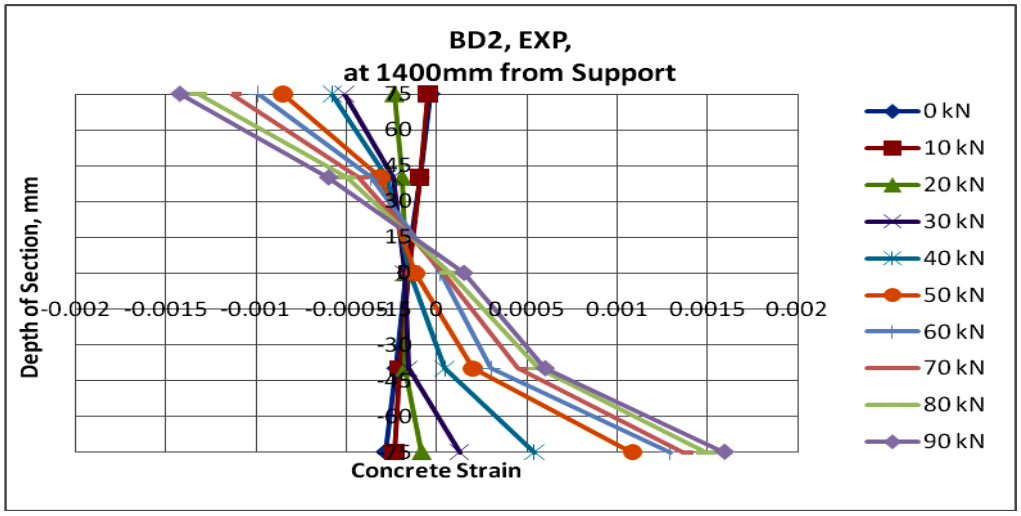

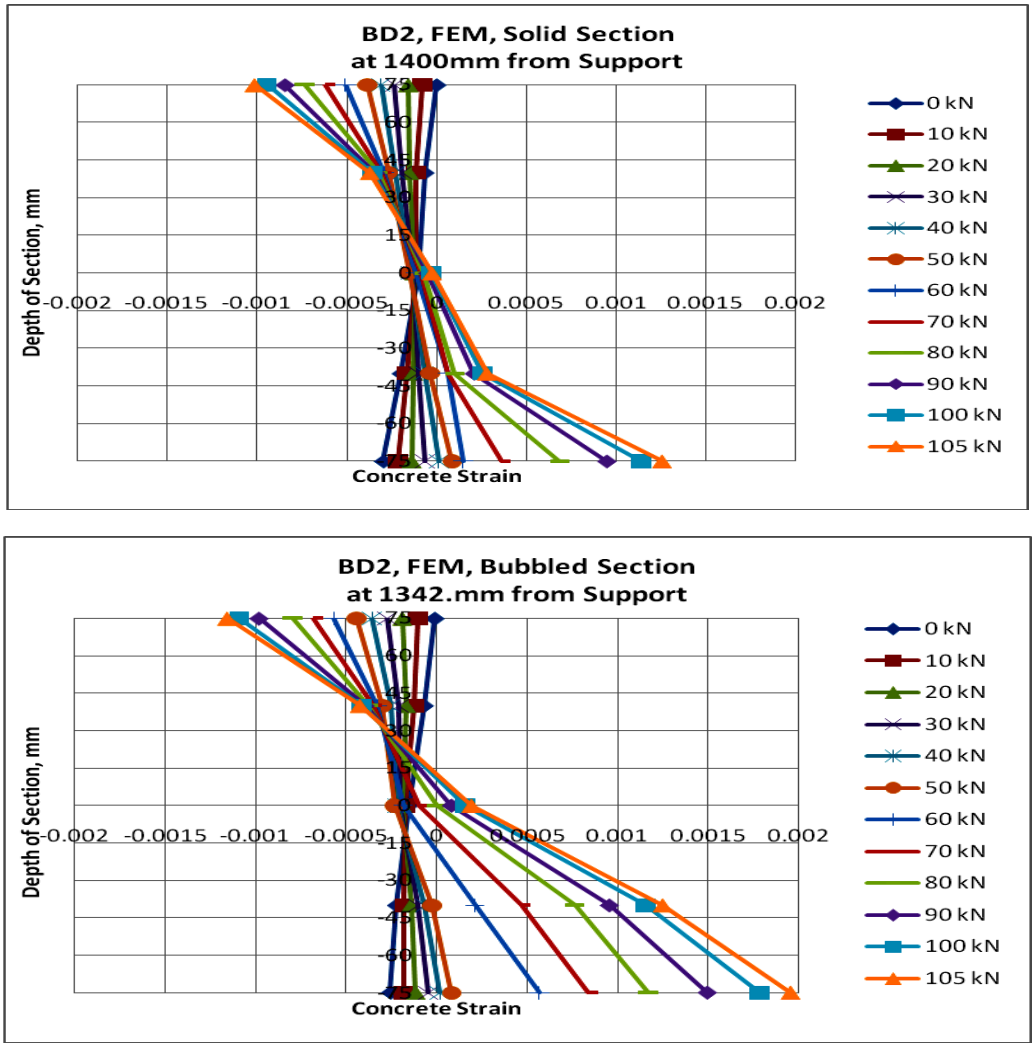

Figure 22. Comparison of experimental and analytical load-concrete strain curves for BD2.

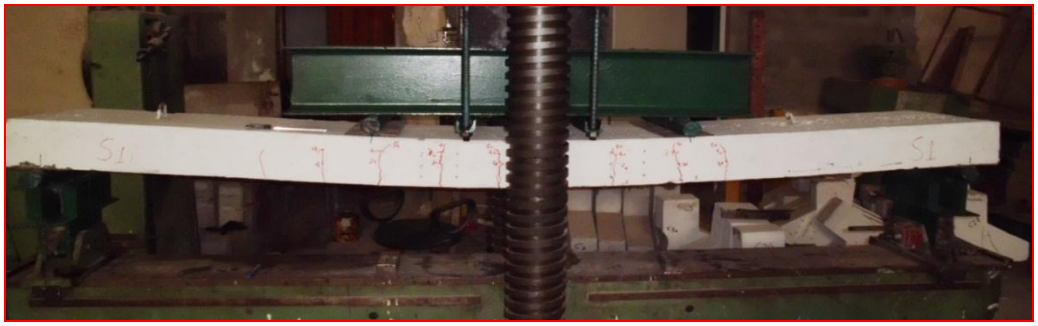

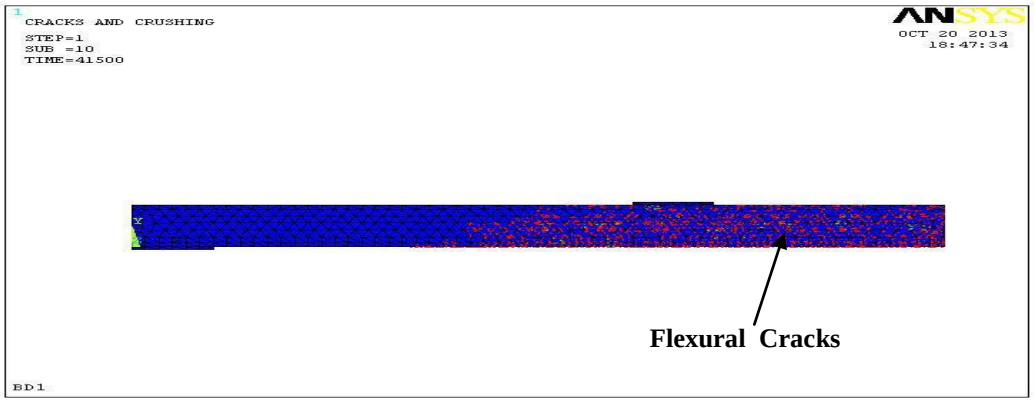

Figure 23. Comparison of experimental and analytical crack pattern at ultimate load for BD1.

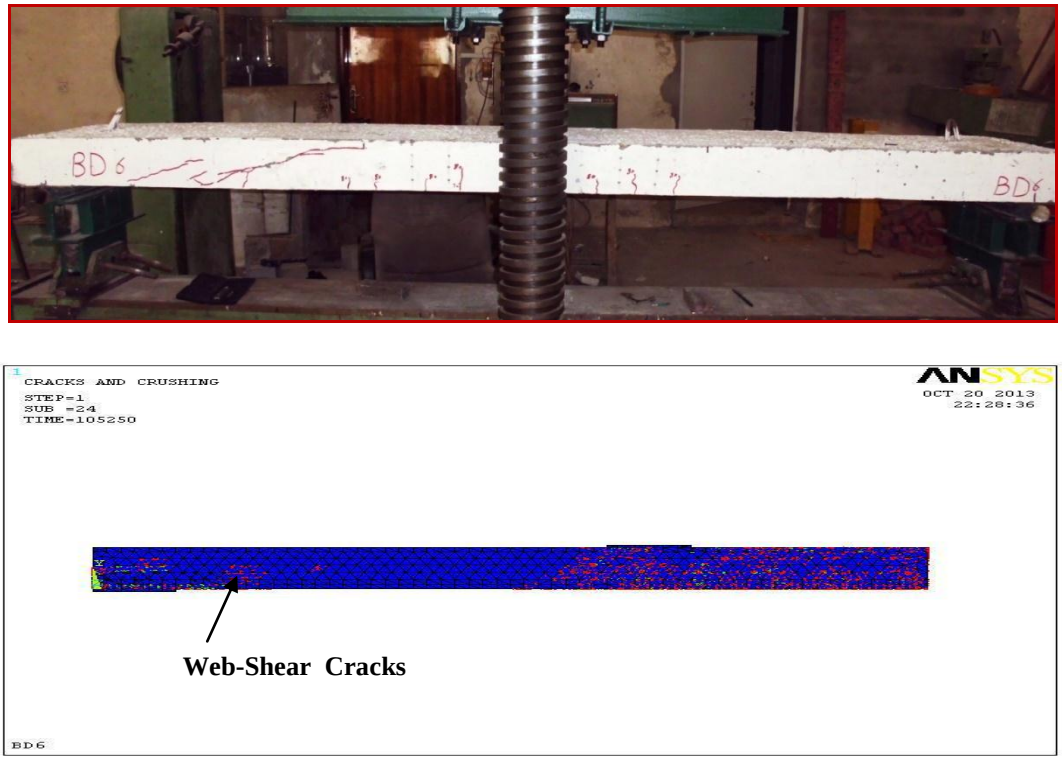

Figure 24. Comparison of experimental and analytical crack pattern at ultimate load for BD6.

Laboratory Preparation of Simulated Sludge for Anaerobic Digestion Experimentation

Mahmood K. H. Al-mashhadani
Lecturer
Department of Chemical Engineering
Engineering of College- University of Baghdad
E-mail: mkh_control@yahoo.com

Stephen J. Wilkinson
Professor
Department of Chemical Engineering
University of Chester, UK
E-Mail: s.j.wilkinson@chester.ac.uk

William B. Zimmerman
Professor
Department of Chemical and Biological Engineering
University of Sheffield, UK
E-Mail: w.zimmerman@sheffield.ac.uk

ABSTRACT

Health and environmental factors as well as operational difficulties are major challenges facing the development of an anaerobic digestion process. Some of these problems relate to the use of sludge collected from primary and secondary clarifier units in wastewater treatment plants for laboratory purposes.

The present study addresses the preparation of sludge for laboratory purposes by using a mixture that consists of the digested sludge, which is less pathogenic, compared to the collected sludge from the primary or secondary clarifier, and food wastes. The sludge has been tested experimentally for 19 and 32 days under mesophilic conditions. The results show a steady methane production rate from the anaerobic digester which used sludge with a rate of 1.5 l/day and concentration around 60%, with comparatively low H_2S gas content (10 ppm). The methane produced from the digester that used only digested sludge decreases during the experimental period.

Keywords: anaerobic digestion, digested sludge, food waste, biogas.

التحضير المختبري للوحل الافتراضي لاختبار الهضم اللاهوائي

د. محمود خزعل حمادي
مدرس
قسم الهندسة الكيمياوية
كلية الهندسة جامعة بغداد

د. ستيف ولكنسن
بروفسور
قسم الهندسة الكيمياوية
جامعة جستر- بريطانيا

د. وليم زيمرمان
بروفسور
قسم الهندسة الكيمياوية والبايلوجية
جامعة شفيلد - بريطانيا

الملخص

العوامل الصحية والبيئية بالاضافة الى الصعوبات التشغيلية هي تحديات رئيسية لا زالت تواجه تطوير عملية الهضم اللاهوائي. بعض هذه المشاكل تتعلق باستخدام الوحل الذي يؤخذ من وحدات الترسيب(الكلاريفاير) الابتدائية والثانوية في وحدات معالجة المياه الثقيلة للاغراض المختبرية. البحث الحالي يتناول تحضير الوحل للاغراض المختبرية مستخدما خليط من الوحل المعالج بايلوجيا في الهضم اللاهوائي, والذي يكون اقل تسبباً للامراض بالمقارنة مع المأخوذ من وحدات الترسيب الابتدائية والثانوية, مع مخلفات الطعام. الوحل المقترح اختبر تجريبيا لمدة 19 يوما و 32 يوما تحت ظروف حرارية متوسطة. النتائج بينت استقرارية معدل انتاج الميثان من الهضم اللاهوائي المستخدم الوحل مع معدل 1.5 لتر/يوم وبتركيز 60% تقريبا, مع محتوى قليل من غاز كبريتيد الهيدروجين (10 جزء بالمليون). بينما معدل انتاج الميثان المنتج من الهاضم الذي يستخدم الوحل المعالج بيالوجيا فقط يتناقص خلال الفترة التجريبية.

الكلمات الرئيسية: الهظم اللاهوائي, الوحل المعالج بايلوجيا, مخلفات الطعام , الغاز الحيوي.

1. INTRODUCTION

Anaerobic digestion is an important economic and biological process. It includes four stages (hydrolysis, acidogenesis, acetogenesis, and methanogenesis) in the absence of oxygen. The main benefits of this process are: sludge stabilisation; reduction of pathogens; reduction of odour and solids content in the sludge; conversion of organic matter into energy (biogas) for use as a renewable energy source; and production of fertilizer for agriculture **,Montgomery and Bochmann, 2014 ,Castellucci et al., 2013 ,Chelliapan et al., 2012 ,Batstone et al., 2002 and Angenent et al., 2004.**

Collection of the sludge from either primary or secondary clarifier units for laboratory purposes has become unacceptable for health and environmental reasons, which have become a major concern for many researchers and being an additional burden when they are conducting their experimental work.

Even though several attempts have been made to resolve these problems through the use of simulated sludge, the results obtained from these experiments have been compromised by the use of simulated sludge, and the question of how closely it conforms to real sludge. In most cases, the physical, chemical and biological properties of fresh sludge, collected from wastewater treatment plants, are unknown; in addition they continually change. Such changes can be influenced by, for instance, the type of wastewater, sampling and storage duration, handlings and transfers from wastewater treatment plant to the laboratory, weather conditions and seasonal changes, variation of water treatment equipment design and operating conditions. Biologically, many types of anaerobic bacteria exist in wastewater, **Baudez et al., 2007.**

The activity and type of these bacteria mainly depend on the characteristics of wastewater and weather conditions at the time of sampling, as well as on the collection method used. These parameters, for instance, would strongly affect the biogas production rate and the efficiency of biodegradation of the organic matter in the sludge. Chemical and physical properties of sewage sludge vary with time; this makes it difficult to link the results obtained from experiments carried out using different sludge batches (e.g. starter inoculums).

Therefore, in an attempt to prevent this problem occurring, the authors of the present study considered using an identical sampling procedure for the sludge by taking sludge samples from one pre-identified source. The sludge inoculums which been simultaneously taken from a wastewater treatment plant would have been introduced into the two reactors under similar operating conditions, in an attempt to produce the most accurate results possible; as is reported in this study. However, the collection of sludge samples from primary and/or secondary clarifiers for lab-tests has become unacceptable due to numerous health and environmental restrictions.

Hence, a process for the simulation of sludge samples has been adopted in an attempt to overcome these restrictions.

In earlier studies, a synthesised sludge consisting of organic and inorganic synthetic components has been used, **Baudez et al., 2007and Dursun et al., 2004.** However, the suggested methods still need to be further clarified through simpler procedures for preparation and use.

This study suggests using a mixture of digested real sludge (which pose less danger than sludge collected from primary and secondary clarifiers) and simulated sludge formed from food waste.

2. MATERIALS AND METHODS

2.1 Synthetic the Suggested Sludge

Achieving secure discharge of the food waste collected from households, restaurants, and residues from the food industry, which makes up about 70% of the total municipal solid waste in Malaysia, **Hassan et al.,2001** and three billion tons in Europe in 2003 **,Pavan et al., 2007** has become a major challenge for the environment. Several methods have been used for the treatment of food waste. Although landfill dumping of food waste has been the most common method of reducing the volume, pathogens and odour of such waste, the incurred costs and comparatively large areas taken up by landfill sites are serious drawbacks of this method. Utilisation of food waste as a source of energy generation has become the best practice both, environmentally and economically, through the use of biological processes such as anaerobic digestion. Such treatments have the combined benefits of reducing the effects of food wastes as well as producing biogas and digested sludge (compost) which can be used as soil fertiliser. The different types of organic matter which make up food waste are presented in **Table 1** ,which shows the substrates that are required for the anaerobic digestion process.

The simulated sludge, which was suggested in this study, consists of a mixture of anaerobic digested sludge mixed with food wastes. The components and quantities of the food wastes constituents used in the present study are presented in **Table 2.**

Fresh meat, red beans, peas, lentils, white beans, chickpeas, carrots, and rice are the principle materials used in the sludge in the present study, since these materials have the organic material (lipids, polysaccharides, proteins and nucleic acids) necessary for anaerobic bacteria. The first six materials were initially boiled at 100 ^{o}C for 1 hour, before being added to the rice, which has been soaked in water for 24 hours. Then, the product from the previous stage was thoroughly mixed for 30 min to make a simulated food waste with more slurry after adding the water.

According to the recommendations provided by earlier studies, feeding the digester with nutrients or trace metals was not necessary**, Perez-elvira et al., 2011 ,Chamy and Ramos, 2011, ,Braguglia et al., 2011, ,Kim et al., 2011 and Siggins et al., 2011.** The studies reported that sludge taken from wastewater treatment plant did not require the addition of any supplementary nutrients or trace metals, as the used sludge already contained lipids, polysaccharides, proteins and nucleic acids that are required for the digestion process.

The digested sludge, used in these experiments, was collected from an outlet stream of a full-scale mesophilic digester at “Woodhouse wastewater treatment plant” in the UK.

2.2 The Experimental Setup

Two main setup procedures were applied in this study. The first procedure was experimental testing of the suggested mixture, which was used in the first setup trial. This mixture consisted of a portion of the digested sludge collected from our earlier experiments and a portion of the digested sludge collected from the anaerobic digester from wastewater treatment, in addition to the food waste which was simulated and prepared in the present study. The aim of the second setup practice was to analyse the prepared simulated sludge in order to create a semi-continues process for long operation periods.

In this experiment, two identical bench-scale anaerobic digesters were setup. The digester has an overall volume of 15 litres, with a working volume of 9 litres. The working days of this experimental work were 19 and 32 days. The digesters were operated under mesophilic

conditions (36^{o}C to 38^{o}C). Continuous measurements of biogas produced from both digesters were achieved by downward displacement of acidic aqueous solution (pH <4). All volumes of biogas given in this study have been corrected to 1atm pressure and 20^{o}C. Thus, the total volume of biogas equals to volume of the collector (i.e volume of cylindrical tube). Continuous measurement of methane, carbon dioxide and hydrogen sulphide concentrations in the biogas mixture was carried out daily by biogas analyser (Data gas analyser, Model 0518) at 1atm pressure. A schematic diagram and photograph of the experimental apparatus is shown in **Fig.1** and **Fig.2** respectively. The digested sludge collected from Woodhouse Wastewater Treatment Plant (WWTP) in the United Kingdom, was used with the same preparation procedure that was used in first stage.

A PID controller was used in the present study to maintain the temperature in the reactor with mesophilic conditions. The digester was fitted with a pH controller, type ON/OFF controller (model BL931700 pH minicontroller) to monitor pH values in the digester. 0.2M sodium bicarbonate ($NaHCO_3$) was used to adjust the digester pH to the optimum pH value, (6.8 - 7.4, which provides a suitable environment for growth of the anaerobic bacteria).

Volatile fatty acids (VFAs) content was measured according to Hach Lange for Water Quality procedure, **Esterification method, 1962** in which the sample was filtered by centrifugal device (Eppendorf centrifuge 5810) at 2000 rpm for 10 min. Then, an aliquot of 0.5 ml of centrifuged sample was pipetted into a dry 25 ml sample cell. While the second dry sample cell has 0.5 of deionised (DI) which was prepared to calibrate the spectrometer device. Ethylene glycol (1.5 ml) and sulphuric acid (0.2 ml and 19.6 N) were also introduced into each sample cell. The hydroxylamine hydrochloride solution (0.5 ml), sodium hydroxide (2.0 ml and 4.5 N) and ferric chloride sulphuric acid solution (10 ml) are used in the evolution of VFAs.

3. RESULTS AND DISCUSSION

Many experiments with different conditions and methods were conducted in order to achieve the best simulation process. The experiments were carried out starting with raw sludge collected from WWTP, followed by the direct use of the food waste and digested sludge. Although many experiments gave negative results, some of the experiments which showed positive results have encountered environmental problems (e.g. producing huge amounts of H_2S gas). For instance, when the food waste was used as a sole feed stock with no added digested sludge; huge amounts of biogas were produced with comparatively high H_2S content, which was out of the range of the biogas analyser used in this experiment. This increase was result of high organic loading rate that led to inhibit the methanogenesis bacteria, **Babaee and Shayegan, 2011.** Thus, hydrogen and acetate produced from the early stage of this process can be consumed by sulfate-reducing bacteria, which considers thermodynamically favourable more than methanogenesis bacteria in consumption of hydrogen and acetate, to produce hydrogen sulphide **,Isa et al., 1985.** Therefore, concentration of hydrogen sulphide in the biogas is an indicator of the success or otherwise of the anaerobic digestion process, **Karhadkar et al., 1986.** This problem, consequently led to a full shut down of the digestion process.

In further experiments, the efficiency of the simulated sludge prepared for use in this study was evaluated by measuring the biogas production rate from anaerobic digestion as methane gas. The latter is produced by methanogenic bacteria through the anaerobic digestion process, which, when encounters any problem, prevents or slows biogas production (methane and carbon dioxide). Methane, carbon dioxide and hydrogen sulphide, as well as oxygen, were continuously monitored during the experimental operation period.

The effect of the addition of the food waste supplement to the feed substrate on biogas production has been investigated in this section. **Figs.3** and **4** show yield of biogas from two anaerobic digesters fed with and without supplementary food waste substrate, respectively. It can be clearly seen that the amount of biogas produced from the first digester, which was fed with supplementary food waste, is more than that produced from the second digester (e.g. fed with only digested sludge).

Fig.5 shows the biogas concentration produced from the digester that was fed with 15 ml of food waste. During the first six days of the experiment, the carbon dioxide produced from the digester was more than the methane. The main reason for this is that high production of carbon dioxide takes place in the second stage of the anaerobic digestion process via converting the propionate and butyrate to acetate, hydrogen and carbon dioxide as shown in the following equations. Moreover, the acidogenesis bacteria are faster growing than methanogenesis bacteria. However, it depends on the activity of anaerobic bacteria, sampling and operational conditions.

$$3C_6H_{12}O_6 \longrightarrow 4CH_3CH_2COOH + 2CH_3COOH + 2CO_2 + 2H_2O$$

$$CH_3CH_2COOH + H_2O \longrightarrow CH_3COOH + CO_2 + 3H_2$$

$$C_6H_{12}O_6 \longrightarrow CH_3CH_2CH_2COOH + 2CO_2 + 2H_2$$

$$C_6H_{12}O_6 + 2H_2O \longrightarrow 2CH_3COOH + 2CO_2 + 4H_2$$

As some of the produced carbon dioxide remains as a dissolved gas in the sludge, another portion of CO_2 gas strips up of the digester to biogas collector.

In addition, in this stage, the methanogenic bacteria have a very slow growth and they need time to complete the fermentation process. These bacteria convert a part of the produced carbon dioxide to methane by reducing the partial pressure of hydrogen produced from the second phase to around 10^{-4} atmosphere, **Schink, 1997 and Stams et al., 2005.** Reduction of hydrogen concentration to this level ensures the success the whole process by reducing the accumulation of volatile fatty acids, as well as increasing the production of methane. The amount of methane produced from the reaction of hydrogen with carbon dioxide is estimated by 30%, **Appels, et al., 2008, ,Sahlstrom, 2003 ,Ahring, 2003 and Metcalf and Eddy, 2003.** Thus, the methane production usually increases day per day until reaches to a known-value (e.g. ≈60%). During the operation of the anaerobic digestion process, 15 ml of food waste slurry was fed into the digester every day. Equally, similar quantities of sludge were removed daily from the digester in order to maintain a constant working volume.

In order to evaluate the efficiency of the degradation process of organic material (food waste) at different stages, the concentration of volatile fatty acid (VFAs) was measured at different intervals during the operating period, considering that the VFAs are raw materials to produce the acetates molecules by acetogenic bacteria. **Fig.6** below indicates that the concentration of VFAs in the digester fed with sludge and food waste show higher values than that in the digester with sludge only. Moreover, there were no significant variations in pH values throughout the experiments, and the pH values were kept at optimal conditions as shown in **Fig.7**. Thus, this finding evidently supports the fact that the increase in VFAs was not because of an accumulation

process, but these values would be converted into acetate by acetogenic bacteria and then to the methane by methanogenic bacteria.

Although the experiment in this stage has shown encouraging results with both digested sludge and food waste, this experiment was repeated but for a longer operation period in an attempt to confirm the obtained results and the behaviour of the process. **Figs.8** and **9** show the methane and carbon dioxide produced from the anaerobic digester, respectively, over 32 days of operation. The trend of methane production has been stable during the operation period.

Fig.10 below shows percentages of biogas components (e.g. CH_4 and CO_2) produced from the anaerobic digester fed with a simulated sludge. It can be seen that the percentages of main gases (methane and carbon dioxide) were around 60-70% and around 20%, respectively. The data obtained from the experiments shows that the use of suggested simulated sludge keeps operation of the anaerobic digestion with desired results, providing that H_2S values are kept low as shown in **Fig.11**.

It would, therefore, be expected that any accumulation of dissolved CO_2 in the digesters without pH control would lead to lowering of pH, however, as shown in **Fig.12**, the results showed the capability of the used pH control system to maintain the pH within an ideal range in both digesters. It should also be noted that there was also a natural buffering effect whereby acids produced can immediately react with ammonia produced from biodegradation of proteins.

4. CONCLUSION

Collecting sludge from either primary or secondary clarifier units in wastewater treatment plants, for laboratory purpose, has been unacceptable due to several health and environmental reasons. The present study suggested mixture, which consists of digested sludge fed with food waste as semi-continuous process, for laboratory purposes. The results obtained from the experiments shows that the use of the suggested simulated sludge through 19 and 32 day, keeps operation of the anaerobic digestion with desired results (60% methane), while the hydrogen sulphide values are kept low no more than 10 ppm. According to these results, the use of such a preparation for the purposes of laboratory when dealing with anaerobic digestion, provides the stability of the process with less environmental and health hazard.

5. ACKNOWLEDGMENT

W.Z. would like to acknowledge support from the EPSRC (Grant No. EP/I019790/1). W.Z. would like to acknowledge the Royal Society for a Brian Mercer Innovation award and the Royal Academy of Engineering for an industrial secondment with AECOM Design Build. MKHaM would like to thank the Iraqi Ministry of Education for a doctoral scholarship. S.W. would like to acknowledge support from MWH UK.

6. REFERENCES

- Ahring, B. K. 2003, *Perspectives For Anaerobic Digestion. Biomethanation I, Verlag I.Springer Berlin / Heidelberg,* Springer, New York, book, Vol. 81, PP. 1-30.

- Angenent, L. T., Karim, K., Al-Dahhan, M. H., Wrenn, B. A. and Domíguez-Espinosa, R. 2004, *Production of bioenergy and biochemicals From Industrial and Agricultural Wastewater.* Trends in Biotechnology, Vol. 22, No.9, 477-485.

- Appels, L., Baeyens, J., Degrève, J. and Dewil, R. 2008, *Principles and Potential of the Anaerobic Digestion of Waste-Activated Sludge*. Progress in Energy and Combustion Science, Vol. 34, No.6, PP. 755-781.

- Babaee, A. and Shayegan, J. 2011, *Effect of Organic Loading Rates (OLR) on Production of Methane from Anaerobic Digestion of Vegetables Waste*. Bioenergy Technology, Linkoping, Sweden.

- Batstone D.J., Angelidaki I., Kalyuzhnyi S.V., Pavlostathis S.G., Rozzi A., Sanders W.T.M., Siegrist H., and Vavilin V.A., 2002, *The IWA Anaerobic Digestion Model No 1 (ADM1)*. Water Science and Technology Vol. 45, No. 10, PP. 65–73.

- Baudez, J. C., Ginisty, P., Peuchot, C. and Spinosa, L. 2007, *The Preparation of Synthetic Sludge for Lab Testing.* Water Science and Technology. Vol. 56, No. 9, PP. 67-74.

- Braguglia, C. M., Gianico, A. and Mininni, G. 2011, *Laboratory-scale Ultrasound Pre-Treated Digestion of Sludge: Heat and Energy Balance*. Bioresource Technology, Vol. 102, No.16, PP. 7567-7573.

- Castellucci S., Cocchi S., Allegrini E., and Vecchione L., 2013, *Anaerobic Digestion and Co-Digestion of Slaughterhouse Wastes*., Journal of Agricultural Engineering., Vol XLIV(s2):e104. PP. 526-530.

- Chamy, R. and Ramos, C. 2011, *Factors in the Determination of Methanogenic Potential of Manure. Bioresource Technology*, Vol. 102, No.17, PP. 7673-7677.

- Chelliapan S., Mahat S. B., Md. Din M. F., Yuzir A., Othman N., 2012, *Anaerobic Digestion of Paper Mill Wastewater*., Iranica Journal of Energy and Environment 3 (Special Issue on Environmental Technology), PP. 85-90.

- Dursun, D., AYOL, A. and Dentel, S. K. 2004, *Physical Characteristics of a Waste Activated Sludge: Conditioning Responses and Correlations with aSynthetic Surrogate*. Water Science and Technology, Vol. 50, No.9, PP. 129-136.

- Esterification Method, 1962, Hach Lange united for water quality, (www.hach-lange.com, VolatileAcid_8196_2800.fm), Adapted from the Analyst, Vol. 87, PP. 949.

- Hassan MN, Chong TL, Rahman M, Salleh MN, Zakaria Z, Awang M, 2001, *Solid Waste Management in Southeast Asian Countries with Special Attention to Malaysia*. Proceeding Sardinia 2001, Eight International Waste Management and Landfill Symposium.

- Isa, z., Grusenmeyer, s., and Verstraete, w., 1986, *Sulfate Reduction Relative to Methane Production in High-Rate*, Applied and Environmental Microbiology, Vol. 51, No. 3. p. 580-587.

- Karhadkar, P. P., Audic, J.-M., Faup, G. M. and Khanna, P. 1987, *Sulfide and Sulfate Inhibition of Methanogenesis*. Water Research, Vol. 21, No.9, PP. 1061-1066.

- Kim, H., Nam, J. and HS.SHIN 2011, *A Comparison Study on the High-Rate Co-Digestion of Sewage Sludge and Food Waste Using A Temperature-Phased Anaerobic Sequencing Batch Reactor System*. Bioresour Technol., Vol. 102**,** PP. 7272-9.

- Metcalf and Eddy. 2003, *Wastewater Engineering Treatment and Reuse*, book, McGraw Hill.

- Montgomery L. F. R. and Bochmann G. 2014, *Pretreatment of feedstock for enhanced biogas production*. IEA Bioenergy. ISBN 978-1-910154-05-2.

- Pavan P., Bolzonella D., Battistoni E. and Cecchi F. 2007, *Anaerobic co-digestion of Sludge with Other Organic Wastes in Small Wastewater Treatment Plants: An Economic Considerations Evaluation*. Water Science and Technology. Vol. 56, No.10, PP. 45-53.

- Pérez-Elvira, S. I., Fdz-Polanco, M. and Fdz-Polanco, F. 2011, *Enhancement of the Conventional Anaerobic Digestion of Sludge: Comparison of Four Different Strategies*. Water Science and Technology, Vol. 64, PP. 375-383.

- Sahlstrom, L. 2003, *A review of Survival of Pathogenic Bacteria in Organic Waste Used in Biogas Plants*. Bioresource Technology, Vol. 87, No.2, PP. 161-166.

- Schink, B. 1997. *Energetics of Syntrophic Cooperation in Methanogenic Degradation*. Microbiology and Molecular Biology Reviews, Vol. 61, No. 2, 262-280.

- Siggins, A., Enright, A. M. and O'flaherty, V. 2011. *Temperature Dependent (37-15°C) Anaerobic Digestion of a Trichloroethylene-Contaminated Wastewater*. Bioresource Technology, Vol. 102, No.17, PP. 7645-7656.

- Stams, A. J. M., Plugge, C. M., De Bok, A. F. M., Van Houten, B. H. G. W., Lens, P., Dijkman, H., and Weijma, J. 2005, *Metabolic Interactions in Methanogenic and Sulfate-Reducing Bioreactors*. Water Science and Technology, Vol. 52, No 1, PP. 13-20.

Table 1. Type of organic matters in food waste.

Organic materials	Source
Lipids	*Butter, Cheese, Whole Milk, Ice Cream, Cream And Fatty Meats*
Polysaccharides	*Potatoes, Wheat, Corn, Rice, and Cassava*
Protein	Lamb, Egg, Beef, Marmite
Nucleic acids	Plant and animal foods like meat, Certain vegetables and alcohol

Table 2. Details of materials which was used in the synthetic sludge.

	Name	Organic content	Quantity (g)
1	Rise	***Carbohydrates (80%)***, Fat, Protein, Vitamin B1,2,3,5,6,9,C, Calcium, Phosphorus, Potassium, Iron	1250
2	Meat	Protien	400
3	Red bean	Protien, Carbohydrates, Fat	600
4	Peas	Carbohydrates, Fat, Protein, Vitamin A, B1,2,3,5,6,9,C, Iron	
5	Lentils	Protien, Sugars, Carbohydrates, Fat, Vitamen B1,9, Cacium, Iron, Phosphorous, Potassium, Sodium	
6	White bean	Protien, Carbohydrates, Fat	
7	Chickpea	Carbohydrates, Fat, Sugar, Protein, Vitamin A, B1,2,3,5,6,9,12,C,E, K Iron, Phosphorus, Potassium, Sodium	
8	Carrot	Carbohydrates, Fat, Sugar, Protein, Vitamin , Iron, Phosphorus, Potassium, Sodium	

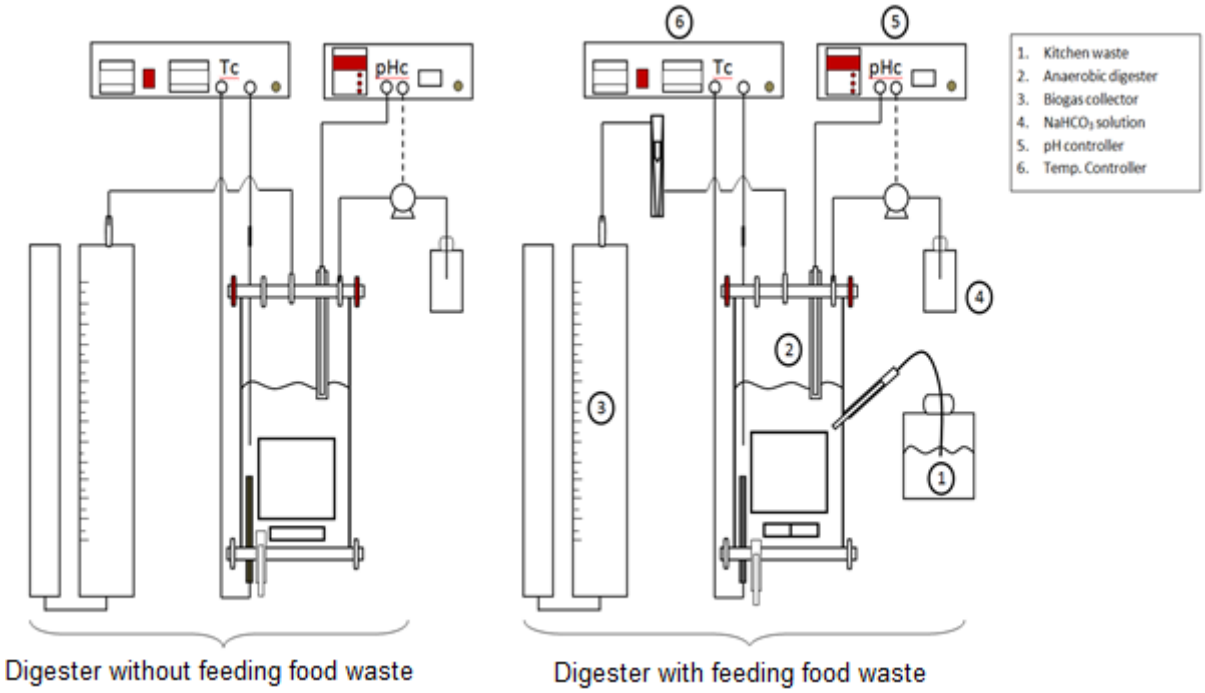

Figure 1. A schematic diagram of the experimental apparatus.

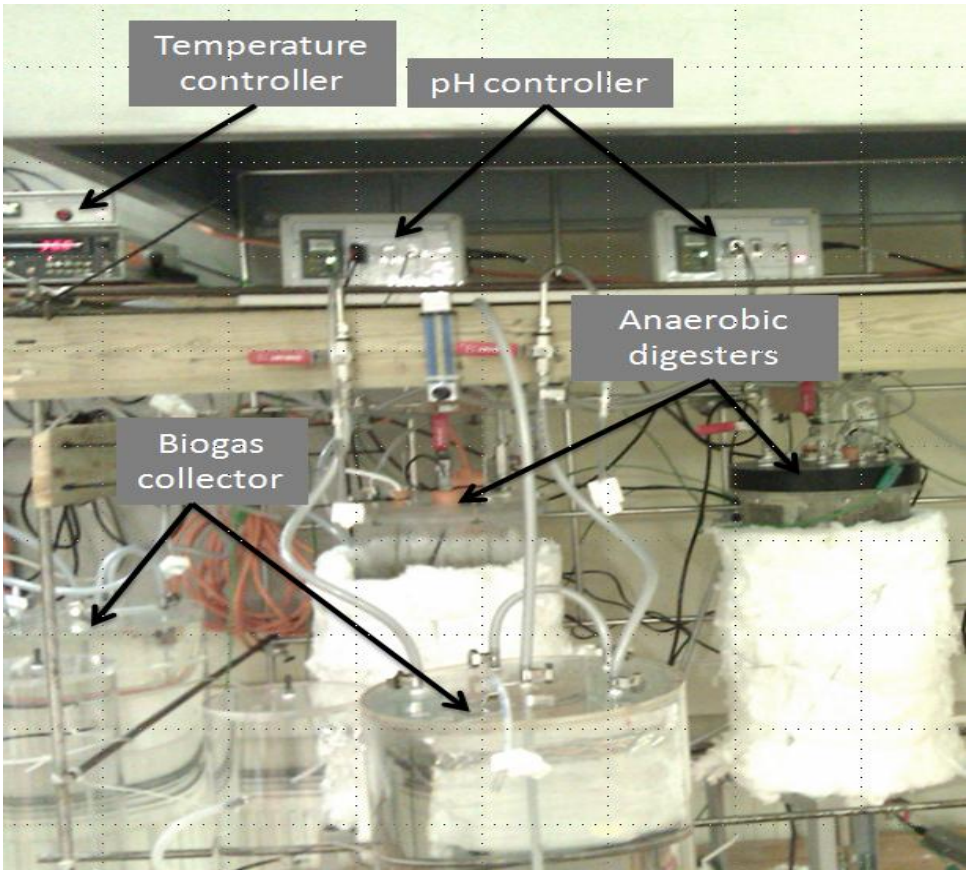

Figure 2. Photograph of the experimental apparatus.

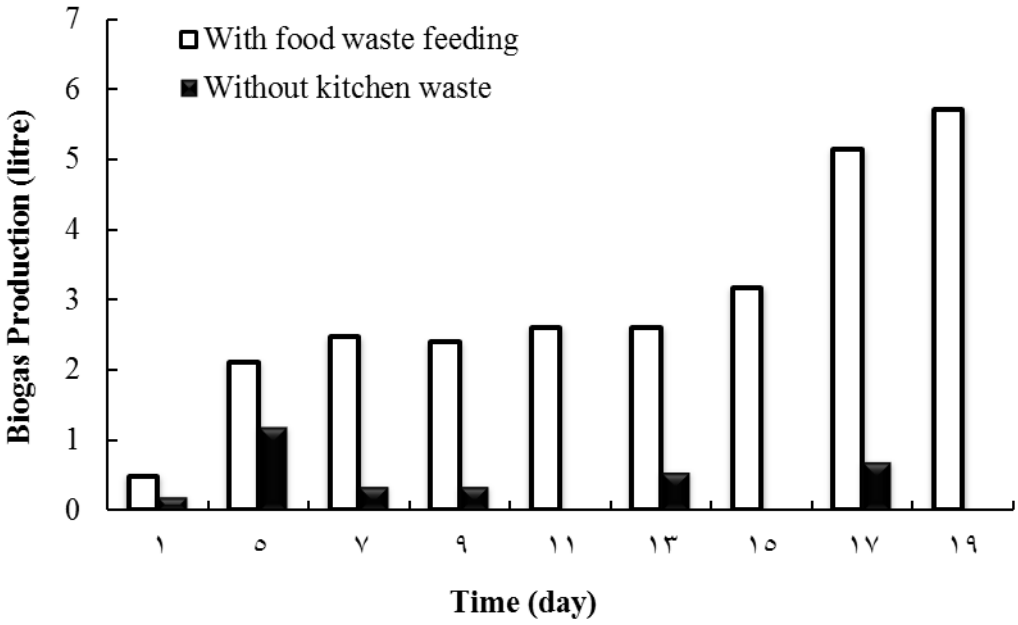

Figure 3. Effect of food waste feeding on biogas production.

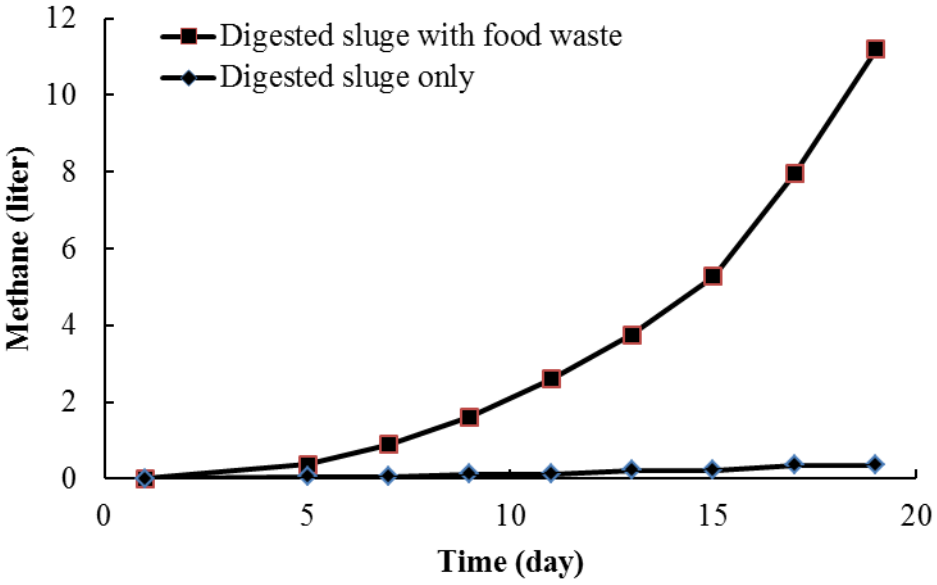

Figure 4. Cumulative methane production from anaerobic digester containing digested sludge only compared to that also fed by food waste.

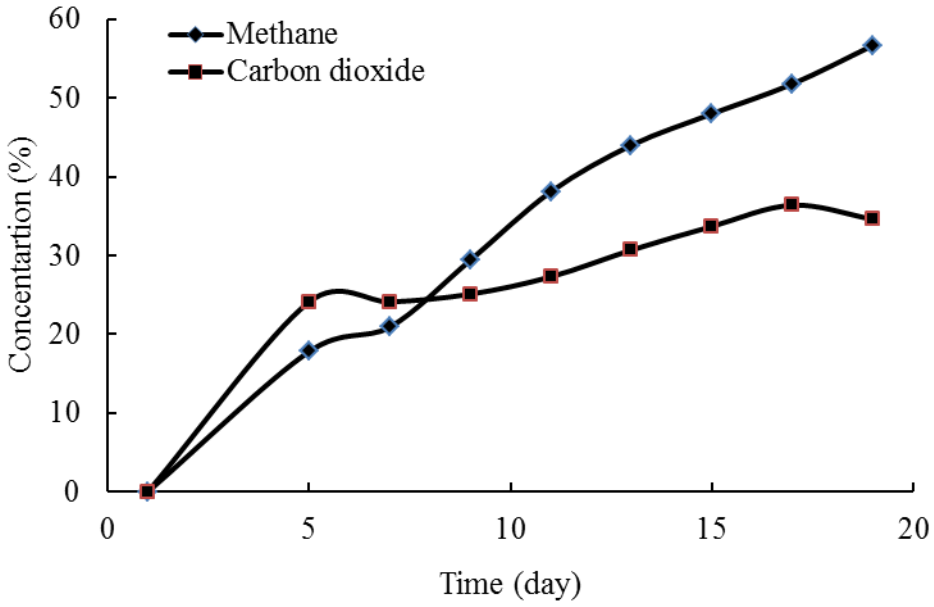

Figure 5. Concentration of methane (CH_4) and Carbon dioxide (CO_2) in biogas produced from the digester containing digested sludge and fed by food waste.

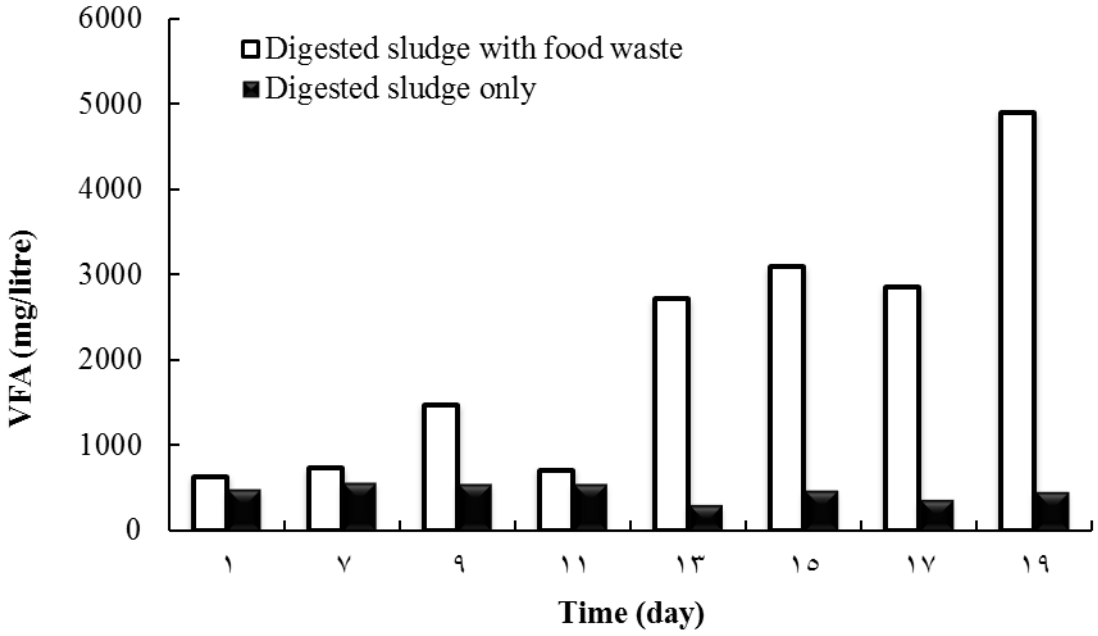

Figure 6. Variation in volatile fatty acids concentration in the digester fed with food waste and the digester fed only with digested sludge.

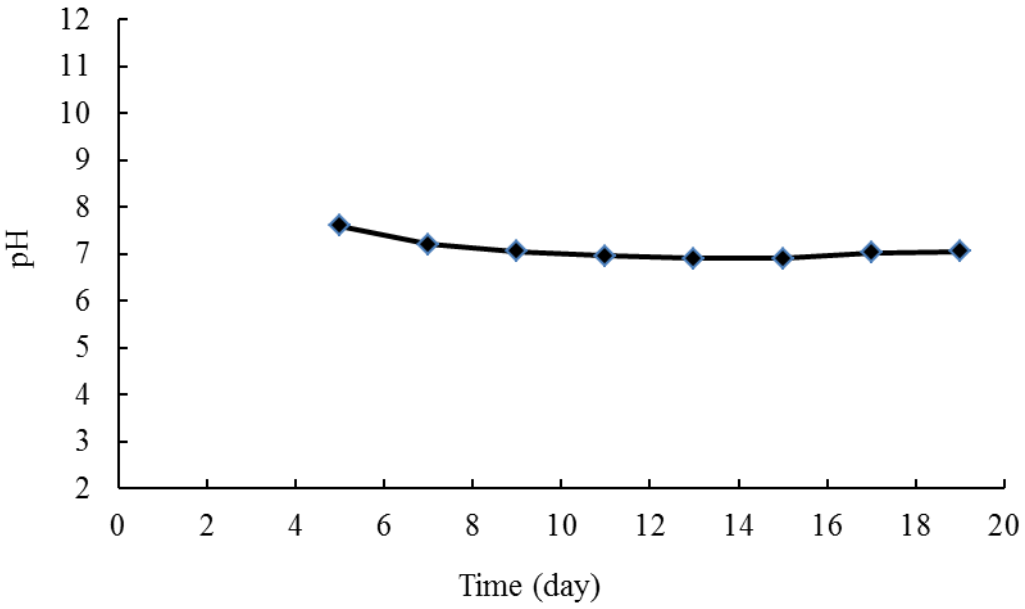

Figure 7. pH values in the anaerobic digester that contain simulated sludge. The pH value remained stable at optimum conditions.

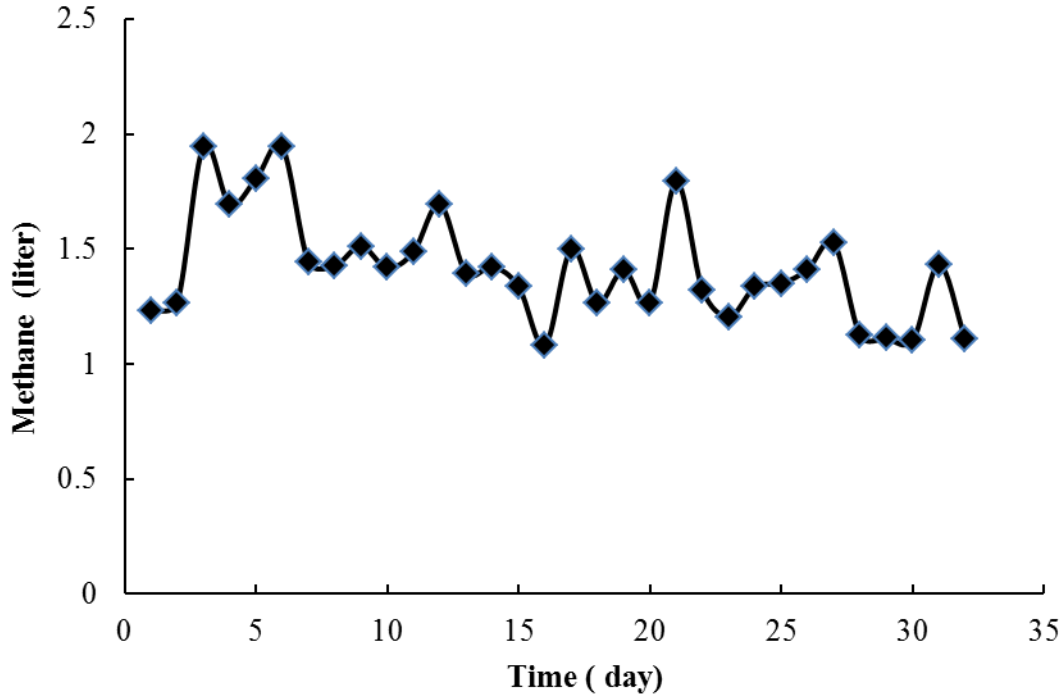

Figure 8. Methane production from the anaerobic digester fed with digested sludge and food waste.

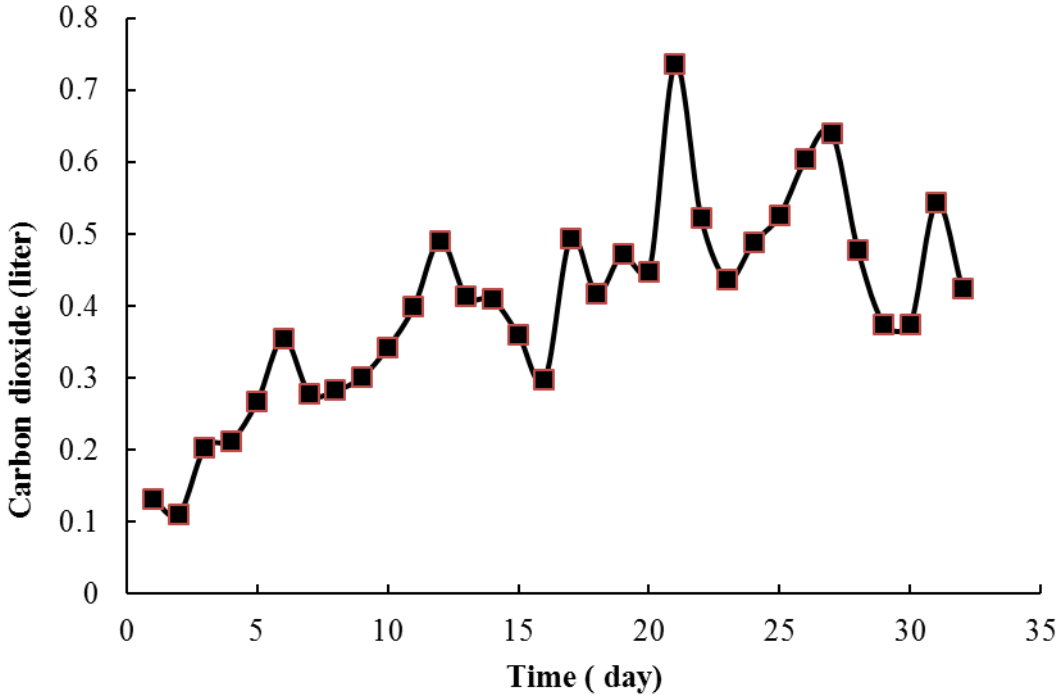

Figure 9. Values of carbon dioxide produced from anaerobic digester fed with digested sludge and food waste.

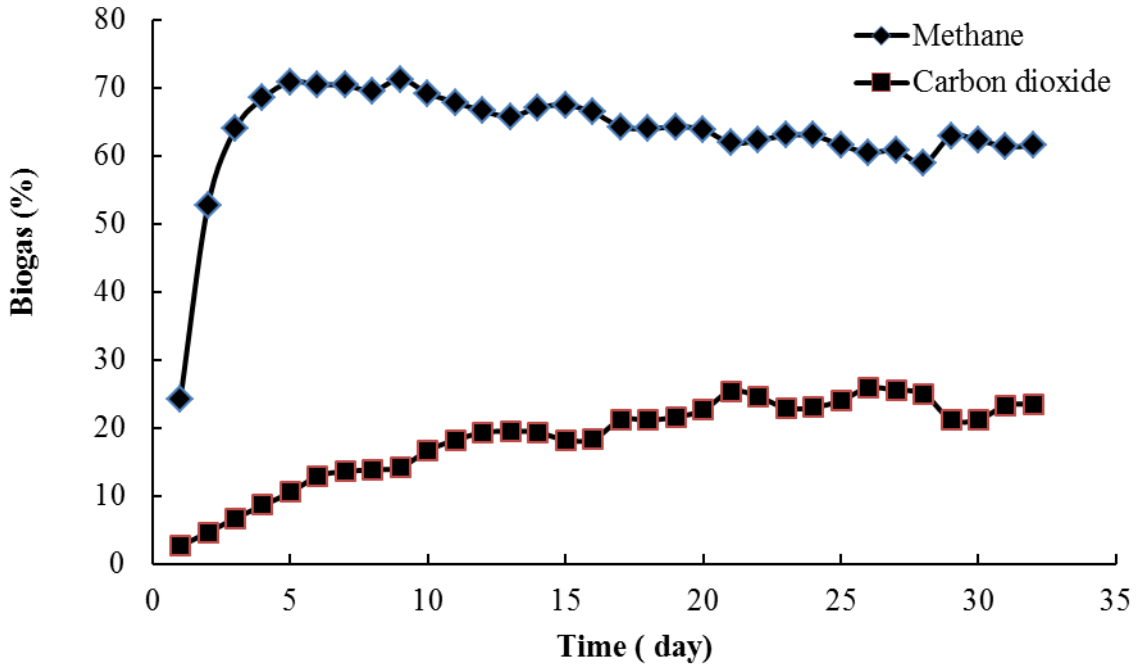

Figure 10. Concentration of methane and carbon dioxide in the biogas produced from the anaerobic digester fed with simulated sludge.

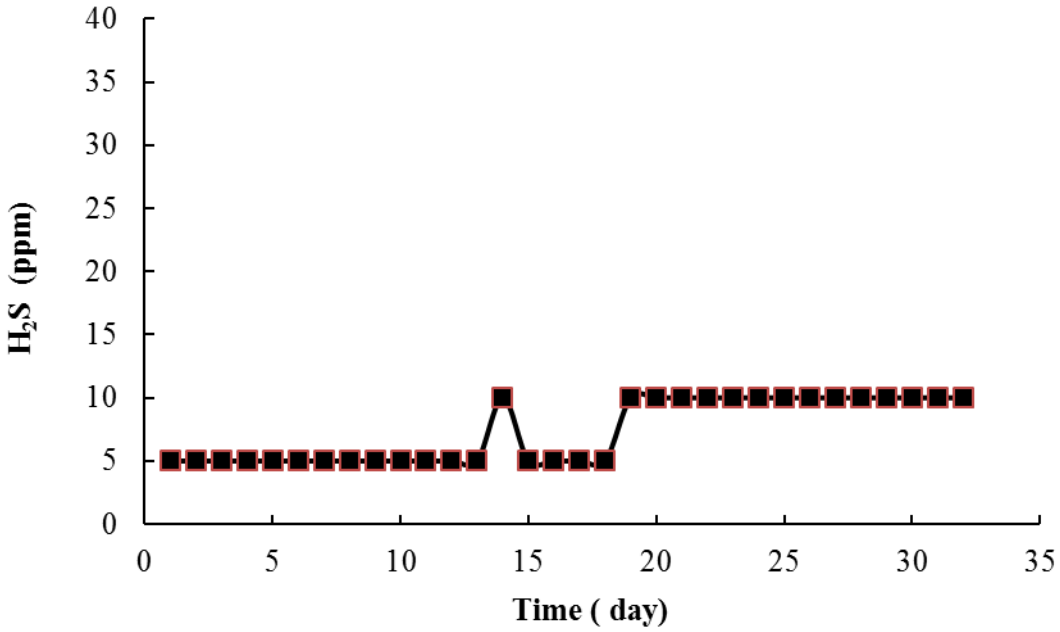

Figure 11. Hydrogen sulphide production by the anaerobic digester fed with simulated sludge.

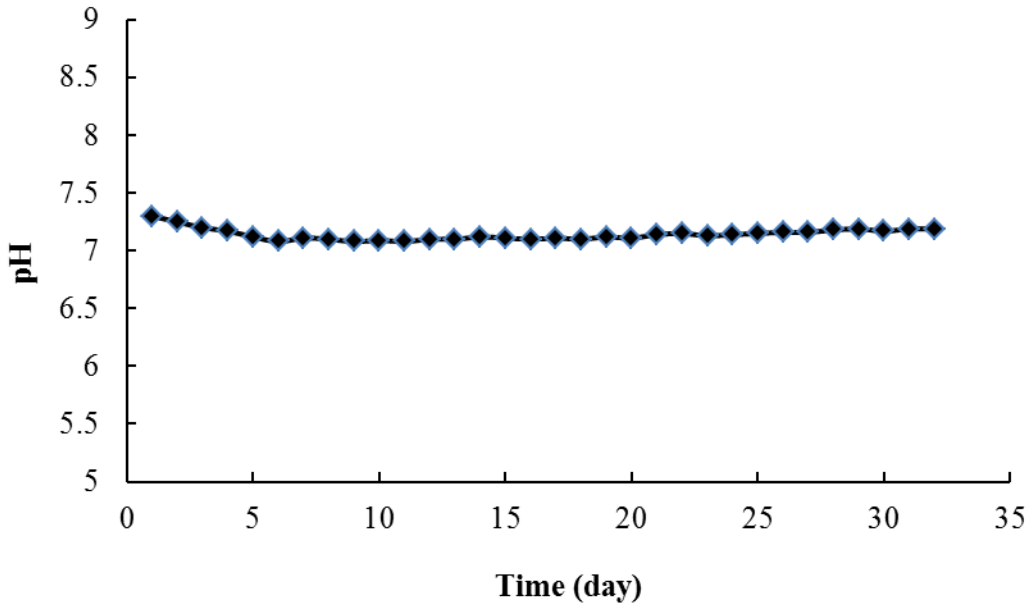

Figure 12. pH value in the anaerobic digester containing simulated sludge.

Assessing Tensile and Shear Properties of Recycled Sustainable Asphalt Pavement

Saad Isaa Sarsam
Professor
Department of Civil Engineering, College of Engineering, University of Baghdad, Iraq
Email: saadisasarsam@coeng.uobaghdad.edu.iq

Ali Muhssin Shahatha AL-Shujairy
M.Sc Student
Department of Civil Engineering, College of Engineering, University of Baghdad, Iraq
Email:alimuhssin83@gmail.com

ABSTRACT

Hot mix recycling of asphalt pavements is increasingly being used as one of the major rehabilitation methods by various highway agencies. Besides general savings in costs and energy expended, it also saves our natural resources and environment. Recycling process presents a sustainable pavement by using the old materials that could be reclaimed from the pavement; these materials could be mixed with recycling agents to produce recycled mixtures. The important expected benefits of recycling process are the conservation of natural resources and reduction of environmental impact. The primary objectives of this work are evaluating the Tensile and Shear Properties of recycled asphalt concrete mixtures, In addition to the resistance to moisture damage. The impact of implementing three types of recycling agents on asphalt concrete properties was also investigated. For this purpose, old materials reclaimed from field, (100% RAP), virgin filler at 3 percent content by weight of mixture and three types of recycling agents (soft asphalt cement of penetration grade 200-300, soft asphalt cement of penetration grade 200-300 blended with 4% silica fumes and soft asphalt cement of penetration grade 200-300 blended with 6% fly ash) at 1.5% content by weight of mixture have been implemented and used to prepare recycled mixtures. Mixtures were subjected to the following tests: Marshall Test (12 specimens), indirect tensile strength test at 20ºC, 25ºC, 40ºC, and 60ºC (48 specimens), indirect tensile ratio (12 specimens), double punch shear test (12 specimens).
It was found that using (soft asphalt cement blended with silica fumes) as a recycling agent revealed better performance results than the other type of recycling agent. The percentages of variation for recycled mixtures with recycling agent of (soft asphalt cement blended with silica fume) when compared to aged mixture were (-13.8%, -25.05%, 229.5%, -47.67%,) for properties of (Marshall stability, indirect tensile strength at 60ºC, tensile strength ratio, double punch test,), respectively.

Key words: recycled mixture, recycling agent, asphalt cement, silica fumes, flyash.

تقييم خصائص الشد والقص للرصفة الاسفلتية المستدامة المعاد تدويرها

سعد عيسى سرسم
استاذ
جامعه بغداد, كليه الهندسه, قسم الهندسه المدنيه

علي محسن شحاذه الشجيري
طالب ماجستير
جامعه بغداد,كليه الهندسه,قسم الهندسه المدنيه

المستخلص

يعد التزايد في استخدام الخلطات الاسفلتية المعاد تدويرها احد الطرق الرئيسية في اعادة تأهيل الطرق من قبل وكالات الطرق السريعة, فهي بالإضافة الى كونها توفر التكاليف والطاقة المبذولة بشكل عام, فهي تحفظ الموارد الطبيعية والبيئية. ان عملية اعادة التدوير تقدم طبقة تبليط مستدامة عن طريق استخدام المواد القديمة التي يتم تهيئتها من هذه الطبقة وهذه المواد من الممكن مزجها مع معاملات اعادة التدوير لإنتاج خلطات الخرسانة الاسفلتية المعاد تدويرها. ان المنافع المتوقعة المهمة لعملية اعادة التدوير هي حفظ المصادر الطبيعية وتقليل التأثير البيئي.

الهدف من الدراسة هو تقييم خصائص الشد والقص لخلطات الخرسانة الاسفلتية المعاد تدويرها بالإضافة الى ذلك تقييم المقاومة لضرر الرطوبة, مع بحث تأثير استخدام ثلاثة انواع من مواد اعادة التدوير على خصائص الخرسانة الاسفلتية. لهذا الغرض فان المواد القديمة التي أحضرت من الموقع بنسبة 100% والمواد المالئة الناعمة الجديدة بنسبة 3% من وزن الخلطة وثلاثة انواع من مواد اعادة التدوير (الاسفلت السمنتي ذو درجة الاختراق 200-300 و الاسفلت السمنتي ذو درجة الاختراق 200-300 مع 4% غبار السيليكا و الاسفلت السمنتي ذو درجة الاختراق 200-300 مع 6% من الرماد المتطاير) عند محتوى معامل تدوير 1.5% من وزن الخلطة , تم استخدامها لتحضير الخلطات المعاد تدويرها.

ان الخلطات في هذه الدراسة تم تعرضها للفحوص التالية : فحص مارشال (12 نموذج) وفحص مقاومة الشد غير المباشر في 20°م, 25°م, 40°م, 60°م (48 نموذج) , فحص نسبة الشد غير المباشر (12 نموذج) , فحص الاختراق المزدوج (12 نموذج).

لقد تم الاستنتاج بان استخدام مادة اعادة التدوير (الاسفلت السمنتي ذو تدرج الاختراق العالي + غبار السيليكا) يعطي افضل نتائج اداء من الانواع الاخرى من مواد اعادة التدوير. ان نسب التغاير في خواص الخلطات المعاد تدويرها باستخدام معامل اعادة التدوير (الاسفلت السمنتي ذو تدرج الاختراق العالي مع غبار السيليكا) مقارنة مع الخلطة المرجعية كانت (-13.8% , -24.05% , 229.5% , -47.67%) لكل من خواص (ثبات مارشال , مقاومة الشد غير المباشر في 60°م , نسبة الشد غير المباشر , فحص الاختراق المزدوج.

الكلمات الرئيسيه: خلطة معاد تدويرها, معامل تدوير, الاسفلت الاسمنتي, ابخرة السيليكا, الرماد المتطاير.

1. INTRODUCTION

Recycling is the process of reusing the existing pavement materials that no longer serve the traffic effectively. The recycling of pavements can be seen as a sustainable option, as it is a production process with environmental and economic benefits. When the pavement mixture reaches the end of its service life it may be disposed or recycled. Using Reclaimed Asphalt Pavement (RAP) is considered as an economical and environmental friendly process; it preserve the natural resources and could produce similar structural performance when compared with virgin asphalt mixtures **,Hussain and Yanjun, 2012.** Most of the local research work on recycling concentrates on the physical properties of recycled mixes; little attention has been paid on the durability issue of recycled mixes. In fact using RAP in pavement construction has now become common practice in many countries. In Iraq, most of asphaltic pavement needs maintenance or rehabilitation; therefore, asphalt pavement recycling could be suggested for maintenance, rehabilitation or even reconstruction process at economical basis with acceptable properties. The most important properties which should be investigated are the Tensile and Shear Properties of recycled asphalt concrete to improve serviceability, reduce maintenance costs and impair safe operations. This Properties is caused by the accumulation of permanent deformation in all or some layers in the pavement structure. In this work, a detailed investigation was carried out to evaluate the durability of recycled asphalt concrete in terms of Tensile and Shear Properties and resistance to moisture damage.

2. MATERIALS CHARACTERISTICS

2.1 Aged Materials

The reclaimed asphalt mixture was obtained by the rubblization of full depth asphalt concrete from highway section. This highway was constructed during 1982; the highway was heavily deteriorated with various cracks and ruts existed on the surface. The rubblized section involves asphalt stabilized base coarse layer and two layers of binder coarse. The reclaimed mixture was heated, combined and reduced to testing size as per AASHTO 2013; a representative sample was subjected to Ignition test according to AASHTO T 308 procedure to obtain binder and filler content, gradation and properties of aggregate. **Table 1** presents the properties of aged materials after Ignition test while **Table 2** presents gradation of old (reclaimed) aggregate obtained from aged mixture. It can be seen that the gradation is finer that that specified for the reclaimed layers (base and binder courses), this may be attributed to the possible degradation of aggregate under traffic through the pavement life.

2.2 Mineral Filler

Mineral filler used in this work is limestone dust obtained from factory in Holy Karbala governorate. The physical properties of the used filler are presented in **Table 3.**

2.3 Recycling Agents

2.3.1 Soft grade asphalt cement

Asphalt cement of penetration grade 200-300 obtained from Al-Dura refinery was adopted for recycling in this work. Its physical properties are listed in **Table 4.** Soft asphalt cement will be referred as "soft AC" in this study.

2.3.2 Soft grade asphalt cement blended with silica fumes

Asphalt cement of penetration grade 200-300 from Al-Dura refinery was blended with 4% of silica fumes which were obtained from local market based on **,Sarsam, 2013.** It is an ultra-fine powder consisting of nearly spherical particles around 100 times smaller than a grain of cement. Soft Asphalt was heated to nearly 110ºc, and the silica fumes were added gradually to the asphalt cement with stirring until homogenous blend was achieved; the mixing and stirring continued for 30 minutes by a mechanical blender. **Table 5** shows physical properties of silica fumes while **Table. 6** presents physical properties of soft asphalt cement 200-300 blended with silica fumes. Soft asphalt cement blended with silica fume will be referred as "Soft AC+Silica fumes" in this work.

2.3.3 Soft grade asphalt cement blended with fly ash

Asphalt cement of penetration grade 200-300 from Al-Dura refinery was blended with 6% of Fly ash which was obtained from local market based on **,Sarsam, 2013.** Soft Asphalt was heated to nearly 110ºc, and the Fly ash was added to the asphalt cement gradually with stirring until homogenous blend was achieved. The mixing and stirring continued for 30 minutes by a mechanical blender. **Table 7** shows physical properties of Fly ash while **Table 8** presents physical properties of soft asphalt cement 200-300 blended with Fly ash. Soft asphalt cement blended with Fly ash will be referred as "Soft AC+Fly ash" in this work. **Fig. 1** shows recycling agent types and the mechanical blender adopted.

3. EXPERIMENTAL PROGRAM

3.1 Preparation of Mixtures

3.1.1 Reclaimed mixture (reference mixture)
Reclaimed mixture was obtained from the reclaimed material from field. It was heated to 145ºC and specimens were prepared for further testing to investigate the performance after recycling.

3.1.2 Preparation of recycled mixture
Recycled mixture consists of reclaimed mixture (RAP) 100%, virgin mineral filler and recycling agent mixed together at specified percentages according to the mixing ratio. First, RAP was heated to approximately 160ºC, mineral filler was heated to 160ºC. and recycling agent was heated to 130ºC separately before it was added to the heated RAP and filler at the desired amount; 3% by weight of mixture of the mineral filler was added and 1.5 % by weight of mixture of the recycling agents was added and mixed for two minutes until all mixture was visually coated with recycling agent as addressed by **,Sarsam, 2007.** The recycled mixture was prepared using three types of recycling agents: soft asphalt cement, soft asphalt cement blended with silica fume and soft asphalt cement blended with Fly ash.

3.1.3 Preparation of accelerated short term aged recycled mixture
Recycled mixtures was heated to 130°C to become loose and then spread in shallow trays with 3cm thickness and subjected to one cycle of accelerated aging process by storage inside an oven at 135°C for 4 hours as per superpave procedure (**PP2**). The mix was stirred every 30 minutes during the short term aging process to prevent the outside of the mixture from aging more than the inner side because of increased air exposure. After the accelerated aging process was completed, Marshall Specimens were constructed from the aged asphalt concrete after heating the material to 150°C.

3.2 Preparation of Marshall Specimens
It is a cylindrical specimen of 102 mm in diameter and 63.5 mm in height. Marshall mold, spatula, and compaction hammer were heated on a hot plate to a temperature between 120-150ºC. A piece of non-absorbent paper, cut to size, was placed in the bottom of the mold before the mixture was introduced. The asphalt mixture was placed in the preheated mold, and then it was spaded vigorously with a heated spatula 15 times around the perimeter and 10 times around the interior. Another piece of non-absorbent paper cut to size was placed on the top of the mix. The temperature of mixture immediately prior to compaction temperature was 150ºC. The mold assembly was placed on the compaction pedestal and 75 blows on the top and the bottom of specimen were applied with specified compaction hammer of 4.535 kg sliding weight, and a free fall in 457.2 mm. The specimen in mold was left to cool at room temperature for 24 hours and then it was extracted from the mold using mechanical jack. Marshall Specimens were subjected to the following tests: Marshall Test (12 specimens), indirect tensile test at 20ºC, 25ºC, 40ºC, and 60ºC (48 specimens), indirect tensile ratio (12 specimens) and double punch test (12 specimens). **Fig. 2** presents a group of prepared specimens.

3.3 Laboratory Evaluation for Asphalt Concrete
3.3.1 Resistance to plastic flow (Marshall test)
This method covers the measurement of the resistance to plastic flow of cylindrical specimen of asphalt paving mixture loaded on the lateral surface by mean of the Marshall apparatus according to ASTM D 1559. The cylindrical specimen was conditioned by placing it in water bath at 60ºC for 30 minute, then it was inserted into the testing device, and compressed on the lateral surface with a constant load rate of 50.8 mm/min until the dial gage reached the maximum load resistance which is recorded as stability, and the corresponding flow value at that point was

also recorded. The entire test was performed within 30 sec after the specimen was removed from water bath. Three specimens for each combination were tested and the average results were reported. **Fig. 3** shows Marshall Test Device.

3.3.2 Indirect tensile strength test and temperature susceptibility

The indirect tensile strength followed the procedure of ASTM D6931-07; Marshall Specimens were used in this test, and percent of air voids for specimens was the same as that for Marshall test. After the specimen was cooled at room temperature for 24 hours, it was conditioned by placing in water bath at four different temperatures 20, 25, 40, and 60 ºC for 30 minutes and then the specimen were centered on the vertical diametrical plane between the two parallel loading strips 12.7 mm in wide. Vertical compressive load at rate of 50.8 mm/min by Versa tester machine was subjected until the dial gage reading reached the maximum load resistance; the reason of conducting this test is to evaluate the tensile strength and temperature susceptibility for the mixtures. **Fig. 4** presents Indirect Tensile Test Device. The indirect tensile strength was calculated by the following equation: ASTM D4123

$$ITS = \frac{2000 * P}{\pi * T * D} \quad (1)$$

where:
ITS = indirect Tensile Strength, kPa
P = maximum load resistance at failure, N
D = diameter of specimen, mm
T = thickness of specimen immediately before test, mm

The temperature susceptibility was calculated by the following equation: **Husham, 1999**

$$\boldsymbol{TS = \frac{(ITS)t1 - (ITS)t2}{t2 - t1}} \quad (2)$$

where:
TS = temperature susceptibility (kPa / ºC)
(ITS)t1= indirect tensile strength at t1 =25ºC
(ITS)t2 = indirect tensile strength at t2 =40ºC

3.3.3 Indirect tensile strength ratio test

The test was performed to evaluate the moisture damage resistance of mixtures, and the procedure followed ASTM D4867. A set of six specimens were prepared, three specimens were tested for indirect tensile strength by storing in a water bath at 25ºC for 30 minutes, and an average value of ITS for these specimens was computed as SI (ITS for unconditioned specimens). The other three specimens were conditioned by placing in volumetric flask 4000-ml heavy- wall glass filled with water at room temperature 25˚C and then a vacuum of 28mm Hg was applied for 5 to 10 min. to obtain 55 to 80 % degree level of saturation. The specimens were then placed in deep freeze at -18˚C for 16 hours. The frozen specimens then were moved to a water bath for 24 hours at 60ºC. Then they were placed in a water bath at 25ºC for 1 hour, and they were tested for indirect tensile strength. The average value was computed as SII (ITS for moisture-conditioned specimens). **Fig. 5** shows the process of conditioning of specimens for

TSR test .The indirect tensile strength ratio could be calculated from the following equation: ASTM D4867

$$TSR = \frac{SII}{SI} * 100 \quad (3)$$

Where:
TSR = indirect tensile strength ratio, %
SI= average ITS for unconditioned specimens, kPa
SII = average ITS for moisture-conditioned specimens, kPa

3.3.4 Double punch shear test
This test procedure was developed at the University of Arizona by Jimenez 1974, and it was used to measure the stripping of the binder from the aggregates. This test was reported by many studies **,Solaimanian, 2004 ,Turos, 2010 ,Sarsam, 2006 and Hasan, 2012.** Marshall specimen was used for this test; it was conditioned by placing in water bath at 60ºC for 30 min. The test was performed by centrally loading the cylindrical specimen, using two cylindrical steel punches placed on the top and bottom surface of the sample. The specimen was centered between the two punches 2.54cm in diameter, perfectly aligned one over the other, and then loaded at a rate of 2.54cm /minute until failure. The reading of dial gage at the maximum load resistance was recorded. **Fig. 6** shows Double Punch test apparatus. The punching strength is computed by the equation:

$$\sigma t = \frac{p}{\pi(1.2bh - a^2)} \quad (4)$$

where:
σt = punching stress, Pa
P= maximum load, N
a= radius of punch, mm
b=radius of specimen, mm
h=height of specimen, mm

4. ANALYSIS AND DISCUSSION OF TEST RESULTS

4.1 Marshall Stability

It was found that recycling decreases Marshall stability, as the stability value was high for aged mixture (19.2 kN), it decreased for recycled mixtures with (Soft Ac), (Soft Ac + Silica Fume) and (Soft Ac + Fly ash) recycling agents by (-17.45%, -13.8% and -5.73%) respectively compared with aged mixture. This may be attributed to the fact that aged mixture contains hardened asphalt, which will lead to increased stability due to higher asphalt viscosity, while recycled mixtures lack necessary bonding effect because of their reduced viscosity (increased workability) and increased binder content (after adding the rejuvenator). This agrees well with the findings of **,AL-Zubaidi, 2013.** Mixtures with recycling agents (Soft Ac) showed lower stability than (Soft Ac + Silica Fume), and (Soft Ac + Silica Fume) showed lower stability than (Soft Ac + Fly ash), which indicates that bonding effect for (Soft Ac + Fly ash) is higher than the other agents. Variation in the stability of mixtures is presented in Figure (4-2). Also it can be seen from **Fig. 7** that all mixtures has stability value more than (8 kN) which represent stability of surface layer according to the specification limits of roads and bridges SCRB, 2003.

4.2 Marshall Flow

Recycling revealed a pronounce increase in Marshall flow value corresponding to aged mixture. All the types of recycled mixtures satisfied Marshall flow criteria of (2-4) mm, except recycled mixture with (Soft Ac). Flow value for mixture with (Soft Ac) was higher than other mixtures. While the Flow value for mixture with (Soft Ac + Silica Fume) was lower than other mixture. **Fig. 8** clarifies the flow results.

4.3 Effect of Recycling Agent Types on Indirect Tensile Strength (ITS)

Mixtures were subjected to indirect tensile strength test at 20ºC, 25ºC, 40ºC, and 60ºC. Three specimens for each mixture type were tested, and the average value was obtained to represent the tensile strength of this type at the specified temperature. Also, the temperature susceptibility for each mixture type was obtained.

Recycling revealed a pronounce increase in (ITS) value at 20˚C corresponding to aged mixture. The percent of increase in (ITS) for recycled mixtures with (Soft Ac, Soft Ac + Silica Fumes and Soft Ac + Fly ash) was (10.86%, 24.58% and 29%) respectively as compared with aged mixture. **Fig. 9** presents the (ITS) values at 20ºC.

Results indicated that tensile strength at 25ºC for all the recycled mixtures was lower than aged mixture value by (-39.62%, -31.57% and -15%) for recycled mixtures with (Soft Ac, Soft Ac + Silica Fumes and Soft Ac + Fly ash) respectively as compared with aged mixture. Also Mixtures with recycling agent of (Soft Ac) showed lower indirect tensile strength value than that with (Soft Ac + Silica Fumes). On the other hand, mix with (Soft Ac + Silica Fumes) shows lower indirect tensile Strength value than that with (Soft Ac + Fly ash). **Fig. 10** presents the (ITS) values at 25ºC.

The reduction in Tensile strength values at 40ºC for recycled mixtures was higher than that of aged mixture. The percent of reduction in (ITS) value for recycled mixtures with (Soft Ac, Soft Ac + Silica Fumes and Soft Ac + Fly ash) was (-33.31%, -22.63% and -6.93%) respectively when compared with aged mixture. The recycled mixture with (Soft Ac + Fly ash) revealed the highest tensile strength value as compared to other recycled mixtures, but it was lower than (ITS) value of aged mixture.

At 60ºC, the tensile strength for aged mixture was higher than that of recycled mixtures. The percentages decrease in (ITS) value for recycled mixtures with (Soft Ac, Soft Ac + Silica Fumes and Soft Ac + Fly ash) was (-38.53%, -25.05% and -4.21%) respectively. The recycled mixture with (Soft Ac + Fly ash) had higher tensile strength value than other recycled mixtures. **Fig. 11** presents the (ITS) values at 40ºC and **Fig. 12** presents the (ITS) values at 60ºC.

The reduction in (ITS)value at (25˚C, 40˚C and 60˚C) for recycled mixtures are in contrast with the findings of **,Hasan, 2012.**

The temperature susceptibility results presented in **Fig. 13** shows that recycled mixtures were less influenced by temperature than aged mixture by (-49.52%, -45.56% and -27.75%) for recycled mixtures with (Soft Ac, Soft Ac + Silica Fumes and Soft Ac + Fly ash) respectively. Mixture with (Soft Ac) revealed the lower temperature susceptibility value than other recycling agents. Mixture with (Soft Ac + Fly ash) was higher than both mixtures with (Soft Ac + Silica Fume) and (Soft Ac) in temperature susceptibility. This might be caused by the properties of the (Silica Fumes and Fly ash), as these agents are more influenced by temperature variation than asphalt cement. The temperature susceptibility value for aged mixture was high due to the nature of aged and hardened asphalt cement which leads to a mixture more susceptible to temperature variation. **Fig. 13** shows the temperature susceptibility results.

4.4 Effect of Recycling Agent Types on Tensile Strength Ratio (TSR)

The results of tensile strength ratio showed that recycled mixtures had good resistance to the action of water. The tensile strength ratio was higher than 80% for all recycled mixtures **Fig. 14**, and the recycled mixture with (Soft Ac) had the highest (T.S.R) value comparing to other recycled mixtures, while mixture with (Soft Ac + Fly ash) was lower than both mixtures with (Soft Ac + Silica Fume) and (Soft Ac) in (TSR). The results revealed high improvement in tensile strength for recycled mixtures with (Soft Ac, Soft Ac +Silica Fumes and Soft Ac + Fly ash) by (241.65%, 229.5% and 192.61%) compared to aged mixture. This agrees well with the findings of **,Hasan, 2012.**

4.5 Effect of Recycling Agent Types on Punching Shear Strength

Double punch test indicates the stripping behavior between binder and aggregate, and since recycled mixture contains recycling agent which has a softening effect in the mixture, the stripping behavior was the concern of the study. The punching shear strength for recycled mixtures was lower than aged mixture by (-48.47%, -47.67% and -10.35%) for recycled mixtures with (Soft Ac, Soft Ac + Silica Fumes and Soft Ac + Fly ash) respectively and this agrees with the findings of **,AL-Zubidi, 2013.** This might be related to the lower viscosity of binder in recycled mix compared to aged mix. Recycled mix with (Soft Ac + Fly ash) had the highest punching shear strength value compared to the other recycled mixtures, and recycled mix with (Soft Ac) revealed the lowest value. **Fig. 15** presents double punch test results for recycled and aged mixtures.

5. CONCLUSIONS

1. Significant reduction in Marshall Stability was noticed for recycled mixtures when compared to aged mixture. The percent of reduction was (-17.45%, -13.8% and -5.73%) for recycled mixtures with Soft Ac, Soft Ac + Silica Fumes and Soft Ac + Fly ash, respectively.
2. Significant improvement in indirect tensile strength at 20˚C was noticed for recycled mixtures as compared to aged mixture. While (ITS) at 25˚C, 40˚C and 60˚C revealed low value for recycled mixtures when compared to aged mixture. The percent improvement in (ITS) value at 20˚C was (10.86%, 24.58% and 29%) for recycled mixtures with Soft Ac, Soft Ac + Silica Fumes and Soft Ac + Fly ash, respectively. While the percent reduction in (ITS) value at 25˚C was (-39.62%, -31.57% and -15%), and at 40˚C was (-33.31%, -22.63 and -6.93%) and at 60˚C was (-38.53%, -25.05% and -4.21%) for recycled mixtures with Soft Ac, Soft Ac + Silica Fumes and Soft Ac + Fly ash , respectively.
3. The results of tensile strength ratio showed that recycled mixtures had good resistance to moisture damage by (241.65%, 229.5% and 192.61%) for recycled mixtures with Soft Ac, Soft Ac + Silica Fumes and Soft Ac + Fly ash, respectively as compared with aged mixture.
4. Punching shear strength for recycled mixtures was lower than that of aged mixture by (-48.47%, -47.67% and -10.35%) for recycled mixtures with Soft Ac, Soft Ac + Silica Fumes and Soft Ac + Fly ash, respectively.

REFERENCES

- AASHTO-PP2 1999, *Standard Practice for Mixture Conditioning of Hot Mix Asphalt (HMA).* The American Association of State Highway and Transportation Officials, Washington, D. C., USA.

- Hasan, E.A., 2012, *Assessing Performance of Recycled Asphalt Concrete Sustainable Pavement* , M.Sc. thesis, College of Engineering, University of Baghdad.

- Husham, A.M., 1999, *Evaluation of Suitable Temperature Susceptibility Index for Local Paving Asphalts*, M.Sc. Thesis, Civil Engineering Department, University of Baghdad.

- Hussain, A., and Yanjun, Q., 2012, *Evaluation of Asphalt Mixes Containing Reclaimed Asphalt Pavement for Wearing Courses*, Proceedings , 2012 International Conference on Traffic and Transportation Engineering, School of Civil Engineering, Southwest Jiaotong University, Chengdu, China, IPCSIT vol. 26 , Singapore, PP. 43-48.

- AL-Zubaidi, I.L., 2013, *Durability of Recycled Asphalt Concrete Pavement*, M.Sc. Thesis, College of Engineering, University of Baghdad.

- Sarsam, S.I., 2006, *Improving Asphalt Concrete Quality for Ramps and Approaches*, Indian Highways, No.3, Vol. 34, PP.61-66.

- Sarsam S.I., 2007, *A Study on Aging and Recycling of Asphalt Concrete Pavement*, University of Sharjah Journal of Pure &Applied Sciences, Vol. 4, No. 2, pp. 79-96.

- Sarsam, S.I., 2013, *Effect of Nano Materials on Asphalt Cement Properties*, International Journal of Scientific Research in Knowledge (IJSRK), 1(10), pp. 422-426, 2013.

- Solaimanian, M. J., Harvey, M., Tahmoressi, and Tandon, V., 2004, *Test Methods to Predict Moisture Sensitivity of Hot-Mix Asphalt Pavements*, Moisture Sensitivity of Asphalt Pavements CD-ROM, Transportation Research Board, National Research Council,Washington, D.C., pp. 77-110.

- Turos, M.I., 2010, *Determining the Flexural Strength of Asphalt Mixtures using the Bending Beam Rheometer*, M.Sc. Thesis, University Of Minnesota.

Table 1. Properties of reclaimed materials after ignition test.

Material	Property		Value
Asphalt binder	Binder content %		4.94%
Coarse aggregate	Bulk specific gravity		2.56
	Apparent specific gravity		2.619
	Water absorption %		1.057%
	Wear% (Los Angeles abrasion)		22%
Fine aggregate	Bulk specific gravity		2.590
	Apparent specific gravity		2.819
	Water absorption %		1.91%
Mineral filler	Percent passing sieve no.200		98%
	Specific gravity		2.82
Aged Mixture	Marshall Properties	Stability	19.2 kN
		Flow	3.3 mm
		Air voids	6.14%
		Bulk density	2.322 gm/cm^3

Table 2. Gradation of old (reclaimed) aggregate obtained from aged mixture.

Sieve no.	Sieve size (mm)	% Passing by weight	SCRB Specification	
			Base course	Binder or leveling cours
1½"	37.5	-----	100	----
1"	25.4	100	90-100	100
3/4"	19	99	76-90	90-100
1/2"	12.5	94	56-80	70-90
3/8"	9.5	85	48-74	56-80
No.4	4.75	61	29-59	35-65
No.8	2.36	49	19-45	23-49
No.50	0.3	19	5-17	5-19
No.200	0.075	4	2-8	3-9

Table 3. Physical properties of filler (lime stone).

Property	Value
Bulk specific gravity	2.87
% Passing sieve no.200	99

Table 4. Physical properties of soft asphalt cement recycling agent.

Property	Test conditions	ASTM Designation no.	Value
Penetration	25ºc, 100gm, 5sec	D5-06	260
Softening point	(ring & ball)	D36-95	36
Ductility	25ºc, 5cm/min	D113-99	80
After thin film oven test properties D1754-97			
Retained penetration of residue	25ºc, 100gm, 5sec	D5-06	51%
Ductility of residue	25ºc, 5cm/min	D113-99	45
Loss on weight	163ºc, 50g,5 hrs		0.37

Table 5. Physical properties of silica fumes.

Property	Value
Specific gravity	2.14
% Passing sieve no.200	100
Specific surface area (m^2/ kg)	20000

Table 6. Physical properties of soft asphalt cement (200-300) blended with 4% silica fumes.

Property	Test conditions	ASTM Designation No.	Value
Penetration	**25°c, 100gm, 5sec**	D5-06	253
Softening Point	**(ring & ball)**	D36-95	38
Ductility	**25°c, 5cm/min**	D113-99	105
After Thin Film Oven Test Properties D1754-97			
Retained penetration of residue	**25°c, 100gm, 5sec**	D5-06	47%
Ductility of residue	**25°c, 5cm/min**	D113-99	35
Loss on weight	**163°c, 50g,5 hrs**		0.22

Table 7. Physical properties of fly ash.

Property	Value
Specific gravity	2.0
% Passing sieve no.200	99%
Specific surface area (m^2/ kg)	650

Table 8. Physical properties of soft asphalt cement (200-300) blended with 6% fly ash.

Property	Test conditions	ASTM Designation No.	Value
Penetration	**25°c, 100gm, 5sec**	D5-06	278
Softening point	**(ring & ball)**	D36-95	34
Ductility	**25°c, 5cm/min**	D113-99	65
After Thin Film Oven Test Properties D1754-97			
Retained penetration of residue	**25°c, 100gm, 5sec**	D5-06	35%
Ductility of residue	**25°c, 5cm/min**	D113-99	22
Loss on weight	**163°c, 50g,5 hrs**		0.27

Figure 1. Recycling agents type and mechanical blender.

Figure 2. Group of prepared specimens.

Figure 3. Marshall test at NCCLR laboratory.

Figure 4. Indirect tensile test device.

Figure 5. Conditioning process of specimens for TSR test at NCCLR laboratory.

Figure 6. Double punch test apparatus.

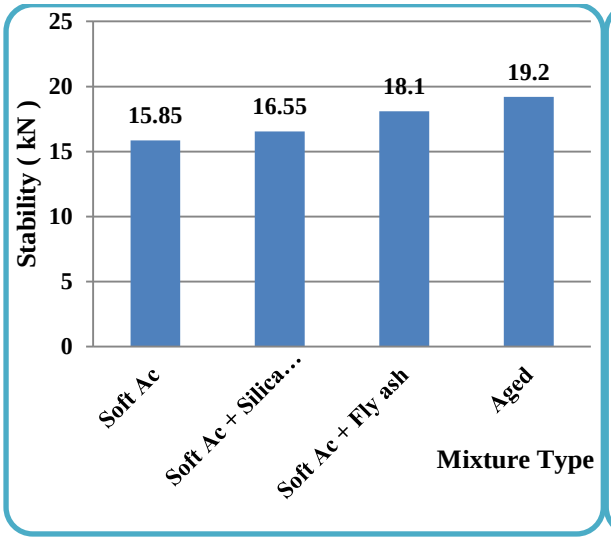

Figure 7. Stability for aged and recycled mixtures.

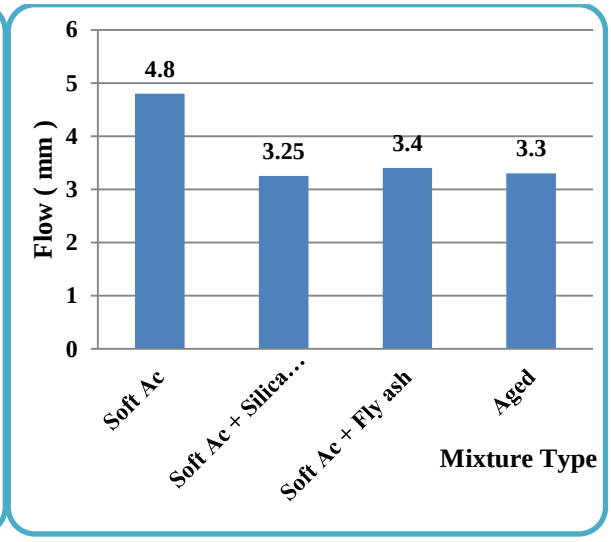

Figure 8. Flow results for aged and recycled mixtures.

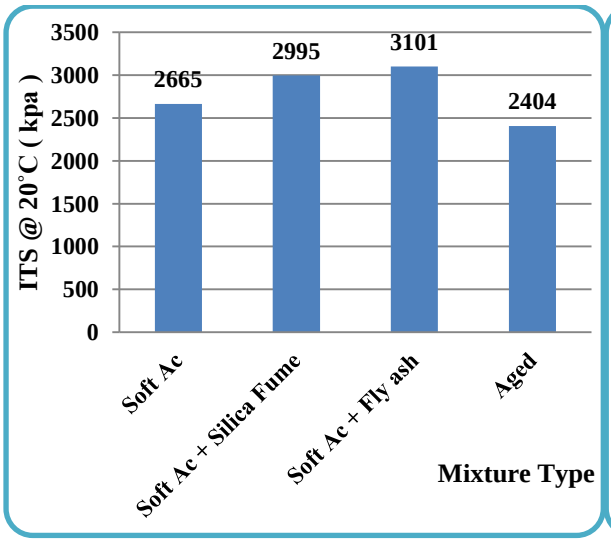

Figure 9. ITS results at 20˚C for aged and recycled mixtures.

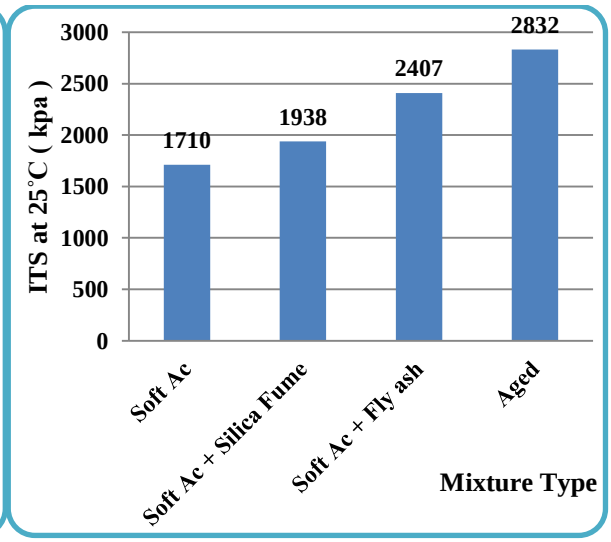

Figure 10. ITS results at 25˚C for aged and recycled mixtures.

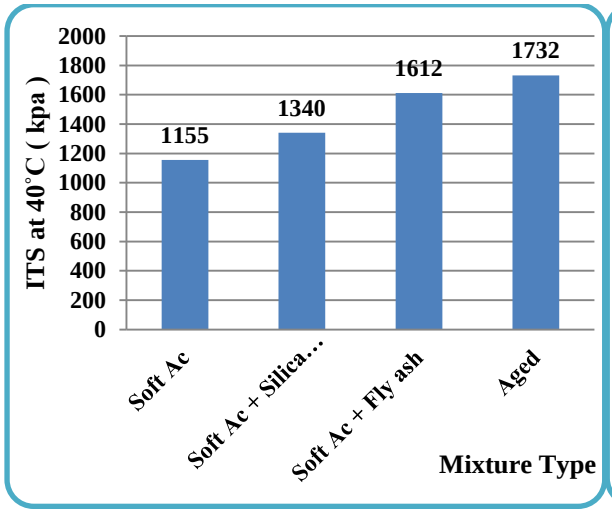

Figure 11. ITS results at 40˚C for aged and recycled mixtures.

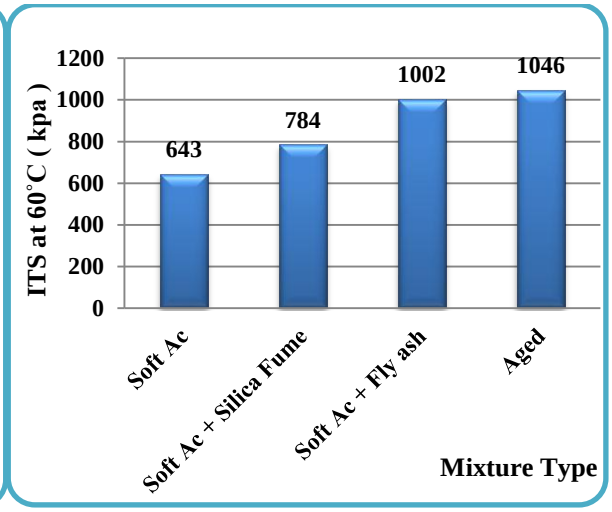

Figure 12. ITS results at 60˚C for aged and recycled mixtures.

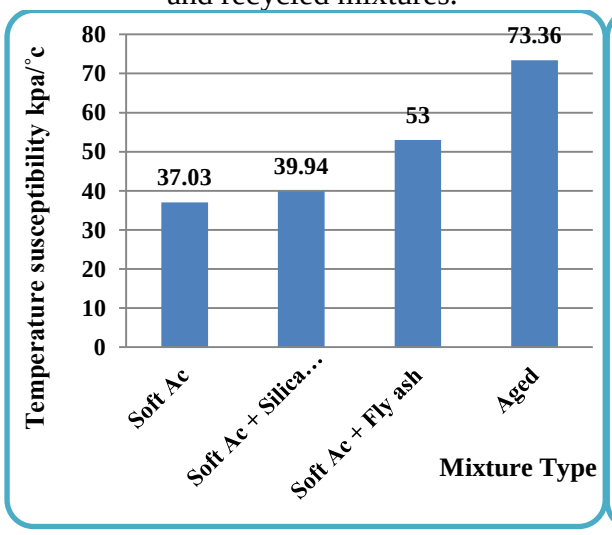

Figure 13. Temperature susceptibility results for aged and recycled mixtures.

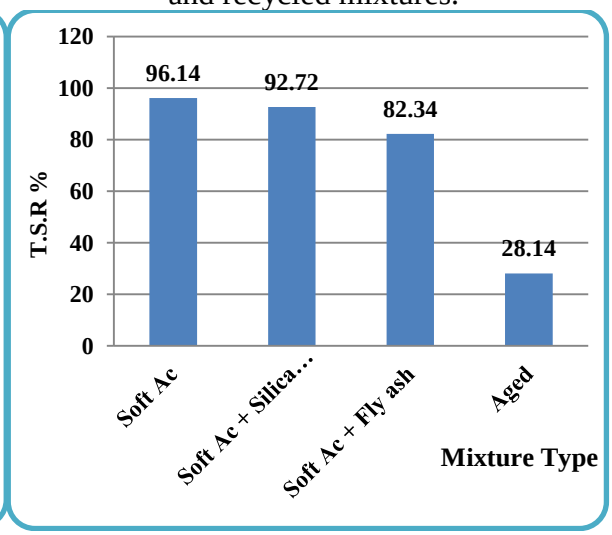

Figure 14. Tensile strength ratio test for aged and recycled mixtures.

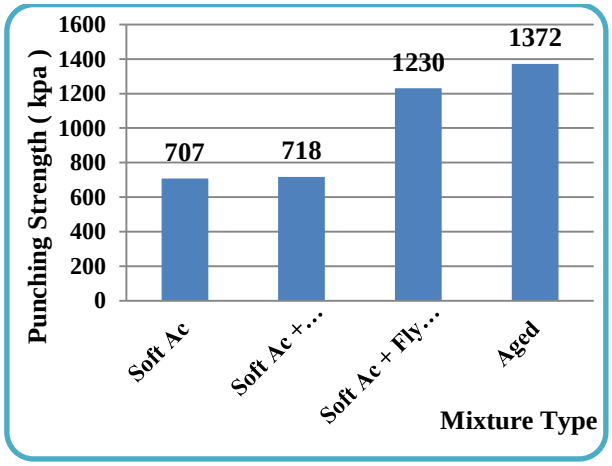

Figure 15. Double punch test results for aged and recycled mixtures.

Artificial Neural Networks Modeling of Total Dissolved Solid in the Selected Locations on Tigris River, Iraq

Dr. Ayad Sleibi Mustafa
Assistant Professor
University of Anbar, Civil Eng. Dept. College of Engineering.
Email: ayad_eng2001@yahoo.com .

ABSTRACT

The study aims to predict Total Dissolved Solids (TDS) as a water quality indicator parameter at spatial and temporal distribution of the Tigris River, Iraq by using Artificial Neural Network (ANN) model. This study was conducted on this river between Mosul and Amarah in Iraq on five positions stretching along the river for the period from 2001to 2011. In the ANNs model calibration, a computer program of multiple linear regressions is used to obtain a set of coefficient for a linear model. The input parameters of the ANNs model were the discharge of the Tigris River, the year, the month and the distance of the sampling stations from upstream of the river. The sensitivity analysis indicated that the distance and discharge have the most significant affect on the predicted TDS concentrations. The results showed that a network with (8) hidden neurons was highly accurate in predicting TDS concentration. The correlation coefficient (r), root mean square error (RMSE) and mean absolute percentage error (MAPE) between measured data and model outputs were calculated as 0.975, 113.9 and 11.51%, respectively for testing data sets. Comparisons between final results of ANNs and multiple linear regressions (MLR) showed that the ANNs model could be successfully applied and provides high accuracy to predict TDS concentrations as a water quality parameter.

نمذجة الشبكات العصيبة الاصطناعيه للاملاح الذائبة الكلية في مواقع مختارة من نهر دجلة في العراق

د. اياد صليبي مصطفى

استاذ مساعد

كلية الهندسه-جامعة الانبار

المقدمة

تهدف الدراسة الى التنبؤ بتراكيز المواد الصلبه الكلية (TDS) بوصفها مؤشرا لنوعية المياه تبعا التوزيع المكاني والزماني لنهر دجلة في العراق باستخدام نموذج الشبكه العصيبة الاصطناعية (ANN).اجريت الدراسة لخمسة مواقع على طول نهر دجلة بين الموصل والعمارة في العراق للفترة (2001- 2011).لمعايرة نمذجة الشبكه العصيبه الصناعية تم استخدام برنامج الانحدار الخطي المتعدد للحصول على مجموعة من المعاملات للنموذج الخطي.ان المدخلات الاساسيه للمتغيرات الداخله لبرنامج (ANNs) هي تصريف النهر، السنة، الشهر، المسافة لمواقع المحطات من مقدم النهر.أظهر تحليل الحساسيه ان المسافة والتصريف لهما تاثيرجوهري على توقعات تراكيز (TDS). بينت النتائج ان الشبكة ذات ثمانية عقده في الطبقه المخفيه (hidden layer) من الخلايا العصيبة كانت دقيقه للغاية للتنبؤ في تركيز (TDS).ان قيمة معامل الارتباط (r) وجذر متوسط مربعات الخطأ (RMSE) ومعدل نسبة الخطأ المطلق (MAPE) بين البيانات المقاسة والبيانات التي تم حسابها من النموذج كالآتي(0.975، 113.9، 11.51%).أشارت

نتائج المقارنة النهائية لنموذج الشبكات العصبية الاصطناعية (ANNs) مع الانحدار الخطي المتعدد (MLR) .ان نموذج (ANNs) يمكن ان يطبق بنجاح ويوفر دقة عالية لتنبؤ تراكيز (TDS) كمؤشر لنوعية المياه.

Keywords: Tigris River , TDS, ANNs, and discharge.

1-INTRODUCTION

River water quality is a significant concern in many countries, considering agricultural and drinking consumptions. Therefore, prediction of TDS as the main water quality condition is a necessary tool for water resources planning and management. Limited water quality data and the high cost of water quality monitoring often pose serious problems for process-based modeling approaches .Artificial Neural Networks (ANNs) provide a particularly good option, because they are computationally very fast and require many fewer input parameters and input conditions than deterministic models, ANNs, however require a large pool of representative data for training **,Ali , et al., 2009.**

In recent years, ANNs have been successfully applied in the area of water quality modeling. The use of ANN model was to be better than other simulations and commonly used statistical models **,Mas and Ahlfeld, 2004** due to the complex interrelated and non-linear relationships between multiple parameters. ANNs had been used successfully for predicting TDS parameter in streams, river and lakes, **Kanani et al., 2008 ,Ali et al., 2009 ,Abudu et al., 2011 ,Asadollahfard et al., 2012 ,Moasheri et al., 2013 and Nemati et al., 2014.** There have been a number of studies for Iraqi researchers on the Tigris River water quality modeling, especially within Mosul and Baghdad, with some examples: **,Al Shami, 2006 ,Abudl Razzak, et al., 2009 ,Abed and Ismail, 2013 and Al-Suhaili, and Ghafour, 2013. , Ali,S.M.2014. ,Ismail et al., 2014. ,Kadhem,2014. and ,Flaieh et al., 2014.** Over the last few years few studied have been conducted to predict some water quality parameters on Iraqi Tigris River by using ANNs model. These studies had demonstrated some degree of success, **,Al-Suhaili et al., 2008 and ,Al-Suhaili and Mahammed, 2014.**

The water quality of the Tigris River, using the parameter TDS as an indicator water quality is varying from place to place along the river and overtime. Water salinity, expressed as TDS, is an increasing problem in Iraq. Salinity increases as the river water flow southward and evaporation, sewage effluent dissolution of limestone and agricultural drainage **,Al Marsoumi et al., 2006.** However, TDS values of the Tigris water at the Turkish Iraqi border are 280 mg/l and the River reaches more than 1500 mg/l at Amarah, Iraq **,Al-Ansari, 2013.** The main objectives of this study are to predict the spatial and temporal changes in TDS parameter throughout the selected sampling stations on the Tigris River using ANNs model.

2- MATERIALS AND METHODS

2-1 Data and Site Description

The Tigris River is one of the most important twin rivers in Iraq, 1850 km long. The total length of the river in Iraq is 1415 km with a catchment area of 235000 km^2. Hydrological behavior of the Tigris River has been changed due to the construction of large dams and irrigation projects in Turkey and Iraq. The Tigris River mean discharge at Mosul city prior to 1984 was 701 m^3/sec and dropped to 596 m^3/sec afterward. This implies that 15% of the river discharges were been decreased. The average discharge in

Baghdad was 544 m^3/sec. This value is far away from the mean daily flow prior to 2005 , 1140 m^3/sec **,Ali et al., 2012.** On the other hand, discharges south of Baghdad reduced in the Tigris to 37 BCM at Kut . Past Kut, the Tigris supplies water for irrigation and public water supply and also discharge to the central marsh combined .These discharges reduced 3 BCM at Qalatsalih during the period after 1990 **,ESCWA-BGR, 2012.** In the present study, ANNs model was applied for TDS water quality parameter of five sampling stations on the Tigris river (Mosul in the north of Iraq, Samarra barrage, Muthanna bridge at Baghdad, Kut barrage and Amarah south of Iraq as shown in **Fig.1**. These data were collected from the **,National Center for Water Resources Management, Ministry of Water Resources, Iraq ,2012.** Water quality stations along the Tigris River are located between 36°20.802′Latitude and 43°08.417′ Longitude at Mosul, North of Iraq and 31°51.338′Latitude and 47°08.618′ Longitude at Amarah, South of Iraq. The ANNs model inputs are the monthly discharge (Q) in m^3/sec, distance (D) in m of the sampling station from the upstream of the Tigris river at Mosul, the year (Y) and the month of the data (M) . The output of the model was TDS as a water quality parameter. The data set has a record length of (11) years covering between 2001 to 2011 based on existing measured values of different variables. The average annual discharge of the selected stations along the Tigris River is shown in **Fig.2**. Also the average recorded annual TDS concentration is shown in **Fig. 3**.

2-2 Overview Artificial Neural Networks

Artificial Neural Networks (ANNs) are a flexible mathematical structure that is capable of identifying a large number of simple processing elements that are called neurons. The basic structure of an ANNs model usually comprised three distinctive layers, the input layer that all data are imported to the network and calculation the weight of each input variables are done; the hidden layer or layers, where data are processed; and the output layer, where the results of ANNs are produced .The number of neurons in the input hidden, and output layers depends on the problem. If the number of hidden neurons is small, the network may not have sufficient degrees of freedom to learn the process correctly. On the other hand, if the number is too high, the training will take a larger time and the network may over-fit the data **,Karunanithi et al., 1994.** Many authors have described the structure and operation of ANNs **,Zurada, 1992.** The most common activation function is sigmoid (logistic) function and is described as follows, **,Diamantopoulos et al., 2005.**

$$f(x) = 1 / 1+e^{-x} \quad (1)$$

2-3 Pre-processing and Data Division

It is a common practice to divide the available data into three sets, training, and validation. In this study, we randomly divide up the 100% of the target time steps into 80% for training and 20% for validation. The training data are further divided into 70% for training set and 30% for the testing set. The training set is used to adjust the connection weights of the neural network.

The testing set is used to check the performance of the network at various stages of learning, and training is stopped once the error in the testing set increases. The validation set is used to evaluate the performance of the model once training has been

successfully accomplished. The way data are divided can have a significant effect one model performance **, Al-Janabi, 2006.** and trial – and – error process was used to select the best division .The data base used for the ANNs model comprises total of (660) individual cases .Missing data were found in each of the water quality sampling stations .Ranges of the data used for the input and output variable are tabulated in **Table 1**. Data pre-processing can have a significant effect on the generalization performance of a supervised neural network **,Dogan et al., 2009.** Normalization and transformation data was scaled or normalized using Eq. (2)

$$x_{scaled} = (x_{\circ} - x_{min}) \ / \ (x_{max} - x_{min}) \quad (2)$$

Where $x_{\circ}$ is the original data point, x_{min} and x_{max} are the minimum and maximum values in the data set, respectively. This is done in order to ensure that the min. value in the data set is scaled to zero, and the maximum value is scaled to one **,Martin and Mohammad, 1994.**

2-4 Performance Evaluation and Modeling Error

The performance of model was evaluated by calculating the following statistical parameter: correlation coefficient (r), root mean square error (RMSE) and mean absolute percentage error (MAPE) defined by Eqs. (3-5), respectively

$$r = \frac{\sum(Q^0 - M^0)(QP - MP)}{\sqrt{\sum(Q^0 - m^0)2 \sum(QP - MP)2}} \quad (3)$$

$$RMSE = \frac{1}{N}\sum(Q_{\circ} - Q_p)^2 \quad (4)$$

$$MAPE = \frac{1}{N}\sum |Q_{\circ} - Q_p| \quad (5)$$

Where $Q_{\circ}$ and Q_p are the observed and estimated concentrations at the time steps, $M_{\circ}$ and M_p are the mean of the observed and estimated concentrations, respectively, and N is the total number of observations of the data set. The RMSE and MAPE measure the errors –however, RMSE is the most popular measure of errors which receives much greater attention than small errors. **,Sabah and Ahmed, 2011** showed that the MAPE around 30% is considered a reasonable prediction.

Neural Network Model Application

Using the default parameters of the ANN model (0.2 for learning rate and 0.8 for momentum rate), a number of network with different numbers of hidden lager nodes (1-10) and with different transfer functions were developed. However the number of hidden unit directly affects the performance of the network. The best performance of these networks was with (8) hidden layer nodes and minimum values of correlation coefficient, RMSE and MAPE , **Table 2.** The best transfer functions for the input, hidden and output layers were linear, tanh and sigmoid respectively more than 150 trials were used in this study. The effect of the internal parameters controlling the back – propagation (momentum and learning rates) on model performance is investigated for the model with eight hidden layer nodes, **Table 2.** .The effect of the learning and momentum rates on the model performance is shown in **Figs.4** and **5**. Different values of learning and momentum

rates were used, **Table 2**. It can be seen that the performance of the ANNs model is relatively sensitive to learning rates in the range (0.1 – 0.8) then the prediction errors increase sharply to (133.4), **Figs. 4** and **5** show the effect of the momentum rate on model performance. It can be seen that the performance of the ANNs model is relatively sensitive to momentum rate value of (0.8). The optimum values for learning and momentum rate used are 0.4 and 0.8, respectively .The coefficient of correlation, RMSE and MAPE were 0.975, 113.9 and 11.51%, respectively. Also, the network with (8) hidden layer nodes has the lowest prediction error for the training and validation tests. However, it is believed that network with (8) hidden layer nodes is considered optimal, Fig. (6).

The statistics of the training, testing and validation sets for the ANN models is shown in **Table 3**.The statistical parameters considered include the maximum, minimum, mean and standard deviation. To examine how representative the training, testing and validation sets are with respect to each other t-test and F-test are carried out. The t-test examines the null hypothesis of no difference in the means of two data sets and the F-test examines the null hypothesis of no difference in the variances of the two sets. For a given level of significance, test statistics can be calculated to test the null hypotheses for the t-test and F-test respectively. Traditionally, a level of significance equal to 0.05 is selected. Consequently, this level of significance is used in this research. This means that there is a confidence level of 95% that the training, testing and validation sets are statistically consistent. The results of the t-test and F-tests are given in **Table 4**. These results indicate that training, testing and validation sets are generally representative of a single population.

3- RESULTS AND DISCUSSION

The ANNs model was then adopted to simulate total dissolved solid (TDS) with respect to discharge of the selected sites along the Tigris River and time .It used ANNs architecture with one hidden layer (eight nodes) and with different activation functions . The optimum learning rate of 0.4 and momentum of 0.8 were selected by many trials, as explained above.

The sensitivities of above parameters for the TDS prediction were estimated by using **,Garson, 1991 and Goh,1995** methods .ANNs connection weights were used in these methods, **Table 5**. The results indicate that the distance and discharge had the a significant effect on the predicted TDS with a relative importance of 58% and 27% , respectively , followed by year and month with a relative importance of 12% and 3% , respectively , **Fig. 7** .The minimum value of relative importance for the month variable is due to the water resources monitoring and management .There are no monthly variations in flow rates from barrages the regulators along the Tigris River as in the flow hydrograph . The developed ANNs models accurately simulated the water quality (TDS) of Tigris river .Typical ANN's prediction model results are TDS concentrations, for the total data (r=0.96), **Fig.8**. Comparison of simulated water quality in Tigris river is shown in **Fig.9** .There is no trend in increasing of TDS concentration in sampling site between Mosul and Samarra sites. The progressive increase in TDS concentrations was directly proportional with distance after Samarra to Kut sites but with low positive slope and high or sharp positive slope for Kut to Amarah sites. This is due to the effects of upstream developments drainage project, direct sewage disposal into the river and agricultural

activities. Using the connection weights and the threshold levels which obtained from ANN model, **Table 5.** the predicted TDS concentration in (mg/l) for Tigris River can be expressed as follows:

$$\mathbf{TDS} = 146 + \frac{2832}{1+e^{(0.58+2.39\tanh(x1)+1.84\tanh(x2)+4.65\tanh(x3)-8.83\tanh(x4)-2.11\tanh(x5)-3.06\tanh(x6)+2.40\tanh(x7)-2.57\tanh(x8))}} \quad \text{.....(6)}$$

Where:

$x_1 = 64.37 + 46.12*10^{-4}Q + 0.07\ M - 3.62*10^{-3}D - 0.033\ Y$ (6-a)

$x_2 = 19.48 - 12.27*10^{-4}\ Q + 0.11\ M - 2.31*10^{-3}D - 9*10^{-3}\ Y$ (6-b)

$x_3 = 264.44 + 3.88\ *10^{-4}\ Q + 0.61\ M + 4.87*10^{-3}D - 0.13\ Y$ (6-c)

$x_4 = 1889.86 + 5.11*10^{-4}\ Q + 0.27\ M + 14.12\ *10^{-3}D - 0.95Y$ (6-d)

$x_5 = 291.38 + 47.15*10^{-4}Q + 0.12\ M - 5.75*10^{-3}D - 0.15\ Y$ (6-e)

$x_6 = -74.93 - 7.13*10^{-4}Q - 0.6\ M + 1.0*10^{-3}D + 0.4\ Y$ (6-f)

$x_7 = -576.14 - 2.12*10^{-4}Q + 0.14\ M - 13.11*10^{-3}D - 0.29\ Y$ (6-g)

$x_8 = -13.10 - 7.03*10^{-4}Q + 0.33\ M - 6.13*10^{-3}D + 0.07\ Y$ (6-h)

It should be noted that Eq.(6) is valid only for the range of value of (M, Y, D, and Q) given in **Table 1**. This is due to the fact that ANN should be used only in interpolation and not extrapolation **,Tokar and Johnsn, 1999.** Eq. (6) is long and complex because it contains four independent variables. On the other hand, it can predict accurately the TDS of Tigris River as shown in **Fig. 8** with a correlation coefficient equal to 0.96 and value of MAPE less than 30% . The equation length depends on the number of nodes in the input and hidden layers. A neural network of four input neurons, eight hidden neurons and one output is found to be the optimum architecture for the current problem as shown in **Fig. 10**.

Multiple linear regression (MLR) may be viewed as a special case ANNs model that uses linear transfer functions and no hidden layers, if the linear model performs as a basis for comparison. The following regression models are derived for the TDS concentration of the Tigris River in (mg/l).

$$TDS = Q^{-0.255}M^{-0.006}D^{0.694}Y^{0.560} \quad (7)$$

where , M is the month , Y is the year , D is the distance in (km) and Q is the discharge in (m^3/sec) .The correlation coefficient r, RMSE and MAPE are 0.78, 610.4 and 58%, respectively, **Fig.11** .Comparison between results of ANNs and (MLR) analysis showed better results in ANNs model (RMSE and MAPE) values. So, ANNs could explain the variability of the TDS concentration Tigris River more efficiency.

4- CONCLUSIONS

The following conclusions could be deduced from this study

1- ANN performed better than MLR model. The results provided sufficient assessment of performance (r=0.975, RMSE=113.9 and MAPE=11.51%) for ANN model and r=0.78, RMSE=610.4 and MAPE=58% for MLR model.

2- The sensitivity analysis indicated that the distance and discharge have the most significant effect on the predicted TDS concentration, while the year and month have the smallest impact on prediction.

3- ANN's model could be translated into practical formula from which TDS may be calculated. However the predicted formula is important in water quality management and finding the missing data, temporally and spatially.

4- According to the results of ANN model, it is found that the TDS increases with increasing time and distance from upstream, and it is negatively correlated with the flow.

5- The results of this study can be utilized in optimized management and planning of water quality management of the study area in Iraq.

REFERENCES

- AbdulRazzak, I.,A.,Sulaymon, A., H., and Al-Zoubaidy, A., 2009, *Modeling the Distribution of BOD and TDS in Part of Tigris River within Baghdad*. Journal of Eng., Vol.15 ,No.2,pp.2673-3691.

- 2-Abudu S, King JP,and Sheng Z., 201,*Comparison of the Performance of Statistical Models in Forecasting Monthly Total Dissolved Solids in the Rio Grande.* Journal of the American Water Resources Association,Vol.48,No.,pp.10-23.

- Al-Ansari, N.A.,2013, *Management of Water Resources in Iraq: Perspectives and Prognoses*, Scientific Research Eng. Vol.5,pp.667-684.

- 4-Al-Janabi, K.R., 2006, *Laboratory Leaching Process Modeling in Gypseous Soils Using Artificial Neural Network (ANN)*, Ph.D. Thesis, Building and Construction Eng. Dept. University of Technology.

- 5-Al-Marsoumi, A, H., Al Bayati, K., M., and Al-Mullah, E., A., 2006, *Hydrogeochemical Aspects of Tigris and Euphrates River within Iraq: a Comparative Study*, Raf. Jour. Sci., Vol.17, No.2,pp. 34-49.

- 6-Ali, A.A., Al-Ansari, N.A.,and Knutsson, S., 2012, *Impact of Growing Islands on the Flood Capacity of Tigris river in Baghdad City* .Environmental and Natural Resources Eng.,Vol.27,No.31,pp.511-518.

- 7-Ali,S.,M.,2014, *Characterizing of Some Hydrochemical Parameters of Tigris River, Iraq with the Aid of GIS*, Journal of Natural Science Res.,Vol.4,No.22,pp.6-18.
- 8-Ali N.,Ahmed E., Othman A.K., and Othman J, 2009, *Prediction of Johor River Water Quality parameters using Artificial Neural Network.*, European Journal of Scientific Res., Vol.28, No.3 pp. 422-435.
- 9-Al-Shami, A., Al-Ani, N. and Al Shalchi, Th., 2006, *Evaluation of Environmental Impact of Tigris River Pollution between Jadirriya and Dora Bridges*. Journal of Eng. No.3, Vol.13,pp.884-861.
- 10-Al-Suhaili R.H. and Ghafour Z.J., 2013, *Genetic Algorithm Optimization Model for Central Marches Restoration Fows with Different Water Quality Scenarios*, Journal of Eng.,Vol.19,No.3,pp.312-330.
- 11-Al-Suhaili, R.,H., Kassim, W., M., and Yousif, Y.M.,2008, *Prediction of Turbidity in Tigris River Using Artificial Neural Networks.* Journal of Eng., Vol. 14, No.2,pp. 2483- 2493.
- 12-Al-Suhaili,R.,H.,and Mohammed,Z.,J.,2014, *Comparison between Linear and Assessing Tigris River Non-Linear ANN Models for Predicting Water Quality Parameters at Tigris River*. Journal of Eng., Vol.20,No.10,pp.1-15.
- 13-Asadollahfard G,Taklify A.and Ghanbari,A.,2012, *Application of Artificial Neural Network to Predict TDS in Talkheh Rud River.* Journal of Irrigation and Drainage Engineering,Vol.138,No.4,pp.363-370.
- 14- Diamantoppoulou, M.J., Antonopoulos V.Z. and Papamichail D.M. ,2005, *The Use of a Neural Network Technique for the Prediction of Water Quality Parameters of Axios River in Northern Greece*, Journal European Water,Vol.11/12,pp.55-62.
- 15-Dogan,E.,Sengorur,B.,and Koklu,R.,2009, *Modeling Biological Oxygen Demand of the Melen River in Turkey Using an Artificial Neural Network Technique*, Journal Environmental Management,Vol.90,pp.1229-1235.
- 16-ESCWA-BGR Cooperation, *Inventory of Shared Water Resources in Western Asia*, (online version) Chapter 3:Tigris River Basin. Beirut , 2012.
- 17-Flaieh,H.,M. Ridha ,M.J and Abdul-Ahad,M.Y.,2014, *Quality in Baghdad City Using Water Quality Index and Multivariate Statistical Analysis*, International Jour.of Eng. Sci. and Res. Tech.,Vol.3,No.7 pp.687-699.
- 18-Garson,G.D.,1991, *Interpreting Neural-Network Connection Weights*. Artifical Intell.Expert.,Vol.(6),No.(7),pp.47-51.

- 19-Goh, A.T.C.,1995, *Back-Propagation Neural Networks for Modeling Complex System,* Artificial Intelligence in Engineering ,Vol.9, pp.143-151.

- 20-Ismail, A., H., and Abed, G., A., (2013). *BOD and DO Modeling for Tigris River at Baghdad City Portion Using QUAL2K Model*., Journal of Kerbala University, Vol.11, No.3,pp. 257-273.

- 21-Ismail, A., H., Abed, B.Sh.and Abudul-Quder,S.,2014, *Application of Multivariate Statistical Techniques in the Surface Water Quality Assessment of Tigris River at Baghdad Stretch*, Iraq, Journal of Babylon University, Eng. Science, Vol.22,No.2 pp. 450-463.

- 22-Kadhem, A., J. ,2013, *Assessment of Water Quality in Tigris River- Iraq by Using GIS Mapping*, Natural Resources, Vol.4, pp. 441-448.

- 23-Kanani S., Asadollahfardi G, and Ghanbari A., 2008, *Application of Artificial Neural Network in Predict Total Dissolved Solids in Achechay River Basin*,World Applied Science Journal, Vol. 5, pp.645-654.

- 24-Karunanithi,N.,Grenney,W.J.,Whitley,D.,and Bovee,K.,1994, *Neural Networks for River Flow Prediction*., J.Comput.Civ.Eng.,Vol.8, No.2, pp.201-220.

- 25-Martin T. H. and Mohammad B. M. ,1994, *Training Feed Forward Networks with the Marquardt Algorithm,* IEEE Transactions on Neural Networks,Vol.5,No.6 pp.989-993.
- 26-Mas,D.M.; and Ahlfeld,D.P.,2004, *Use of Artificial Neural Network Models to Predict Indicator Organisms Concentrations in an Urban Watershed*., American Geophysical , Spring Meeting,Abstract H53A-06.

- 27-Moasheri S.A., Khammar G.A., Poornoori Z.,Beyranvand Z. and Soleimani M. 2013, *Estimate the Spatial Distribution TDS the Fusion Method Geostatistics and Artificial Neural Networks.,* International Journal of Agriculture and crop sciences,Vol.(6) ,No.(7),pp.410-420.

- 28-Nemati, S., Naghipour, L., and Fezeli, M.H., 2014, *Artificial Neural Network Modeling of Total Dissolved Solid in the Simineh River*, Iran, J. of Civil Eng. and Urbanism, Vol.4, No.1 pp.8-14.

- 29-Sabah,S.S.and Ahmed,S.,2011, *Performance of Artificial Neural Network and Regression Techniques for Simulation Model in Reservoir Interrelationship*, International Journal of the physical Science,Vol.69,No.34 pp.7738-7748.

- 30-Tokar, A. S., and Johnson,P. A. ,1999, *Rainfall-Runoff Modeling Using Artificial Neural Networks,* J. of Hydrol. Eng.,Vol. 4,No.3, pp.232– 239.

- 31-Zurada,J.M.,1992, *Introduction to Aritifical Neural Systems*,West Publishing Company,St.Paul.

Table 1. Ranges of variables data used for the ANNs model.

Model Variables	Min. Value	Max. Value
Discharge of river (m^3/sec)	15.0	1949
Distance from upstream (km)	150	1100
Month	1	12
Year	2001	2011
TDS (mg/l)	146	2832

Table 2. Performance of ANNs models for prediction (TDS) of Tigris River.

					Training		Testing		Validation		
Parameter effect	Model No.	Learn Rate	Moment Rate	Hidden layer model number	Correlation Coefficient	RMSE	Correlation Coefficient	RMSE	Correlation Coefficient	RMSE	MAPE for all data (%)
Default Values	1	0.2	0.8	1	0.906	214.6	0.897	497.8	0.838	533.6	32.20
	2	0.2	0.8	2	0.945	170.2	0.863	688.1	0.805	712.2	17.51
	3	0.2	0.8	3	0.952	173.3	0.851	810.7	0.791	831.6	18.49
	4	0.2	0.8	4	0.955	149.8	0.866	690.5	0.824	700.1	13.20
	5	0.2	0.8	5	0.963	137.8	0.880	550.6	0.585	557.2	13.56
	6	0.2	0.8	6	0.963	144.8	0.857	741.89	0.814	752.3	14.49
	7	0.2	0.8	7	0.966	127.38	0.834	873.5	0.789	871.7	12.14
	8	0.2	0.8	8	0.967	124.67	0.846	783.43	0.805	788.11	12.18
	9	0.2	0.8	9	0.968	124.98	0.848	785.5	0.812	782.8	12.18
	10	0.2	0.8	10	0.968	125.79	0.850	777.2	0.809	782.6	12.07
Momentum Rates	11	0.2	0.1	8	0.958	137.7	0.855	685.7	0.808	697.5	11.88
	12	0.2	0.2	8	0.959	137.5	0.854	691.5	0.808	703.9	11.94
	13	0.2	0.3	8	0.959	136.9	0.856	687.8	0.809	701.5	12.02
	14	0.2	0.4	8	0.960	135.9	0.857	684.1	0.811	699.1	12.03
	15	0.2	0.5	8	0.960	134.7	0.857	687.5	0.812	702.7	12.03
	16	0.2	0.6	8	0.961	133.4	0.858	688.7	0.814	702.9	12.24
	17	0.2	0.7	8	0.964	128.7	0.849	744.7	0.805	749.4	12.14
	18	0.2	0.8	8	0.967	124.6	0.896	783.4	0.804	783.1	12.18
	19	0.2	0.9	8	0.970	118.0	0.828	893.1	0.790	884.1	12.07

	20	0.2	0.95	8	0.972	119.0	0.831	907.4	0.787	908.4	12.01
Learning Rates	21	0.1	0.8	8	0.961	133.4	0.895	687.0	0.814	701.1	12.21
	22	0.2	0.8	8	0.967	124.7	0.845	783.4	0.804	783.1	12.18
	23	0.3	0.8	8	0.968	121.4	0.832	863.6	0.791	857.1	12.17
	24	0.4	0.8	8	0.970	118.6	0.829	890.1	0.791	880.8	12.19
	25	0.5	0.8	8	0.970	120.7	0.831	895.9	0.796	880.6	12.96
	26	0.6	0.8	8	0.972	118.6	0.840	852.9	0.8	848.5	12.10
	27	0.7	0.8	8	0.975	113.9	0.869	856.8	0.850	668.1	11.51
	28	0.8	0.8	8	0.975	115.4	0.872	532.6	0.865	563.5	11.87
	29	0.9	0.8	8	0.974	115.4	0.861	402.1	0.894	393.8	12.84
	30	1	0.8	8	0.975	114.6	0.852	394.7	0.916	306.5	12.42

Table 3. Input and output statistics for the ANN model.

Data Set	Statistical Parameter	Month (month)	Year (year)	Distance (m)	Q (m^3/sec)	TDS (mg/l)
Training N=369	Maximum	12	2011	1100	1494	2991
	Minimum	1	2001	150	15	197
	Mean	6.425	2004.91	714.0921	379.8699	726.916
	Sta.dv.	3.452	3.284536	272.078	229.0094	485.3027
Testing N=159	Maximum	12	2011	1100	1582	2877
	Minimum	1	2001	150	22	146
	Mean	6.622	2005.298	592.4528	335.3459	730.1132
	Sta.dv.	3.498	2.696331	399.1759	270.1845	705.6958
Validation N=132	Maximum	12	2011	1100	1360	2986
	Minimum	1	2001	150	36	156
	Mean	6.537	1989.825	588.7925	325.8328	673.3861
	Sta.dv.	3.427	3.342669	409.4047	266.7569	595.345

Table 4. Input and output statistics for the ANN model.

Variable and data set	t-value	Lower critical value	Upper critical value	t-test	F-value	Lower critical value	Upper critical value	F-test
Month								
Testing	-1.911	-1.975	1.975	Accept	1.579761	1.3001	2.556	Accept
Validation	-1.54856	-1.978	1.978	Accept	0.390277	1.334	2.936	Reject
year								
Testing	2.118442	-1.975	1.975	Reject	1.437779	1.3001	2.556	Accept
Validation	1.346531	-1.978	1.978	Accept	1.183871	1.334	2.936	Reject

Distance								
Testing	-1.42187	-1.975	1.978	Accept	1.584163	1.3001	2.556	Accept
Validation	-1.53378	-1.978	1.975	Accept	1.383798	1.334	2.936	Accept
discharge								
Testing	-1.13612	-1.975	1.975	Accept	1.449	1.3001	2.556	Accept
Validation	1.163922	-1.978	1.978	Accept	2.660403	1.334	2.936	Accept
TDS-output								
Testing	1.140016	-1.975	1.975	Accept	1.934	1.3001	2.556	Accept
Validation	1.667779	-1.978	1.978	Accept	1.453	1.334	2.936	Accept

Table 5. Weights and threshold levels for the ANN model.

Hidden layer node	**Wji (weight from node i in the input layer to node j in the hidden layer)**							
	i=4		**i=3**		**i=2**		**i=1**	
j=5	-0.326		-3.449		0.773		8.922	
j=6	-0.085		-2.203		1.186		-2.373	
j=7	-1.287		4.643		6.655		0.752	
j=8	-9.527		13.449		2.933		0.989	
j=9	-1.455		-5.482		1.356		9.115	
j=10	0.372		0.949		-6.637		-1.382	
j=11	2.909		-12.493		1.536		-0.409	
j=12	0.655		-5.842		3.670		-.1357	
Output layer node	Wji (weight from node i in the hidden layer to node j in the output layer)							
	i=12	i=11	i=10	i=9	i=8	i=7	i=6	i=5
j=13	2.570	-2.396	3.062	2.108	8.826	-4.653	-.184	-2.39

Figure 1. Location of the study area.

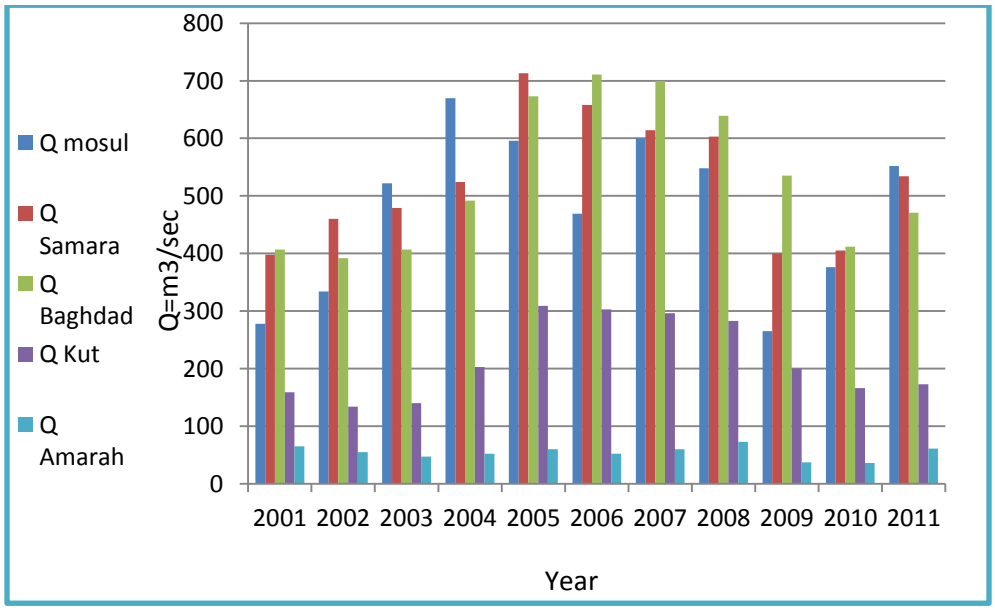

Figure 2. Discharge patterns of selected sites of Tigris river of the period(2001-2011).

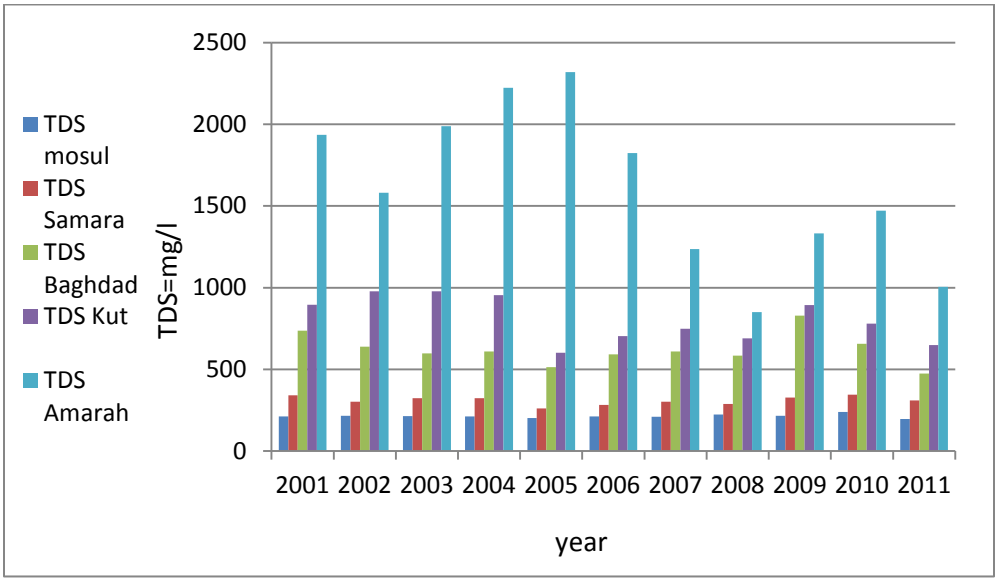

Figure 3. TDS concentrations patterns of selected sites of Tigris river of the period (2001-2011).

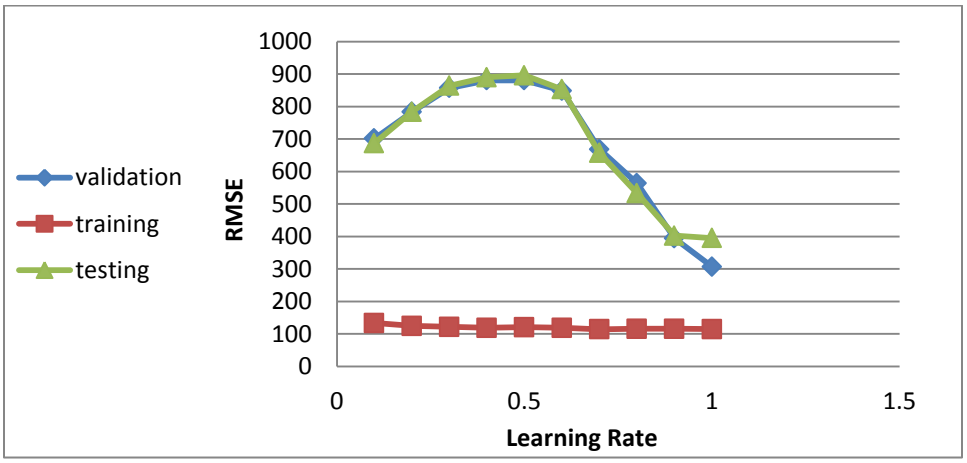

Figure 4. Performance of ANN model with different values of learning rates (β=0.8).

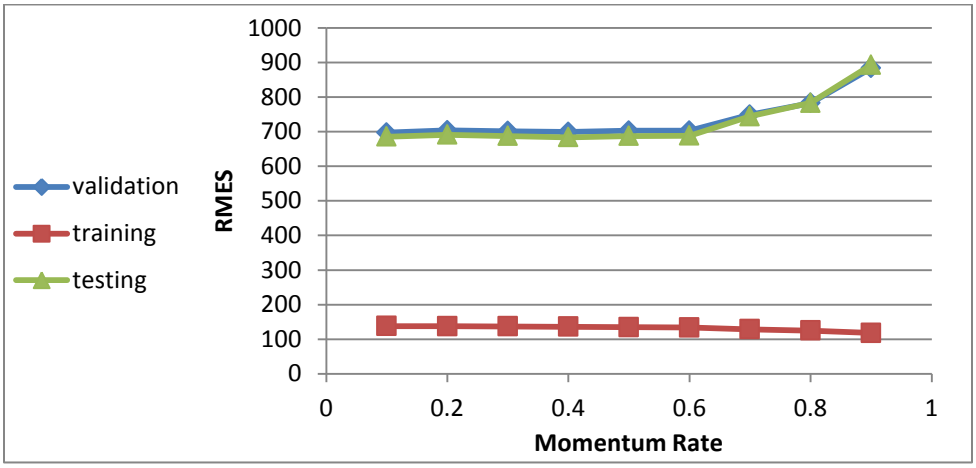

Figure 5. Performance of ANN model with different values of momentum rates,($\alpha = 0.2$).

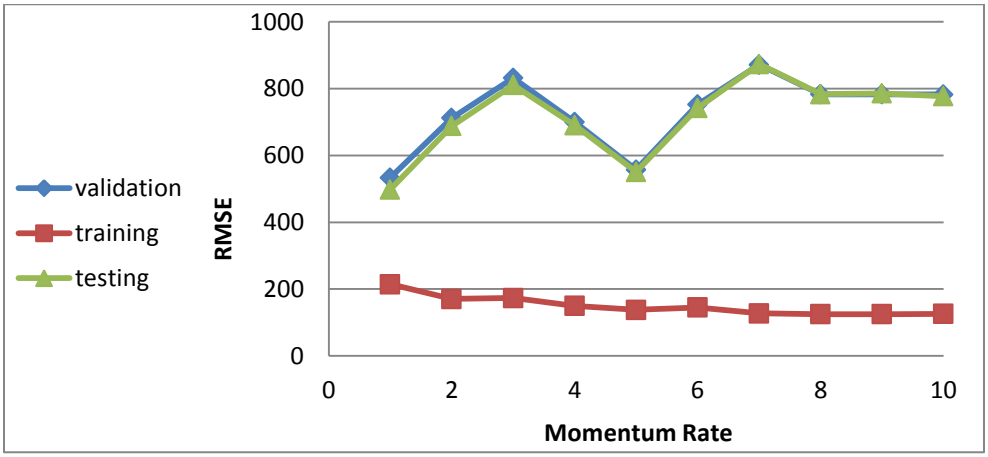

Figure 6. Performance of ANN model with different values of hidden layer nodes,(α=0.2 and β=0.8).

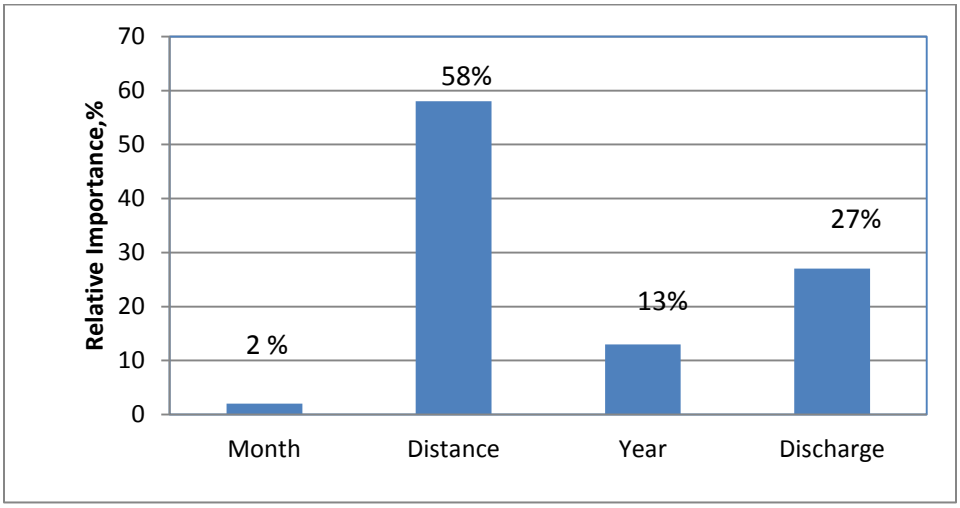

Figure 7. Relative importance of the input variables for the ANN model.

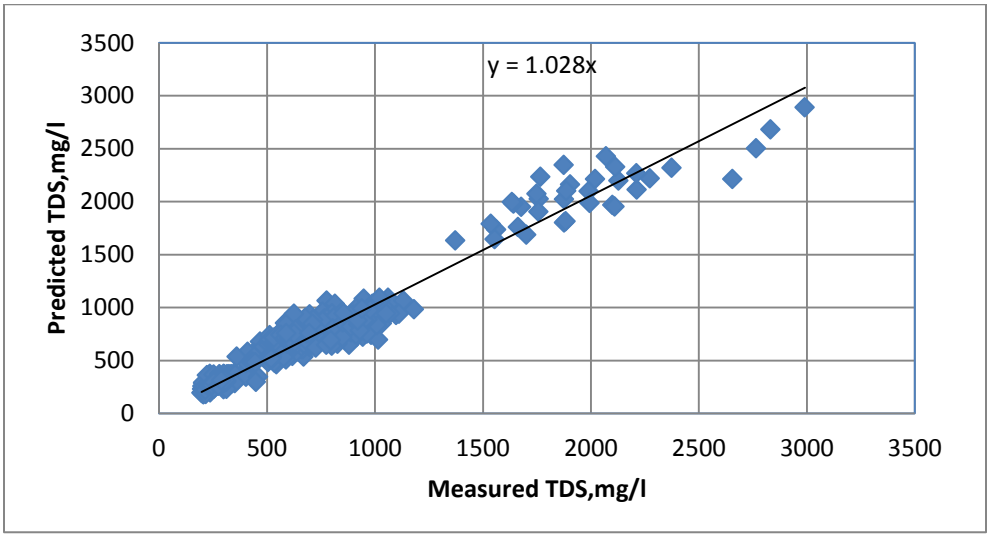

Figure 8. Simulated versus measured valued of TDS concentration of Tigris River.

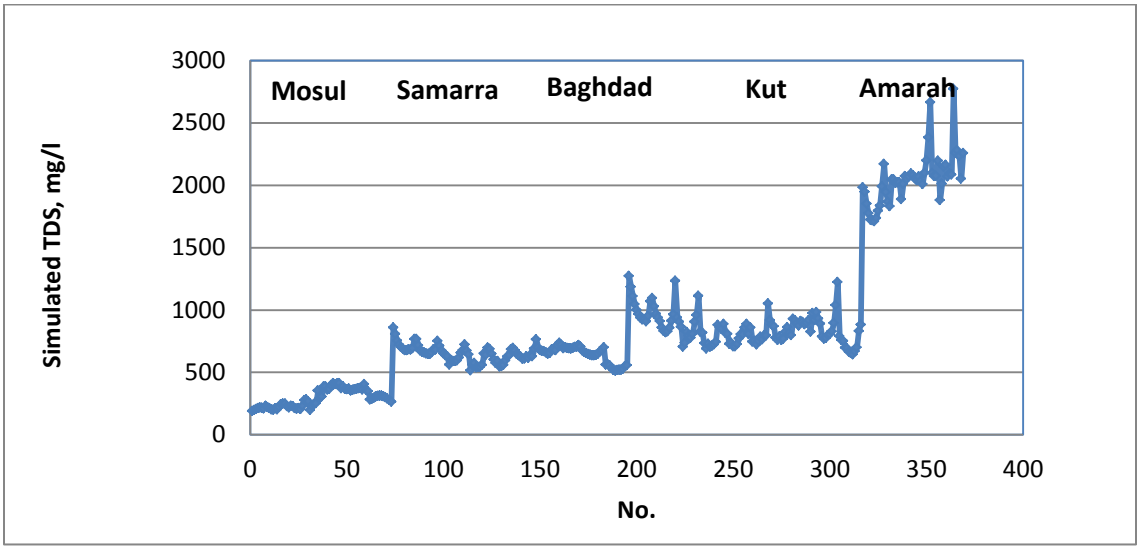

Figure 9. Change of simulated TDS with distance and years, Tigris River.

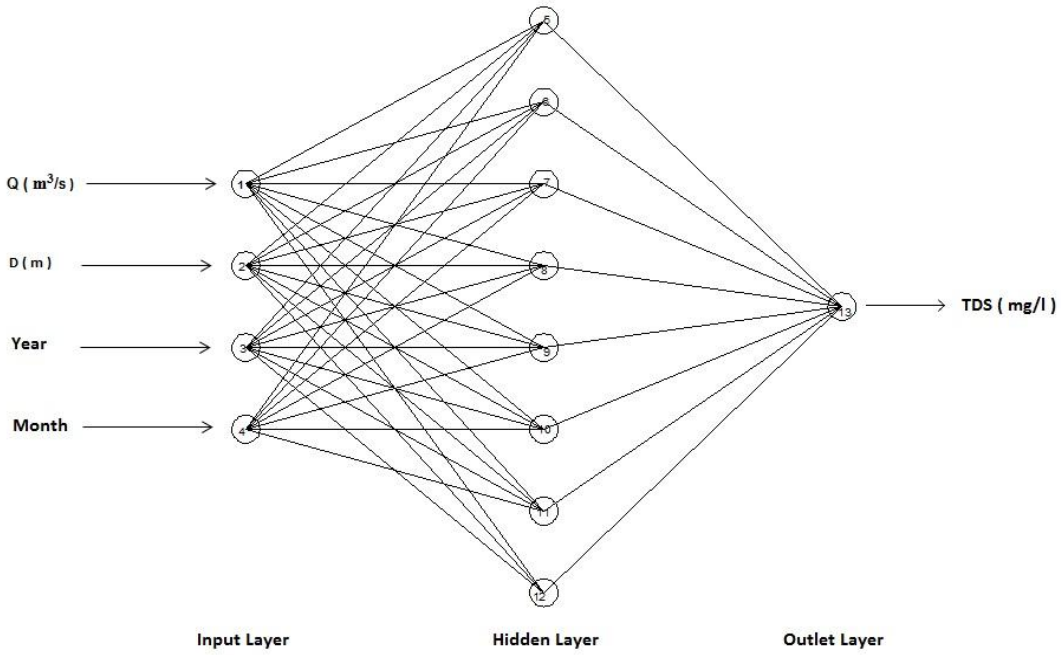

Figure 10. Schematic representation of the ANN architecture Model.

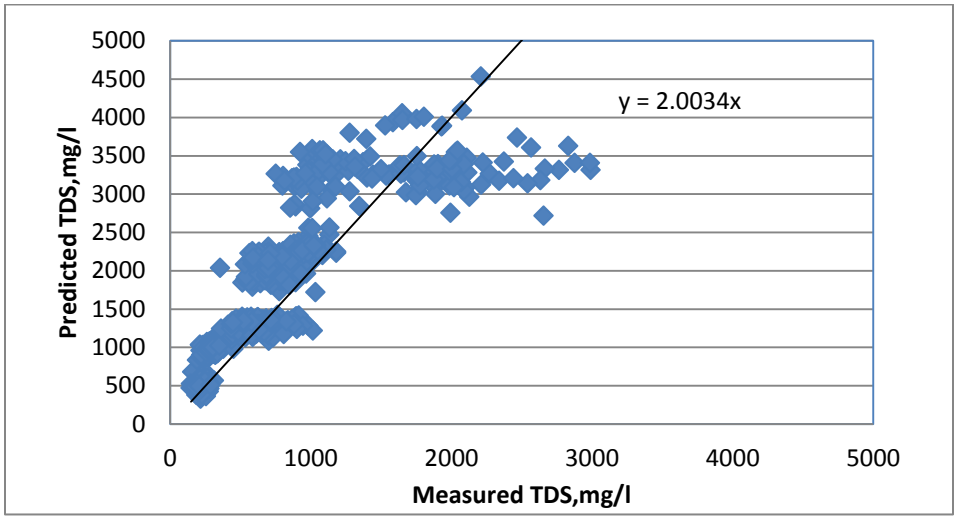

Figure 11. Simulated versus measured values of TDS concentrations for total.

ISSN 1726 - 4073

مجلة الهندسة

مجلة علمية محكمة تصدرها
كلية الهندسة ـ جامعة بغداد

حزيران
2015

العدد 6
المجلد 21

قـائـمـة الـمـحـتـويـات

القسم العربي:

النظم المنشأية لعمارة الحداثة في العراق
دراسة تحليلية لعمارة قحطان المدفعي

المدرس محمد رضا شاكر مجيد
ماجستير هندسة معمارية
قسم الهندسة المعمارية – كلية الهندسة – جامعة بغداد

الخلاصة

مايميز عمارة المعمار الدكتور قحطان المدفعي صفة التفرد وهي استخدام التغطيات الانشائية ذات الاشكال الثلاثية الأبعاد المتميزة واستغلال الهيكل المنشأي في اعطاء جمالية اضافية لتكوين المبنى وتطبيقا لافكاره الكونية والتي امن بها بشدة ودافع عنها وقد إستخدم بشكل خاص مادة الخرسانة المسلحة كمادة إنشائية أساسية لتحقيق هدفه. وفي ظل حقبة من التراجع الملحوظ في المستوى العمراني الذي يجعلنا بموقع يدفعنا نحو تحليل ودراسة ما بدأت به العمارة العراقية الحديثة ومسارها المتصاعد وصولا الى قمتها وفترات تراجعها حتى وصلت الى وضع لاتحسد عليه حاليا و التي تطرق اليها العديد من النقاد والمختصين في هذا المجال ولكي لاتكون الحلول خاضعة لمبدا الفعل ورد الفعل، من هنا برزت المشكلة البحثية وهي التحري عن الجذور السليمة لهذه العمارة وإنشائها وتعريف المجموع بافكارها وانجازاتها والسبل التي اتخذها روادها للنهوض بواقع العراق العمراني وايجاد نمط عراقي خالص مفعم بالمعاصرة والتجديد والجرأة في إستخدام النظم المنشأية والمواد الإنشائية المتوفرة محلياً لخلق عمارة متميزة في هذا النتاج والذي كان المعمار الدكتور قحطان المدفعي احد رواده المتميزين والذي يمكن اتخاذها مثالا ممتازا على تلك الفترة لنستخلص منه ومن نتاجه العمراني امورا عديده لايمكن تجاهلها.

من هنا سيتضمن البحث تحليلاً لمجموعة منتخبة من أبنية المدفعي المصممة والمنفذة كإطار نظري وعملي للبحث ومن ثم مقارنتها بأعمال أقرانه من المعماريين العالميين وصولاً الى الهدف الذي ينشده البحث وهو إستخلاص أمور عديدة من هذا النتاج المعماري من اهمها:

- مقومات النهوض بالواقع العمراني للبلاد من خلال التصميم والإنشاء كما حدث للرواد من قبل.
- الافكار التي اسس لها رواد الحداثه وما تطورت عنه لاحقا وصولا الى عصرنا الحالي.
- إيضاح الاشكال المعماريه والمنشأية والتقنيات البنائية المتبعة فيها والتي تميز بها المدفعي.

الكلمات الرئيسيه: قحطان المدفعي، ديناميكية، حداثه، تكنلوجيا، الأشكال السرجية، النحتيه، المنشأيه.

Structural Systems for Modern Architecture in Iraq Analysis Study to Dr. Qahtan Al-Madfa'i's Architecture

Mohammed Ridha Shakir Majeed
Lecturer
Engineering College-Baghdad University
E-mail:mridhachalabi@gmail.com

ABSTRACT

Dr. Qahtan Al-Madfa'i's architecture has been characterized by a particular characteristic that may be unique and extreme at the same time, that is the use of the distinctive three-dimensional structural coverings and the exploitation of structural construction to give an extra aesthetic touch to the composition of the building, to achieve the application of his universal ideas, which he strongly believed and defended.

In the period of the marked urban decline that the country undergoes now, which urges us toward making a comparison between the beginning of the modern Iraqi architecture and its ascending path up to its peak and the periods of its decline until it reached a very bad condition which has been referred to by many critics and specialists. In order not to have solutions that are subject to action-and-reaction principle, it is necessary to search for the intact origins of this architecture and its construction, define its concepts and achievements and the methods adopted by its pioneers to scaffold the urban status of Iraq and to find a pure Iraqi touch full of modernity and innovation. Dr. Qahtan Al-Madfa'i is one of those distinguished pioneers whose works and urban outcome can take as excellent examples of that period and to deduce from him and from his work many things that cannot be ignored.

All of this will be done through the illustration and analysis of selected group of Al-Madfa'i's buildings, designed and implemented, and to be compared with the works of his international architects and thereby reaching the goal of the research.

Key Words: Kahtan Al Madfai, Dynamic, Modernism, Technology, Saddle shapes, Sculpture, Structural.

1. المقدمة

بدأً لابد من الحديث عن الحقبة الذهبية للعمارة العراقية في عصرها الحديث (الستينات والسبعينات) وعن اهم منجزاتها وروادها والاشارة الى النتاج العمراني المتميز الذي قدمه الدكتور قحطان المدفعي في تلك الفترة وقد يكون من الصعب اختصار منجزاته واعماله التي تجاوز بها حدود الابداع وخرج بها عن المالوف متحررا بذلك من القيود التقليدية التي كانت سائدة انذاك وغالبا مايجد النقاد والمحللون صعوبة في تصنيف اعماله او ادراجها ضمن توجه معين فقد شكلت عمارته حدثا مميزا في الخطاب المعماري العراقي والاقليمي كونه (تجاوز سابقيه , وتميز على اقرانه , وتاثر به بشدة من لحقه) وكيف لا وهو احد مؤسسي العمارة العراقية الحديثة في مرحلتها الثانية و أحد مؤسسي جمعية الفنانين التشكيليين العراقية فضلا عن مايتميز به من مواهب متعدده يعتبرها طيفا متداخلا مع العمارة لايمكن فصل احدها عن الاخر تجسدت فيه من خلال ملكته الشعرية وما ابدعه من لوحات فنية فهو بذلك يتخذ مسارا خاصا به ميزه عن غيره من معاصريه في فترة كان التجديد والافكار التحديثية محط اهتمام المعماريين والفنانين والتي

كانت تاثيرات احدها سرعان ماتتدفق الى الاخرى والتي غيرت كثيراً من القناعات والرؤى في الممارسة المعمارية وغيرت من اساسياتها ومنطلقاتها. (مصدر – 2) .وقبل الولوج في افكار المعمار ونتاجاته فلا ضير من توطئة تبين ظروف نشأته وتاثيراتها عليه لاحقا، فهو قحطان حسن فهمي المدفعي ولد في منطقة الاعظمية عام 1926 من عائلة معروفة ومن بيئة فنية وادبية كانت مثالية الى حد ما لنشوء المعمار الدكتور قحطان المدفعي وهذا مايفسر ولعه الشديد بالفنون والشعر وإمتلاكه روح الاعتداد بالنفس والاعتماد على الذات والتي ظهرت لديه في عدة مواقف فانعكست لاحقا في ابنيته المتفرده شكلا ومنشأً ومضمونا واصراره على هذه الاشكال بالرغم من النقد الكثير والاراء المعارضة لتوجهاته والتي كانت تبدو غريبة للوهلة الاولى على الفكر والمفاهيم العمرانية السائدة في تلك الحقبة.

تلقى تعليمه الثانوي في الاعدادية المركزية في بغداد وتخرج منها عام 1946 ليغادر بعدها الى انكلترا لاكمال دراسته في الكارديف في ويلز والتي فضل الدراسة فيها على لندن لكونها اكثر هدوءا واقل تناقضا عن ما اعتاده من حياة في بلده الام وكانت الدراسة المعمارية في الجامعات الانكليزية محافظة الى حد كبير وتميل بشدة الى التوجه التقليدي وهو ماحاول قحطان التصدي له والتحول عنه بشدة والذي كان عادة ماينتهي بعقبات يواجهها مع مشرفي التصميم والرسم اليدوي حيث كان قحطان يبحث عن ذاته دائما متطلعا الى التجديد والتطوير المستمر المرتبط بالتطور العلمي والفيزيائي والذي كان في ذروته في تلك الفترة.(مصدر – 1)

واعجب المعمار في تلك الفترة بافكار الحداثة واعجبته ابنيه المعمار اوسكار نيماير Oscar Niemeyer‘والحداثة التي تبنتها البرازيل بقوة في تلك الفترة في عمارتها.

وبعد هذه السنين التي لاتخلو من النشاط والاحداث المحبطة والمحفزة اتم دراسته الجامعية وعاد الى بغداد وذلك في نهاية عام 1952 ليباشر بوضع بصماته الاولى في العمارة العراقيه من خلال ابنيته ذات التعبير الواضح القوي والذي مر بفترات من التطور المقترن بتغير نظره المعمار للكون وما يكتسبه من خبرة ودراية وتبادل وجهات النظر مع عمالقة الحداثة امثال والتر غروبيوس (Walter, Gropius) فنتج عن كل ماتقدم عمارة ناضجة شكلت مساحة مميزه ومؤثرة في عموم المشهد المعماري العراقي والاقليمي على حد سواء والذي كان ينطوي على اهمية خاصة ان كان لحساب تحديث العمارة.

وقد تميزت عمارته بصفة قد تكون متفردة ومبالغ فيها في الوقت ذاته وهي استخدام التغطيات الانشائية ذات الاشكال الثلاثية الأبعاد المتميزه واستغلال الهيكل المنشأي والخبرات المحلية الحرفية المتوفرة آنذاك كتقنيات بنائية في اعطاء جمالية اضافية لتكوين المبنى وتطبيقا لافكاره الكونية التي امن بها بشدة ودافع عنها .كما يتضح على نتاجه المعماري والفني الاطلاع الواسع والبراعة اللغوية فهو متقن لاربعة لغات (الانكليزية والالمانية واليونانية فضلا عن لغته العربية الأم) وممارس دائم لكتابة الشعر وممارسة الرسم[1].

2. مقدمات الإنجاز المعماري:

لابد من تشخيص أسباب التراجع الملحوظ في المستوى العمراني الذي يمر به العراق حاليا الامر الذي يجعلنا بموقع يدفعنا نحو المقارنة بين ما بدأت به العمارة العراقية الحديثة ومسارها المتصاعد وصولا الى قمتها وفترات تراجعها

[1] وبعد سنين طويله من الانجازات والابداعات وبعد ان تجاوز عمره الخامسة والثمانين عاما لازال المعمار مفعما بالحيوية وحب الاطلاع وممارسة الفن ومتابعة اخر اخباره ومستجداته في العالم فهو لا يشعر بالملل ولا بالفراغ فهو يعرف كيف يملئ وقته على حد قوله.
فهو بعد كل هذا العمر المليء بالمغامرات والتحديات لا يزال يتطلع الى تحد اخير يثبت فيها تميزه وابداعه في مجال العمارة مقدما امكانياته وكل مايستطيع ان يقدمه في خدمة بلده وابنائه الذين امدوه بالطاقه طيلة سنين الغربة ولحين إعداد هذا البحث عام 2014.

حتى وصلت الى وضع لاتحسد عليه و التي تطرق اليها العديد من النقاد والمختصين في هذا المجال ولكي لاتكون الحلول خاضعة لمبدا الفعل ورد الفعل لابد من البحث عن الجذور السليمة لهذه العمارة والتعريف بافكارها وانجازاتها والسبل التي اتخذها روادها للنهوض بالواقع العمراني وايجاد نفس عراقي خالص مفعم بالحداثه والتجديد في هذا النتاج والذي كان الدكتور قحطان المدفعي احد رواده المتميزين.

وبذلك نكون قد حددنا ولو بشكل مبسط مواطن الضعف والقوة التي يمكن العمل عليها للعوده الى مسار الركب المعماري والابداعي الذي تلتزمه اغلب الدول.

لكل انجاز مجموعة من المقدمات سواء اكانت واضحة للعيان أو خفيه فتوفرت في فترة الاربعينيات والخمسينيات من القرن الماضي عوامل وفرص نادرة وبصورة مجتمعة والتي كان ولابد ان تؤثر على مسار العمارة العراقية وتوجهاتها متمثله بأزدياد الموارد المالية للعراق بصورة كبيرة نتيجة لازدياد صادرات واسعار النفط العراقي.

وقد شهدت فترة الخمسينيات عودة عدد من الفنانين التشكيليين والمعماريين الى العراق وعودة مجموعة من المعماريين والفنانين المهنيين والموهوبين والذين اكملوا دراستهم في خيرة المؤسسات التعليمية الفنية والمعمارية الاوربية وما كان يرافق ذلك من ضرورة ايجاد اشكال وتكوينات جديدة تلبي احتياجاتهم وتتفاعل مع هذه التغيرات وقد توجه العديد من المعماريين العراقيين في تلك الفترة نحو التجديد والتحديث وتوسيعه في الفعالية التصميمية والإنشائية مستثمرين قواعد الحداثة ومحاولين ربطها بخصوصية المكان ونتيجة لتنوع خلفيات معماريي تلك الفترة على الصعيد الثقافي والاجتماعي والعلمي ظهر نوع من التباين في الرؤى والافكار باحثين عن طرز تبعدهم عن التقليد لذلك لم يهتموا بالعمل الجماعي او التأسيس لقاعدة مشتركة لذا كان التشابه في تجديدهم ينحصر في حل المتطلب البيئي والوظيفي في نتاجهم المعماري بل انجر معظمهم نحو الالتزام بالقواعد والاشكال المتعارف عليها منطويين تحت جناح الحداثة العالمية وهذا مالم يعجب المعمار قحطان المدفعي الذي وجد في اعماقه صوتا خاصا ومتميزا في مسار العملية التجديدية، صوتا يطمح الى تكثيف الخصوصيه والنزعة الفردية والتي تحدت بأشكالها قناعات الكثيرين في عصره الذين كانت عمارتهم تنطوي على ايفاء الجانب الوظيفي والبيئي وجزءا من الجانب الشكلي الذي كان غالبا مايميل الى التقليد والإقتباس تحد من التطوير والابداع وان كانت هذه الابنيه ذات سمة وظيفية بحته .لذلك لجأ الى التوجه التعبيري الذي وجده الاقرب الى افكاره ليوصله الى عمارة ذات طابع متميز ذو نكهة خاصة ومتفردة تمكنه من الخروج بأشكال معماريه تتسم بالحركة والديناميكية المشبعة بومضات الحس الانفعالي وما ساعد على ذلك من رغبته المستمرة للاطلاع على احدث التقنيات الانشائية في عصره وابتداعه اشكالا ميزته عن غيره والتي كانت في اغلب الاحيان موفقة في اداء المبتغى منها. (مصدر – 2)

الفكر التصميمي للمعمار الدكتور قحطان المدفعي

إن النخبة الصالحة من المعماريين التي تنافست في العطاء منذ لحظة عودتها الى الوطن قد تفاعلت فيما بينها فكرياً وتبادلت المفاهيم وأعلنت بجرأة عن تقبلها للمسؤولية فأسسوا مكاتبهم وأشغلوا مناصب أساسية في أجهزة الدولة الهندسية فلعبوا دوراً واضحاً في رسم سياساتها العملية وليس ثمة شك في أن هذا التنافس قد اسهم في إستخلاص القدرات الكامنة لأفكار هذه النخبة وضخها الى أرض الواقع لتضيف رصيداً الى رصيد وترسم بالخط العريض الذي ترتبط حافته الأخرى بالشكل المرسوم لمدرسة معمارية عراقيه تتناوب الأجيال في رفع بنيانها ورسم ملامحها...ولقد كان قحطان المدفعي واحداً من هذه النخبة وأسهم بفاعلية الى جانب أقرانه من أمثال د. محمد مكيه، هشام منير، رفعت الجادرجي، عبدالله إحسان كامل، وغيرهم في صياغة محاور أساسية للحركة المعمارية في العراق.

لقد ساهم المعمار قحطان المدفعي برفد النتاج المعماري بحيوية إضافية من خلال تحركه وتطلعاته وتقصيه لكل مايظهر على الساحة من شواخص الأعمال...وكيف إستهوتنا وراقت لنا تلك التكوينات الديناميكية والتكوينات المتناغمة التي طالعناها في متنزه الأوبرا ومدينة الألعاب في بغداد والتي أقترنت بإسم المعمار قحطان المدفعي..وحيوية الشباب التي تتوافق مع كل مايوحي بالحركة والتغيير.

لقد كان قحطان من قلائل المهندسين المعماريين الذين يحملون صفات أخرى وتطلعات أخرى الى جانب تطلعاته وإهتماماته المهنية فقد كان يعنى بسماع الشعر والشعر الشعبي...بل وينظمه أيضاً..ويروق له سماع الموسيقى..وكان إجتماعياً ومتبسطاً.

لقد أثبت المعمار قحطان المدفعي شغفه بالتجديد وإعتماده أسلوب التجريد والتركيز على عناصر ديناميكية الأشياء– وهذه هي نظرته للكون– في أعماله وتصاميمه. إن أسلوب المعمار قحطان المدفعي هذا قد أغنى الحركة المعمارية في العراق بمحور آخر شد إليه عدد من جيل الشباب.

ولايمكن انكار تبني المدفعي لافكار الحداثة الا انه قام بأدخال تفسيراته الذاتية على نتاجاته المعمارية والتي اكد فيها على الناحية الجمالية وفق مفهوم نحتي حيث كان عادة ما يستخدم اسلوب لايخرج عن روح الحداثة مدخلا عناصره النحتية بأسلوبه الخاص والمميز ولقد كان له نظرة خاصة ميزته عن اقرانه من رواد الحداثة العراقيين وذلك لالتزامه منهجا فكريا يتمحور حول الرؤية الكونية الجديدة والتي اشهرها علماء الفيزياء والفلك في تلك الفترة وحاول ان يطبقها على نتاجه المعماري بنفس يعكس خصوصية البلد وخصوصية ذاته المتفردة.

وتنص هذه النظريات على (ان ألبرت أينشتاين Albert Einstein اعتقد ان الكون كل موحد وكل شيء في جوهره يساوي كل شيء اخر ويتحول اليه فالمادة تساوي الطاقة والجاذبية تساوي التعجيل والمكان يساوي الزمان.....).

وقد اسندت معادلات النظرية النسبية الجديدة المستخدمة لوصف الكون الاحدب من قبل الاكتشافات الثورية لعلم الفلك في العشرينيات على يد العالم الفلكي ادوين هابل (مصدر 5،9) والذي استبدل صورة الكون الساكن ذي الحجم المحدود المستقر بصورة الكون الدائم التوسع والاستمرارية والتغيير فهو يتكون من عدد هائل من المجرات التي تبتعد نحو افاق فضائية متسعة باستمرار.

واصبحت بذلك مجرة درب التبانة التي نحن فيها والتي يبلغ قطرها حوالي 100 الف سنة ضوئية تقريبا لاتعتبر الا اكبر بقليل من كرة متناهية الصغر في كون ممتد مليء بالمجرات لذلك يمثل الكون المنفجر خصائص الكون غير المستقر والمتغير بمرور الزمن نتيجة لتمدد المادة الموجودة فيه والذي فرض نوع جديد من الانظمة تدعى بالانظمة المفتوحة المعتمدة على مبدأ الغائية[2] (Teleology) والتوسع او الامتداد (Expansionism) وماجاءت به هذه الافكار عن التوسع وشكل الكون الجديد انعكست في اعمال المعمار قحطان المدفعي عن طريق تبنيه لنظرية السطوح السرجية[3] Hyperbolic- Paraboloidal Surfaces (شكل–2)، الذي اعتمد عليه في افكاره التصميمية.

وقد تبنى المدفعي هذه الافكار بعد فترة من المحاولات لادخال الحركة والحداثة في اعماله ففي فترة الستينات نلاحظ هذا التحول والنضوج المهني ونتلمس مقدرته المتمكنة في استخدام عناصر التكوين الممزوجة بالخبرة العالية لطبيعة

[2] الغائية (Teleology) قسم من الميتافيزيقا، يقوم على مبدأ ارتباط العالم بعضه ببعض ارتباط العلّة بالغاية.

[3] السطح السرجي (Saddle surface) هو سطح أملس يحتوي على نقطة مقعرة أو أكثر. أتت التسمية من شبهه بسرج الفرس والذي ينحني صعودا وهبوطا.

المواد الانشائية التي يستخدمها مع نظام التراكيب التي يوظفها لكن هاجس التعبيرية المتسمة على تعقيد كتلوي (مصدر– 12) التي وسمت عمارة المدفعي بسمة خاصة كانت حاضرة في هذا العقد المزدحم بالمشاريع المتنوعة والتي طالما تطلع المعمار من خلالها ليكون صوتا معماريا منفردا ومتميزا لخلق منجز معماري ناضج وذو تعبيرية مكثفة قائمة على حرية التجريب وتفعيل المخيلة لذا كانت مبانيه تعايش في تكويناتها قرارات تصميمية تبدو متضادة ومتناقضة سواء اكانت لدلالاتها ام لناحية اسلوب توظيفاتها وقد يكون تجاور هذه القرارات المتباينة في التكوين هو الذي يمنح الاخير تلك القوة الاسرة من الحيوية والتشويق والذي يصل الى حد الغرابة وصولا الى فك ارتباط مفهوم العمارة عن ما ارتبطت بها من قيم ومنطق وتمثيل وتاريخ كما دعت له استراتيجيات عمارة التفكيك في تلك الفترة وكمثال على تصاميمه المثيرة للنقاش والتي يحظر تكويناتها البساطة مع التعقيد والوضوح مع الابهام هي مبنيي جمعية الفنانين التشكيليي (شكل–3) ومبنى متحف التاريخ الطبيعي في بغداد (شكل–4).

ويرى المدفعي في احد ندواته (مصدر– 13) ان هنالك فنانين يؤمنون بقوة العقل وتراهم يبتعدون عن المرسم وينتقلون الى الميادين مباشرة كي تحفزهم على العمل وتدريب العين على الرؤية من الامور التي تقابل العقل وفي القابلية على الخزن وحمل الرؤى لبعض الوقت وقد ذكر (كاندنسكي)[4] في هذا الاعتبار وخصوصا عندما يتحدث عن طفولته انه كان يروض عقله اي يتجاوز اختباراته ليس عن طريق الاحصاءات الرياضية بل يتجاوز ذلك عندما يرد عن نفسه من خلال الرؤية والتسجيل وسط عقله وقد حصر المدفعي مبادئه في اربع نقاط :

أ– التلقائية في الفن

ب– اللاجدوى والنهلية

ج– التلقائية في الشعر

د– اللغة التعبيرية في العمارة

يرى كاندنسكي انه توضع بها مستويات الجمال ، وان يعرض على المتلقي مايفيده من مصطلحات قد تبدو في الفنون قريبة من الذهن ولكنها عند المتلقي بعيدة نوعاما وهذا يتم من خلال عرض أشكال وتكوينات ورسومات تفصح عن مكنونات الفنان المادية التي لم ترد في ذهنه فحسب وإنما في المادة ذاتها.

ونرى ان المدفعي يصارع أموره الأربعة من خلال ، الصراع مع الطبيعة وأسرارها وعملية اكتشاف المعرفة من خلال التجربة ، إذ يحاول أن يوظف الرباعية بإيجاد صيغة للجمع التشكيلي في رؤى لثقافة تبدو أكثر معاصرة ، وخصوصا مخاطبته للموضوع إن كان لوحة مرسومة اوتصميم عمارة بناء أو قصيدة شعرية ، هنا لم يجد فرصة لاستخراج كل ماموجود في الرباعية وجعله حالة سهلة للمتلقي ، وإنما الواجب عليه أن يتعامل مع مفردات أكثر إبراز في الحالة الظاهرة والمعمولة.

ويرى المدفعي (مصدر– 14) أن كل التقاء للألوان في الأشكال والمساحات ، يكون تكرار موجب باللوحة لان عادة هناك توافقات تحدث نتيجة هذه التكرارات ، المدفعي أعطى لهذه الحالة دور في الرسم والعمارة والشعر ، لأنه عبر عن تلك الأفكار باتجاهات فلسفية للنظر إلى الحياة والبحث والتعلم من الطبيعة ، دون إحداث أي خلل يذكر . والخلل

[4] فاسيلي كاندينسكي فنان روسي (16 ديسمبر 1866 – 13 ديسمبر 1944) أحد أشهر فناني القرن العشرين، اكتشافاته في مجال الفن التجريدي جعلته واحدا من أهم المبتكرين والمجددين في الفن الحديث. في كلتا الحالتين، كفنان وباحث نظري لعب دوراً محورياً ومهماً جدا في تطور الفن التجريدي (abstraction art). تنسب اليه جائزة كاندينسكي للفنون، ومن أشهر تصاميمه كرسي كاندينسكي الذي اخذ طابع مدرسة باوهاوس في ألمانيا.

هنا ليس المقصود بالأفكار باعتبار أن الفكرة ناضجة ، ولم يبقى سوى الأداء والفعالية والنظر إلى الحياة الجديدة من خلال الفن .

(ويقول المدفعي عندما تكون نهاية الحياة الموت وهذه مصيرية الإنسان ونهايته فيقول ما الجدوى من العمل والانتاج والفن والبناء والشعر والعمارة ، هذه لم تكن لاجدوى لها عنده وإنما ربما ينطلق من إعدام الموضوع أو التخلص منه ، والانتقال إلى شيء آخر سواء في لوحة الرسم أو تصميم فنون العمارة أو الشعر هو الذي بالإمكان انجازه دون غيره في الفن) .

والتلقائية المعتمدة في الشعر ، أقحمها المدفعي كونها لغة درامية ، ناضجة من تغيرات أثرت على الحياة ، بدرجة اوجدها النقاد في فترة الحداثة عندما شمل الشعر ، الكلام العفوي والكلام التلقائي والكلام أثناء الأحلام كل هذه كانت أفكار المدفعي تنطلق ، بدافع التجربة لانه اوجد لها أرضيات مشتركة ، في المنفعة والتداول ومن الصعوبة أن يفهم هذا الموضوع بسهولة من قبل المتلقي وإنما من المحتمل ان يوف نوع من القناعة ، عندما يكون الشعر بمعناه العفوي ليس إلا؟.

وحسب مايقول المدفعي (مصدر–8) **(لم تكن العمارة لي إلا تركيباً زمانياً ومكانياً وهي تعبير عن شيء وخصوصا بداياتي المعمارية)** الحالة الخاصة التي يمتلكها ، المدفعي تظهر إلى حد ما في قائمة تتصدر الأشياء المحسوسة ، وتبقى عنده المتضادات هي التي تثير الجدل بدليل أن المعماري لحد الآن هو معادي للطبيعة عندما يحول كل مافيها إلى بناء ، المدفعي يريد التخلص من الأمر بأي شكل من الأشكال ، وعندما يستخدم التصميم يبدو انه يكون ضد الطبيعة كمبدأ ، ولكن الأمر يمكن أن يكون ضمن صورة المشهد الراقي الذي أدرك الحيز بالفضاء ،ومن ثم الصياغة التصميمية ليبقي للزمن تداوليته المعبرة بأفكار ومشاعر وأحاسيس فنون العمارة ، وعندما يكون المدفعي معماريا تعبيريا يتوجب عليه أن يعطي دورا اكبر لأعماله بالظهور لتكتمل الرباعية ونقول إنها رباعيات المدفعي.

3. رؤية المدفعي للواقع العمراني الحالي

لقد عبر المدفعي (مصدر– 9) في العديد من المناسبات واللقاءات عن عدم قناعته بمجمل مايجري على ارض الواقع لعمارة بغداد خصوصا والعراق عموما وقد وصف ذلك بقوله **(مع الاسف لايعجبني، والذي لا يعجبني بها اكثر من الذي يعجبني وهذا يشعرني بالالم لان بغداد تستحق جمالا اكثر وعمرانا اجمل فالسفر داخل بغداد مؤلم واتمنى ان يكون هذا الشعور مؤقتا ، من الصعب ان اجد قاموسا تعبيريا عن ماهية عمارة بغداد ولكن كأي واحد يبحث عن اموره القديمة يجد هنا وهناك اماكن لها اهمية ولها ذكرياتها وطرازها الواضح)**، كما اكد المدفعي على ان **(عمارة بغداد عمارة وقورة وهي بالضد مما يحدث حاليا وهذا لايشوه بغداد فقط بل سوف يمحي ملامحها التي نعرفها وتجعلنا نشعر بأننا نسكن في مكان لا ننتمي اليه)** مشيرا بذلك الى مواد التغليف الجديدة واهمها (الألكيوبوند) معتبرها فضلات الحضارة الغربية وكونها مادة تجارية يراد من استخدامها سهولة التنفيذ وسرعته والكسب المادي طارحة بذلك كل القيم الشكلية والمناخية والاجتماعية العراقية عرض الحائط واعطى مثالا على ذلك **(مكعب من الزجاج على ماذا يدلل)**، (مصدر – 5) ولاسيما اذا لم يكن ملبيا للمتطلبات المناخية المحلية القاسية.

وهو يعزو واقع بغداد الحالي الى مجموعة من العوامل من اهمها والذي له علاقة بالبحث: (مصدر– 18)

أ– التعجل في وضع الحلول للمشكلات واختيار الجهات المنفذة وتفضيل ماكان سريعا منها واقل كلفة دون الالتفات الى النوعية والفكر المتبع واحيانا انعدامه .

ب- انتشار المهمة التصميمية لدى شركات المقاولات المحلية والتي تشكلت معظمها حديثا والتزامهم بتنفيذ المشاريع بغياب كلي او شبه كلي عن الرقابة الاكاديمية والمتخصصة .

ج- استخدام مواد البناء الرخيصة والرديئة النوعية والالتزام بمجموعة من التكوينات المكررة والتي يتم اقحامها في مختلف المشاريع باختلاف اغراضها فضلا عن استخدام الالوان دون دراسة مدى تناسقها وتضادها مع المجاورات ومع غرض المبنى او المحددات البيئية الشكلية او الوظيفية .

د- الاقتصار في عملية التنفيذ على نظام البناء المصمت الكونكريتي في المشاريع الصغيرة والهياكل ذات الفضاءات المتكررة في المشاريع المتوسطة والكبيرة وكانما لاوجود لانظمة اخرى او الاعتقاد بان تنفيذها مستحيل.

هـ- استخدام اليد العاملة البعيدة عن الاحتراف الفني وعدم تزويدهم بالمخططات التنفيذية الكاملة التفاصيل وانعدام وجود دورات او شركات منظمة تمتلك كادرا متخصصا في تنفيذ الابنية من المهندس المشرف وحتى العامل البسيط مما يؤدي الى نتائج سلبية وغير مرضية في تنفيذ التصاميم وان كانت على مستوى معين من العناية .

و- ميل معظم المصممين المعماريين نحو التقليد والاشكال المعمارية التي لاينطوي وراءها اي فكر تصميمي معماري او انشائي وربما يعود ذلك الى التسرع في اتخاذ القرارات وحذف مرحلة الدراسة التحليلية قبل الشروع بوضع التصاميم .

ز- الضعف الواضح والكبير في التكنولوجيا الانشائية واقتصار معظم المصممين الانشائيين على مجموعة من النظم والمعادلات والمواد التي تعتبر متخلفة في وقتنا الحالي ودون الطموح الذي يتطلع اليه المصمم المعماري مما يفرض عليه قيودا في عمله التصميمي من خلال التبسيط الشديد للواجهات الخامسة (اشكال الاسقف) وتقليل الارضيات البارزة عن الهيكل وبأقل مسافات ممكنة والتقيد بميلان محدد وفتحات وتداخلات بسيطة على مستوى الجدران والارضيات.

ح- ضعف في التواصل مع الجهات التي تمثل الخبرات الانشائية والتنفيذية في دول العالم المتقدم على المستوى الاكاديمي والتطبيقي .

وفي ظل التطورات (مصدر- 1) التكنولوجية المتسارعة الخطى في العالم المتقدم مازال العراق بلد الحضارات واول مؤسس للقوانين المدنية للعالم يرزح تحت وطأة التشوهات البصرية للمنظر المدني والنسيج الحضري على الرغم من اننا بلد يقود موسساته دستور ديمقراطي، ينبغي ان تؤمن من خلاله حياة كريمة تليق لبناء مجتمع مدني متقدم وتكمن المشكلة الكبرى باننا لا نزال نعاني من ازمة مستعصية تتمثل في توفير الطاقة الكهربائية والتي تعد عصب الحياة في جميع انحاء العالم لما لها من اهمية ستراتيجية وحيوية وقد استمرت هذه المعاناة لاكثر من عقد من الزمن بانتظار انشاء محطات توليد الطاقة الكهربائية واستيرادها من مناشئ عالمية وبالاعتماد على طاقة البترول كوقود للتوليد الكهربائي علما بان اغلب دول العالم اتجهت منذ فترة ليست بالقصيرة لايجاد حلول بديلة للطاقة الكهربائية تعتمد الطاقة النظيفة الصديقة للبيئة لاسباب ايجابية تستند الى تخفيض مستوى النفقات والمحافظة على نقاء البيئة.

4. دراسة مقارنة بين نتاج المدفعي وعمالقة الحركة المعمارية الحديثة:

يشير المعمار المدفعي في كثير من الندوات واللقاءات الى اعجابه بتوجهات واعمال العديد من المعماريين العالميين من امثال لو كوربوزييه Le Corbusier.

واوسكار نيماير بالاضافة الى العالم والمعمار ريتشارد بوكمينستر فولر Richard Buckminster Fuller

و فرانك أوين غيري Frank Owen Gehry.

وعادة مابين المدفعي (مصدر– 14) العديد من المقارنات بين اعمالهم واعماله مظهرا الاختلاف في تبني الافكار ضمن التوجه او الحركة الواحدة واذا ما نظرنا الى اعمال المدفعي بعين التفحص لوجدناها ملتزمة باساسياتها لمبادئ وافكار الحداثة من تجريد واختزال للتفاصيل والحركة مع اعطاء نوع من التعبيرية البارعة من خلال الهيكل المنشأي البسيط ذو المواد المحلية فنجد تاثره الواضح بابنية لو كوربوزييه الوحشيه ذات الملمس الكونكريتي المكشوف والخشن، ككنيسة الرونتشام في فرنسا Notre Dame du Haut, Ronchamp, Fr., 1950–55 (شكل–5).

فطبق ذلك في عدد من ابنيته مثل بناية مركز تدريب المواصلات السلكية واللاسلكية في منطقة العلاوي ببغداد (شكل–6).وعدد من الدور السكنية مثل دار السيد امين الياسين ودار السيد هشام المدفعي (شكل–7).

فضلا عن تاثره بالاطر التكوينية العامة للدور السكنية التي صممها مع الالتزام باعطاء طابع عراقي وخصوصية مكانية ومناخية في معظم ابنيته. وشهد مسار المدفعي تحولا كبيرا بعد لقائه بعملاق الحداثة والتر غروبيوس حيث نقل له الاخير فكر النسبية في العمارة ودور الزمن والحركة ضمن هذا المفهوم فكانت تلك الحادثة طفرة لمسار المعمار الابداعي وبما اسماه انفلاق فكري تجسد في عدد من ابنيته المميزه مثل مبنى سكرتارية الطاقة الذرية (شكل–8) وجامع آل بنية (شكل–9) ومبنى البريد المركزي كما نجد تأثير الحركات الفنية الحديثة واوجهها المعمارية واضحة في نتاجه المعمارى كالموسيقى الحديثة وتضمينها في المعرض الزراعي (حالياًنقابة المهندسين الزراعيين) (شكل–10) كفكرة لونية وايقاعية في الوقت ذاته والتوجه التكعيبي الذي تبناه في دار محمد حميدان ومعهد الاتصالات السلكية واللاسلكية وغيرها من التوجهات والتيارات والتي تباينت فتراتها واهدافها ولا يخفى التعطش الشديد للاشكال والتكوينات الجديدة والحرة (ذات الطابع النحتي) والتي تبرر مبالغتها وافراطها التعبيري استنادا لمبررات الحركة والتنوع البصري وقد كان المصمم المعماري ايرو سارنين Eero Saarinen احد اعلام هذا التوجه ولعل ابرز اعماله كانت في قاعة الهوكي (شكل–11) المغلقة وفي مطار كينيدي (TWA) (شكل–12) ويلاحظ فيهما تعاملاً نحتياً مع هيكل المبنى وتفاصيله فاندمجت العناصر الانشائية والوظيفية مع بعضها البعض لتكون تحفة نحتية تمتاز بالاستمرارية والتجانس.

فوجد المدفعي (مصدر– 4) في هذا التوجه مجالا للتعبير عن ذاته المتفردة بالرغم من عدم توفر الخبرة الانشائية والوسائل الكافية ومثال على ذلك مبنى إداري في شارع الخلفاء (شكل–13) واعمدة حدائق الاوبرا وبواباتها المتكررة (شكل–14) الامر الذي لم يسبقه اليه احد في العمارة العراقية التي لطالما التزمت بالاشكال الكلاسيكية.

ولريتشارد بوكمينستر فولر Richard Buckminster Fuller نظرة مختلفة عن كوننا وحياتنا حيث اكتشف ان الاساس الهيكلي لنقل القوى في الحجيرة الحية اساسها قوى الشد فيرى ان الابنية يفترض ان تكون عاملة قدر الامكان بمبدا الشد مع تبنيه للنظرة الكونية الجديدة فكان للمدفعي قناعة الى حد كبير في ذلك المبدا وطالما رغب

بالعمل على اساسه الا ان عددا كبيرا من المعوقات جعلته يلتزم قوى الانضغاط كاساس لعملية توزيع ونقل الاحمال وكان اهم تلك المعوقات يتمثل بالضعف في الجانب التكنولوجي والعوامل الاقتصادية (مصدر – 24) .

وفي الثلاثينات جاءت نظرية الشكل السرجي الكونية لتشغل عددا كبيرا من الفنانين والمعماريين فتبناها بعضهم وحاول ترجمتها الى واقع ملموس كجزء من فكر التشبه بالكون الاكبر وكان المعمار فيلكس كانديلا Félix Candela احد اشهر مبدعي الاشكال السرجية والمطورين على تشكيلاتها فله العديد من الهياكل القليلة السمك نسبيا والمعتمدة على تداخل اجهادات الشد والانضغاط في عملية نقل الاحمال عبر مساند نقطية تمثل مفصل الارتباط (شكل–15). فغالبا ما اعجب المدفعي وحذى به نحو تطويعه للخصوصية العراقية ومناخها المتطرف فانتج مجموعة واسعة منها وان لم تكن موفقة الى حد كبير في الايفاء بالجانب البيئي واحياننا الوظيفي . ومن امثلتها مبنى خلط وتعليب الشاي في بغداد (شكل–16).

وبعد فترة من انتشار هذا المبدا في الاوساط المعمارية وما تبع ذلك من نقد ونتائج للتجارب السابقة حدث نوع من التحولا ت الفردية في الناحية التطبيقية للمفهوم فمنهم من التزم التبسيط والايحاء الشكلي ومنهم من بالغ في تعقيد تلك الاشكال نظرا لتوافر الالية الانشائية وتطورها بصورة متسارعة .

اما المجموعة الثالثة فقد اجرت تعديلاتها الخاصة على المفهوم واعتماد مبادئ الالتحام الشكلي والتكامل بين اتجاهات توزيع القوى وشكل المنشا وكان المدفعي احد هؤلاء المحدثين عن طريق ادخالها على الاشكال المعمارية العراقية التاريخية والتي يرى انها تحمل دلالات ميتافيزيقية مميزة ويعتقد بتوصل الحضارة (البابلية والآشورية) الى نتائج وعلوم لم نتوصل اليها لحد الان .

ولم يقتصر ادخال تلك الاشكال والافكار على الابنية التعبيرية والرمزية بل تجاوزها الى انواع اخرى من الابنية الوظيفية كالابنية الادارية والصناعية. وقد واجه الدكتور المدفعي ماواجهه من تحديات في التعاون مع المختصين في مجال الانشاء الذين تعاون معهم وذلك لكونه يمتلك خبرة واسعة في هذا المجال وكانت احياننا تفوق قدراتهم او مخيلاتهم ان صح التعبير فغالبا ما كان يبادر بالحلول الانشائية الذكية والسهلة التنفيذ كما حدث في تنفيذ تصاميم حدائق الاوبرا (شكل–17) (مصدر – 17). ومن مجمل الامور التي حدت من قدرة المدفعي في التعامل الانشائي هي رغبته بانحصار العملية التصميمية والتنفيذية بايادي عراقية قدر الامكان وهو بذلك يلتزم بمبادئ الاستدامة والتوصيات التي نادى بها العديد من مؤسسي العمارة البيئية أو المكانية امثال المعمار المصري الكبير حسن فتحي والاستاذ الدكتور محمد مكية فكان المواد المستخدمة في تنفيذ ابنيته مواد محلية وقابلة في معضمها لاعادة التدوير وتلائم في الوقت ذاته المتطلبات الانشائية والبيئية وتعكس القيم التراثية والتاريخية العراقية اما بحد ذاتها او بطريقة تنضيمها . كما اعتمد في اغلب مشاريعه على الايدي العاملة العراقية وعمل على تدريبهم وصقل قدراتهم عن طرق تزويدهم بكافة التفاصيل اللازمة للتنفيذ واحياننا التناقش معهم ومساعدتهم بصورة مباشرة الامر الذي لم نعتد على رؤيته لدى معظم المصممين وهو بذلك يذكرنا بالاسباني أنطوني غاودي (Antoni Gaudi) الذي كان يشرف بنفسه على تنفيذ ابنيته وبادق تفاصيلها، الامر الذي جعل الكثيرين من المقيمين والدارسين لمجال العمارة والاقتصاد والاجتماع ينظرون له بعين الاشادة والامتنان لكونه ساهم وبدرجة كبيرة في احياء طرز البناء القديمة وتطوير الحديثة منها عن طريق مجموعة من الحرفيين البسطاء ومساعدتهم في رفع مستوى خبرتهم التنفيذية .

وجاء جامع آل بنية يحمل هذا التوافق بين المحافظة على العناصر الاساسية والتراثية للمسجد وبين الافكار الاهتدامية [5]والحركية التي تبناها المدفعي سواء اكانت في الهيكل الانشائي او في مواد وطبقات الانهاء.

وتشهد الساحة المعمارية تنوعا كبيرا في المرجعيات الشكلية والفكرية واتاحة الحيز الاكبر في العملية التصميمية للجانب الفردي وتراجع في تطبيق القواعد الفنية التقليدية فبات الامر اشبه بسباق لانتاج ابنية اكثر تميزا و جرئة وتراها في كثير من الاحيان تستند الى افكار للتجميع الكتلي والتحريك او النحت الانفعالي والتي سبق وظهرت في فترات سابقة في المجالات الفنية والعلمية المختلفة كالرسم والنحت وعلوم الحياة فما فكرة اعمدة البارابوليود Parapoliod في حدائق الاوبرا للمدفعي في منتصف القرن الماضي ومبنى الجذع المفتول Turning Torso لسنتياغو كالاترافا [6] (شكل-18) الا تطبيقات مختلفة للموضوع ذاته ولكن التقنية الانشائية المتطورة والتقبل الثقافي للمجتمع الجديد مكن لكالاترافا من تنفيذ مبناه. كما مكن المدفعي من قبل في تصميم مبنى سكرتارية الطاقة الذرية والذي لم يتم تنفيذه .

كما نرى ان العديد من الاشكال والافكار التي توصل لها المدفعي في فترات ليست بالقريبة بدات تنتشر بصورة تلقائية في العديد من دول العالم حتى وان لم يكن هنالك اطلاع مسبق عليها لكونها تتبع من نهج واحد يجمع بين العلم وطيف الفنون التنوعة ويضع مسألة التجديد في اولوياته لذا فيمكننا القول ان المدفعي وبالرغم من صعوبة طرح تلك الافكار في العراق فانه تمكن وبطريقة بارعة من ان يتفوق على معاصريه ويسبق عصره بعقود من الزمن.

5. الفكر المنشأي للمدفعي:

يشير المعمار الدكتور قحطان المدفعي في اجابته على سؤال عن المنظومه الهيكلية لمبانيه[7] بقوله **(احاول ان اعطي لكل بناية معياراً اجتماعياً – ذوقياً – انشائياً)** فهو يبرر بذلك هياكله البنائية بقوله (مصدر- 14) **(اعتمدت على ما هو متوفر من الامكانيات والالات والمواد والخبرات العراقية لذلك لجأت الى توزيع الاحمال ونقلها عن طريق قوى الانضغاط وكانت البحور في اغلب الابنية صغيرة او متوسطة تعتمد على نظام الفسح المتكررة المتشابهة واحياننا المتغيرة لايجاد فضاءات اكبر ضمن الهيكل ذاته فكانت التصاميم الانشائية تخضع للجداول القياسية لمسافات الاسناد المثالية).**

ويتابع بقوله **(ان الاوربيين يرون ان الزاوية 90° هي الزاوية المقدسة كما ذكر لو كوربوزيه اي النظام المتعامد بينما نرى نحن (البابلواشوريين) ان الهيكل يجب ان يكون مائلا كما في الزقورات والقلاع وغيرها الكثير من الابنية الاخرى).**

---

[5] (الاهتدام) وهو الاسم المعرب لمصطلح (DECOSTRACTION) والتي يرى المدفعي ان ترجمتها بكلمة تفكيك امر غير مقبول ولايمت للفنان والمعمار بصلة

[6] سنتياغو كالاترافا (Santiago Calatrava) معماري ونحات إسباني من فالنسيا (مواليد عام 1951)، معروف عالميا بمشاريعه ذو الطابع المستقبلي.

[7] زيارة الباحث الى منزل المعمار الدكتور قحطان المدفعي في شهر تشرين أول 2011

واشار المدفعي الى ان الحضارة التي نعيشها حاليا معتمدة على فكر المهندسين الانشائيين لذا وكنتيجة لكون المادة وثقلها هي الاساس لهذا فانه يتم التاكيد على قوى الشد و التقليل من ارتكازات الانضغاط كما نصت نظريات فولر الانشائية والذي اكتشف ذلك ضمن الخلية الحيوية فالمدفعي اراد وبشدة استخدام مبادى الشد لفولر ولكن الامكانيات لم تكن متاحة.

ويمكننا أن نرى إن المدفعي إستخدم الهياكل والتسقيفات ذات الاشكال المتسمة بالحركة بالرغم من عدم توافر التقنية الكافية لذلك لذا كانت ابنيته وكما ذكرنا سابقا تتناقض بين جدرانها الحاملة او اعمدتها المنتظمة التوزيع اليسيرة التنفيذ من جهة وبين التسقيفات المبتكرة ذات التقنية الانشائية المميزة في محاولة لايجاد تميز انشائي وشكلي فكانت جمالية ابنيته تعتمد على جمالية الانشاء بطريقة تحقق النواحي الاقتصادية والشكلية والبيئية.

ومن ابنيته ذات الطراز الانشائي المميز انذاك:

أ- مبنى جمعية الفنانين التشكيليين في بغداد (شكل-19) **ذو الاقبية البرميلية المتوازية المتكررة.**

ب- متحف التاريخ الطبيعي في بغداد (شكل-20) **ذو التسقيف المعتمد على اشكال البارابولويد Parapoliod.**

ج- مبنى البريد المركزي في بغداد (شكل-21) (لم ينفذ) الذي يبين النضج الواضح للفكر الانشائي للمدفعي والمعتمد في تسقيفه على **الاقبية المتحدة المركز والمكررة.**

د- جامع ال بنية في بغداد (شكل-22) حيث الابداع الانشائي في هيكل في كافة عناصره وتفاصيله الانشائية من **قبة بيضية الشكل واعمدة مندمجة باسلوب بارع مع الجسور ذات الشكل المميز ساحبة نقطة التقاء الاقواس الى الخارج فضلا عن المنارة التي وفق المدفعي في توقيعها وطريقة ربطها بهيكل المبنى.**

هـ- برج ربيعة في ابو ظبي (شكل-23) (لم ينفذ) وبلغ المدفعي فيهما مراحل اعمق في الفكر الانشائي وكانت خبرته الإنشائية قد بلغت مرحلة مكنته من انجاز **مبنى برجي بنظام الاحمال العمودية وبتوفيق مع الشكل الخارجي للفتحات المتنوعة المواقع.**

و- مبنى سكرتارية الطاقة الذرية في بغداد (شكل-8) (لم ينفذ) فقد تميزت إستخداماتهاالإنشائية لاختيار نظام انشائي يتناسب مع فكرة المبنى المستوحاة من حركة الالكترونات (مصدر- 16) حول النواة وذلك عن طريق اللجوء الى **النظام الناتئ للمستويات الكونكريتية المتغيرة الزاوية بالتدريج عن طريق اعتماد كتلة كونكريتية دائرية** استغلها المدفعي كفضاءات داخلية تضم فضاءات الحركة العمودية وبعض الفضاءات العامة فنتج عن ذلك مبنى غاية في الروعة والتميز وللاسف لم يتم تنفيذه وبقي اسير الورق لحد الان في الوقت الذي يجري حاليا تنفيذ العديد من الابراج ضمن هذا المفهوم ولكن بنسب اكثر رشاقة وباعتماد التغليف المستمر للمستويات وبما يتناسب مع روح العصر وتوافر التقنيات التنفيذية الدقيقة والمحوسبة.

6. الإستنتاجات

- تميزت أعمال المدفعي بإستخدامات منشأية متفردة وتميزت بالحركة العالية وذلك من خلال تبني الأفكار الحديثة وإدخال التفسيرات الذاتية والخصوصية المحلية عليها.
- الواقع العمراني والإنشائي المحلي وتشخيص الأسباب والعلل التي يعاني منها ووضع الحلول الملائمة لها توفرت للروادفرص لتقديم أعمالهم ضمن ظروف أتاحت للنخبة المثقفة من إيصال الفكر لأصحاب القرار

في حقبة الخمسينات فضلاً عن نضوجهم ومنهم المعمار المدفعي وإندفاعه لتجارب جديدة في الستينات والسبعينات.

- إستمرار عطاء المدفعي عقوداً ولايزال حتى ساعة إعداد هذا البحث.

7. التوصيات

مما تبين في أعلاه فإن الباحث يوصي بما يأتي:

- لابد للمصمم المعماري من الاحاطة بتاريخ تطور التقنيات البنائية على مستوى الحضارات المختلفة بصورة عامة وعلى مستوى العمارة المحلية التاريخية والتراثية بصورة خاصة والافادة منها لكونها تحمل في مضمونها حلولا لبيئة وعادات المنطقة بعد تجارب عديدة قد تعود لالاف السنين.
- ضرورة الاطلاع على الانظمة المنشأية المتطورة واستخدامها او التعديل عليها لتتناسب مع المتطلبات البيئية والشكلية المحلية.
- ان المنظومة المنشأية المتطورة والامكانيات الاقتصادية العالية غير كافية لتحقيق التميز في المنتج المعماري اذ ان فكر المصمم وخياله هما العامل الاهم في العملية الابداعية وهنالك امثلة عديدة لابنية تميزت ببساطتها من ناحية المواد المستخدمة وبايادي محلية ولكنها كانت غاية في الروعة والجمال.
- العمل المستمر على ابتكار وتطوير اشكال وانماط انشائية جديدة فالامر ليس بالصعوبة التي يبدو عليها متحررا بذلك من التقليد للتقنيات الانشائية الغربية.
- الدعوة الى اختراق المنظومات الانشائية التقليدية من قبل المصممين المعماريين وايجاد مايعبر عن ذاتهم بصورة صادقة بعيدا عن التقليد والحلول المتكررة.
- التاكيد على دور التكنولوجيا الحديثة والبرامج الحاسوبية وما تقدمه من تسهيلات باختصار الزمن وتقييم متانة الهيكل ومواطن الضعف فيه دون اجراء التجارب الموقعية كما يفتح للمصمم افاق جديدة من خلال المقترحات التي يقدمها .
- الجرأة في طرح الافكار الانشائية وان كانت بعيدة عن التنفيذ فقد تنتهي الامور الى حل مبتكر او تؤدي لابداع انشائي على اقل تقدير .
- استشارة الاختصاصيين وذوي الخبرة في المجال التطبيقي الانشائي من خلال عرض المشاريع عليهم في مراحلها الاولية وذلك لغرض الافادة من خبراتهم .
- اعتماد مبدا النقد الذاتي للفرد من خلال التطوير على الفكرة الانشائية من خلال دمجها مع انظمة اخرى او التعديل عليها او التخفيف من العناصر الغير ضرورية وصولا الى النظام الاكثر اقناعا.
- الافادة من التجارب السابقة وعلى المستوى المحلي والعالمي واعتماد التقييم النهائي مابعد التنفيذ وذلك لتلافي الوقوع في الاخطاء ذاتها او للتاكد من سلامة الحس الانشائي لهذا النظام والتطوير عليه في مشاريع مماثلة .
- الاهتمام بالجانب الفكري للهيكل الانشائي ومايرمز اليه فان ذلك يعطي للمبنى بعدا محسوس غير مرئي ويساهم في دعم فكرة المشروع ومثال ذلك فكرة الاشكال السرجية المرتبطة بالفيزياء الكونية .
- محاولة التنويع في الهياكل الانشائية باستمرار فان ذلك يزيد من خبرة المعمار وخياله ويتيح له مقدار اكبر من الحرية في العملية التصميمية.

8. المصادر والمراجع

1. الراوي، خالد ثابت، عمارة قحطان عوني دراسه تحليليه وتوثيقيه، أطروحه مقدامه الى مجلس كلية الهندسة – جامعة بغداد، 1990
2. السلطاني، خالد، عمارة ومعماريون، الطبعة الاولى 2009
3. الطائي، نهاد، مقال منشور عن دار الهنا الثقافي 2007
4. العبيدي، محمد، مقال عن توجهات المدفعي.
5. العتابي، عبد الجبار، لقاء مع المعمار في معرض الفنانين التشكيليين 2010/4/1
6. العلاف، عماد هاني، حوار مع المعمار الدكتور قحطان المدفعي
7. المدفعي، قحطان، الاهتدام، كتاب غير منشور
8. المدفعي، قحطان، زمكانية العمارة التقليدية ودلالاتها، كتاب غير منشور
9. المدفعي، قحطان، كلمة في حفل التكريم في وزارة الثقافة 2004
10. المدفعي، قحطان، مقال مقتطع من صحيفة المدى بعنوان (بغداد بين التصميم الماضي والرؤية المعاصرة)2012
11. المدفعي، قحطان، مكان الكامن، رسالة دكتوراه
12. المدفعي، قحطان، محاضرة في قسم هندسة العمارة، جامعة بغداد، 2010
13. المدفعي، قحطان، محاضرة في مؤتمر الحفاظ على مراكز المدن، 2010
14. المدفعي، قحطان، لقاءاته مع الطلبة في داره، بغداد، 2012
15. جمعية المهندسين البحرينيين، اشكالية النظرية والتطبيق في العمارة التقليدية، البحرين 16 يناير 1995
16. زيارة الدكتور قحطان المدفعي في محل اقامته
17. صور الابنية من ارشيف الاستاذ قحطان المدفعي
18. غزوان، معتز، محاضرة للدكتور المدفعي عن الدار العراقية التقليدية والنسبج التقليدي بغداد 2010/7/29
19. لقاء مع الدكتور قحطان المدفعي في قناة الفيحاء (برنامج مقهى الفيحاء) نيسان 2011
20. مجلة ur، العدد الخريفي لسنة 1979
21. لقاء منشور في موقع موطني الثقافي مع الدكتور قحطان المدفعي
22. محاضرة للدكتور قحطان المدفعي في جامعة ال البيت الاردنية في عمان 1998
23. مقال في مجلة الاتحاد حول الندوة التي اقامها الدكتور قحطان المدفعي في قاعة دجلة للفنون .
24. مقال للدكتور خالد السلطاني في جريدة المدى الثقافي العدد 158، 20 تموز 2004
25. موسوعة The international who's who 1997-1998
26. Al-kalily, JIM, The house of wisdom
27. Asensio, Francisco, New Architecture An International Atlas, Printed in China, 2007
28. Bandel, Struture Systems, 1967 by Deutsche Verlags – Anstalt Gmbttgart
29. Kuhl, Isabel, and others, 50 Architects you should know, Germany, 2008
30. Sharp, Dennis, Twentieth century architecture, A visual study, Australia, 2002

www.ahewar.org .31
www.wikipedia.org .32

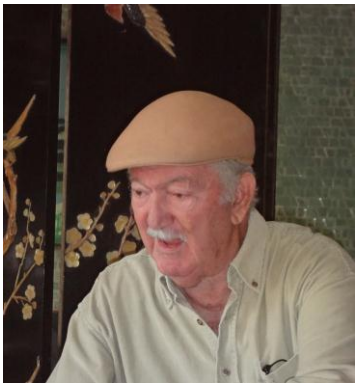

(شكل-1) المعمار الدكتور قحطان المدفعي

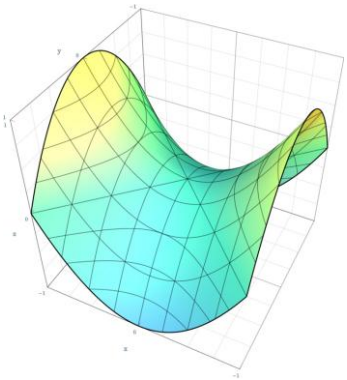

(شكل-2) السطح السرجي (Hyperbolic-Paraboloidal surface)

(شكل-3) مبنى جمعية الفنانين التشكيليين في بغداد

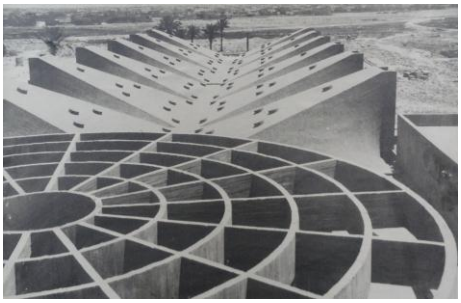

(شكل-4) مبنى متحف التاريخ الطبيعي في بغداد

(شكل-5) كنيسة الرونتشام Le Corbusier- Notre Dame du Haut, Ronchamp, Fr., 1950-55

(شكل-6) بناية مركز تدريب المواصلات السلكية واللاسلكية في منطقة العلاوي بغداد

(شكل–7) دار السيد امين الياسين في البصرة

(شكل–8) مبنى سكرتارية الطاقة الذرية (لم ينفذ)

(شكل–9) جامع آل بنية بغداد

(شكل–10) مبنى المعرض الزراعي بغداد (حالياً نقابة المهندسين الزراعيين)

(شكل–11) قاعة الهوكي في جامعة ييل Eero Saarinen–D. S. Ingalls Hockey Rink, Yale University,New Haven, CT, 1956 – 1958

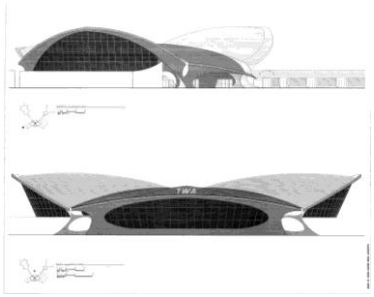

(شكل–12) مطار كينيدي –Eero Saarinen TWA Building, Kennedy Airport, NYC

(شكل–13) مبنى إداري في شارع الخلفاء بغداد

(شكل-14) احد الاعمدة الخارجية لحدائق الاوبرا - بغداد

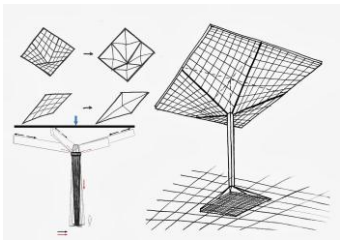

(شكل-15) مسقف من تصميم المعمار فيلكس كانديلا يوضح الفكر الانشائي المميز حيث تندمج العناصر الانشائية منسحبة نحو البعد الثالث

(شكل-16) سقف معمل تعبئة الشاي- بغداد

(شكل-17) حدائق الاوبرا خلال عملية التنفيذ- بغداد المعمار قحطان المدفعي

(شكل-18) مبنى الجذع المفتول Turning Torso للمعمار سنتياغو كالاترافا

(شكل-19) مبنى جمعية الفنانيين التشكيليين في بغداد

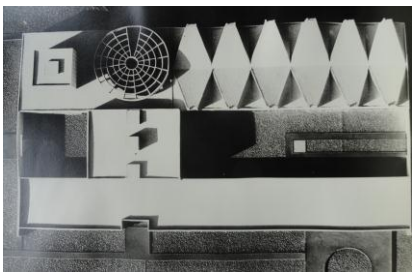

(شكل-20) متحف التاريخ الطبيعي في بغداد

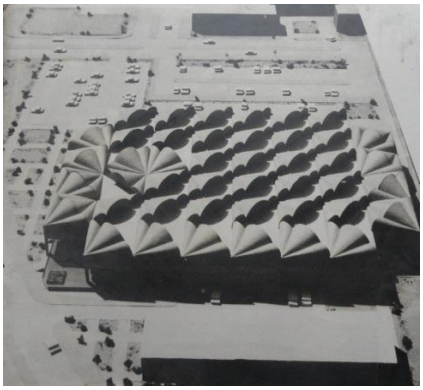

(شكل–21) مبنى البريد المركزي–بغداد (لم ينفذ)

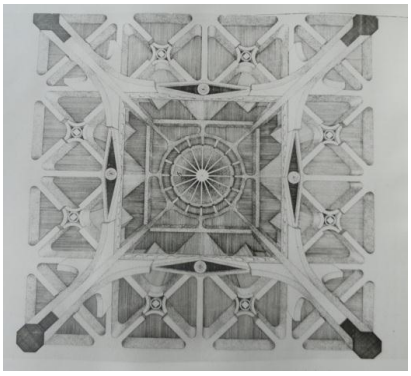

(شكل–22) لقطة منظورية داخلية لجامع آل بنية – بغداد

(شكل–23) برج ربيع في أبو ظبي (لم ينفذ)